NASA Contractor Report 178095

AEROACOUSTICS OF SUPERSONIC JET FLOWS FROM CONTOURED AND SOLID/POROUS CONICAL PLUG-NOZZLES

Darshan S. Dosanjh and Indu S. Das

SYRACUSE UNIVERSITY
Syracuse, New York

(NASA-CR-178095) AEROACOUSTICS OF SUPERSONIC JET FLOWS FROM CONTOURED AND SOLID/POROUS CONICAL PLUG-NOZZLES Final Report (Syracuse Univ., N. Y.) 187 p CSCL 20A G3/71

N87-17484

Unclas 44018

Grant NAG1-129
January 1987

National Aeronautics and Space Administration

Langley Research Center
Hampton, Virginia 23665

TABLE OF CONTENTS PAGE

TABLE OF CONTENTS (CONT'D)

NOMENCLATURE

A	Area
a	Acoustic speed
D	Diameter
f	frequency
K	Annulus radius ratio (R_p/R_N)
M	Mach number
p	Pressure
R	Radius (Also Radial Distance from the Nozzle-Exit to the Measuring Location).
R_N	Radius of the nozzle lip
R_p	Radius of the plug at the sonic point
V	Velocity
W	Annulus width of plug nozzle
α	Inclination of the convergent nozzle lip to the nozzle axis.
β	Parameter, $\sqrt{(M_j^2 - 1)}$
γ	Ratio of specific heats
ν	Prandtl-Meyer angle
ρ	Density
σ	Percent porosity defined as 100 x the ratio of the total area of the perforations to the surface area of the conical plug.
ψ	Inclination of the surface of the contoured plug at the sonic point.
ξ	Ratio of reservoir absolute pressure to the ambient pressure = p_R/p_a
θ	Azimuthal angle of the location of measurement (angle between the center of the nozzle-exit to the center of the microphone and the downstream jet flow axis).

Subscripts

a	Ambient conditions (in the anechoic chamber)
d	Design condition
e	Exit condition
ISA	Standard atmospheric condition
j	Fully expanded jet flow
R	Reservoir conditions
t	Throat (the sonic condition)

I. INTRODUCTION

The noise radiated by high pressure ratio improperly-expanded turbulent heated jet flows (or turbo-jet exhaust) is intense [1-5].* In the acoustic field of such high speed single-stream jet flows, often the mixing and the shock-related noise components are concomitantly present. The intensity of jet-mixing noise from a single subsonic turbulent jet flow is predicted by Lighthill relation [6]. The aerodynamic noise generated by jet flows depends upon the mean speed, the mean flow velocity gradients just downstream of the nozzle exit and the turbulence and mixing characteristics. In a high-speed shockless heated turbulent jet flow, if the turbulence eddies are convected at supersonic phase-speed relative to the ambient conditions, Mach wave radiation may be generated [7].

In an improperly-expanded jet flow, repetitive shock structure is present. The passage of flow fluctuations through such repetitive shock structure results in the generation of either the broadband shock-associated noise [8] and/or the feed-back type screech noise [1,9]. For high pressure ratio improperly-expanded turbulent jet flows, the noise generating mechanisms of the major components of the radiated noise are often coupled. The strength and the spacing of the repetitive cellular shock structure, and the strength and the coherence of the flow fluctuation passing through the repetitive shock-fronts play an important role in the generation of the shock-related noise. Normally, the weaker the repetitive shock fronts are, the lower the level of the shock-associated noise intensity is [10,11]. Moreover, for the same shock strength, if the fluctuations of the turbulent flow convected through the shock front are more intense, the acoustic radiation is stronger [12]. Therefore, to suppress the aerodynamic noise components radiated by improperly-expanded single stream jet flows, the strength of the repetitive shock structure and its spacing, and the strength and the coherence of jet flow

---

*Numbers in brackets refer to the references listed on pp. 114-116. Only a limited number of typical references are cited.

fluctuations convected through the shock fronts need to be modified such that both the noise-contributing sources and the noise generating mechanisms are reduced in strength and effectiveness. Moreover, it is imperative that the desired changes in the exhaust flows are achieved at an acceptable and minimum thrust and weight penalty.

To achieve such acoustically favorable flow and shock structure modifications in improperly-expanded jet flows, the use of the 'equivalent' dual-stream coaxial co-flowing contiguous supersonic jet flows operated in the inverted pressure mode (i.e. the outer (annular) jet is at a higher above-critical pressure ratio than the weakly super-critical pressure ratio of the inner jet) have been shown to be effective [13-17]. Also, a contoured convergent-divergent nozzle is often considered favorably as a design option for controlling the shock-associated noise component of modern high specific thrust engine exhaust. The shock-associated noise component is eliminated if the exhaust flow of a contoured convergent-divergent nozzle is shock free. However, such exhaust-nozzles, of necessity, are operated over an extended range of pressure ratios. Therefore, at the off-design pressure ratios of a contoured C-D nozzle, the repetitive shock structure is present in the jet flows. At low supercritical pressure ratios, the shock structure may be present even in the diverging part of the contoured C-D nozzle. Still, the overall sound pressure level as a function of the fully-expanded jet flow Mach number M_j or the shock-associated noise from both the over- and the under-expanded C-D nozzle, (especially at higher azimuthal angles with reference to exhaust flow) is significantly lower than those of underexpanded jet flows from an equivalent (i.e. of the same mass flow rate, thrust, pressure ratio and exhaust area) single convergent round nozzle [18,19].

Some recent acoustic studies of supersonic jet flows from plug-nozzles have also shown appreciable noise suppression effects [20-23]. As a part of the present study, the use of a contoured plug-nozzle operated either at its design pressure ratio or even over an extended range of off-design pressure ratios has been reported to result in substantial reductions in shock-related noise from supersonic jet flows [20]. Even when an uncontoured conical plug is incorporated in either an externally-expanded convergent plug-nozzle or an externally-internally

expanded convergent-divergent plug nozzle of high radius-ratio K, compared to an equivalent convergent nozzle, significant reductions in shock-related noise components have been reported [20,21].

Mastrello [22] has shown experimentally that a conical convergent round nozzle modified by a porous cylindrical center-body of a tapered conical termination mounted along the nozzle-axis when operated at higher than the critical pressure ratios, results in considerable noise reductions. Because of the distributed porosity of the center-body, the repetitive shock-structure of the underexpanded jet flow is weakened and the observed noise-reductions are mostly in the shock-associated component. More recently such aeroacoustic investigations were extended by Kibens and Wiezien [23] for center-bodies similar to the one's used by Maestrello. The gasdynamical aspects of the underexpanded jet flows from such combinations of convergent nozzle and porous center-bodies were examined and the reductions in shock-related noise observed by Mastrello were confirmed. In these studies, for most configurations of the convergent nozzle and center-body combinations, the porous center-body with a tapered conical termination was extended through the entire length of the supersonic region of the underexpanded jet flow. The geometrical configuration of such a combination of a convergent nozzle with a long cylindrical center-body of high annulus radius ratio does not serve efficiently the aerodynamic function of a conventional plug-nozzle which is to reduce the thrust loss of a contoured C-D nozzle operated in the overexpanded mode at low super-critical pressure ratios. Therefore, the elimination of the repetitive shock structure by the use of a short contoured externally expanded plug with a pointed termination suggests itself as an attractive alternative. The aeroacoustics of such short plug-nozzles with low annulus radius ratios have not been studied before. The aeroacoustic investigations reported here, were undertaken to study the far-field overall sound pressure levels, the shock-related noise component and the nature of the repetitive shock structure of supersonic jet flows of plug nozzles with contoured and short conical plugs of solid surface and pointed termination. Furthermore, the effects of porosity of the conical plug surface on the repetitive shock structure and the resulting noise reductions were also studied.

PLUG-NOZZLE AT SUPERCRITICAL PRESSURE RATIOS

A plug-nozzle is a modification of a conventional convergent-divergent nozzle where downstream of the sonic throat, the supersonic expansion either in part or completely occurs externally [24-26]. A schematic of an externally-expanded plug nozzle is shown in Fig. 1. The contour of the externally-expanded plug surface at the design pressure ratio is such that all the rays of the centered expansion fan originating at the nozzle lip are intercepted at the plug surface and cancelled. The final expansion-ray intersects the plug at its pointed apex. At the throat of a contoured plug nozzle, the angle at the lip of the convergent nozzle is so selected that at the design pressure ratio of the plug-nozzle, the free boundary of the isentropic jet flow is parallel to the nozzle axis and an exit to throat area ratio for an isentropic flow at the selected design Mach number is achieved at the apex of the contoured plug (i.e. at the plug-nozzle exit). For a given design Mach number, such an isentropic plug has the shortest possible length and is shorter than that of the divergent part of an conventional contoured C-D nozzle with its initial expansion section, of the same design Mach number and throat area.

When a contoured plug nozzle is operated at a pressure ratio below the design pressure ratio (designated here as the over- expanded mode), the final ray intersects the plug surface at a location upstream of the plug-apex and the compression wave fronts originate from the remainder of the plug surface. Depending upon the pressure ratio, repetitive oblique shock structure may develop on the plug surface and/or farther downstream in the jet flow. For the pressure ratio higher than the design pressure ratio (underexpanded mode), part of the expansion waves escape the plug surface and result in repetitive shock structure in the jet flow.

The nature of the shock-structure and the jet flows issuing from a solid/porous plug-nozzle operated at the super-critical pressure ratios are dependent upon a large number of geometrical and configurational variables of the plug-nozzle noted below.

(1) The annulus-radius ratio K:

If the design flow Mach number of the contoured-plug nozzle is fixed, then its annulus-radius ratio K is also fixed (see Appendix I).

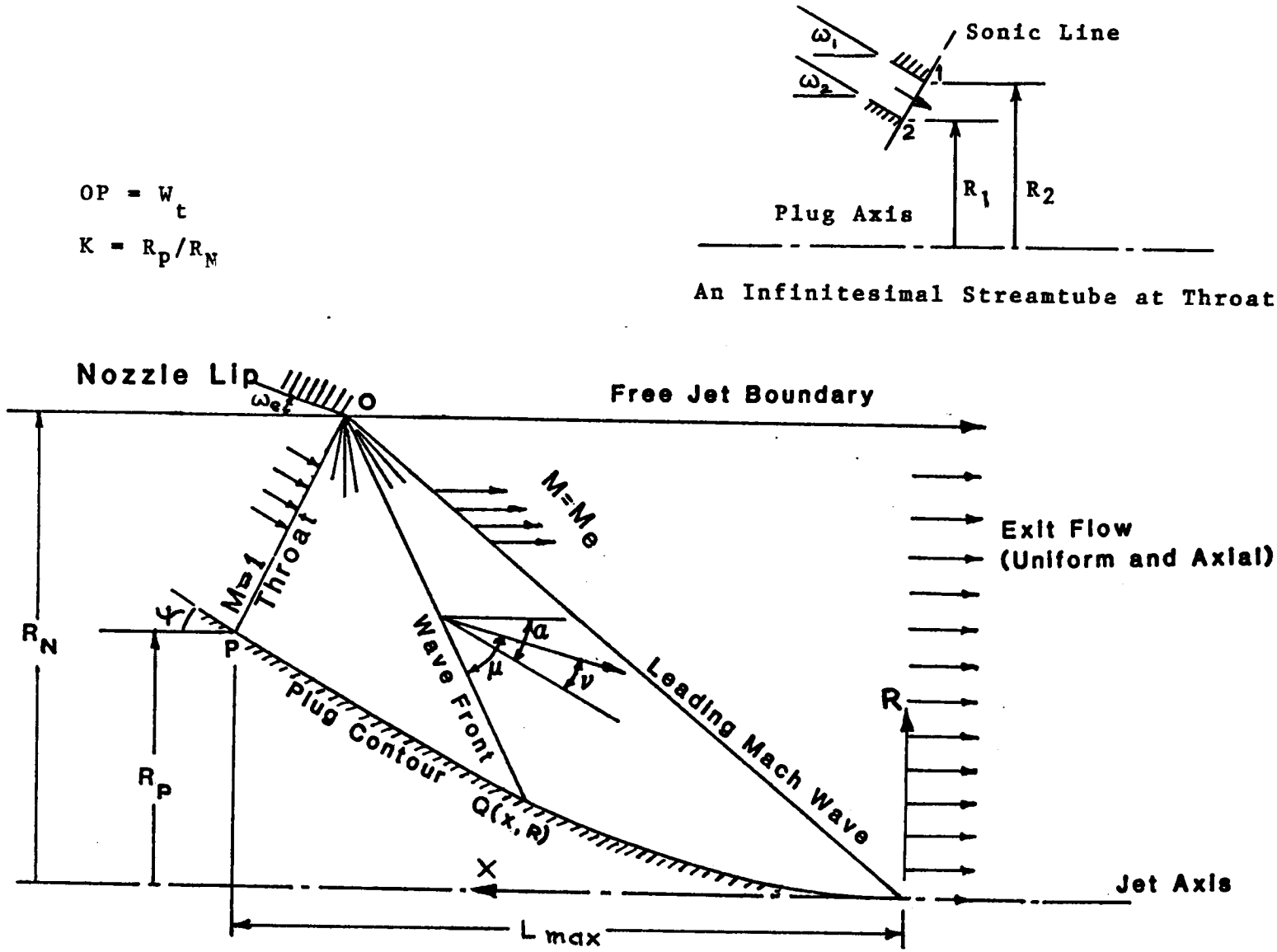

Fig. 1. Configuration and Nomenclature of a Plug-Nozzle with an Externally-expanded Contoured Plug.

The higher the design Mach number, the larger is the associated annulus-radius ratio to achieve an isentropic (shockless) jet flow. The mismatching of the annulus-radius ratios and operating pressure ratio or flow Mach number will result in repetitive shock structure.

(2) Configuration of the nozzle and plug combination:

Commonly either a combination of a convergent nozzle and an externally- expanded plug (Fig. 1) or a combination of a C-D nozzle and an externally-expanded plug [24], are used.

(3) Other relevant geometrical parameters of plug-nozzles:

The half-angle of the conical plug, the plug length and the initial convergent nozzle wall angle at the nozzle lip also influence the repetitive shock structure in the jet flow. The shock structure downstream of the plug-nozzle exit is strikingly different depending upon whether the plug termination is pointed (Fig. 8) or truncated [27].

(4) Porosity of the Plug Surface:

To optimize the modifications and the weakening of the repetitive shock structure of plug-nozzle flows by the porosity of the conical plug, the diameter, the location along the plug surface, the distribution and the depth of the perforations are relevant factors. Whether or not these are through-perforations opening into the hollow body of the conical plug and whether or not the perforated hollow plug is vented to the ambient surrounding, may also play a role in the flow and shock structure modifications.

Obviously, a parametric study of the roles of such a large number of geometrical and operational variables of a plug either with a solid surface or a combination of solid/porous surface is unwieldly. Therefore, to underscore the aeroacoustic role of plug-nozzles with short plugs and the importance of porosity in short plug nozzle flows at supercritical pressure ratios, the plug-nozzles of a few selected key geometrical parameters and configuration were selected.

The objectives of this experimental study are:

(i) To design a contoured plug to obtain a shockless supersonic jet flow at a relatively low design pressure ratio (i.e. of a low supersonic low Mach number):

The shock-associated noise component from the shockless supersonic jet flows issuing from such a plug-nozzle with a contoured pointed plug at its design condition will be absent. Since the contoured plug-nozzle flow is essentially wake-free, the dominant noise generating mechanism will primarily be due to turbulent mixing of the free-jet flow.

The far-field acoustic studies of such contoured plug-nozzle flows will generate the baseline acoustic spectral data for comparative assessment of the noise suppression of the improperly expanded supersonic jet flow issuing from 'equivalent' plug-nozzles of other configurations.

(ii) To study the role of a short solid uncontoured conical plug with a pointed termination as a design option for controlling the shock-associated noise in improperly expanded jet flows: The configuration of the uncontoured short conical plug is to be so selected that its acoustic and the aerodynamic performance is close to that of the contoured plug when both plug-nozzles are operated at the design pressure ratio of the contoured plug- nozzle.

(iii) How best to adapt the plug-porosity concept to optimize the design of a short solid/porous conical plug to maximize reductions of shock-associated noise:

The aim is to modify, by an appropriate selection of the porosity of the plug, the repetitive shock structure in the improperly expanded jet flow issuing from a plug-nozzle with an uncontoured plug such that the jet flow features nearly similar to those of an isentropic contoured plug at the design pressure ratio, are achieved. This means that porosity effects should lead to the weakening of the repetitive shock structure and that the free flow boundary at the plug apex (plug- nozzle exit) ought to be nearly parallel to the plug or jet flow axis.

II. EXPERIMENTAL FACILITIES AND PROCEDURE

II.1 Compressed Air, Flow Controls and Plug-Nozzle Supply System.

The compressed air is supplied by a Worthington HB-2 two stage oilless reciprocating air compressor of pumping capacity 7.9 scm/min. and the maximum discharge pressure of 3.435 MPa. The compressed air is cooled, dried and stored in five tanks of total capacity 31.15 m^3 . The line pressure is reduced through a 2" Masoneilan camflex valve from a maximum of 3.435 MPa to 1.037 MPa in the 10.16 cm. diameter, 45.72 m. long supply line between the storage tanks and the jet room in the acoustic facility. Upstream of the supply chamber, a 5.08 cm pressure control valve and pressure regulator is provided to maintain the supply chamber stagnation pressure at a pre-selected constant value. In the blow-down mode of operation of the compressed air facility, it is possible to operate a plug-nozzle of throat area equivalent to a convergent nozzle of 5.08 cm exit diameter, at a nozzle pressure ratio $\xi \doteq 4.5$ with run time of about 11 minutes.

The details of the stainless steel plenum chamber for the plug-nozzle jet rig are shown in Fig. 2. This plenum chamber is mounted in the anechoic chamber in series with an existing cylindrical plenum chamber (diameter 25.4 cm; length 1.52 m) with a 5.08 cm exit diameter which was used in earlier aeroacoustic studies to supply the inner nozzle of the coaxial dual-stream supersonic jet flow configuration [14]. The new plenum chamber has an overall length of 72.06 cm. and an inside diameter of 30.48 cm. The flow velocity in the cylindrical part of the plenum chamber when the convergent-nozzle of exit d = 4.45 cm is choked, is noted to be about 7 m/s. This ensured that the noise generated by the flow in the plenum chamber duct is comparatively low.

The plenum chamber incorporates a removable plug holder. A wire screen (50% porosity) is installed downstream of the plug-holder. The mechanisms have been provided to ensure sufficiently accurate alignment of the plug holder in three transverse directions. The plug is mounted axially aligned with a slender cylindrical plug holder. This type of axial support for the plug was preferred over the usual lateral strut supports as the former is less likely to cause flow inhomogeneity and to generate unwanted tones and excess-noise.

II.2 Acquisition of the Acoustic Data.

The acoustic data were recorded in an anechoic chamber with free-space dimensions from wedge-tip to wedge-tip of approximately 8m x 6.5m x 4.28m. The chamber is anechoic down to a frequency of 150 HZ [14].

One-third octave sound pressure level spectra of the far-field noise of the various plug-nozzle configurations and modes of operation were recorded at eight equally spaced locations, 15° apart between azimuth angles $\theta = 15^{\circ}$ to 120°, measured with reference to the downstream jet flow axis on an arc of radius R = 3.05m from the nozzle exit in a horizontal plane containing the nozzle axis and the axis perpendicular to the face of the condenser microphone. For a convergent nozzle of exit diameter $D \approx 4.5$ cm, the microphone location is at $R/D \approx 65$. Thus, the noise measuring stations are in the acoustic far-field of the jet noise. The microphone positioning is accurate within $\pm 1^{\circ}$. Standard B and K acoustic instrumentations comprising of B & K, Type 4135, 1/4" condenser microphone, with grid in place, at normal incidence (i.e. zero angle of incidence) band-pass filter set centered at 12.5 to 100 kHz; B and K Type 2305 level recorder were used to record the acoustic data. The condenser microphone was calibrated by B & K type 4220 piston-phone before and after each test run.

The recorded one-third octave sound pressure level spectra were analysed in the range of frequency 200 Hz to 100 kHz. The lower frequency limit was based on the consideration that the design cut-off frequency for the anechoic chamber is 150 Hz. The upper limit of frequency 100 kHz was dictated by the frequency content and the noise levels measured for the various configurations of the model solid/porous plug-nozzles. The ambient pressure, and the dry and wet bulb temperatures in the anechoic chamber were measured during the entire course of acoustic data accumulation. For analysis of acoustic data, the lossless spectral data were obtained by applying the microphone free-field and absorption (humidity) corrections to the recorded 1/3 octave sound pressure level spectra. The microphone corrections of the 1/4" condenser microphone with grid and normal incidence were applied from calibration data provided by the manufacturer. These corrections are listed in Table I-1 of Appendix I.

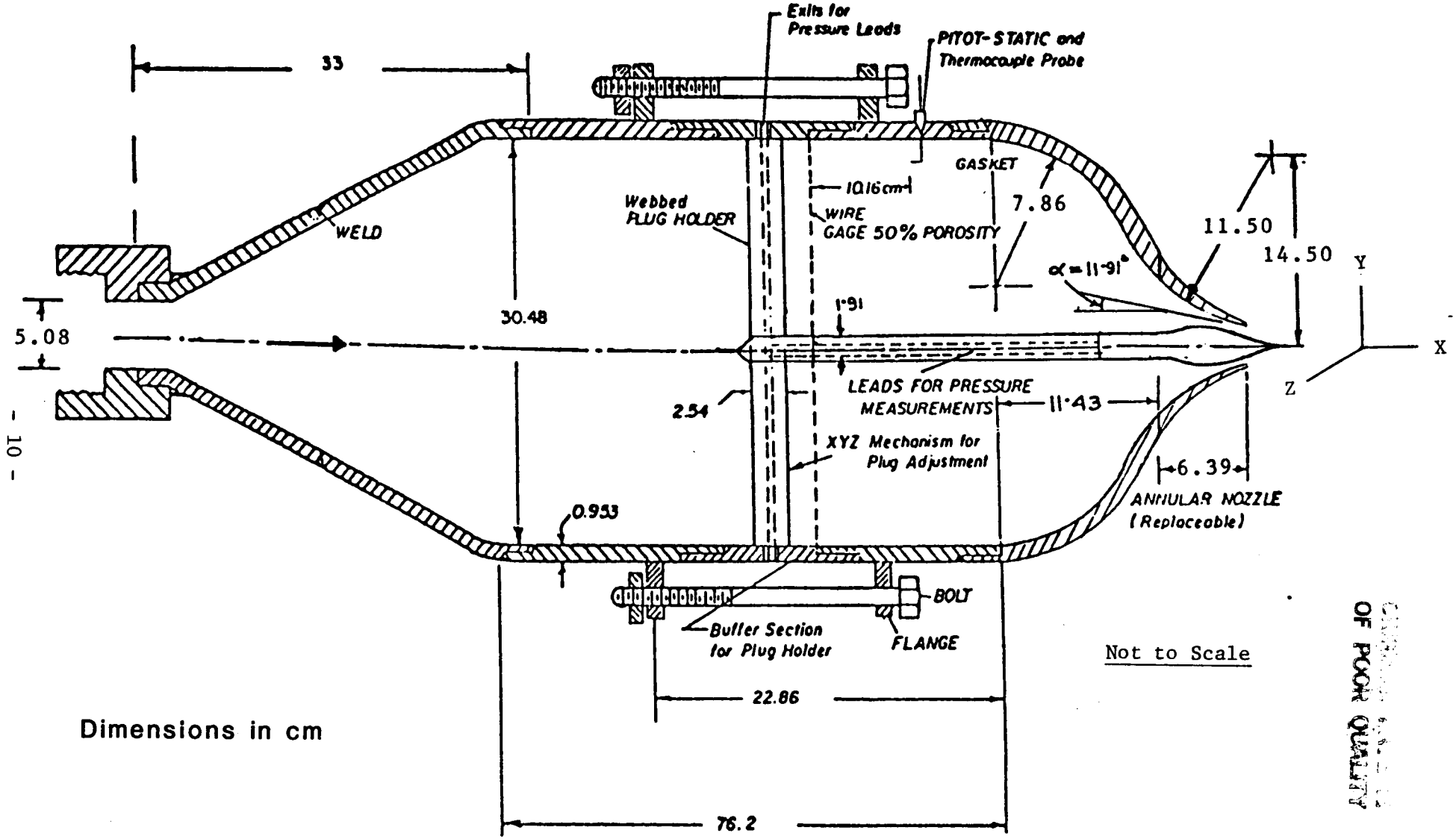

Fig. 2. Plenum-Chamber and Plug-Mounting Assembly for the Plug-Nozzle.

The corrections for acoustic absorption due to humidity based on a relation by Evans and Bass [28], were applied. The details of these corrections especially at higher frequency spectral content for the model plug-nozzles and their bearing on the schemes of reduction of the acoustic spectral data are available in Ref. 43.

The experimental facility and procedure for recording acoustic data were validated by operating the convergent nozzle (plug-nozzle with the plug and its mounting assembly removed) at a range of subsonic velocities and showing the noise intensity (OASPL at $\theta = 90^{\circ}$) to follow $V_j^{7.7}$ which is very close to the expected V_j^{8} dependence [6].

II.3 Optical Records.

A condenser-spark light source, a 48" focal length, front coated 12" diameter parabolic mirror and a film holder are the basic components of the optical system used to record spark shadowgraphs of the jet flows issuing from the convergent nozzle and the various plug-nozzles. Spark source of light of about 1 μsec duration was generated by discharging, six cylindrical low inductance condensers, each of 0.04 μfd capacity (maximum 10 kV; normally used at 7.5 kV), arranged on a ring around the magnesium electrodes. The front electrode had a 1 to 2 mm adjustable diameter hole to serve as the point source of light. The angle between the incident light beam and the axis of the parabolic mirror was adjusted to be within 7° by mounting a front coated plane mirror between the light source and the parabolic mirror. To record the spark shadowgraphs, the film was mounted at a distance of about 7" from the jet axis.

III. NOZZLE CONFIGURATIONS AND MODES OF OPERATION

III.1 Convergent Nozzles

For the aeroacoustic studies reported here, the basic plug-nozzle assembly is a combination of a convergent nozzle with a centrally mounted externally-expanded short plug of pointed termination. The plug-nozzle operated without the plug and its mounting assembly was used as the basic convergent nozzle.

One of the plug-nozzles was designed with a contoured plug to achieve an isentroph an isentropic (shockless) jet flow at its design pressure ratio,

$$\xi_d = \frac{\text{Absolute Reservoir Pressure}}{\text{ambient pressure}} = P_R/p_a = 3.67$$ (i.e. the design Mach

number $M_d \doteq 1.5$). Therefore, for the free jet flow boundary of the fully-expanded jet flow to be straight and parallel to the plug axis, the inclination of the wall of the convergent nozzle must be equal in magnitude and opposite in direction to the Prandtl-Meyer angle $\nu = 11.905°$. To avoid acoustic reflections and screech generation, a fairly sharp nozzle-lip (thickness of approximately 0.5 mm) was provided.

The stainless steel convergent nozzle used in the present studies was machined in two parts. The first portion is carefully welded to the plenum chamber avoiding any inside protuberance or misalignment and the second portion is a detachable extension of the first. This was done so that this convergent nozzle could be adapted for use in any other future plug-nozzle studies at different design Mach numbers. The two parts of the converging nozzle have finely polished extremely smooth matching inner profiles insuring the absence of flow separation at the joint. The detachable part of the converging nozzle is carefully contoured to terminate smoothly at the throat of plug-nozzle into a conical lip having a wall angle of 11.90° with the central nozzle axis.

The exit diameter of the convergent nozzle is 4.5 cm and its overall length is 17.85 cm. The area ratio of the nozzle inlet to the nozzle exit is about 46. The geometry and installation of the convergent nozzle is shown in Fig. 2.

III.2 Contoured Plug

The design of an isentropic contour of the plug for an externally-expanded plug-nozzle is based on the following key considerations* .

(i) The expansion waves are assumed to be centered at the lip of the convergent nozzle. For the free jet boundary at the lip to be straight and parallel to the nozzle axis, the convergent wall has to have an inclination, α , to the jet axis, given by,

$$|\alpha| = |\nu(M_d)| = \sqrt{\frac{\gamma+1}{\gamma-1}} \cdot \tan^{-1} \sqrt{\frac{\gamma-1}{\gamma+1} \cdot (M_d^2 - 1)} - \tan^{-1} \sqrt{M_d^2 - 1}$$

where $\nu(M_d)$ is the P-M function for the design flow Mach number.

* An alternate simple approximate method for a nearly isentropic plug contour developed in the course of the present investigation is outlined in Appendix II (also see Reference 29).

(ii) The individual expansion waves emanating from the nozzle lip and incident on the plug-surface are all cancelled by suitable local compression turns provided at the plug surface. The last expansion wave (corresponding to the design Mach number M_d) must end at the plug tip (or apex) and it has to be straight, being the start of the uniform simple region. The plug contour as such is a streamline of the potential (isentropic) flow issuing from the plug-nozzle.

The exact method of plug contour design is based on the method of characteristics (MOC). The main difficulty in using the method of characteristics for axisymmetric jet flows lies in the flow region near the jet axis (radial distance $R \rightarrow 0$) where a very fine characteristic mesh is required for reasonable accuracy and the problem of numerical instability is known to plague the computations in the center-line region.

A methodology of designing an isentropic supersonic inlet-plug using the MOC was developed by Connors and Meyer [30]. To avoid the computational difficulty near the flow centerline, a finite inlet-plug tip angle and a finite strength shock extending from the inlet-plug tip to the plug-nozzle lip were assumed. The plug contours were predicted for relatively high pressure ratios. The approach, as suggested by this study, also applies to prediction of isentropic plug contours for plug-nozzles. For an ideal contoured plug-nozzle, the annulus-radius ratio K (ratio of the plug radius R_p at the sonic point to the nozzle lip radius R_N) is a unique function of the design flow Mach number. Therefore, at high design pressure ratios, the corresponding values of K's are also high. This, when applied to plug-nozzles to be operated at high pressure ratios encountered in rocket engines, results in small annulus-widths (or heights) of the throat of the plug-nozzle. Therefore, the assumption made by Connors and Meyers that the sonic line at the inlet throat is straight, is reasonably satisfied. The present aeroacoustic studies, however, are aimed at the use of plug-nozzles at a lower range of design pressure ratios such as those normally encountered in turbo-jets for supersonic jet propulsion. This lower range of pressure ratio was not covered in the earlier predictions by Connors and Meyers of the contours of isentropic inlet-plug. At lower design pressure ratios ξ_d, the annulus-radius-ratio K of the plug-nozzle are smaller and consequently, the plug-nozzle throat-

width would be comparatively larger. Therefore, the non-uniform flow at the plug nozzle-throat would result in appreciable curvature of the sonic line. Consequently, Connors and Meyer method which prescribed a straight sonic line at the throat, would not predict the exact plug contour for an isentropic plug- nozzle flow at low super-critical design pressure ratios.

Prediction of the Isentropic Plug Contour

The design parameters that must be determined for the start of the MOC solution are: the geometrical annulus-radius-ratio K, the inner wall (i.e., the plug) slope at the sonic line and the shape of the sonic line. Consider the flow near the throat in an infinitesimal annuls of an axisymmetric plug-nozzle (for nomenclature see Fig. 1). The throat area is given by,

$$A_t = \pi \, (R_1^2 - R_2^2) \, / \cos \left(\frac{\omega_1 + \omega_2}{2}\right)$$

for $\omega_1 \doteq \omega_2$.

The geometrical condition of Mach number gradient at the throat in the stream direction being zero,

$$\frac{dA_t}{dL} = 0, \text{ gives}$$

$$\omega_2 = \sin^{-1} \left|\frac{\sin \omega_1}{k}\right|$$

where $k = R_2/R_1$

The mean flow direction of the streamline in the infinitesimal annulus is,

$$\omega_m = \frac{\omega_1 + \omega_2}{2}$$

Also,

$$k = \left| 1 - \frac{\cos \omega_m}{(A_e/A_t)} \right|^{\frac{1}{2}}$$

where (A_e/A_t) is given by the area-Mach number relation for an isentropic flow.

The preceding set of equations may be used for establishing an iterative scheme, starting from the nozzle lip, to obtain the shape of curved sonic line along with the values of the geometrical configuration parameter K of the plug and slope of the plug at the sonic line. The starting values of ω_1 is given by,

$$\omega_1 \leftarrow \alpha = \nu\ (M_d)$$

where M_d is the design Mach number. The iterative scheme is initiated by guessing a value of k and the process is so rapidly convergent that the points on the curved sonic line are obtained with ease.

Having obtained the sonic line shape, the geometrical annulus- radius-ratio K and the initial slope of the plug at the sonic line ψ, the method-of-characteristics (MOTC) solution, as described in references 31 and 32, was used for obtaining the plug profile which is a bounding stream surface of the plug-nozzle potential flow. The method consisted of treating the flow in two domains (see sketch on the following page). The domain I is a mixed region having both the left running and right running characteristics and the bounding surface of this domain is straight being adjacent to the uniform exit flow region. The domain II is a simple region having only one type of characteristics. The lines of constant characteristics, starting from the nozzle lip, were traced in fifteen small intervals and the plug profile was generated in successive stages by providing suitable local compression turnings at the surface to cancel the incident expansion waves. It may be noted that a line of constant characteristic is necessarily curved in an axisymmetric flow. A combination of computational and graphical approach was used.

In the present study a plug-nozzle with a contoured plug of design Mach number $M_d \doteq 1.5$ was used. This resulted in a specific annulus-radius-ratio $K = R_p/R_N = 0.43$ and a convergent nozzle wall inclination $\omega_e = 11.905^\circ$ and the inner plug wall slope $\psi = 28.37^\circ$. For the same design Mach number, a plug contour was predicted by an approximate method and K and ψ were respectively, 0.41 and 21° . For details see Appendix II. The coordinates of the plug designed by the method of

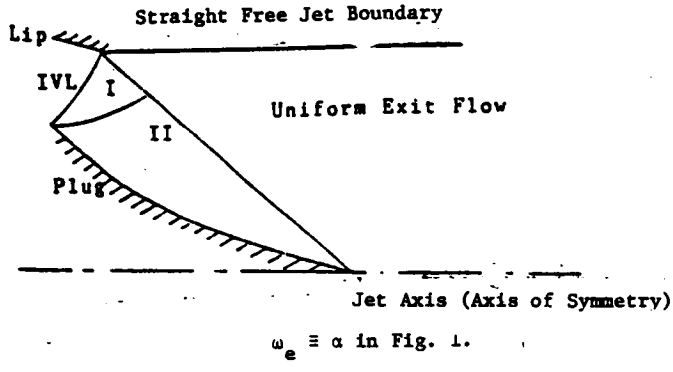

$\omega_e \equiv \alpha$ in Fig. 1.

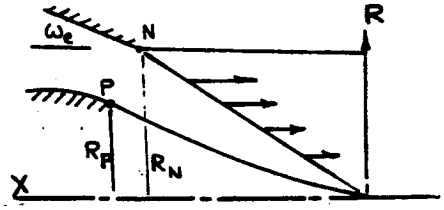

Table 1. Coordinates of the Contoured Plug (in mms)

X	R	X	R
0.00	0.00	15.71	3.45
1.01	0.05	17.66	4.17
3.05	0.25	19.46	4.89
5.59	0.64	21.26	5.69
7.31	0.99	23.06	6.46
8.96	1.40	25.16	7.59
11.21	2.02	27.26	8.70
13.76	2.80	29.27	9.77

Design Mach Number $M_d \doteq 1.50$

Radius at the Nozzle Lip $R_N = 22.5$ mm.

Radius of the Plug at the throat $R_p = 9.77$ mm.

(Annulus-Radius-Ratio) $K = R_p/R_N = 0.434$

Width of the Plug-Nozzle throat $w_t = R_N - R_p/\cos(\frac{\psi + \omega_e}{2}) = 13.56$ mm.

$\omega_e \equiv \alpha_e$ Inclination of the wall of the convergent nozzle

characteristics and by the approximate method are tabulated in Table 1, (p.16) and Table II.1 (p.127) respectively.

To circumvent the difficulties encountered in machining a stainless steel contoured plug with an extremely sharp pointed termination, an aluminum contoured plug was machined with a thickness of the pointed termination of only 0.025 cm.

III.3 Selection of Plug-Nozzle Configurations with a Solid Short Conical Plug.

One of the stated objectives of the aeroacoustic studies reported here was to assess the effectiveness of an uncontoured short conical plug-nozzle in suppressing the shock-associated noise radiated by an underexpanded jet flow issuing from an 'equivalent' convergent (plugless) nozzle.

The plug-nozzle with a contoured plug operated at its design pressure ratio provides the base-line acoustic data for a shock-free plug-nozzle supersonic jet flow. This is an ideal to be approached when the objective is to achieve the suppresion of the shock-related noise components of improperly expanded jet flows issuing from plug-nozzles. Therefore, the shock-associated noise components of improperly expanded jet flows issuing from a conical plug-nozzle can also be assessed by comparison with the noise radiated by an isentropic shockless supersonic jet flow issuing from an 'equivalent' contoured plug-nozzle at its design pressure ratio.

In addition, the role of porosity of the plug surface in weakening the repetitive shock structure in improperly-expanded conical (uncontoured) plug-nozzle jet flows is to be assessed. The aim is to weaken the repetitive shock structure of uncontoured conical plug-nozzle flows such that the features of the improperly expanded jet flows of a plug nozzle with a combination of porous and solid surface are nearly similar to those of a contoured plug-nozzle at or around its design pressure ratio.

Many shapes and geometrical configurations of the conical plugs with a solid surface are possible. An uncontoured conical short plug-nozzle with a throat area equal to that of a contoured plug-nozzle was selected. This facilitates the simultaneous matching of both the pressure ratio and the

mass flow rate for the conical and contoured plug-nozzle flows. Furthermore, when the plug-nozzle configurations are operated without the plug besides the matching of pressure ratio of the resulting convergent nozzle with that of the plug-nozzle, the exit area (or the mass flow rates) of the plug-nozzle and the convergent nozzle flows can be matched by scaling down the exit area of the plugless convergent nozzle (for additional remarks, see the discussion of the acoustic results in Section V.).

Keeping the annulus-radius-ratio K the same, the conical plug may be chosen on the basis of any of the following additional considerations.

(i) The length of the short conical plug is exactly the same as that of the contoured plug. For a given K, this fixes the semi- angle of the conical plug.

(ii) The surface area of the conical plug is equal to that of the contoured plug.

(iii) At the throat of the plug-nozzle, the conical plug surface has the same slope as that of the isentropic contoured plug.

(iv) The geometry of the conical plug could be selected purposely to be radically different from that of a contoured plug. For example, the plug apex angle could be much larger than those obtained from conditions (i) to (iii) or the conical plug could be much longer than the contoured plug. The repetitive shock structure in the improperly expanded jet flows from such conical plug-nozzles will be comparatively stronger than if the geometry of the conical uncontoured plug were selected to be rather similar to that of a contoured plug.

These aeroacoustic studies of plug-nozzle flows were directed at using rather short plugs as center-bodies. Simple quasi-one-dimensional estimations of the pressure distribution over the plug surface and the thrust, and the role of the plug length in intercepting (either in part or in-full) the incident expansion waves, suggested the choice of a solid conical plug semi-angle which results in a surface area equal to that of the contoured plug (option (ii) above). For this experimental study, the

solid conical plug-nozzle so chosen has a annulus-ratio K = 0.43 and semi-angle at the plug apex of 23.9^{o}. The ratio of the plug-length from the sonic point to the plug lip (L_{max}) to the nozzle radius R_N for the contoured plug is 1.30 and for the uncontoured conical plug is 0.97. When operated at the same pressure ratio as that of the contoured plug, such a solid uncontoured conical plug-nozzle is expected to have the same mass flow rate and nearly the same specific thrust with aerodynamic performance close to that of the isentropic contoured plug-nozzle. For additional details of the conical plug geometry, see Fig. 3. The geometrical parameters of the various plug nozzle configurations are summarized in Table 2.

III.4 Porous Conical Plug

The contoured plug-nozzle, the solid conical plug-nozzle and the solid/porous plug- nozzles with plugs of different porosity, all have the same annulus- radius-ratio K (or the throat area). Therefore at the same pressure ratio, the mass flow rates are matched. A comparison of the aeroacoustics of the various plug-nozzle flows is, therefore, possible when these plug-nozzles are operated at the same pressure ratio.

The transonic wind-tunnel studies indicate preference for low porosity at higher speeds if the weakening of the shock fronts from the aerodynamic model incident on the tunnel wall was to be promoted. From the studies of Spiegel et al [33], one may expect a porosity of 15% or lower to be preferable for shock wave cancellation. However, the effects of flow through perforations and the flow resistance introduced by the porosity of the surface on the aerodynamic performance of the plug-nozzle need to be assessed. The flow over perforated surface is known to be a generator of unwanted tones, for values of the Strouhal number around 0.2 [34,35]. Thus, the geometry of the perforations (i.e. the diameter and the depth of the perforation) and whether the porous hollow plug is vented to the ambient atmosphere or not, would influence the gas dynamics of the porous surface in supersonic jet flows and the possible generation of the porosity-dependent acoustic radiation.

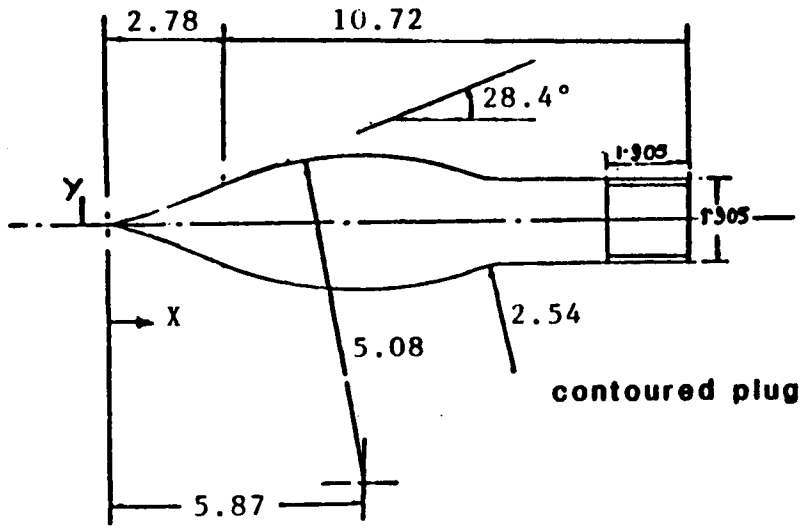

contoured plug

$R_N = 2.225$

$R_P = 0.96$

$K = 0.43\ (R_p/R_N)$

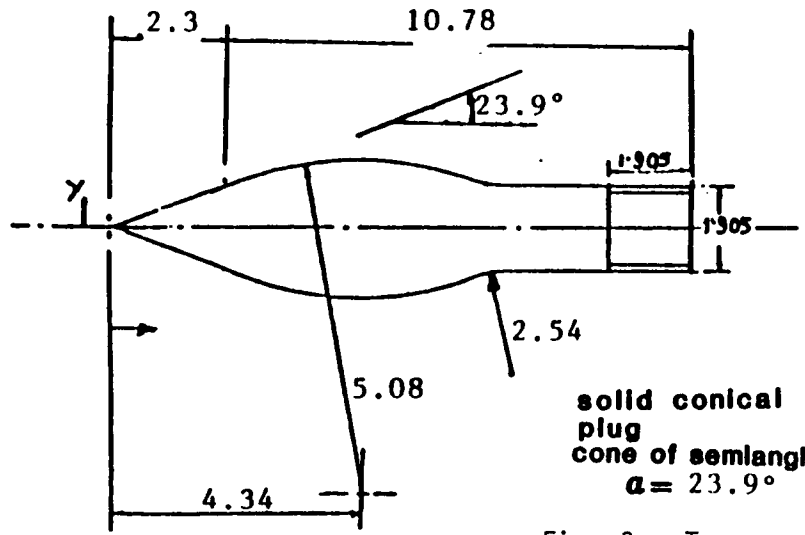

solid conical plug
cone of semiangle
$\alpha = 23.9°$

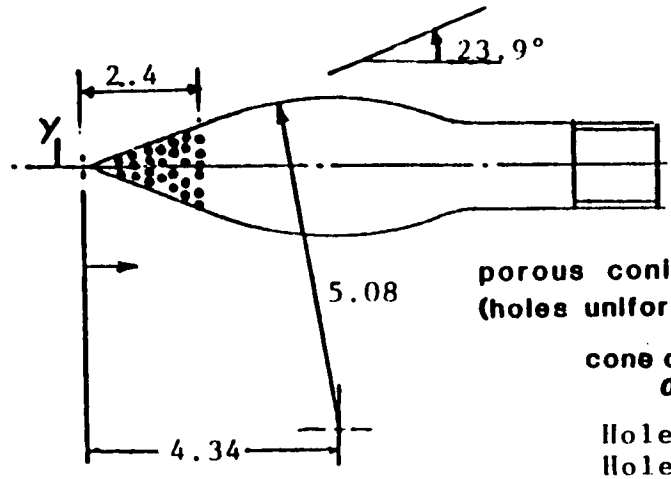

porous conical plug (σ-10%)
(holes uniformly distributed)

cone of semiangle
$\alpha = 23.9°$

Hole Dia. = 0.1
Hole Depth = 0.2

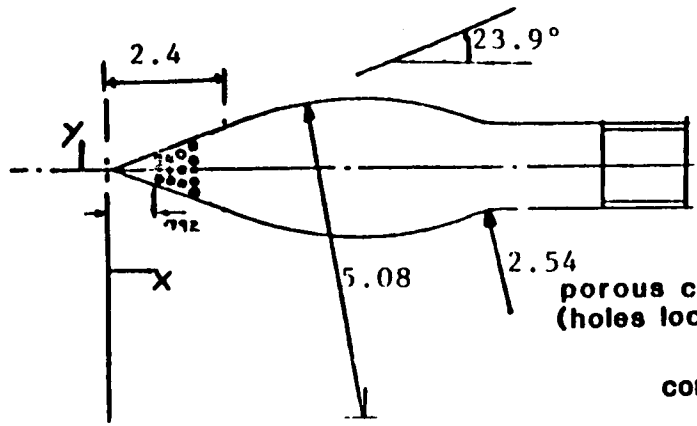

porous conical plug (σ-4%)
(holes locally distributed)

cone of semiangle
$\alpha = 23.9°$

ALL DIMENSIONS IN CMS.

Fig. 3. Type and Geometrical Details of Different Model-Plugs.

With the aforementioned porosity considerations in mind, for the present experiments, a non-vented porous plug having a ten percent porosity σ, with perforations open to the hollow body of the plug (the perforation diameter of 1 mm and the depth of 2 mm) was used. The perforations were uniformally distributed along seven evenly spaced rings over the conical plug surface. The degree of porosity is high enough for promoting either interaction between waves of opposite polarity and/or wave cancellation, and low enough not to significantly affect the thrust of a conical plug without perforations.

The relatively large ratio of the depth of the perforation to its diameter (= 2), increases the damping to the flow in and out of the perforation which diminishes the intensity of self-excitation as noted by Tsui and Flandro [34]. An examination of the spark shadowgraphs recorded during the preliminary studies indicated that strong reflected waves originating from the middle-third of the solid conical plug, play a relatively more significant role in the formation of the repetitive shock structure in the plug nozzle jet flows. Therefore, to modify this shock structure, a second plug having perforations (σ = 4%) only in the middle-third of the plug was also studied. The two porous plug models are shown in Fig. 3.

III.5 Role of Plug Hump

The location of the nozzle throat relative to the plug hump and the radius of curvature of the plug-hump are known to be critical considerations in the design of plug-nozzles [36]. For the contoured plug-nozzle, in particular, the hump may lead to the expansion of the flow around its curved portion just upstream of the geometrical throat. The throat (the narrowest cross-section) of the plug-nozzle, therefore, must always be located downstream of the point where the curved section at the hump becomes tangent to the expansion section of the plug.

In the present study, the largest possible value of the radius of curvature of the plug hump was selected such that, for the prescribed outer wall profile, the minimum flow area occurred at the theoretical location of the sonic line. Further, the approach to the supersonic expansion of the plug was made straight (approximately 0.8 mm long), smoothly joining the curved hump. This ensured the occurrence of the actual throat downstream of the curved portion of the hump.

The actual locations of the throat may deviate slightly from the theoretically predicted location due to three dimensional effects and flow inhomogeneity inherent in the actual flow. To attain shockless jet flow from the contoured plug-nozzle at its design pressure ratio, a slight axial adjustment in the plug location may be helpful to achieve coincidence of the actual and the theoretical location of the sonic point on the plug surface. Therefore, a provision was made in the plug holder so that with proper fillers, the throat location could be moved backward or forward up to 0.8 mm.

The geometrical specifications of the various model externally-expanded plug-nozzles with pointed plug termination are tabulated below.

Table 2. Summary of Geometrical Parameters of the Model Plug-Nozzle Configurations.

S.No.	MODEL	R_N mm	ω_e	K	ψ	w_t mm	L_{max}/R_N	$L_{max}w_t$
1.	Convergent Nozzle	22.5	11.9°	-	-	-	-	-
2.	Contoured P.N.	22.5	11.9°	0.43	28.4°	13.56	1.30	2.16
3.	Solid Conical P.N.	22.5	11.9°	0.43	23.9°	13.56	0.9	1.61
4.	Porous Conical P.N. Porosity 10%	22.5	11.9°	0.43	23.9°	13.56	0.97	1.61
5.	Porous Conical P.N. (Porosity 4%)	22.5	11.9°	0.43	23.9°	13.56	0.97	1.61

R_N Radius of the nozzle lip: R_p radius of the plug at the sonic point

K Annulus-Radius Ratio of R_p to R_N

$\omega_e \equiv \alpha_e$ Inclination of the wall of the convergent nozzle:

w_t width of the annular throat of the plug-nozzle

ψ Inclination of the plug surface to the jet axis, at the sonic point

L_{max} Axial length of the plug from the sonic point to its tip

IV. THE SCOPE OF THE EXPERIMENTAL DATA

The acoustic and optical data of the supersonic jet flows issuing from the contoured plug nozzle, uncontoured conical plug-nozzles and a combination solid/porous plug nozzles were recorded to explore their comparative performance for suppression of shock-associated jet noise. The range of pressure ratios at which these were studied and the extent of the experimental data recorded, are tabulated below.

Nozzle Configuration	Jet Pressure Ratio ξ					
	2.0	2.5	3.0	3.6	4.0	4.5
a) Convergent Nozzle	†	†	†	†	†	†
b) Contoured Plug-Nozzle	†	†	†	†	†	†
c) Uncontoured Solid Conical P-N	†	†	†	†	†	†
d) Porous Conical P-N (σ = 10%)	*	*	†	†	*	†
e) Porous Conical P-N (σ = 4%)	*	*	†	†	*	†

The symbol † indicates that the acoustic data were gathered at all eight azimuthal angles, 15 degrees apart, from $\theta = 15^{\circ}$ to 120° (measured with respect to the downstream axis of the jet flow. The symbol * indicates that the acoustic data were gathered only at $\theta = 90^{\circ}$.

The spark shadowgraphs and the acoustic data of the supersonic jet flows issuing from each of these nozzle configurations operated at the range of pressure ratios ξ = 2.0 to 4.5 were recorded. Since in the present studies the theoretical design pressure ratio for the contoured plug-nozzle is $\xi_d \doteq 3.67$, the range of pressure ratios ξ covers the off-design pressure ratio for the over-expanded ($\xi < \xi_d$) and for the underexpanded ($\xi > \xi_d$) modes of operation. For the contoured plug nozzle, shock-free flow was achieved at $\xi \doteq 3.60$ ($M_j \doteq 1.49$).

The 1/3 octave SPL's were recorded at azimuthal angles $\theta = 15^\circ$, to 120° for the convergent nozzle flows (i.e. the plug-nozzle operated without the plug) operated at $\xi \doteq 2.0$ to 4.5 as well as for the contoured plug-nozzle operated at the design pressure ratio $\xi \doteq \xi_d$ and the off-design pressure ratios. For the combination solid/porous conical plug nozzles operated at ξ = 3.05, 3.6 and 4.5, the 1/3 octave spectral data were also recorded at all eight θ locations. However, for ξ = 2.0, 2.5, 4.0 the acoustic data for the solid/porous plug-nozzle were recorded only at $\theta = 90^\circ$. Since at higher angular locations around $\theta = 90^\circ$, the shock-associated component of radiated noise is dominant over the jet-mixing noise, for shock-associated noise studies, limiting the recording of SPL's to only $\theta = 90^\circ$ for some of these pressure ratios was considered to be adequate. Any shock-structure modifications through the porosity-effects and the related shock associated noise will be manifested more strongly through the reduction of OASPL's at θ around 90°.

In the preliminary stage of these investigations some acoustic data and spark shadowgraphs of the corresponding jet flows of the contoured plug designed by the approximate method were recorded (see Appendix II) where the annulus-radius-ratio of both the solid conical plug and the solid/porous conical plug K = 0.41. Some of the acoustic results along with the optical records of the supersonic jet flows are reproduced in Appendix II (for further details, see Reference 29).

V. EXPERIMENTAL RESULTS AND DISCUSSION

All the plug-nozzle configurations used in these studies, as noted earlier, are a combination of a basic convergent round nozzle and short plug with pointed termination. For various plug-nozzle configurations, only the plug is changed and different plugs have either solid or a combination of solid/porous surfaces of different contours. For each of the plug-nozzles, the annular radius ratio K is the same. The angle of the converging wall ($\omega_e = 11.9^o$) of the basic convergent nozzle was selected such that at the design flow Mach number ($M_d \doteq 1.5$) of the contoured plug-nozzle, the free jet flow boundary is parallel to the nozzle axis. The plug-nozzle is operated as a convergent nozzle by removing the plug and its mounting assembly.

V.1 Noise Radiated by Underexpanded Jet Flow Issuing from Convergent Nozzle.

The acoustic data gathered with the convergent nozzle operated at various above-critical pressure ratios provide the baseline data for the evaluation of the noise-suppression effectiveness of the various 'equivalent' model plug-nozzle flows.

Acoustic radiation at discrete frequencies is often observed from underexpanded jet flows issuing from convergent nozzles. This is commonly attributed to a feedback mechanism [1]. To develop a prediction model for shock-associated noise of full scale engines based on acoustic data acquired from model nozzles, the characteristics of the broadband shock associated noise (without screech contamination) radiated by model jet flows should be known. Hence, the generation of such discrete tones from model underexpanded jet flows, need to be eliminated. This is often achieved by providing protuberances or roughness just inside the nozzle lip [9]. Such a physical modification of the nozzle lip is likely to alter the flow and the shock-structure of the underexpanded jet, thereby affecting the level of the shock-associated noise generation itself. In the present investigation, the elimination of the screech tones was achieved not by resorting to any physical modifications of the nozzle exit, but by making the convergent-nozzle wall at the lip extremely thin (only 0.05 cm). Furthermore, the fiberglass padding of the jet rig was extended and terminated at the nozzle exit plane into a cylindrical layer

of approximately 3/8 inch thickness.

For the operating pressure ratios and the exit-diameter of the convergent nozzle used in these studies, the fundamental screech frequency and its harmonics were calculated by using the relation proposed by Tam, Seiner and Yu [37]. These are marked by vertical arrows in Fig. 4 on a typical 1/3 octave SPL spectral records at $\theta = 90^{\circ}$ at pressure ratios $\xi = 4.0$ and $\xi = 4.5$ of the convergent nozzle jet. The spectral data do not reveal the presence of any very sharp spiked SPL peaks (the usual characteristic of screech tones) in the spectra at or around the calculated values of the fundamental screech frequency and its harmonics. Therefore, the recorded 1/3 octave SPL spectra of the noise radiated by the convergent nozzle jet flows at super-critical pressure ratios are considered to be screech-free and as such the recorded acoustic data are primarily a superposition of the turbulent mixing and the shock-associated noise components.

Peak Frequency Variations

The variation of peak frequency with observer angle θ, for the underexpanded jet flow from the model convergent nozzle, operated at $\xi \doteq 3.60$ is shown in Fig. 5. For clarity, the one-third octave SPL spectra at various angles are plotted on a sliding scale. The broad band but strongly humped spectra at higher angles shown in Fig. 5(a). are typical of the broadband shock-associated noise radiated by underexpanded jet flows from convergent round nozzles. At higher angles to the jet axis, where shock associated noise is dominant, the peak frequency decreases with the observer angle θ indicating a Doppler-shift type of phenomenon. Such characteristics of the spectra have been observed before by Harper-Bourne and Fisher [8] and Tanna [38].

For $\xi = 3.05$, 3.6 and 4.5, St. numbers vs θ are plotted in Fig. Fig. 6. For each ξ, the St. number is seen to vary broadly with peaks and plateaus between approximately 0.2 to 1.2 approaching 0.4 at higher θ's. At each $\theta < 45^{\circ}$, the St. number for different pressure ratios $\xi = 3.05$ to 4.5 and, thus, different repetitive shock structure, is nearly the same. The variations in the St. number at different above-critical pressure ratios are most pronounced for the intermediate angles $45 < \theta < 75^{\circ}$. The experimentally observed peak frequencies at different

θ's for the above-critical pressure ratios ξ = 2.0 to 4.5 are tabulated in Table 3 as Strouhal number $St = f_p D/V_j$ where V_j is the fully-expanded jet flow velocity and D is the exit diameter of the convergent nozzle.

Far-Field Noise Intensity

Since the shock-associated noise is dominant at higher angles to the jet axis, the acoustic intensity (or OASPL) at $\theta = 90^o$ is compared with the shock associated noise for choked convergent circular nozzle jet flows as predicted by Harper-Bourne and Fisher [8]. A plot of the OASPL's at $\theta = 90^o$ measured for the improperly-expanded jet flows from the model convergent nozzle of the present study versus $\log_{10} \beta$ where the parameter, $\beta = \sqrt{M_j^2 - 1}$, is presented in Fig. 17. In the intermediate range of the fully expanded flow Mach number $1.2 < M_j < 1.5$, the agreement between the experimental and the predicted OASPL's is excellent. For jet Mach number less than 1.2, the agreement is poor. This behavior has also been noted by Harper-Bourne and Fisher [8] and Tanna [38]. For flow Mach number $M_j >$ 1.6, the experimentally observed shock-associated intensity levels are lower than those predicted. This is attributed to the appearance of the Mach reflection in the axisymmetric underexpanded jet flows and the mixed supersonic and subsonic flow regimes which develop downstream of it. In the present studies, the appearance of Mach disk in underexpanded jet flows emanating from converging nozzle at $\xi \doteq 4.0$ ($M_j \doteq 1.6$) is quite evident in the spark shadowgraphs (see Figs. 12 and 13). The observed agreement between the experimentally observed and the analytically predicted acoustic intensity for $1.2 < M_j < 1.5$ confirms the reliability and the validity of the acoustic data recorded in the present study of the improperly- expanded jet flows.

Recently, the theoretical models for the predictions of shock-associated from improperly expanded jet flows by Harper-Bourne and Fisher (8), Tam and Tanna (19) and Seiner and Norum (30) have been incorporated by Stone (40) in an empirical relation for the prediction of OASPL's generated by supersonic jet flows issuing either from a circular convergent nozzle operated at super-critical pressure ratios or from a convergent-divergent nozzle operated at the off-design pressure ratios. To account for the absence of shock-associated noise from fully-expanded

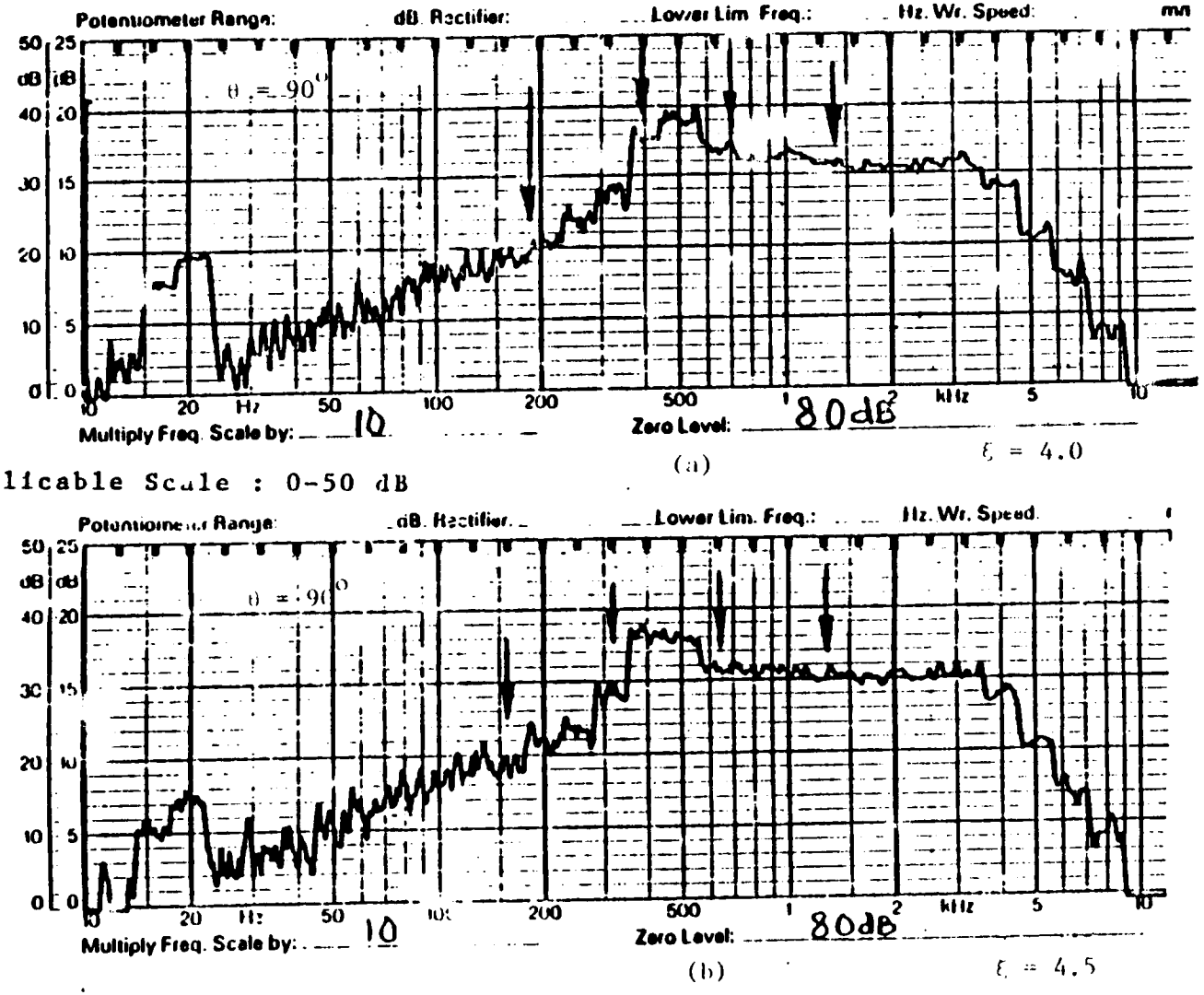

Fig. 4. Typical One-Third Octave Sound Pressure Level Spectra of Underexpanded Jet Flows from the Convergent Round Nozzle.

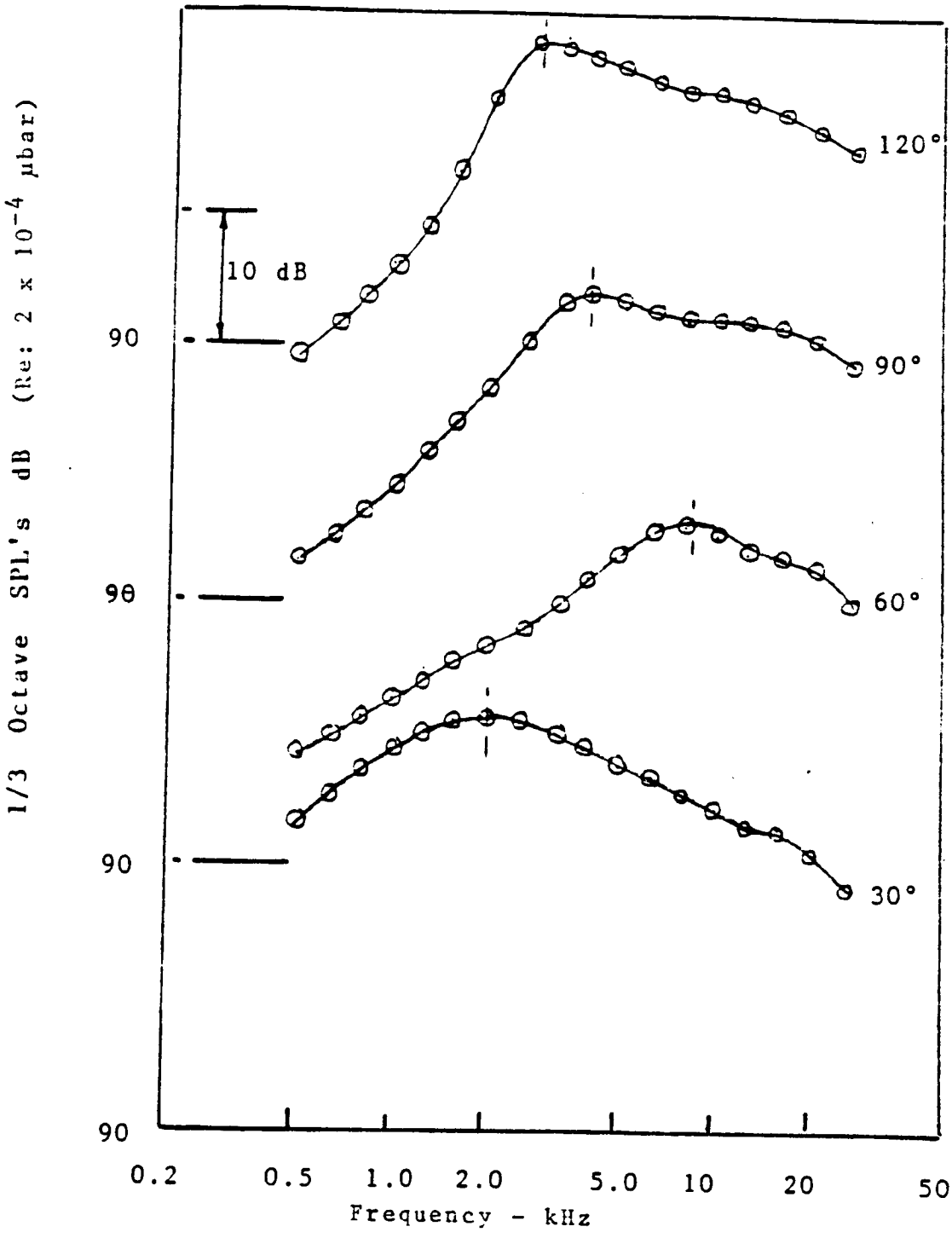

Fig. 5 Variation of Peak-Frequency with Azimuthal Angle for Convergent Nozzle Jet Flows at Pressure Ratio $\xi = 3.6$ ($M_j \doteq 1.49$).

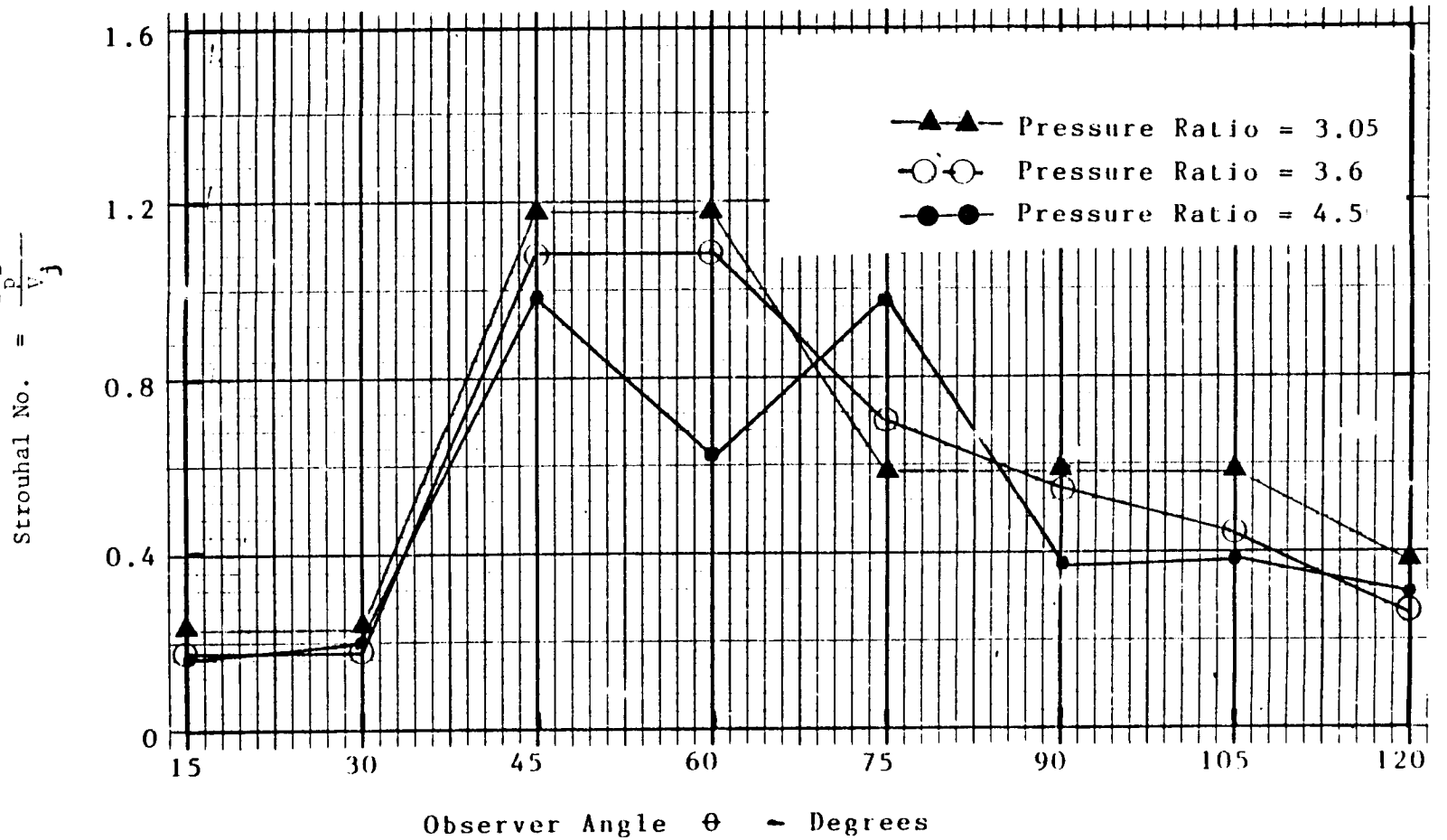

Fig.6 Variation of Strouhal Number with Azimuthal Angle for the Convergent Round Nozzle Jet Flows at Different Pressure Ratios.

Pressure Ratio	Azimuthal Angle θ							
	15°	30°	45°	60°	75°	90°	105°	120°
2.00	0.15	0.24	0.61	0.61	1.52	1.52	1.52	0.97
2.50	0.17	0.21	0.84	1.31	0.66	0.66	0.66	0.66
3.00	0.235	0.235	1.18	1.18	0.59	0.59	0.59	0.38
3.65	0.175	0.175	1.09	1.09	0.70	0.55	0.44	0.26
4.00	0.13	0.17	0.66	0.52	0.41	0.41	0.33	0.26
4.50	0.16	0.197	0.98	0.63	0.98	0.39	0.39	0.31

Table 3. Strouhal number ($St = \frac{f_p D}{V_j}$) variation with Azimuthal angles for Convergent Nozzle Jet Flows at Different Pressure Ratios.

C-D nozzle flows as well as the appearance of the Mach-Disk in improperly expanded jet flows and the related levelling off of the shock-noise at higher $\beta^2 = (M_j^2 - 1)$, the acoustic intensity level is taken to be proportional to $(M_j^2 - M_d^2)/(1+(M_j^2 - M_d^2))$, instead of β^4 used by Harper-Bourne and Fisher for underexpanded jet flows from convergent nozzles. For the convergent nozzle, the design Mach number $M_d = 1$ and the Stones relation takes the following form,

$$OASPL = 162 + 10 \log \{ (\frac{\rho_a}{\rho_{ISA}})^2 \cdot (\frac{a_a}{a_{ISA}})^4 \}$$

$$+ 10 \log [\frac{(M_j^2 - 1)^2}{1 + (M_j^2 - 1)^2}] + 10 \log (\frac{A_j}{R^2}) + F \cdot (\theta_m - \theta)$$

where θ_m is the Mach angle given by $\sin^{-1} (1/M_j)$. The function F, accounts for the directivity of the radiated noise and

$F = 0$, for $\theta > \theta_m$

$F = -0.75$, for $\theta < \theta_m$

In Fig. 7, the typical OASPL's at different θ's for the convergent nozzle operated at pressure ratio $\xi = 4.5$ ($M_j \doteq 1.65$), are compared with those predicted by Stone's relation. For pressure ratios $3.0 < \xi < 4.5$ (i.e. flow Mach numbers $1.3 < M_j < 1.7$), and at higher angles to the jet axis, there is good agreement between the experimental and the predicted OASPL's. For lower supercritical pressure ratios (flow Mach numbers $M_j < 1.2$), the agreement at higher angles is not as good. At lower angles to the jet axis, the predicted intensity by Stone's relation indicates a substantial departure from the experimental values. To account for the fact that at lower angles, the turbulent mixing noise component is dominant and, comparatively, the contributions of the shock-associated noise component are less significant, Stone introduced a correction term to what otherwise is a prediction scheme for shock-associated noise. No physical basis for this empirical term is advanced. According to the acoustic data gathered in the present study the Stone's relation does not seem to predict well the acoustic intensity of the underexpanded jet flows from convergent round nozzle at lower azimuthal angles ($\theta < 45^o$) to the jet axis.

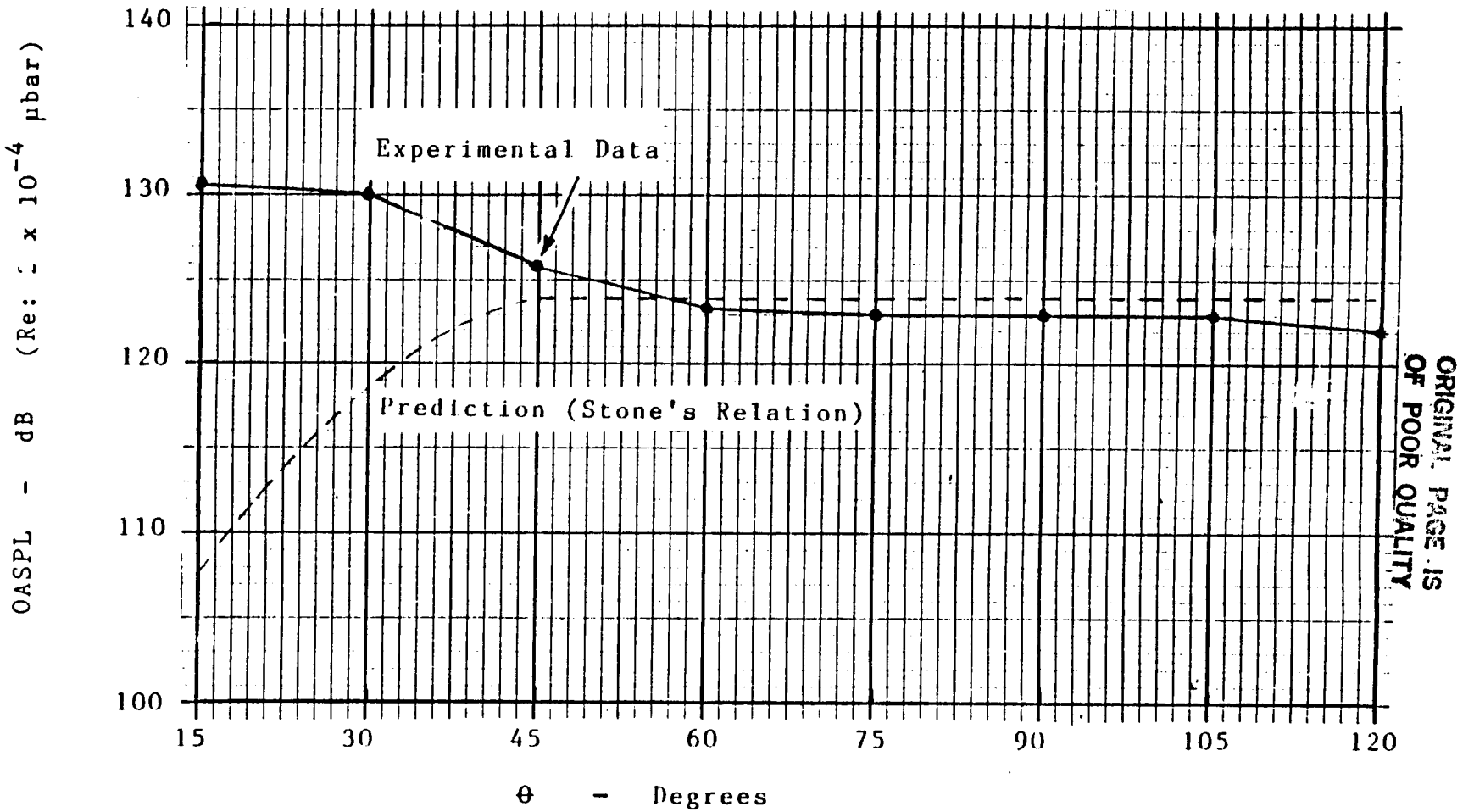

Fig. 7 Comparison of the Overall Sound Pressure Level Variations vs. Azimuthal Angle of Underexpanded Jet Flow from a Convergent Nozzle with those Predicted by Stone [40].

$\xi = 4.5$

V.2. AEROACOUSTIC PERFORMANCE OF A CONTOURED PLUG-NOZZLE OPERATED AT ITS DESIGN/OFF-DESIGN PRESSURE RATIOS.

V.2.1 Shockless Supersonic Jet Flows of Contoured Plug-Nozzle.

The spark shadowgraphs of the supersonic jet flows issuing from plug-nozzles of different geometrical specifications operated at operating pressure ratios ξ = 2.0, 2.5, 3.05, 3.6, 4.0, and 4.5 are presented in Figures 8 to 13 respectively.

The shadowgraph of the contoured plug-nozzle jet flow at pressure ratio $\xi \doteq 3.6$ (Fig. 8b) shows that the supersonic jet flow in the plug-region as well as farther downstream, is free from any repetitive shock structure. This pressure ratio $\xi \doteq 3.6$ ($M_j \doteq 1.49$) is quite close to the theoretical design pressure ratio $\xi_d = 3.67$ ($M_j = 1.50$) of the contoured plug. Moreover, the free jet flow boundary just downstream of the nozzle lip is straight and parallel to the axis of the plug-nozzle, indicating that the supersonic jet flow at $\xi = 3.6$ is fully-expanded. Also for $M_j \doteq 1.49$ (shockless flow condition), the area ratio A_e/A_t as measured from the shadowgraph of the fully expanded jet flow, agrees well with that calculated from Area-Mach number relation for an isentropic supersonic flow. Therefore, shockless (isentropic) supersonic jet flow issuing from a contoured externally-expanded plug-nozzle is achieved at pressure ratio $\xi \doteq 3.6$ ($M \doteq 1.49$). In such flows, the source and the mechanism for the generation of the shock-associated noise component is considered to be absent. Because of the very sharp pointed plug termination, in the spark shadowgraphs of the fully-expanded plug-nozzle flows there is hardly any visible wake. Also, in the shadowgraphs, the boundary layer over the smooth polished contoured plug surface is extremely thin. Therefore, the acoustic performance of such shockless and virtually wake-less plug nozzle supersonic jet flows provides the base-line noise data. These data are used for comparative assessment of the effectiveness of plug nozzles with short conical plugs of different configurations in the suppression of shock-related noise from improperly expanded jet flows.

The shadowgraphs of the contoured plug-nozzle operated at off-design ($\xi<\xi_d$) pressure ratios in the overexpanded mode (Figs. 9 to 11) show the presence of weak shock structures only in the plug region. The formation of the shock cells further downstream of the plug tip is not clearly

discernible.

Figures 12 and 13 show shadowgraphs of the contoured P-N underexpanded ($\xi > \xi_d$) jet flows. The shock structures in the underexpanded jet flows issuing from a contoured plug-nozzle are rather weak as the oblique shock angles of these conical shocks are nearly equal to the expected Mach angles calculated from the local flow Mach number achieved by isentropic flow expansion. Therefore, the corresponding repetitive oblique shock structure farther downstream is also expected to be weak. (For further discussion on the nature of such shock structure and its effects on the shock-associated noise, see Section V.2.5).

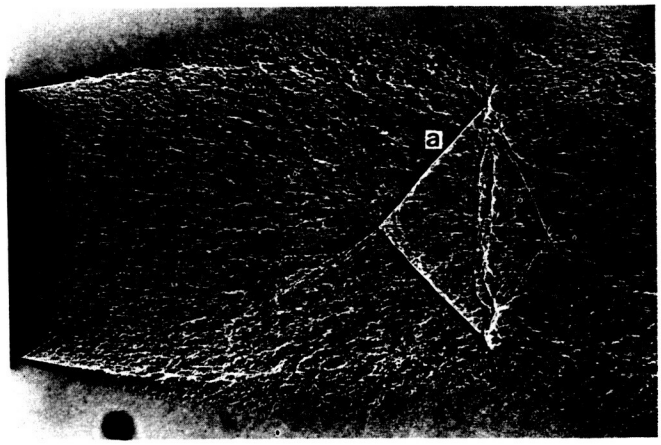

Convergent Nozzle

Solid Conical Plug-Nozzle

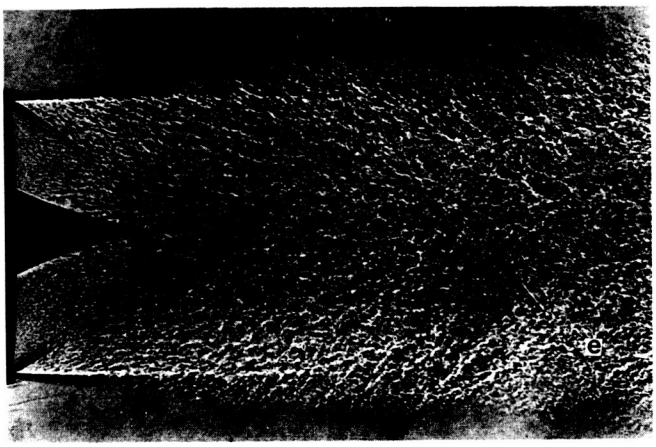

Contoured Plug-Nozzle

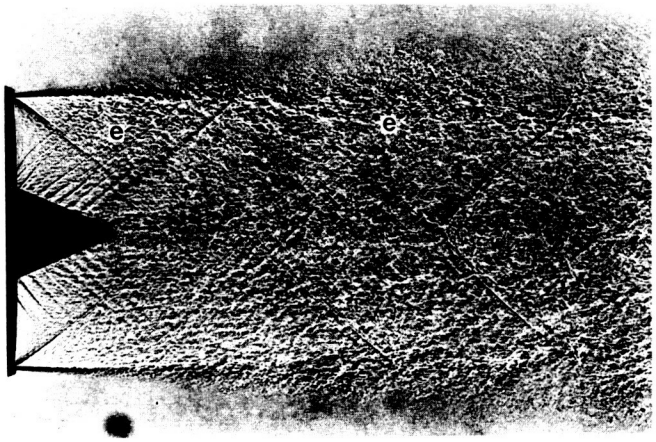

Porous Conical Plug-Nozzle (σ=10%)

Legend of Flow Features in shadowgraphs
(Figs. 8-13)

(a) Repetitive shock structure
(s_1) Shock related to reflections from plug surface
(c) Lambda shock at jet flow boundary
(s_2) Shock formed from the reflection of expansions unintercepted by the plug
(e) Compression wave front
(f) Mach Disc
(g) Slip surface

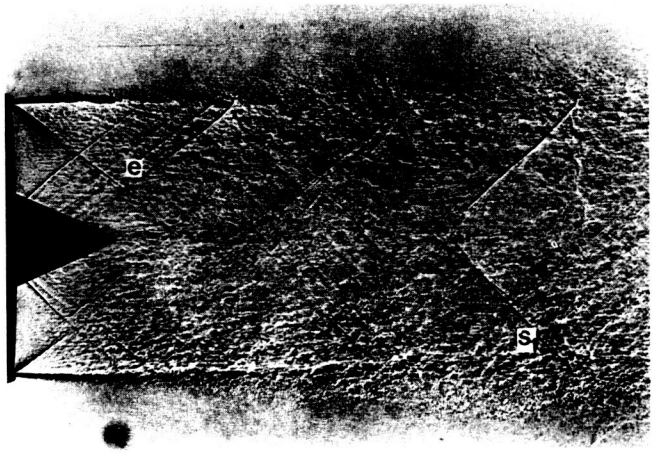

Porous Conical Plug-Nozzle (σ= 4%)

Fig. 8 Shadowgraphs of Convergent Nozzle and Different Plug-Nozzle Flows

(ξ=3.6 : shock-free condition for the contoured plug-nozzle)

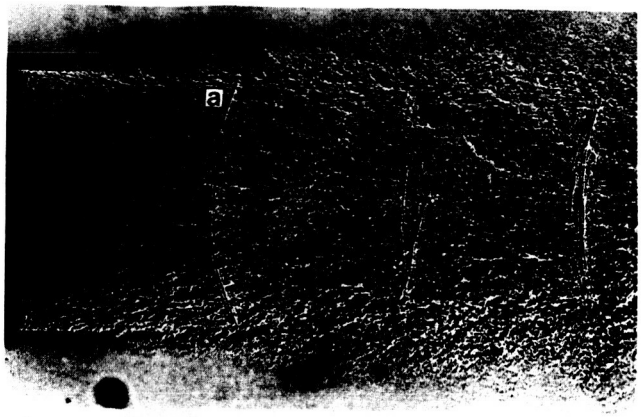

Convergent Nozzle

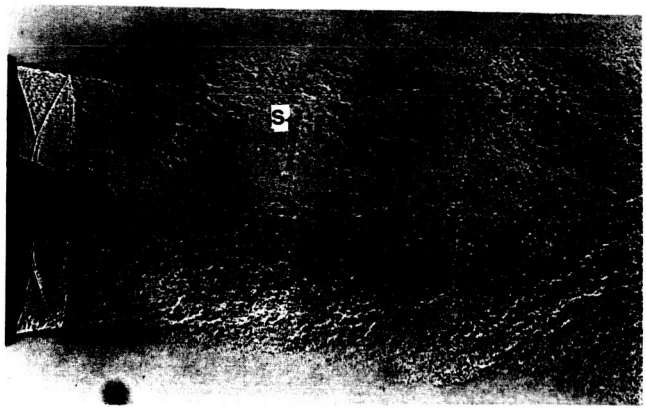

Solid Conical Plug-Nozzle

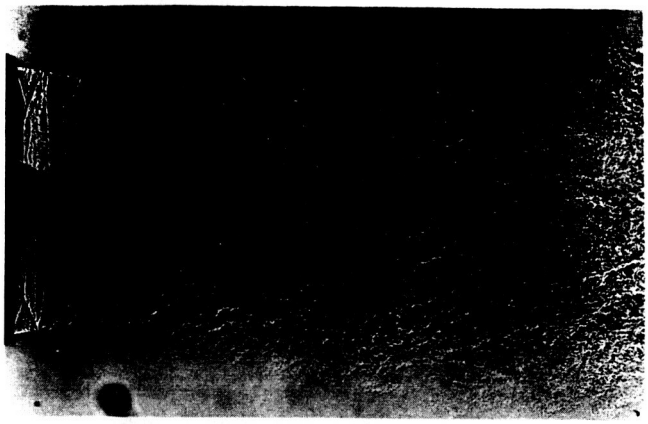

Contoured Plug-Nozzle

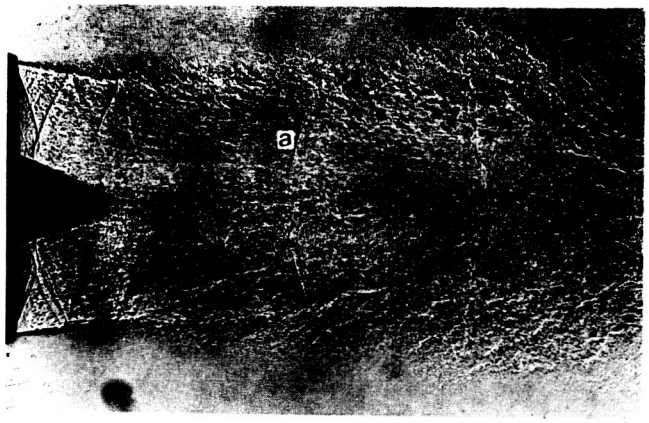

Porous Conical Plug-Nozzle (σ=10%)

Legend of Flow Features in shadowgraphs (Figs. 8-13)

(a) Repetitive shock structure
(s_1) Shock related to reflections from plug surface
(c) Lambda shock at jet flow boundary
(s_2) Shock formed from the reflection of expansions unintercepted by the plug
(e) Compression wave front
(f) Mach Disc
(g) Slip surface

Porous Conical Plug-Nozzle (σ= 4%)

Fig. 9 Shadowgraphs of Convergent Nozzle and Different Plug-Nozzle Flows (ξ=2.00)

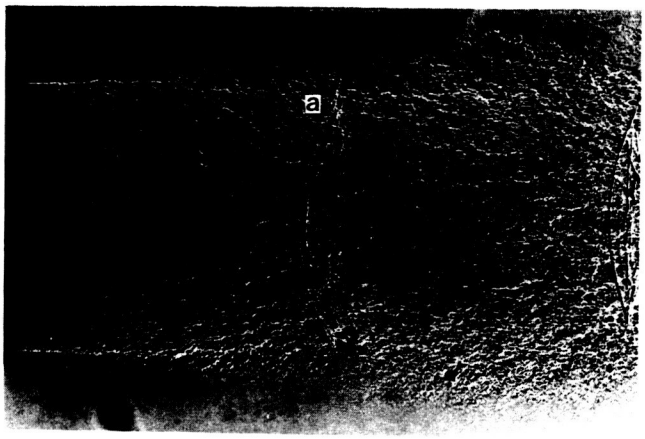

Convergent Nozzle

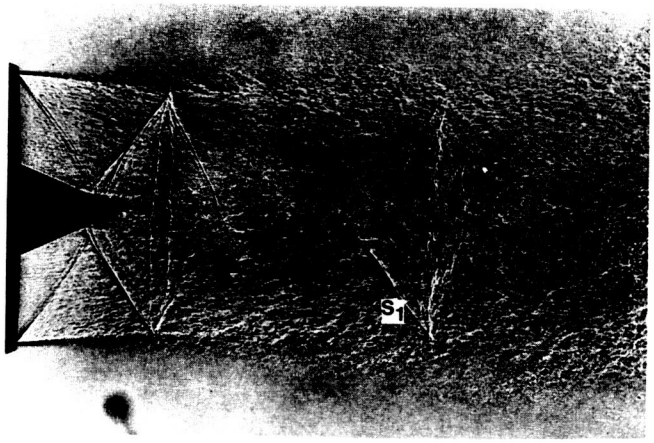

Solid Conical Plug-Nozzle

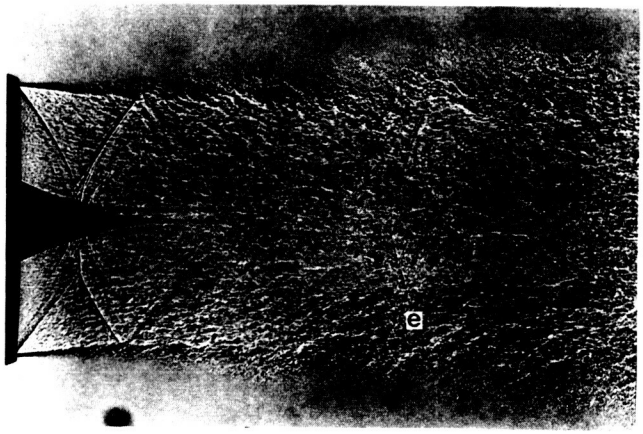

Contoured Plug-Nozzle

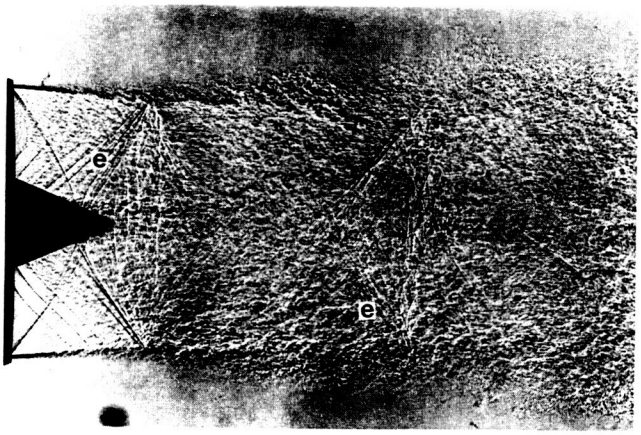

Porous Conical Plug-Nozzle (σ=10%)

Legend of Flow Features in shadowgraphs (Figs. 8-13)

(a) Repetitive shock structure
(s_1) Shock related to reflections from plug surface
(c) Lambda shock at jet flow boundary
(s_2) Shock formed from the reflection of expansions unintercepted by the plug
(e) Compression wave front
(f) Mach Disc
(g) Slip surface

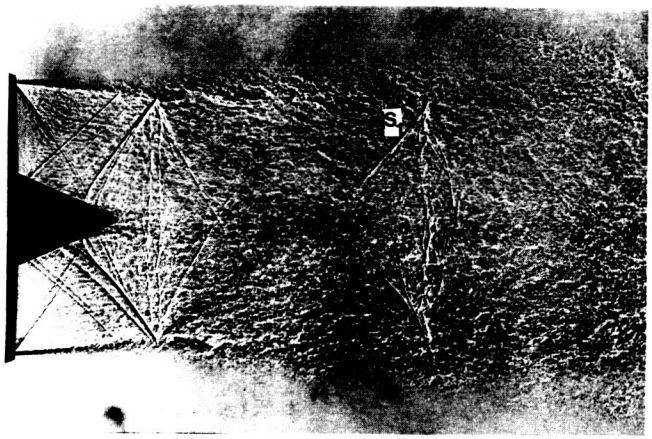

Porous Conical Plug-Nozzle (σ= 4%)

Fig. **10.** Shadowgraphs of Convergent Nozzle and Different Plug-Nozzle Flows (ξ=2.5)

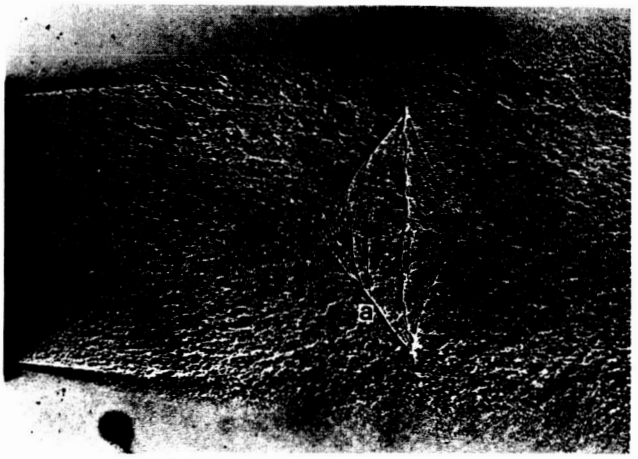

Convergent Nozzle

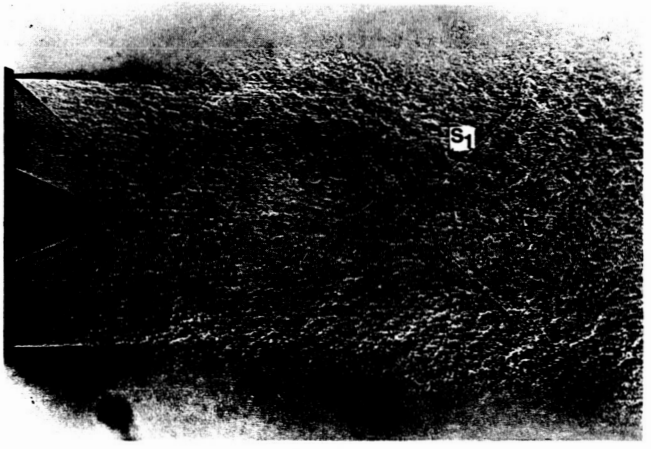

Solid Conical Plug-Nozzle

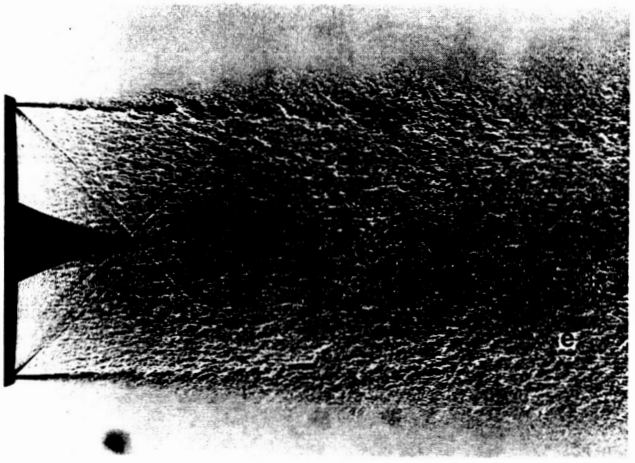

Contoured Plug-Nozzle

Porous Conical Plug-Nozzle (σ=10%)

Legend of Flow Features in shadowgraphs (Figs. 8-13)

(a) Repetitive shock structure
(s_1) Shock related to reflections from plug surface
(c) Lambda shock at jet flow boundary
(s_2) Shock formed from the reflection of expansions unintercepted by the plug
(e) Compression wave front
(f) Mach Disc
(g) Slip surface

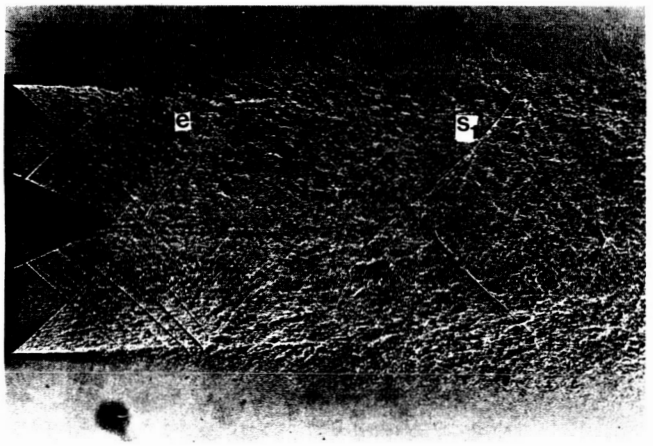

Porous Conical Plug-Nozzle (σ= 4%)

Fig. 11. Shadowgraphs of Convergent Nozzle and Different Plug-Nozzle Flows (ξ=3.05)

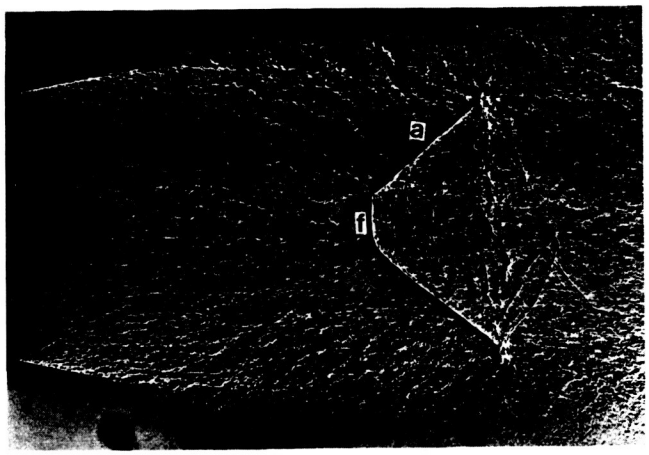

Convergent Nozzle

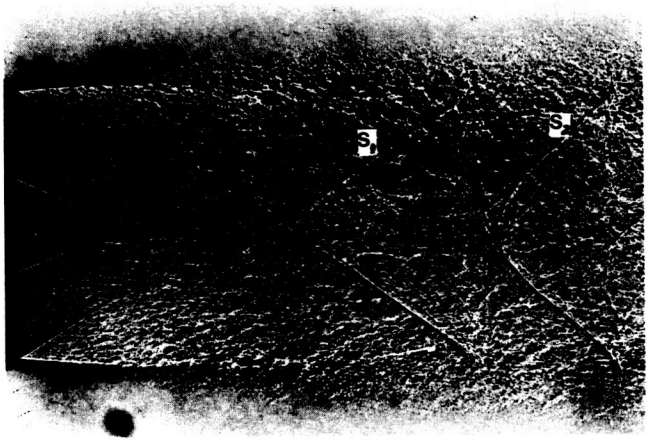

Solid Conical Plug-Nozzle

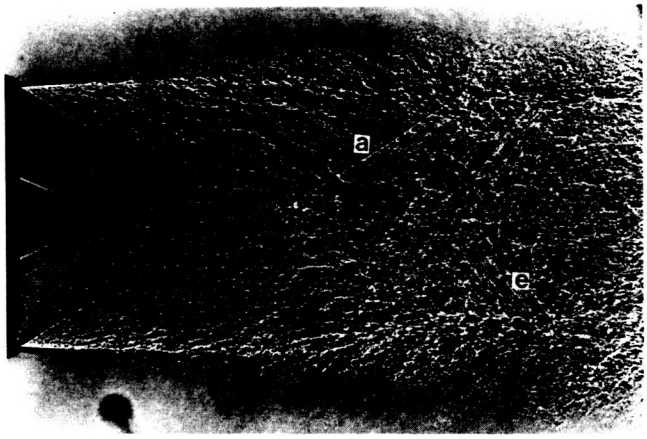

Contoured Plug-Nozzle

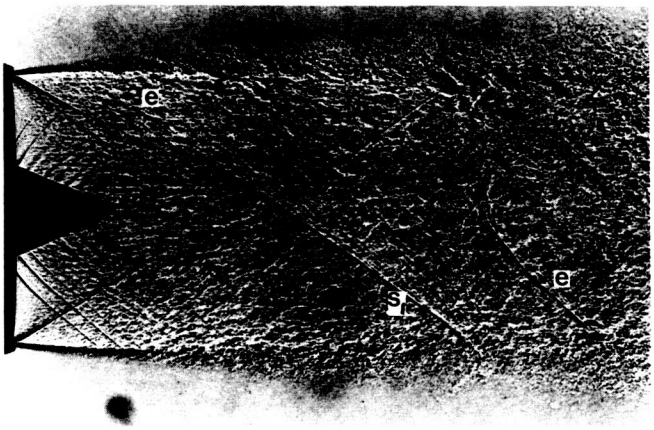

Porous Conical Plug-Nozzle (σ=10%)

Legend of Flow Features in shadowgraphs (Figs. 8-13)

(a) Repetitive shock structure
(s_1) Shock related to reflections from plug surface
(c) Lambda shock at jet flow boundary
(s_2) Shock formed from the reflection of expansions unintercepted by the plug
(e) Compression wave front
(f) Mach Disc
(g) Slip surface

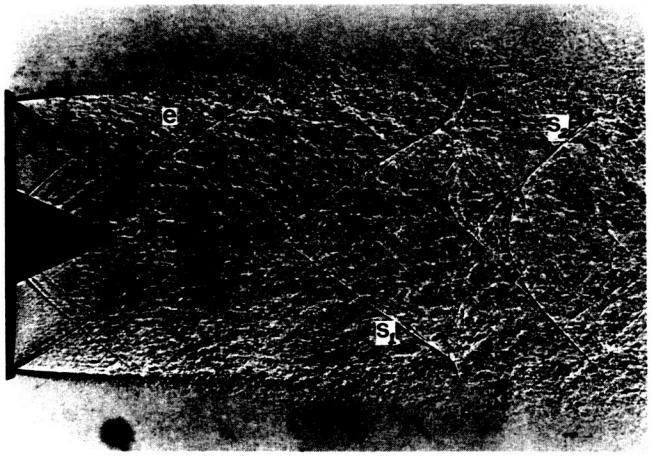

Porous Conical Plug-Nozzle (σ= 4%)

Fig.12. Shadowgraphs of Convergent Nozzle and Different Plug-Nozzle Flows (ξ=4.0)

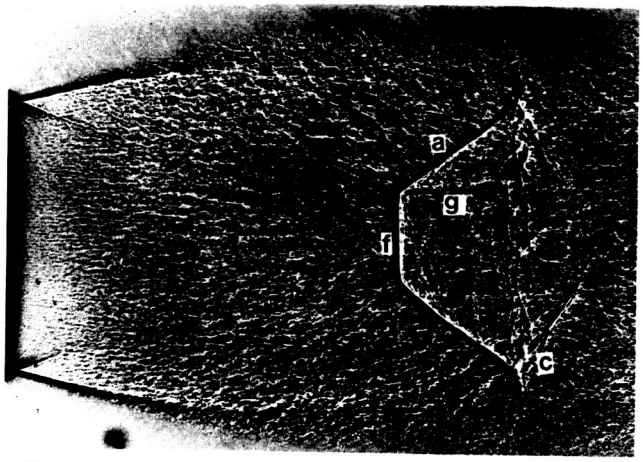

Convergent Nozzle

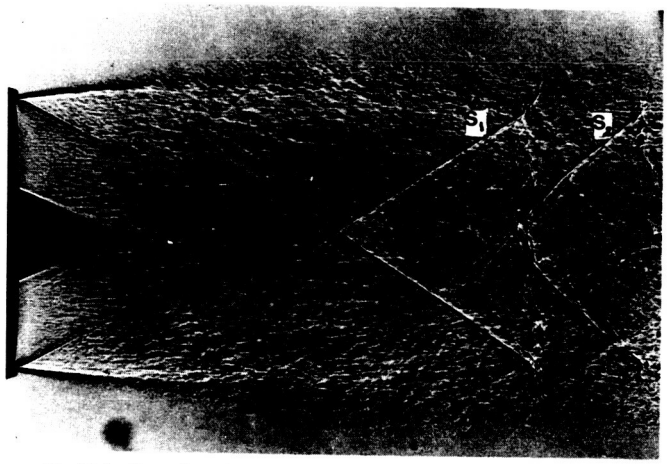

Solid Conical Plug-Nozzle

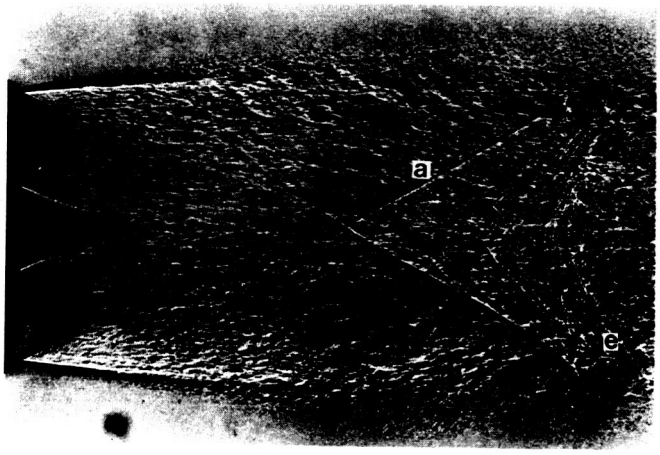

Contoured Plug-Nozzle

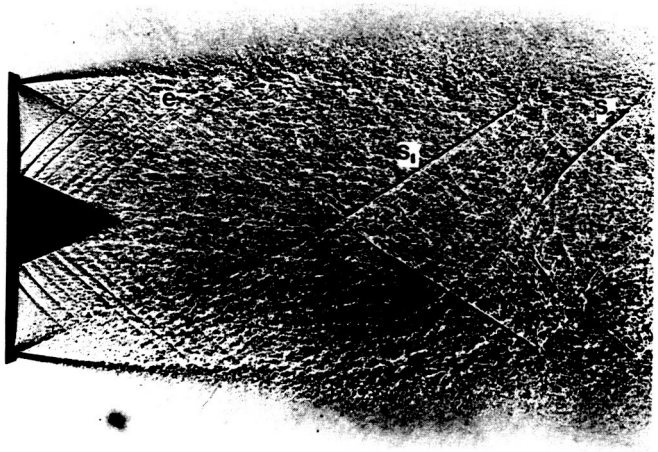

Porous Conical Plug-Nozzle (σ=10%)

Legend of Flow Features in shadowgraphs (Figs. 8-13)

(a) Repetitive shock structure
(s_1) Shock related to reflections from plug surface
(c) Lambda shock at jet flow boundary
(s_2) Shock formed from the reflection of expansions unintercepted by the plug
(e) Compression wave front
(f) Mach Disc
(g) Slip surface

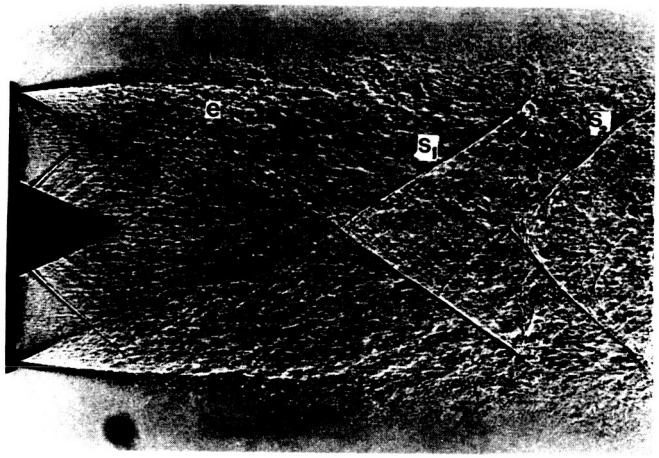

Porous Conical Plug-Nozzle (σ= 4%)

Fig. 13. Shadowgraphs of Convergent Nozzle and Different Plug-Nozzle Flows (ξ=4.5)

V.2.2 ACOUSTIC PERFORMANCE OF CONTOURED PLUG-NOZZLE JET FLOWS.

On the basis of a survey of the available literature, it was concluded that the acoustic performance of a truly shockless supersonic jet flow issuing from a plug-nozzle having a contoured plug with a pointed termination has not been studied before. The noise radiated by a shockless contoured plug nozzle jet flow is considered to be an ideal baseline data for assessing the shock-noise reduction from improperly expanded jet flows issuing from plug nozzles with either a solid or a combination of solid/porous conical plugs. Therefore, to make the comparative acoustic studies of plug nozzles of different contours and configurations possible, extensive acoustic spectral data were gathered for the externally-expanded contoured plug nozzle at its design as well as at a wide range of off-design pressure ratios. Moreover, the experimentally observed acoustic characteristics of such contoured plug-nozzle jet flows may prove to be helpful in future theoretical formulation of noise-generation mechanisms of exhaust flows from an important class of nozzles for propulsion. Furthermore, these noise data set a standard for optimization of the shock-associated noise suppression using plug-nozzles of practical geometries.

The 1/3 octave SPL spectra were recorded for supersonic jet flows issuing from an externally-expanded plug nozzle with a contoured plug having a pointed termination operated at pressure ratio $\xi = 3.60$ (shockless flow) as well as at the off-design pressure ratios ($\xi = 2.0$ to 4.5) at azimuthal angles $15° \leq \theta \leq 120°$. Both the corrected and the uncorrected acoustic data are tabulated in Appendices III and IV, respectively.

The dominant noise generating mechanism for fully-expanded (shock-less) jet flows at the design pressure ratio is due to turbulent mixing and it is only at the off-design conditions that a combination of shock-associated and turbulent mixing noise is present. For typical 1/3 octave SPL data recorded at $\theta = 90°$ for underexpanded contoured plug-nozzle at pressure ratios $\xi = 4.0$ and 4.5, see Fig. 14. In the test-range of pressure ratios and angular locations, there was no evidence of sudden sharp peaks in the one-third octave SPL spectral records, indicating the absence of screech tones.

The variations of peak frequencies with angular location θ at the pressure ratio $\xi \doteq 3.6$ for shockless flow and at the off-design pressure ratios $\xi = 3.05$ and 4.5 are shown, respectively, in Figs. 15a to c. For clarity, at each pressure ratio the one-third octave SPL spectra at different angles θ are plotted on a sliding scale. The corresponding Strouhal number St. vs θ where the annulus width w_t is taken as the characteristic length, are plotted in Fig. 16. The St. numbers for pressure ratio $\xi = 2.0$ to 4.5 at angular locations $15° < \theta < 120°$ are listed in Table 4.

For the contoured plug-nozzle operated at pressure ratio $\xi \doteq 3.6$ (shockless flow), the peak frequency (Fig. 15a) or the Strouhal number (Fig. 16) does not indicate any significant change at higher angles $75° < \theta < 120°$ with respect to the downstream flow axis. The peak frequency f_p at the higher angles is noted to be around 10 kHz; the St. numbers is 0.05 (at $\theta = 15°$) and 0.3 (at $\theta = 120°$) with peak St. number $\doteq 0.5$ at $\theta = 60°$.

The variation of peak frequency with θ for the contoured plug-nozzle at off-design pressure ratio $\xi = 4.5$ (underexpanded mode) and $\xi = 3.05$ (overexpanded mode) are nearly the same between $\theta = 15°$ to 120° except for a second peak at $\theta = 105°$ for $\xi = 3.05$ (Fig. 16).

For $\xi = 4.5$, the peak frequency or St. number decreases to a constant value $\doteq 0.2$ at θ between 75° to 120°. The peak St. number is 0.40 between $\theta = 45°$ to 60°.

The comparison of peak frequency or St. number variations with θ of an underexpanded convergent nozzle flow and the contoured plug-nozzle flows at the same pressure ratio shows that the ratio of the peak frequencies of the contoured P-N to that of the plugless convergent nozzle studied here is approximately 2, suggesting that most likely it is the effect of the characteristic length (annulus throat width w_t = 13.56mm) of the plug-nozzle of annulus-radius ratio K = 0.43 being smaller than the exit radius (22.5mm) of the convergent nozzle. For additional specifications of nozzles see Table 2 on p. 22 .

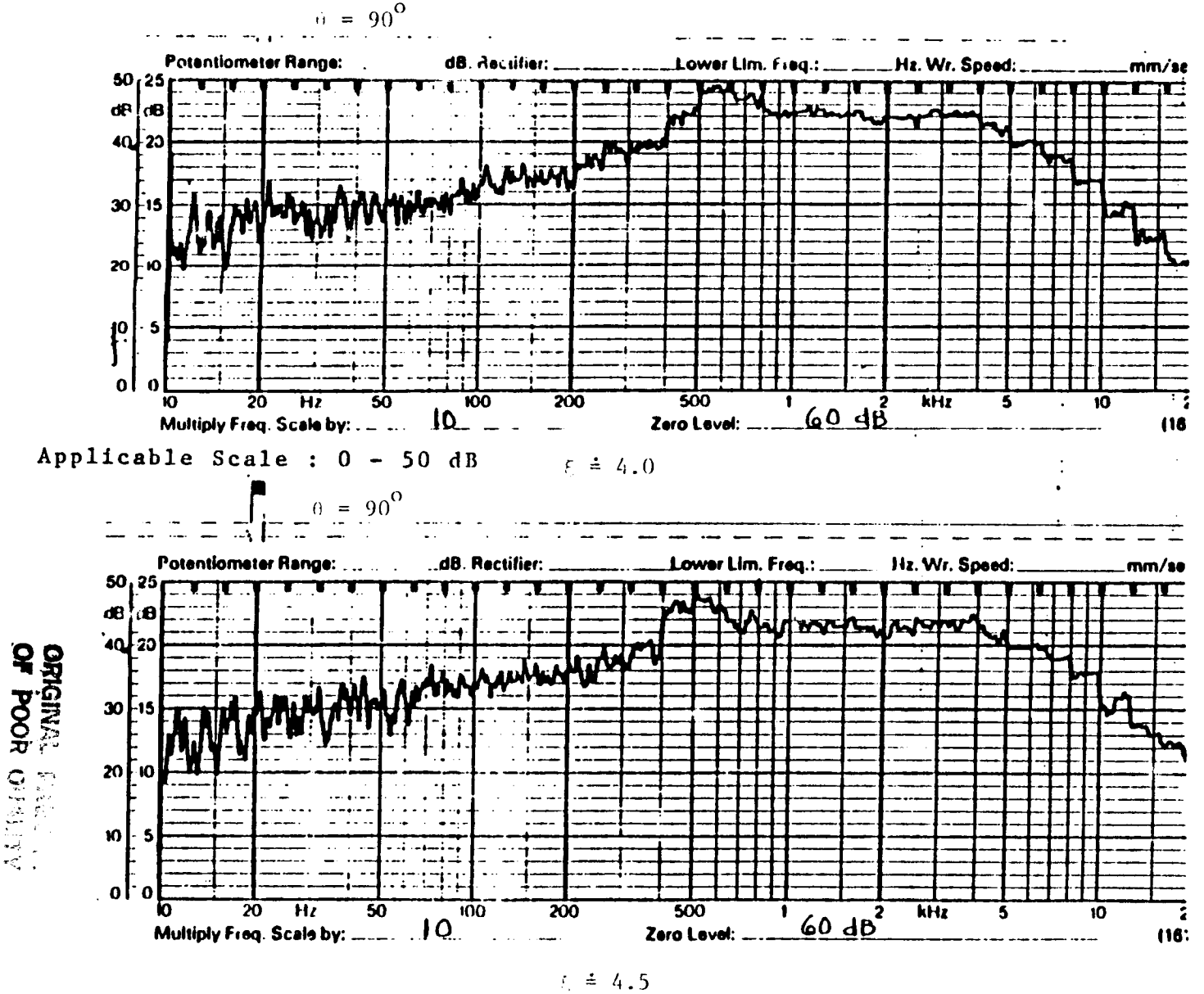

Fig. 14. Typical One-Third Octave Sound Pressure Level Spectra of Underexpanded Jet Flows from the Contoured Plug Nozzle.

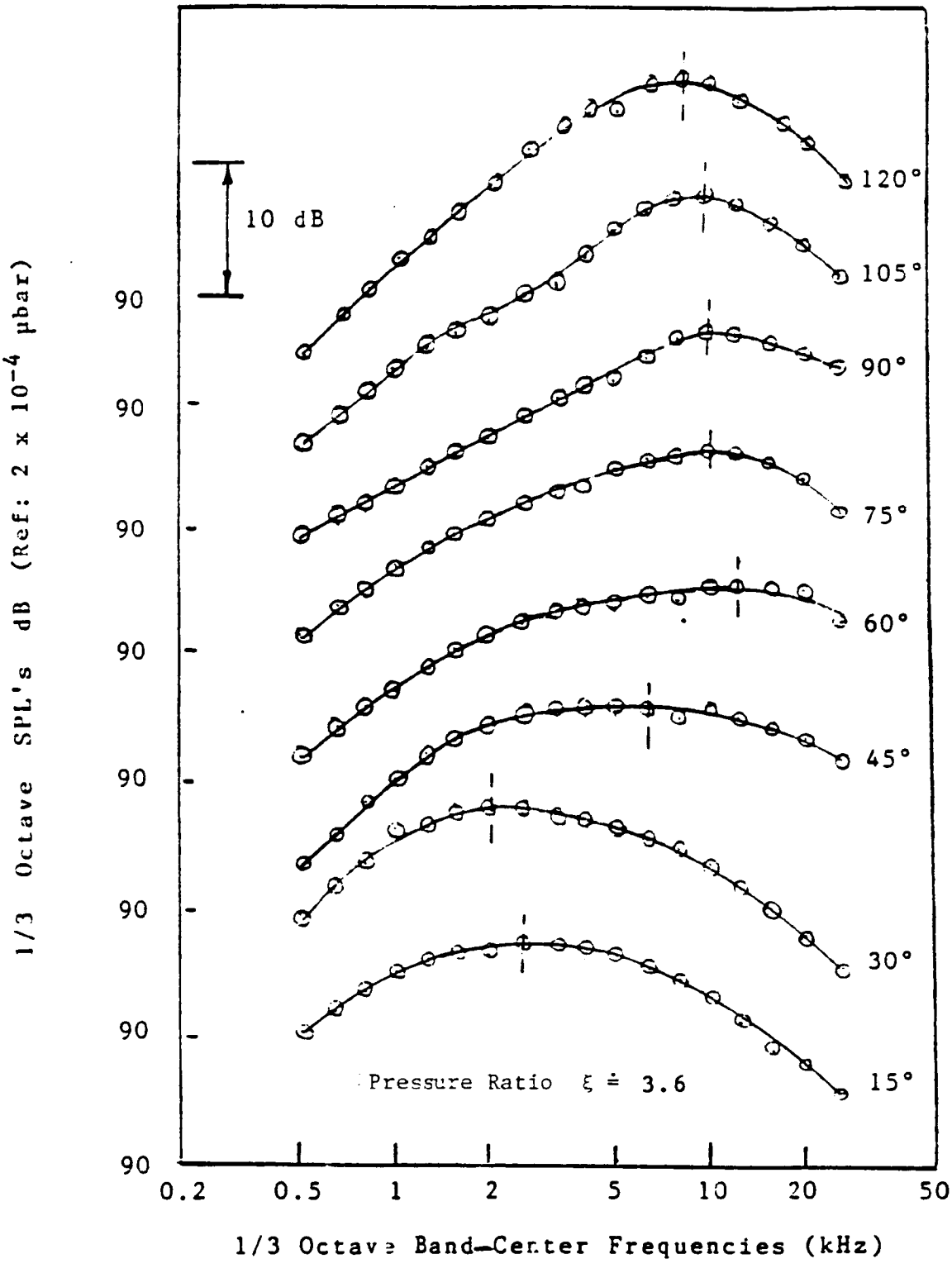

Fig. 15(a) .ariation of Peak Frequency with Azimuthal Angle of the Contoured Plug-Nozzle Jet Flow.

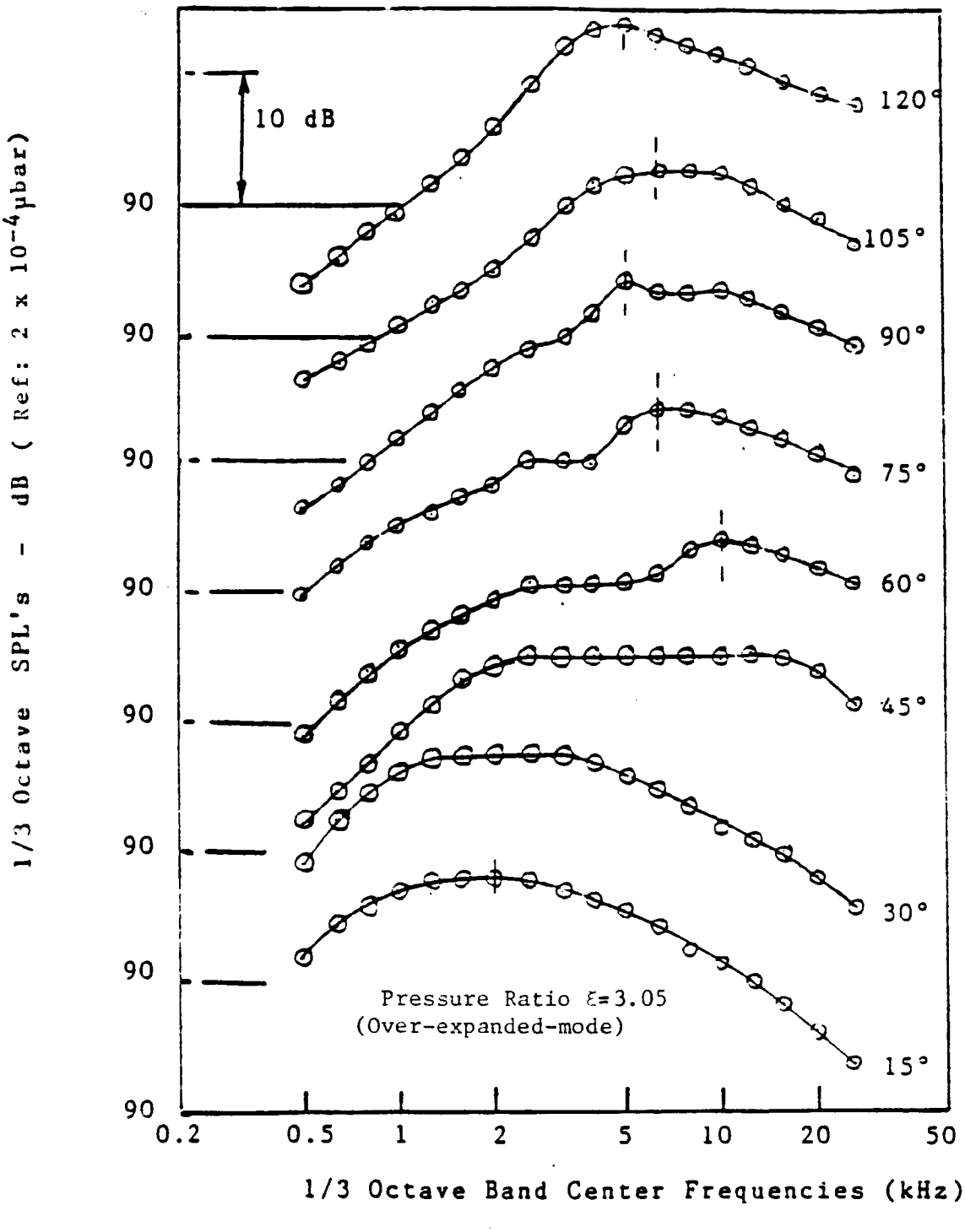

Fig. 15(b) Variation of Peak Frequency with Azimuthal Angle of the Contoured Plug-Nozzle Jet Flow.

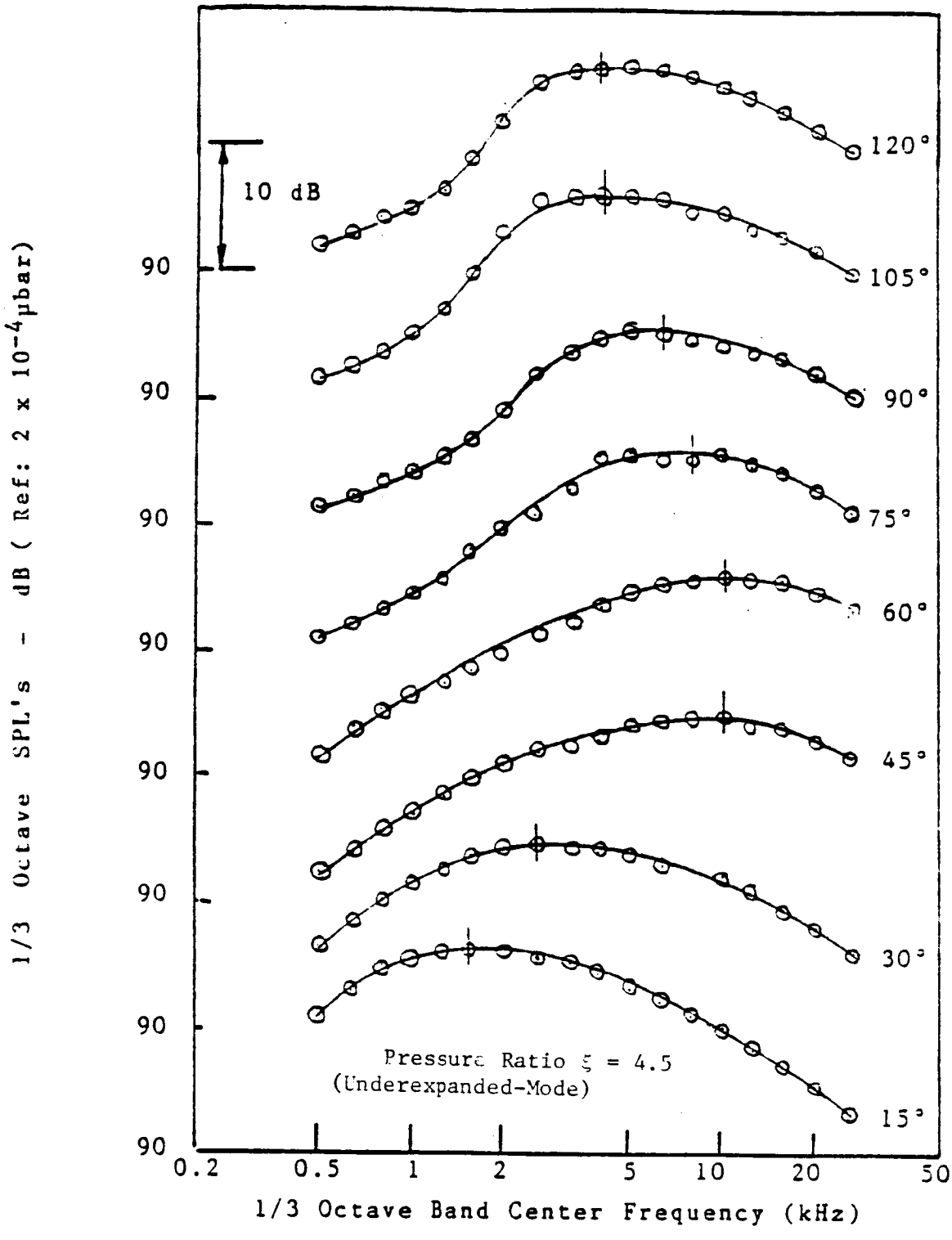

Fig. 15(c) Variation of Peak Frequency with Azimuthal Angle of the Contoured Plug-Nozzle Jet Flow.

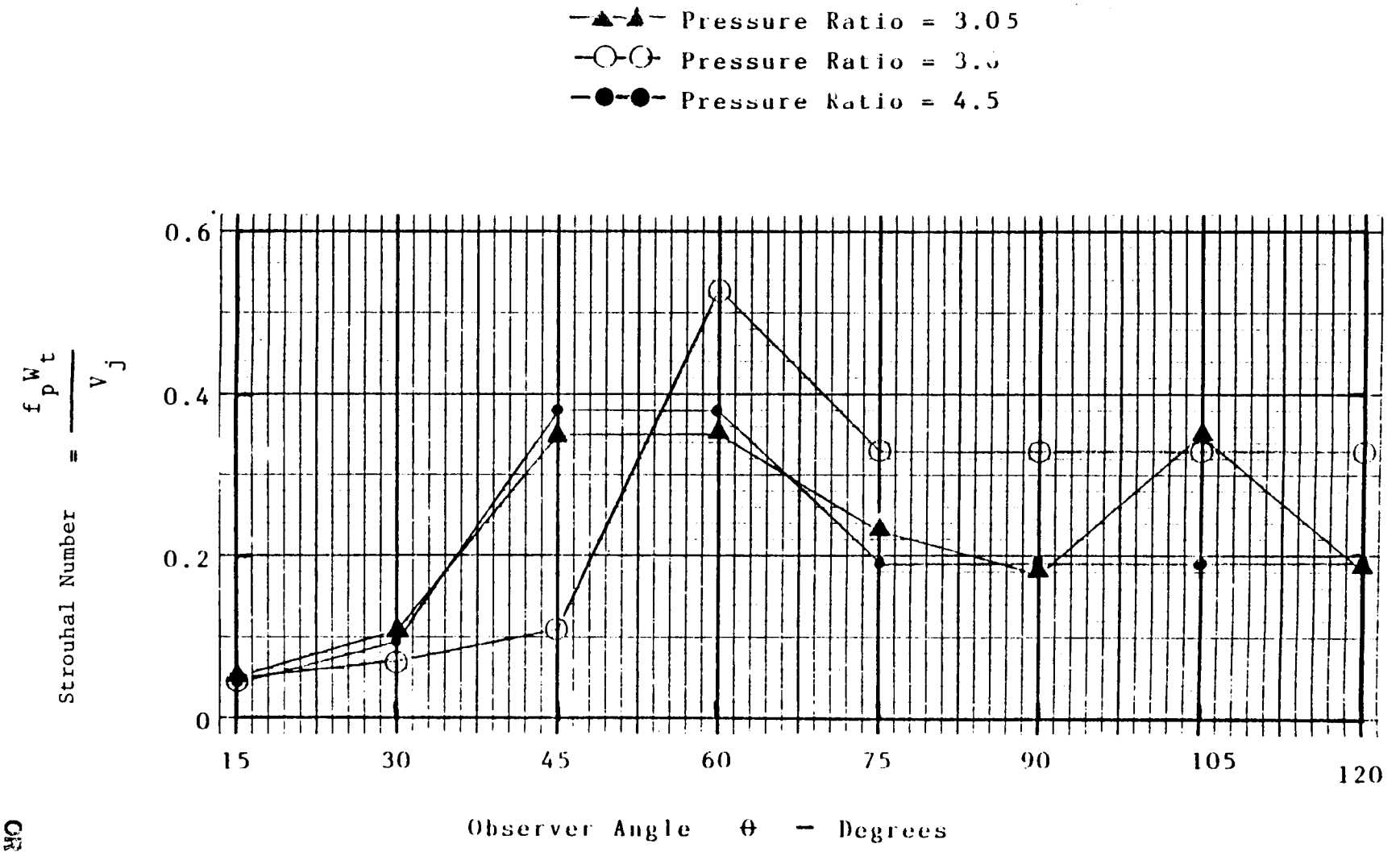

Fig. 16. Variations of Strouhal Number with Azimuthal Angle for the Contoured Plug-Nozzle Jet Flows at Different pressure ratios.

Pressure Ratio	Azimuthal Angle θ							
	15°	30°	45°	60°	75°	90°	105°	120°
2.00	0.059	0.092	0.18	0.59	0.46	0.37	0.37	0.37
2.50	0.063	0.063	0.13	0.50	0.25	0.40	0.20	0.20
3.00	0.057	0.11	0.35	0.35	0.23	0.18	0.35	0.18
3.65	0.053	0.066	0.11	0.53	0.33	0.33	0.33	0.33
4.00	0.062	0.062	0.31	0.25	0.16	0.16	0.16	0.12
4.5	0.047	0.095	0.38	0.38	0.19	0.19	0.19	0.19

Table 4. Strouhal Number ($St = \frac{f_p w_t}{V}$) Variation with Azimuthal Angle for the Contoured Nozzle Jet Flows at Different Pressure Ratios.

V.2.3 NOISE SUPPRESSION EFFECTIVENESS OF A CONTOURED PLUG-NOZZLE

To assess the effectiveness of a contoured plug-nozzle as a supersonic jet noise suppressor, its acoustic performance is compared with that of an 'equivalent' convergent nozzle. The convergent nozzle and the contoured plug-nozzle are operated at the same pressure ratio. Since the contoured plug-nozzle has annulus-radius-ratio $K = R_p/R_N$ $K = R_p/R_N = 0.43$, the ratio of the throat area A_e of the plugless convergent nozzle to the annular throat area A_p of the plug-nozzle ≈ 1.33. To obtain an 'equivalent' convergent nozzle, throat area of the convergent nozzle is scaled down to the annular throat area of the plug-nozzle. Therefore, the intensity levels or OASPL's of the plugless convergent nozzle data need to be reduced by $10 \log_{10} (A_e/A_p)$. For the present case this correction is only 0.68 dB. These 'equivalent' nozzle corrections have been applied to the comparative acoustic results presented in this report. For plug-nozzles with low values of annulus-radius-ratio K, the OASPL correction due to the scaling down of the throat area of the convergent nozzle for 'equivalence' with plug-nozzles is rather small. However, if the aeroacoustics of the plug-nozzles with higher annulus-radius-ratio $K = R_p/R_N$ (i.e. plug-nozzles designed for higher M_j's) were to be studied, the magnitude of this correction would be more noticeable.

The variations of OASPL at $\theta = 90°$ for the jet flows issuing from the contoured plug-nozzle and an equivalent convergent nozzle operated at a range of pressure ratios $\xi = 2.0$ to 4.5 ($M_j = 1.05$ to 1.67) is plotted as a function of the logarithmic shock strength parameter $\log_{10} \beta$ where $\beta = \sqrt{M_j^2 - 1}$ and M_j is the fully-expanded flow Mach number (Fig.17). Substantial noise reductions are obtained by the use of the contoured plug nozzle with a maximum reduction of about 10 dB around $M_j = 1.5$ (the shockless jet flow condition). The OASPL vs $\log_{10} \beta$ variation for the convergent nozzle flows follows the Harper-Bourne and Fisher β^4-scaling. For the contoured plug-nozzle operated in the overexpanded range of pressure ratios ($\xi < \xi_d$; $M_j < M_d$), OASPL varies as $\beta^{1.8}$; over the underexpanded range ($\xi > \xi_d$; $M_j > M_d$), it varies as $\beta^{2.7}$. The OASPL over the entire range of M_j's varies approximately as β^2. Therefore, the OASPL's for the contoured plug-nozzle increase comparatively less steeply than that for the convergent nozzle. Such

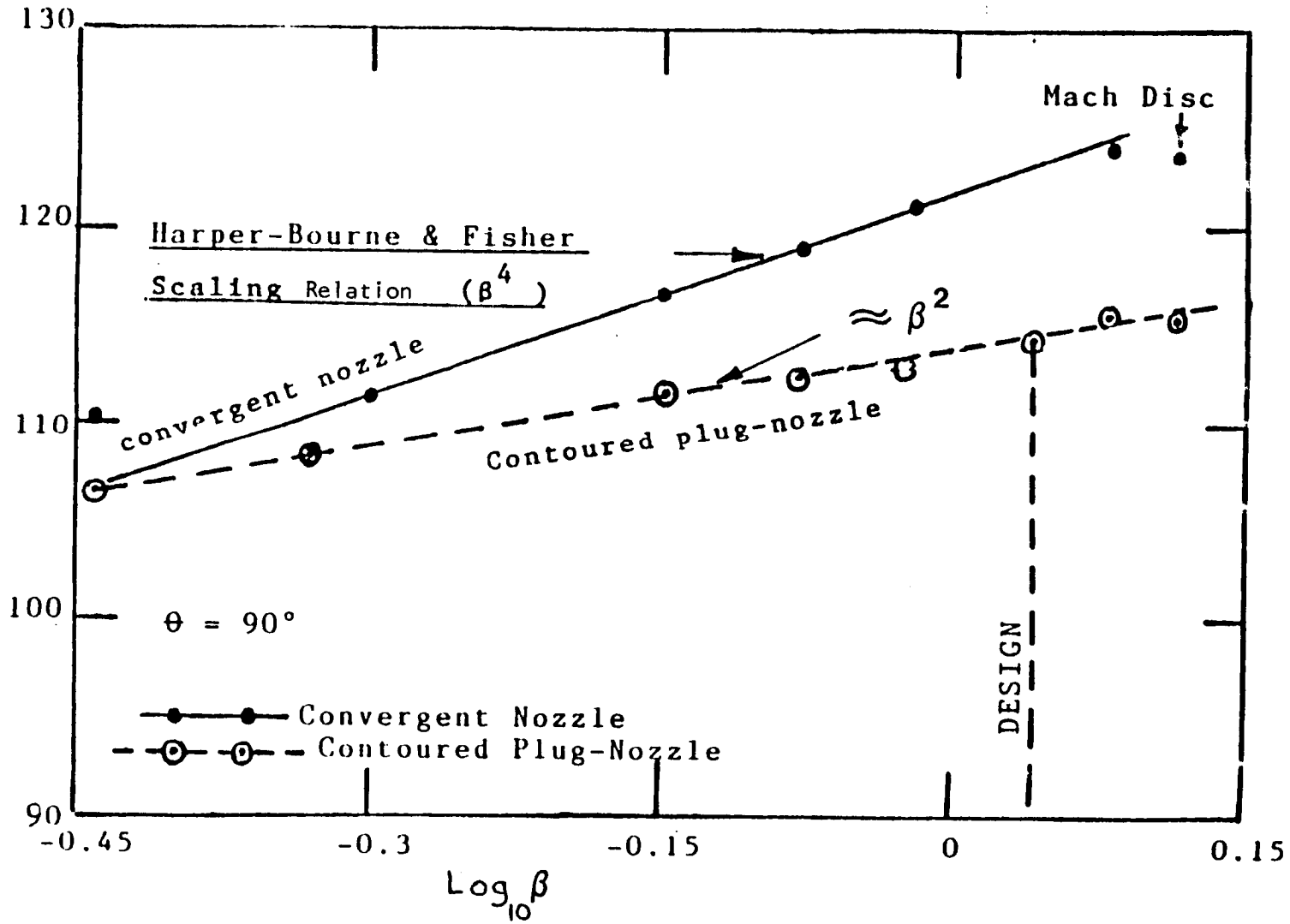

Fig. 17 Comparison of OASPL with logarithmic shock parameter from the contoured plug-nozzle and equivalent convergent nozzle flows.

$$\beta = (M_j^2 - 1)^{\frac{1}{2}}$$

comparative variations of OASPL vs $\log_{10} \beta$ for the contoured plug nozzle and the convergent nozzle jet flows show that when operated at the same pressure ratio the strength of the shock structure in the jet flows from the over- and underexpanded modes of operation of the contoured plug nozzle is weaker than in the underexpanded jet flows from an equivalent convergent nozzle. Consequently, the shock-associated noise component from the contoured plug-nozzle flows is also comparatively weak.

At higher angles to the jet axis, noise intensity vs M_j for a contoured C-D nozzle operated at a range of pressure ratios in the over-expanded modes through the fully-expanded to the underexpanded modes, shows a pronounced "bucket" (i.e. the OASPL rapidly falls to a minimum at the design Mach number and then rapidly rises for higher pressure ratios [19]. However, when OASPL vs. M_j is plotted for a contoured plug-nozzle, operated at a range of pressure ratios, this pronounced characteristic "bucket" variation in OASPL vs. M_j , observed for the C-D nozzle, is not noticeable for the contoured plug nozzle (Fig. 18(a)). The OASPL increases with the increasing M_j from over-, through fully-, to underexpanded mode of operation. Moreover, for $M_j \gg M_d$ and for $M_j \ll M_d$ the OASPL's from C-D nozzle jet noise intensities are observed to approach those of the equivalent convergent nozzle. However, for the contoured plug-nozzle jet flows, the noise intensities are considerably lower than those of the underexpanded jet flows from the equivalent convergent nozzle in almost the entire range of pressure ratios (or M_J's) from the highly overexpanded through to the highly underexpanded mode of operation (Fig. 18(a)).

The OASPL's at $\theta = 90°$ for the contoured plug nozzle operated over a range of pressure ratios (ξ = 2.0 to 4.5 or M_J = 1.05 to 1.67) were also plotted against the Tam and Tanna scaling parameter $(M_j^2 - M_j^2)$ for the intensity of the shock associated noise from a contoured C-D nozzle where the parameter $\beta_\star = \sqrt{M_j^2 - M_d^2}$. The OASPL varies as $\beta_\star^{2.5}$ in the overexpanded mode of operation of the contoured plug nozzle $\xi < 3.6$ (or $M_j < 1.49$), and in the underexpanded mode $M_j > 1.49$ as $\beta_\star^2$ variation for the shock-associated noise intensity for the C-D nozzle flows [19].

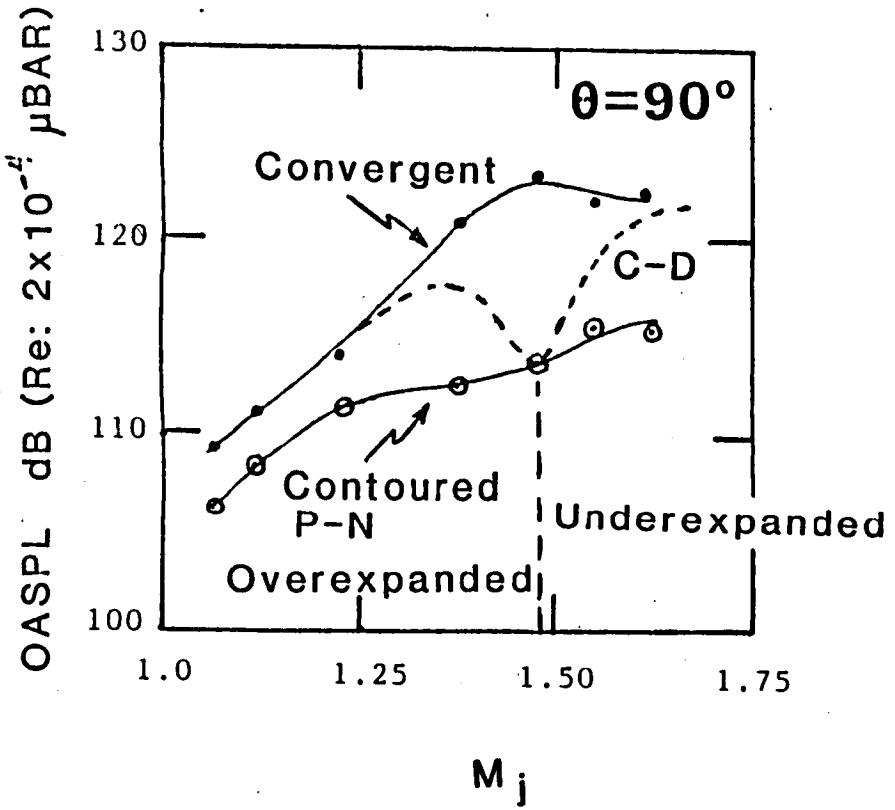

Fig. 18(a) Comparison of overall sound pressure levels of contoured plug-nozzle and equivalent convergent nozzle jet flows at different fully-expanded jet flow Mach Number

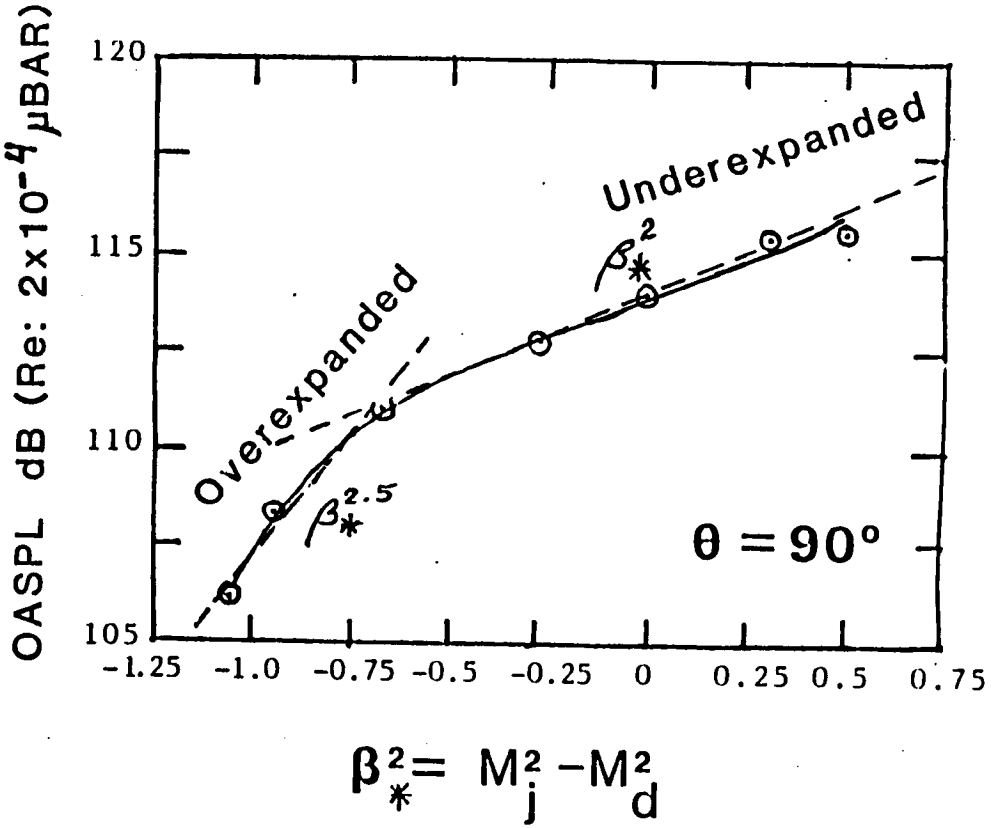

Fig. 18(b) Variation of overall sound pressure levels of contoured plug nozzle operated in the overexpanded and underexpanded modes at different $\beta_*^2 = M_j^2 - M_d^2$

The observed differences in the variation of the combined intensity of the components of the mixing noise and shock-associated noise from a contoured C-D nozzle and a contoured plug-nozzle as a function of the fully- expanded flow Mach number (or the pressure ratio ξ), may be explained with reference to the differences in the development of the shock structure in an off-design overexpanded mode of operation of the contoured plug nozzle and the contoured C-D nozzle. When the above critical pressure ratios for the contoured C-D nozzle are low, such that a normal shock front is present at the nozzle exit, the OASPL are relatively high approaching those of an underexpanded flow from an equivalent convergent nozzle operated at the same pressure ratio. As the pressure ratio is increased (still attaining the design flow Mach number at the C-D nozzle exit), the exit pressure is still lower than the ambient pressure but the difference in the exit flow pressure and the back pressure decreases, requiring the formation of an oblique shock structure in the jet flow to meet the pressure condition at the free jet flow boundary. The strength of the oblique shock progressively decreases as the pressure ratio is increased. The shock structure disappears at the design pressure ratio. This results in the observed minimum in the OASPL vs. M_j plot (Fig. 18(a)). When the pressure ratio or the fully-expanded jet flow Mach number is further increased, the oblique shock structure of a progressively increasing strength reappears in the underexpanded jet flow and the OASPL increases [19]. However, in the over-expanded mode of the C-D nozzle, to raise the exit flow pressure to the back pressure, the oblique shock fronts at the nozzle lip are formed abruptly. But for the off-design pressure ratio of the overexpanded contoured plug ($M_j < M_d$), the jet flow expands through the centered expansion fan at the lip of the convergent nozzle. The expansion fan incident on the contoured plug surface is cancelled. The oblique shocks may be formed by the coalescence of the compression wave fronts originating from only part of the plug surface where the local flow Mach number is lower than the design Mach number. Moreover, the coalescence of the compression fronts into possible oblique shocks is spatially spread out (Fig. 32(a)). This process of oblique shock formation results in comparatively weak oblique shocks. Therefore, the shock-related component of the OASPL from the overexpanded mode of operation of the contoured plug-nozzle does not vary as steeply

with M_j (or the pressure ratio) as it does for jet flows from an overexpanded contoured C-D nozzle.

The OASPL vs θ variations for the contoured P-N at the pressure ratio at which shockless flow is achieved ($\xi \doteq 3.6$) and for the 'equivalent' convergent nozzle operated at the same pressure ratio are compared in Fig. 19.

The difference between the OASPL's of the contoured plug-nozzle and the equivalent convergent nozzle operated at $\xi = 3.6$ at various θ's are plotted in Fig. 20. The use of a contoured P-N of design Mach number 1.5 results in significant noise reductions in OASPL (of the order of 8 dB) when compared with those of an 'equivalent' convergent nozzle. The noise suppression is noted both at the lower angles to the jet axis where turbulent mixing noise predominates as well as at the higher angles to the jet axis, where the shock-associated noise is dominant. Tam and Tanna [19] have reported a reduction of up to 9 dB in the OASPL at $\theta = 90°$ for a C-D nozzle of design Mach number = 1.67 as compared to that of an 'equivalent' convergent nozzle (Fig. 20). For a C-D nozzle of design Mach number of 1.44 Yamamoto et al. [41] showed at higher angles a noise suppression of about 5 dB over their 'equivalent' convergent nozzle. In these experiments by Yamamoto, the comparatively lower levels of reductions in OASPL's may be due either to the lower design Mach number of the C-D nozzle ($M_d = 1.44$) and/or the jet flow may not have been entirely free of the shock structure.

The variations of OASPL's either at $\theta = 90°$ or at $\theta = 120°$ at a range of pressure ratios ξ of the contoured P-N and the equivalent convergent nozzle are very similar (Fig.21). Therefore, any deductions about the shock-associated noise based on the acoustic data recorded either at $\theta = 90°$ or $\theta = 120°$ are equally viable.

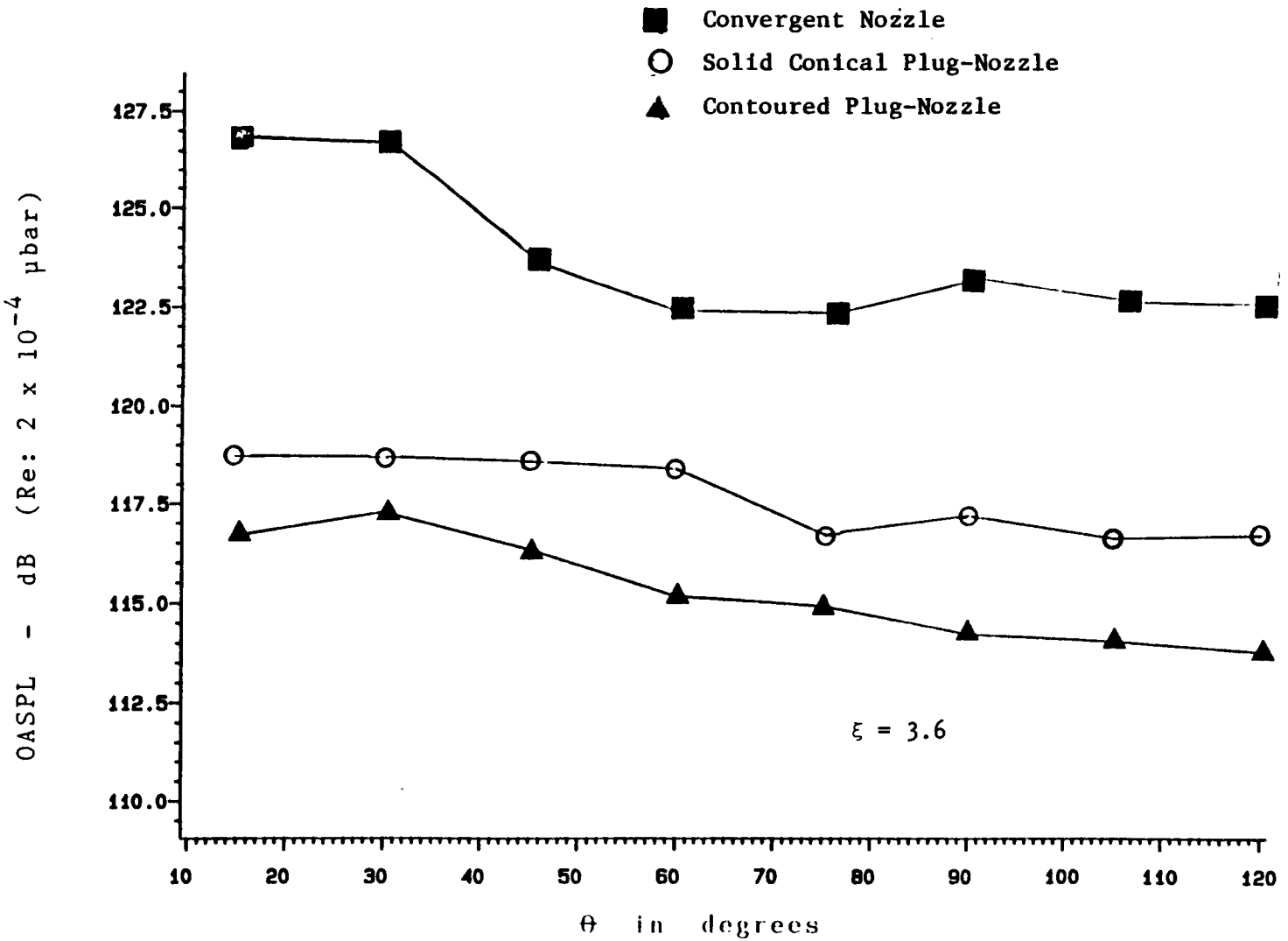

Fig. 19 Comparison of Overall Sound Pressure Level Variations with the Azimuthal Angle of Convergent Round Nozzle and Contoured and Conical Plug-Nozzle Jet Flows.

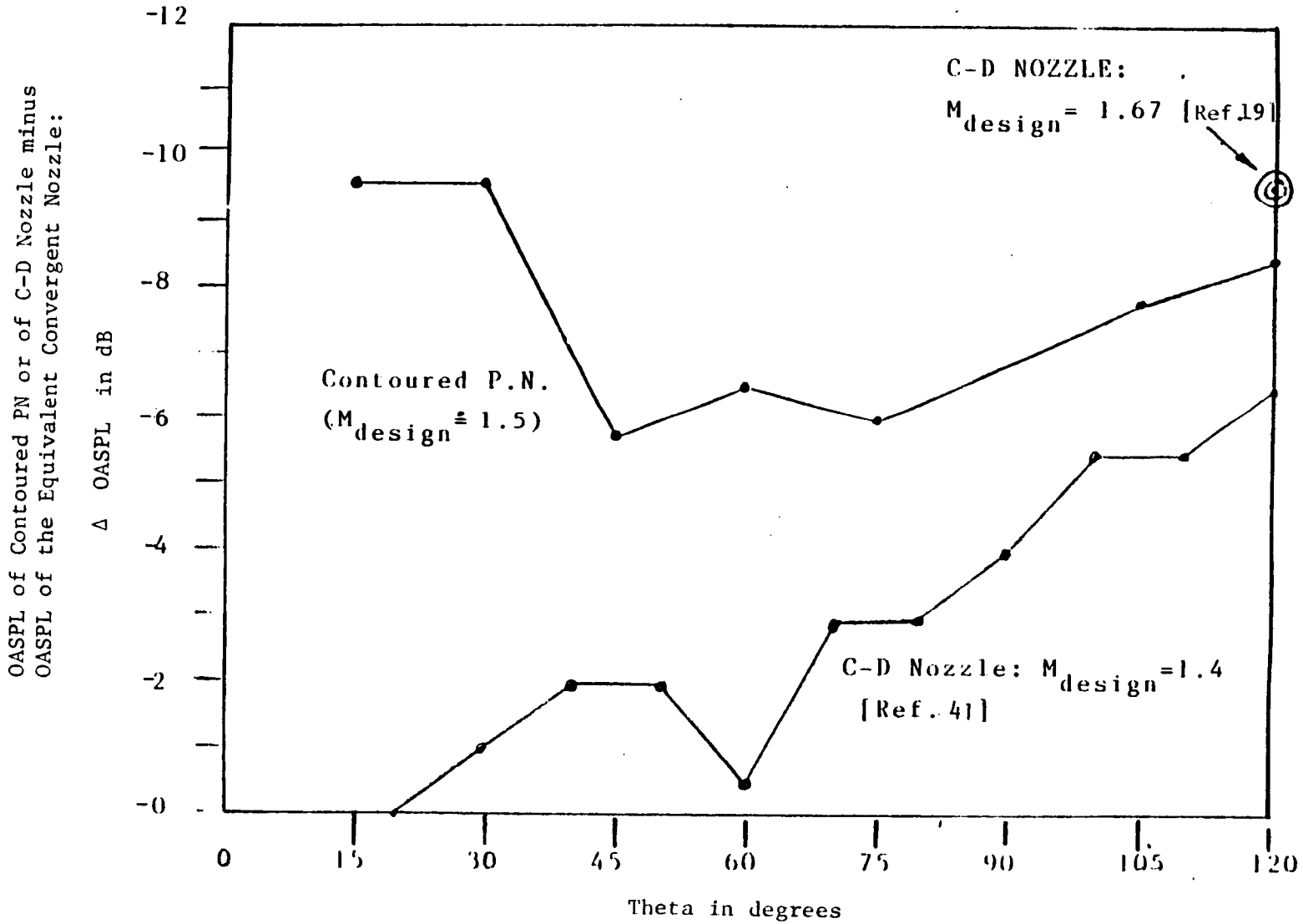

Fig. 20 Noise Suppression Effectiveness of Contoured Plug-Nozzle and Convergent-Divergent Nozzle Jet Flows at Design Pressure Ratios as Compared with that of an Underexpanded Equivalent Convergent Round Nozzle Jet Flow.

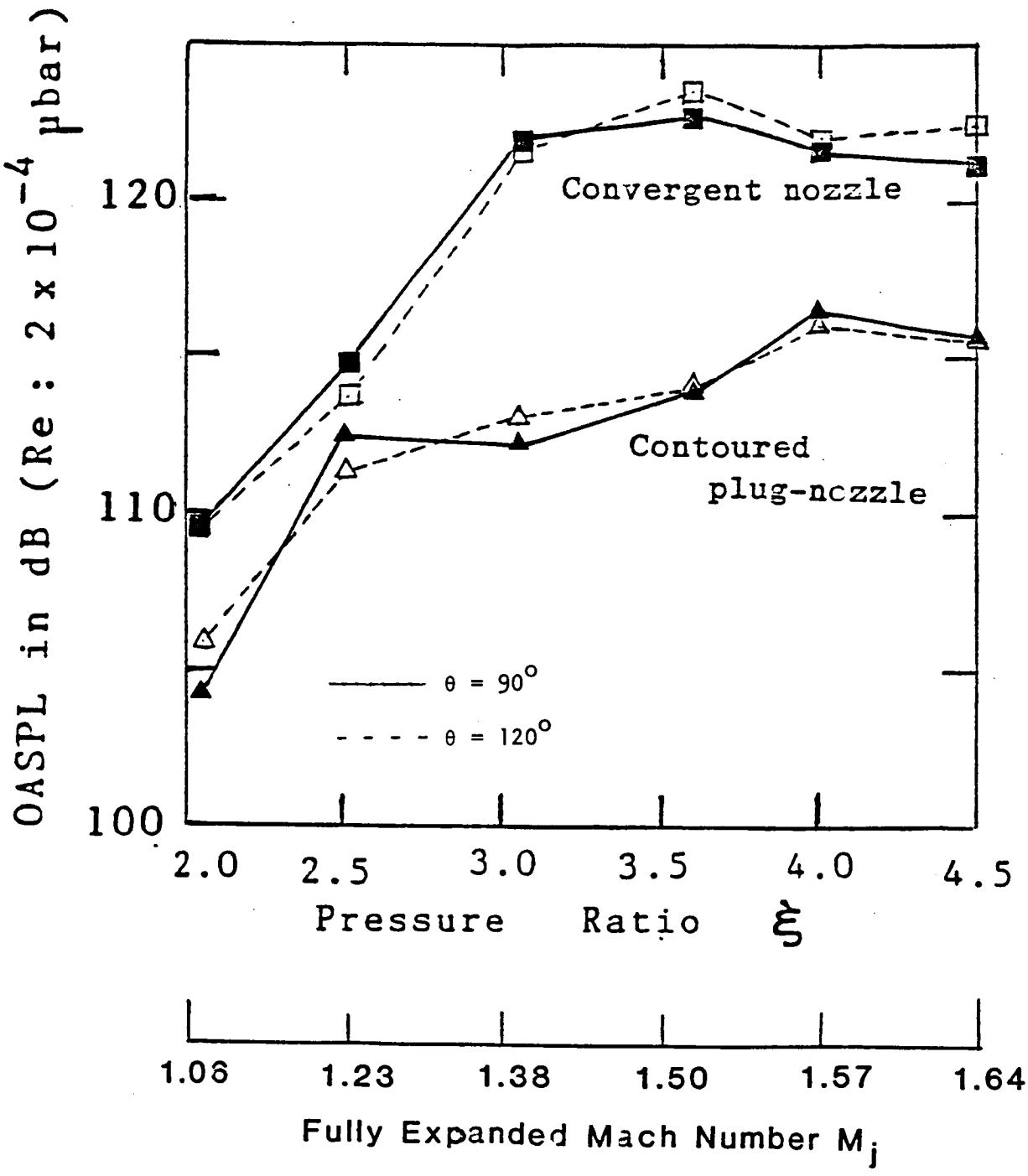

Fig. 21 Overall sound pressure variation with pressure ratio of equivalent convergent and contoured plug-nozzle jet flows.

V.2.4 ADDITIONAL COMPARATIVE ACOUSTIC RESULTS

The one-third octave SPL's of the contoured plug-nozzle for the shockless flow condition, i.e., at pressure ratio $\xi \doteq 3.60$ recorded at $\theta = 90°$ are compared with the corresponding SPL's of the convergent nozzle (Fig. 22). The hump in the SPL spectra around 15 kHz for the contoured P-N is noted to be comparatively broader and lower than that for the convergent nozzle; the acoustic spectra of the convergent nozzle exhibits relatively a sharp hump around 7 kHz. The SPL's in the entire range of 1/3 octave band-center frequencies of the contoured P-N are significantly lower than those of the model convergent nozzle. The contoured plug-nozzle jet flow at $\xi \doteq 3.6$ is shockless (Fig. 8). Therefore the observed reductions in SPL's at $\theta = 90°$ as compared to those from the underexpanded jet flow from a convergent nozzle also operated at $\xi = 3.6$ are by and large attributable to the absence of the shock-associated noise from the shock-free flows of the contoured plug-nozzle. In Fig. 23, the comparison of the PWL's vs frequency of jet flows from the contoured plug-nozzle and the convergent nozzle at pressure ratio $\xi = 3.6$, gives similar results.

Variations of the OASPL's with θ for the contoured plug-nozzle jet flows are shown in Fig. 24 for three pressure ratios, $\xi = 3.05$ (typical of the overexpanded mode); $\xi = 3.6$ (shockless flow), and $\xi = 4.5$ (typical of the underexpanded mode). For each of the fixed pressure ratios, the OASPL's of the contoured plug-nozzle are nearly constant at the observer angle $60° < \theta < 120°$ and the OASPL's increases with the increasing pressure ratio from its slightly overexpanded ($\xi = 3.05$) through fully-expanded mode ($\xi = 3.6$) and the underexpanded mode ($\xi = 4.5$).

The one-third octave SPL spectra, one-third octave PWL spectra and directivity of the OASPL for the contoured P-N at $\xi = 3.0$ (the over-expanded mode) are compared with those of the convergent nozzle in Figs. 25, 26, and 27, respectively. Similar comparisons of the acoustic performance of the contoured P-N at $\xi = 4.5$ (underexpanded mode) are presented in Figs. 28, 29, and 30.

In Fig. 31, the variations of OASPL's at $\theta = 90°$ for a range of pressure ratio ξ of the contoured P-N and the equivalent convergent nozzle are compared. These acoustic plots clearly show that for a range of off-design supercritical pressure ratios, the improperly expanded jet

flows issuing from an externally-expanded contoured plug-nozzle with a pointed termination radiate lower OASPL's as compared to the 'equivalent' convergent nozzle operated at the same pressure ratio. For calculating OASPL at all θ's from the corrected SPL data, the throat area of the convergent nozzle is scaled down to the throat area of the plug-nozzles. Comparatively, the reductions in the OASPL's at the off-design pressure ratios higher than the design pressure ratio are found to be somewhat less but are still significant (about 4 dB, Fig. 29).

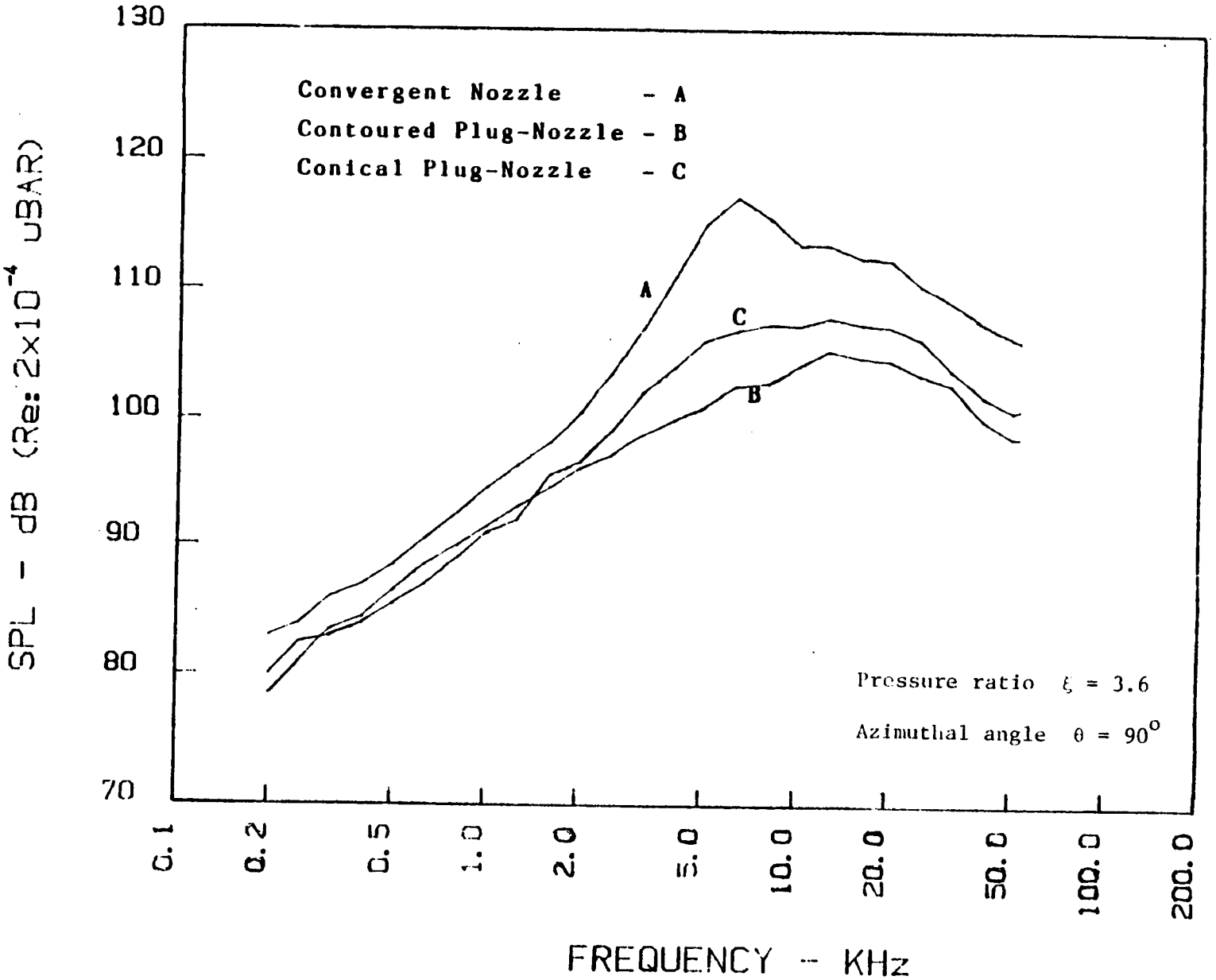

Fig. 22 One-third octave sound pressure level spectra of a convergent nozzle and contoured and conical plug-nozzle jet flows.

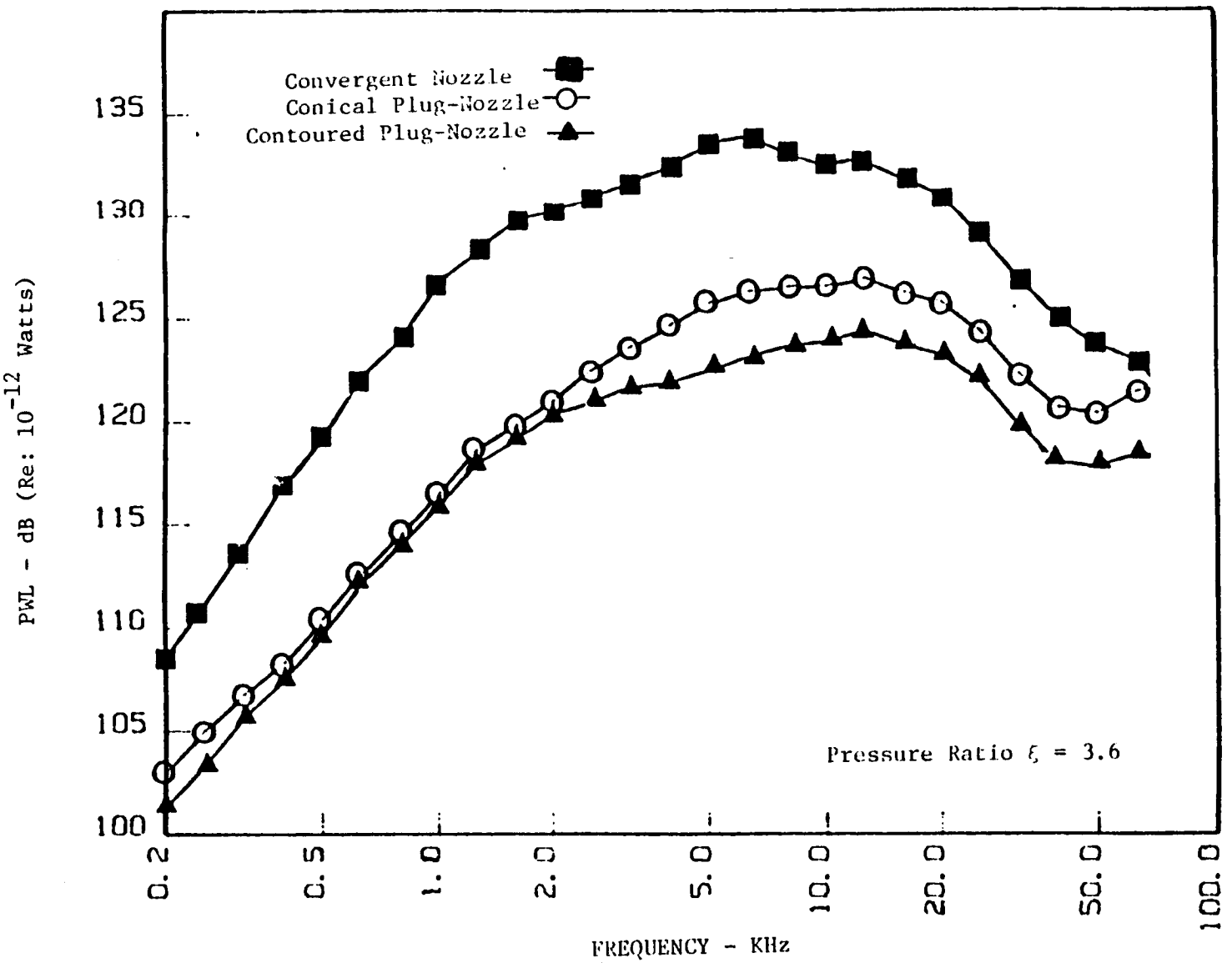

Fig.23 Comparison of Power Watt Level Variation with Frequency of Convergent Nozzle and contoured and Conical Plug-Nozzles Jet Flows.

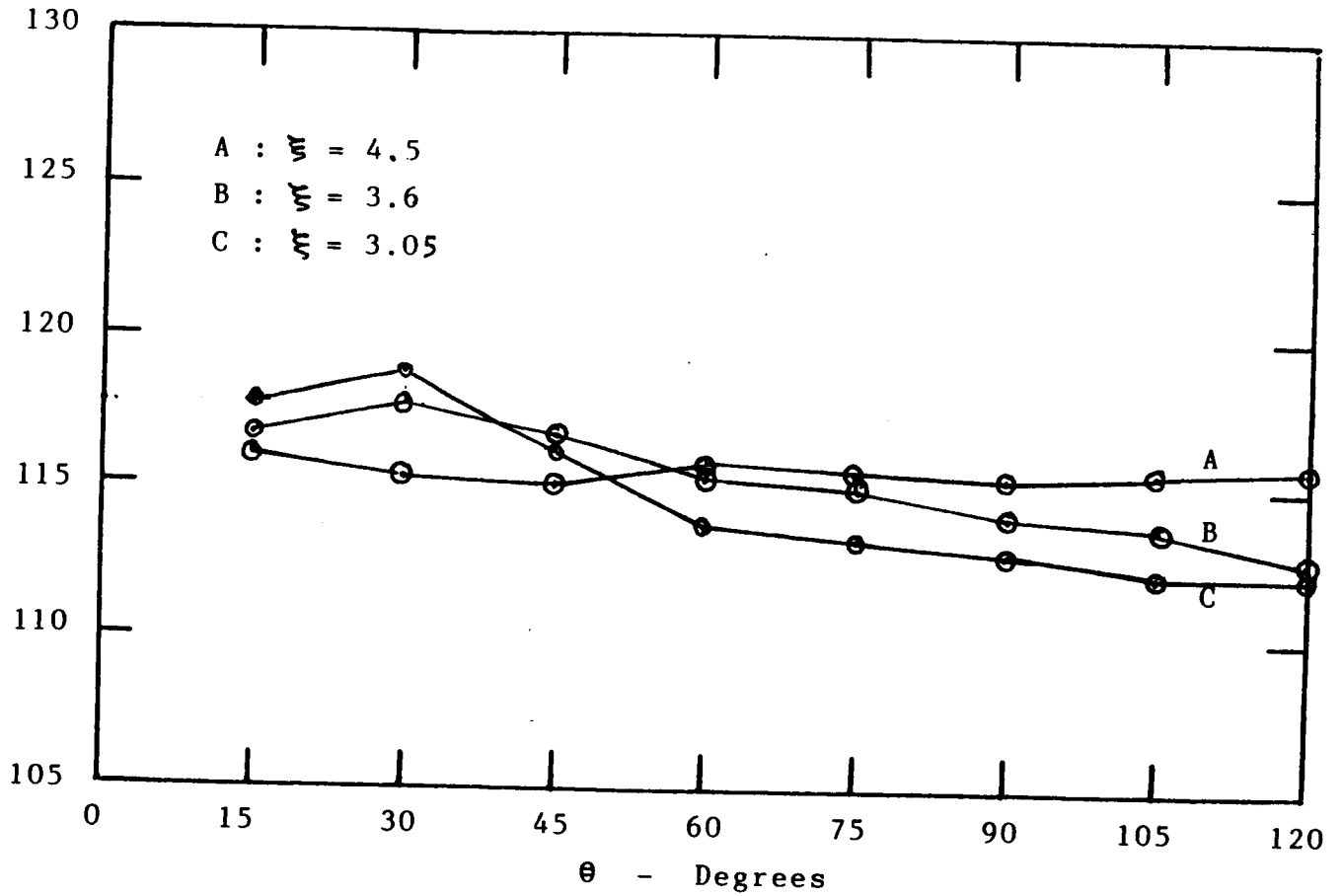

Fig. 24 OASPL's vs Azimuthal Angle of the Contoured Plug-Nozzle Jet Flows at Different Pressure Ratios.

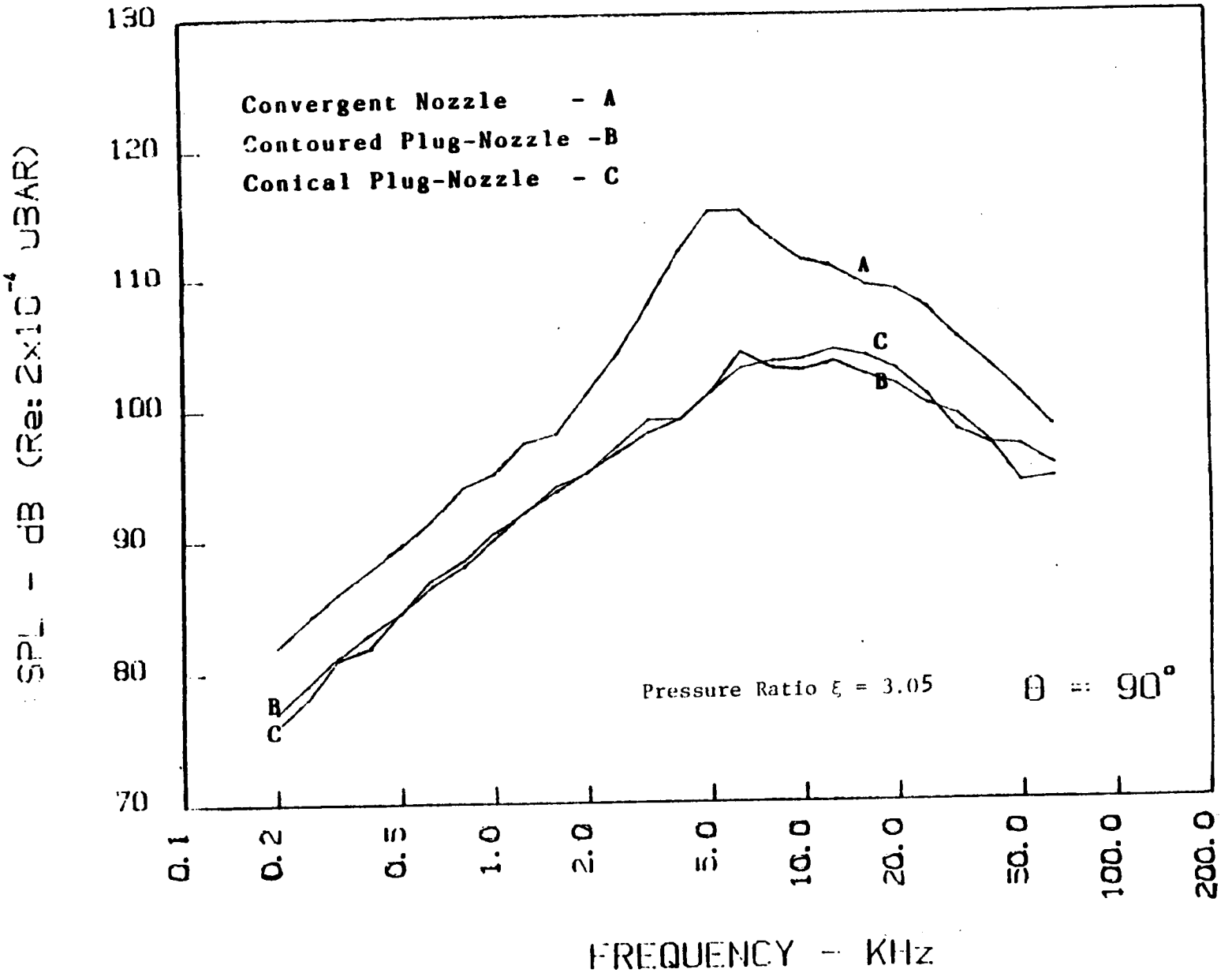

Fig. 25 One-Third Octave Sound Pressure Levels Spectra of the Convergent Nozzle and Contoured and Conical Plug-Nozzle Jet Flows

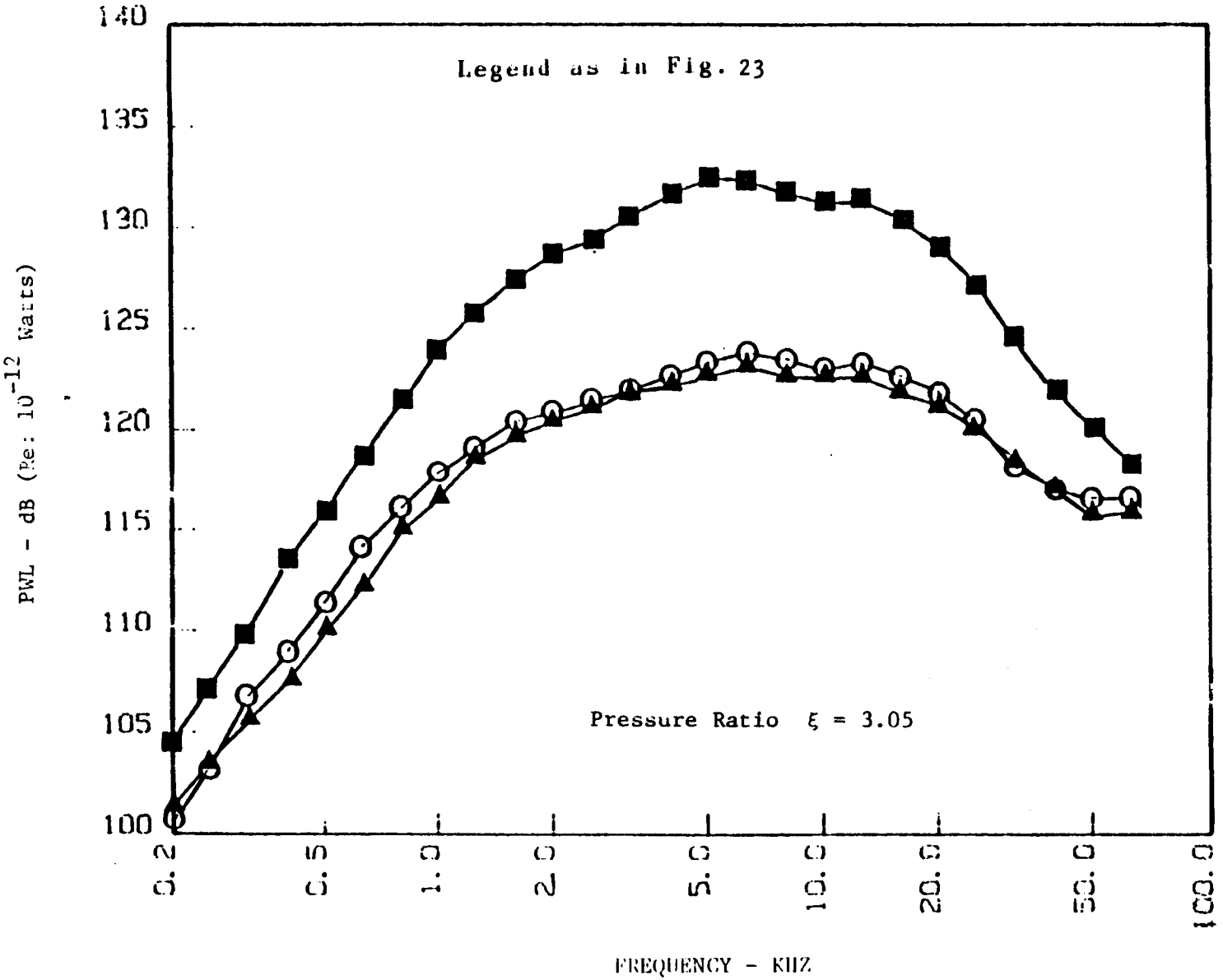

Fig. 26 Comparison of Power Watt Level Variation with Frequency for the Convergent Nozzle and Contoured and Conical Plug-Nozzle Jet Flows.

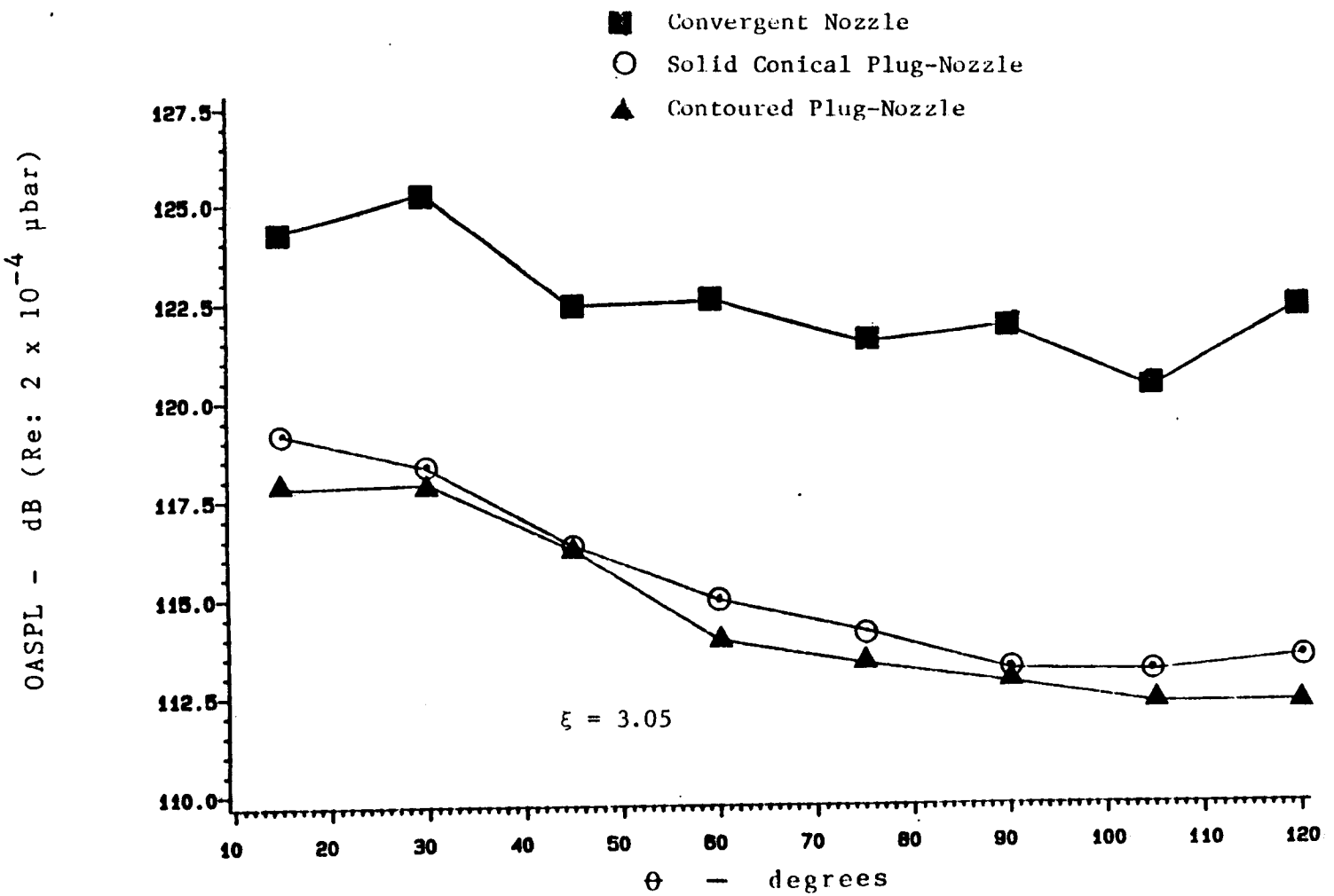

Fig. 27 Comparison of Overall Sound Pressure Level Variation with Azimuthal Angle of Convergent Nozzle and Contoured and Conical Plug-Nozzles.

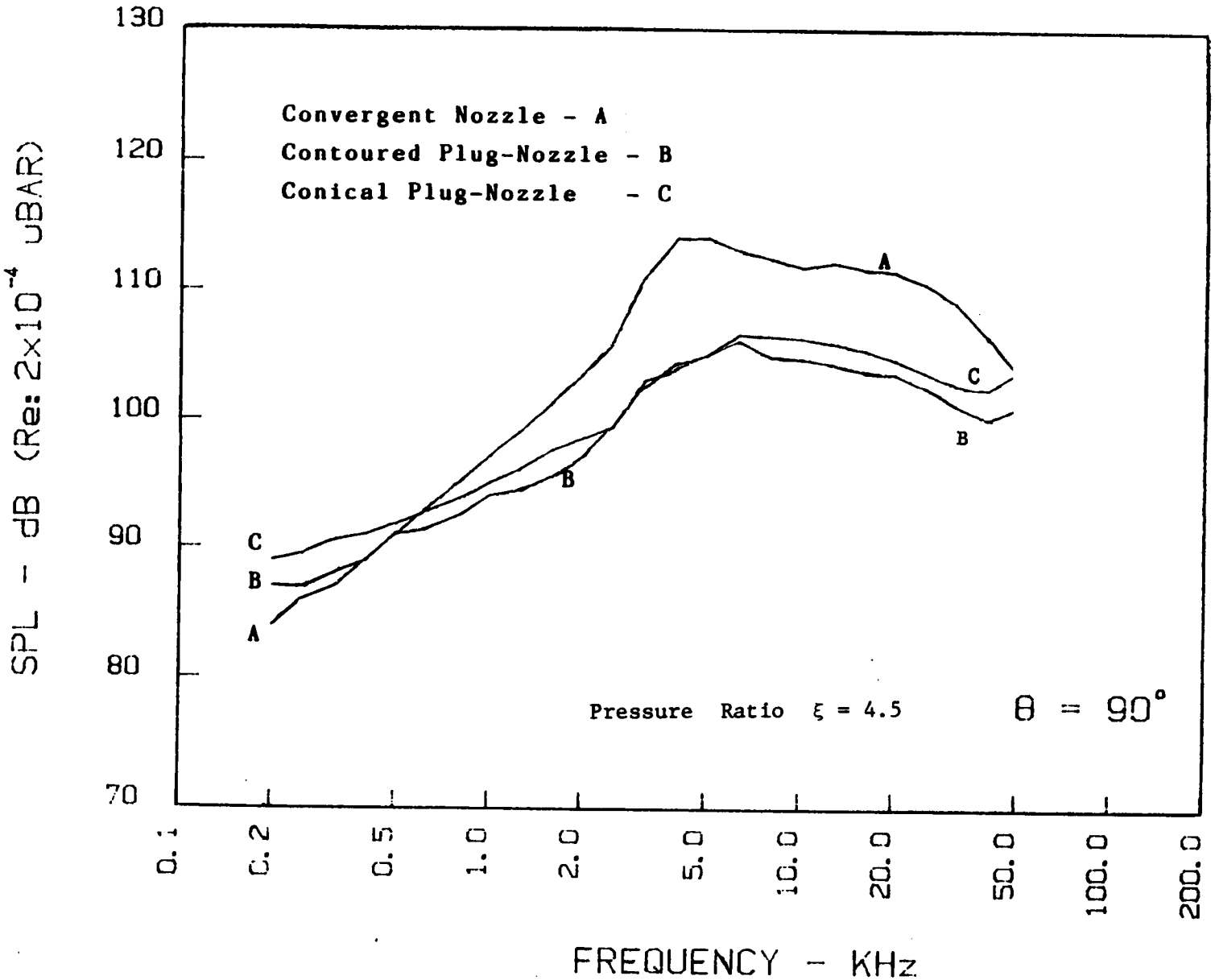

Fig. 28. One-Third Octave Sound Pressure Level Spectra of Convergent Nozzle and Contoured and Conical Plug-Nozzle Jet Flows.

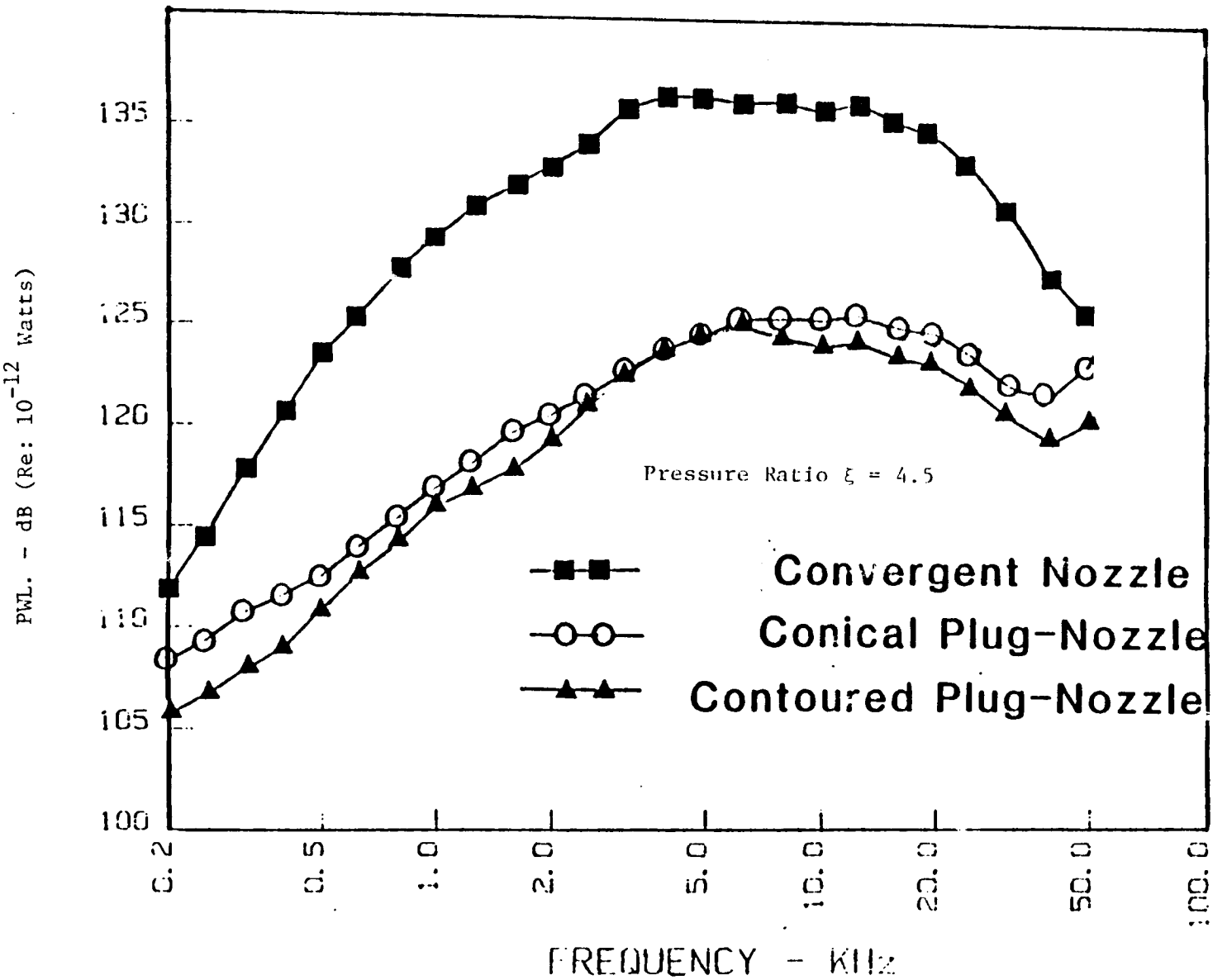

Fig. 29. Comparison of Power Watt Level Variations with Frequency of Convergent-Nozzle and Contoured and Conical Plug-Nozzle Jet Flows.

For Legend See Fig. 27

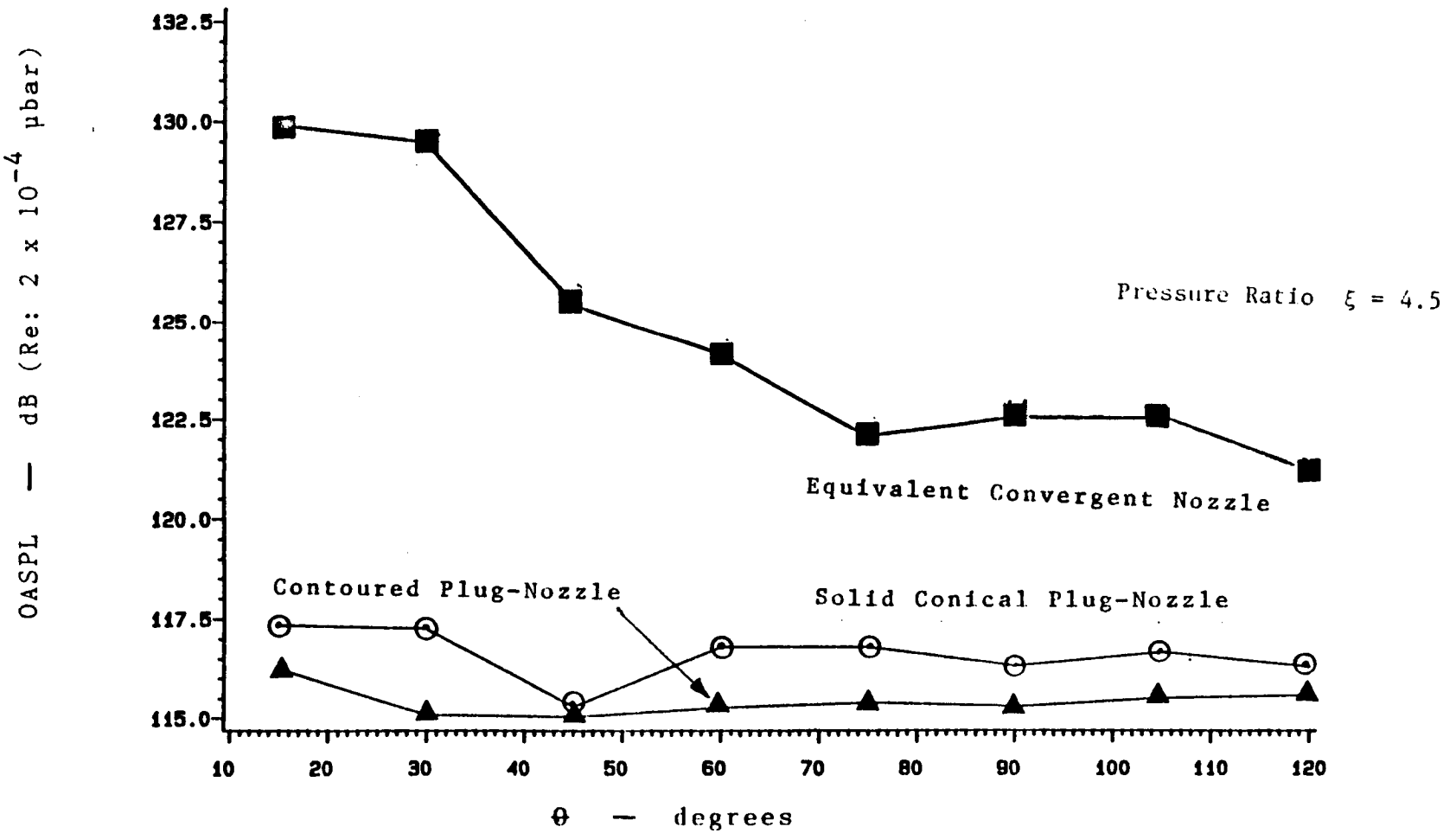

Fig. 30 Comparison of Overall Sound Pressure Level Variations with Azimuthal Angles of Equivalent Convergent Nozzle and Contoured and Conical Plug-Nozzle Jet Flows.

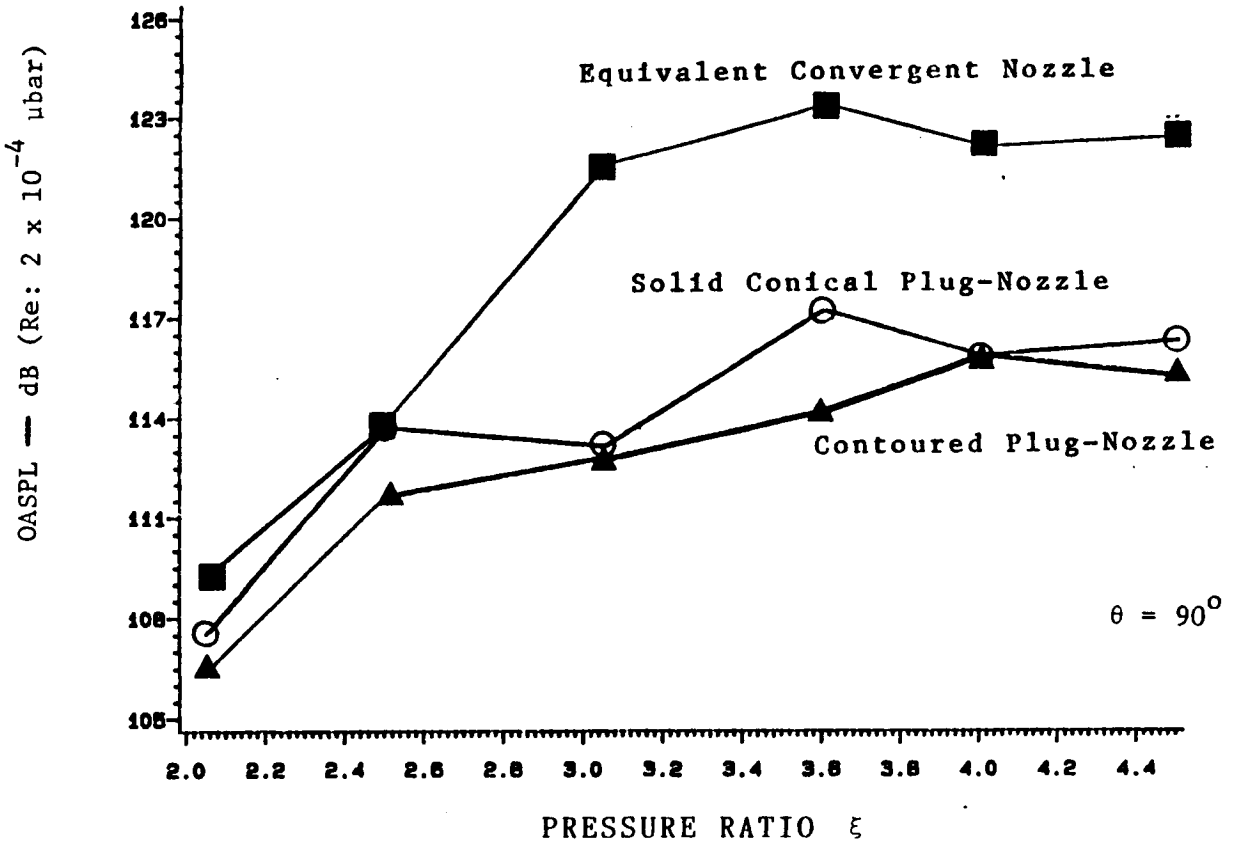

Fig. 31 Overall Sound Pressure Level Variation with Pressure Ratio of Convergent-Nozzle and Contoured and Conical Plug-Nozzle Jet Flows.

V.2.5 Shock-Noise Reduction Mechanism of Contoured Plug-Nozzle Jet Flows.

The spark shadowgraphs of the jet flows presented in Figs. 8 to 13 for the contoured plug-nozzle when compared with those of the underexpanded jet flows from a convergent (plugless) nozzle operated at the same pressure ratio, show significant modifications of the shock structure. At the design pressure ratio $\xi \doteq 3.6$, the contoured plug nozzle is free of shock structure (Fig. 8). At the same pressure ratio, repetitive shock structure is present in the underexpanded convergent nozzle jet flow. The strength of the shock cells increases with increase in the pressure ratio ξ or M_j . At higher pressure ratios, the Mach disk appears in the convergent-nozzle jet flow, with the attendant mixed subsonic and supersonic flow regions downstream (Figs. 12 and 13).

In a contoured P-N jet flows at supercritical pressure ratios, the expansion waves centered at the nozzle-lip are intercepted and cancelled by the contoured surface of the plug. At the design pressure ratio, the contoured P-N jet flow at the nozzle-exit is uniform, axial and shockless (see Figs. 1 and 8). Therefore, the experimentally observed reductions in SPL, PWL and OASPL for the contoured plug nozzle at its design pressure ratio are primarily achieved by plug-induced elimination of the shock structure in the underexpanded jet flows of the basic convergent nozzle.

If the contoured P-N is operated at less than the design pressure ratio (i.e. at $M_j < M_d$ in the overexpanded mode), all the expansion waves between the leading and tail wave fronts of the expansion fan emanating from the nozzle lip are cancelled. However, the compression-turning of the supersonic flow by the contoured plug surface downstream of the location where the tail Mach front of the expansion fan is incident on the plug, generates a set of compression waves (see illustration in Fig. 32). Depending upon the degree of the overexpansion of the contoured plug, these compression waves may or may not coalesce into a shock in the plug region. For overexpanded plug-nozzle, $\xi = 3.05$, such coalescence of compression fronts does not take place in the region of the plug (Fig. 11). The compression wave-fronts reflect as expansions from the free jet boundary - which in turn reflect as compressions from the opposite jet boundary. These reflected-compressions may lead to the formation of a conical

oblique shock in the plug-nozzle jet flow. Further reflections to meet the constant pressure condition at the jet flow boundary result in weak repetitive shock cells. Such oblique shock-structure formed by the successive reflections of the wave fronts originating from only part of the plug surface, are weaker than the oblique shocks in the underexpanded jet flow from a convergent nozzle operated at the same pressure ratio. If the super-critical pressure ratio for the overexpanded mode of operation is lowered, the compression waves generated by the compression-turn of the contoured-plug surface downstream of (and relatively close to) the nozzle throat, lead to the formation of multiple shocks in the plug region. This is well demonstrated in the spark shadowgraphs of the contoured P-N jet-flows in Figs. 9 and 10, and is illustrated in flow sketch in Fig. 32 . These multiple shocks in the plug region are rather weak and there is no evidence of the repetitive shock cells downstream of the plug apex. Therefore, at these off-design low pressure ratios, the relative significance of shock associated noise generation would be reduced. Hence, in such weakly overexpanded contoured plug-nozzle jets the shock associated noise component even at higher θ's, is not dominant and the turbulence mixing noise component plays relatively a more important role. The noise intensity (OASPL's) of the weakly overexpanded jet flows from the contoured P-N nozzle increases as the operating pressure ratios is increased approaching the design pressure ratio where the jet flow is shock-free. It is in this range of pressure ratios that the plug nozzle has a clear aerodynamic advantage over an equivalent contoured C-D nozzle which at such low pressure ratios ($\xi < \xi_d$) develops shock-structure within the nozzle, resulting in shock- related noise and greater loss of thrust.

In the underexpanded mode of operation of the contoured plug nozzle ($\xi > \xi_d$), the tail expansion wave corresponding to $\xi = \xi_d$ (the design Mach number M_d) is incident at the plug tip. In an underexpanded contoured P-N jet ($M_j > M_D$), the plug surface does not quench all the incident expansion wave fronts from the nozzle lip. The expansion Mach fronts with the local flow Mach number $M_j > M_d$, and Mach angles $\mu_j < \mu_d$, are not interceped by the plug surface (Fig. 33). The escaped expansion wave fronts reflect from the free jet boundary on opposite side as compression fronts and may coalesce to form weak repetitive shock in the flow farther downstream of the plug apex. These repetitive shock- cells are more likely to decay

ORIGINAL PAGE IS
OF POOR QUALITY

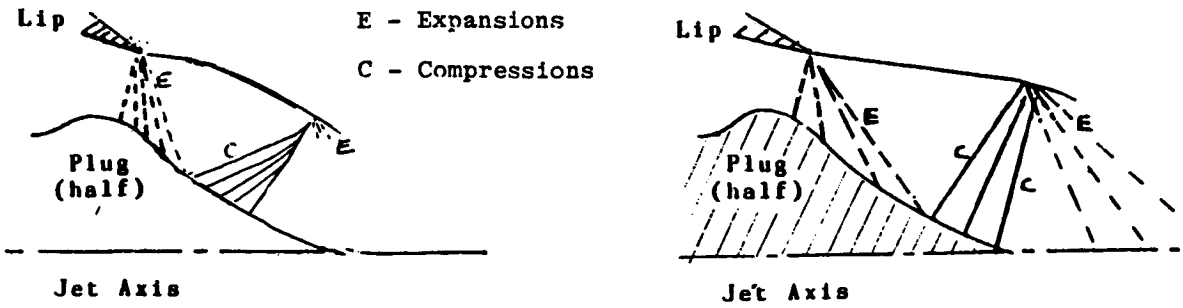

Oblique Shock Formation in the Flow Region of an Overexpanded Contoured Plug. $\xi << \xi_d$ ($M_j << M_d$).

Shock Formation Downstream of the Plug Apex (Exit) of an Overexpanded Contoured Plug $\xi < \xi_d$ ($M_j < M_d$).

Fig. 32 Sketch of Wave Structure of the Contoured Plug-Nozzle Jet Flows in the Over-Expanded Mode.

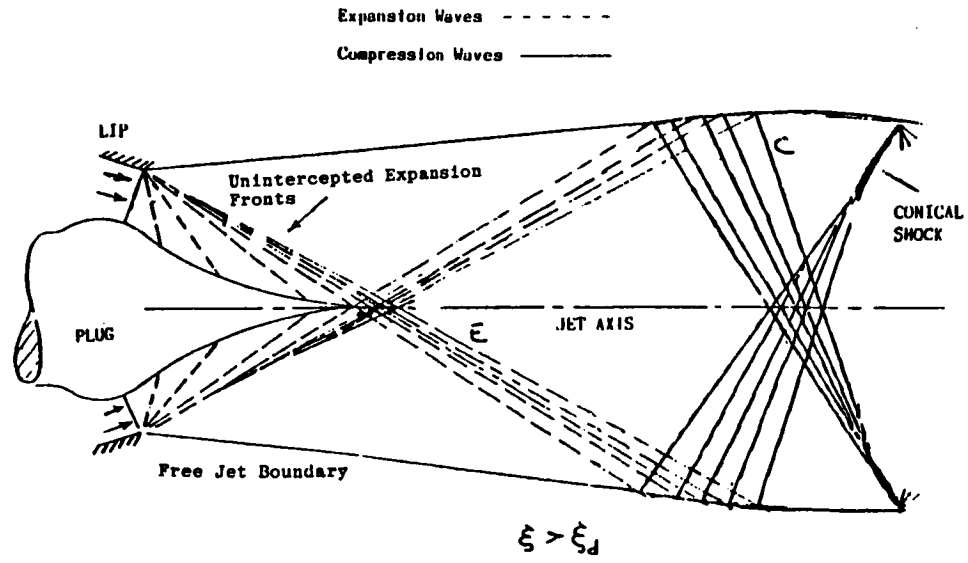

Fig. 33 Sketch of the Wave Structure of the Contoured Plug-Nozzle in the Underexpanded Mode.

faster than those in an underexpanded jet flow issuing from an 'equivalent' convergent nozzle and the underexpanded contoured P-N jet flow, therefore, is likely to have a fewer cycles of the repetitive weak shock cells. Since it is the strength, the number of shock cells, and their spacings and the interaction of the flow fluctuations convected through the shock-structure in the jet flows which contribute to the intensity of the shock-associated noise, one may conclude that the shock associated noise generation would be less significant in underexpanded jet flows issuing from a contoured plug- nozzle operated at off-design pressure ratios ($\xi > \xi_d$) than is the case for underexpanded jet flows issuing from an 'equivalent' convergent nozzle operated at the same pressure ratio. These deductions are supported by the comparative assessment of the shock related noise components at higher observer angles by the contoured plug nozzle and the basic convergent (plugless) nozzle operated at a range of pressure ratios (see Figs. 15-31).

V.3 AEROACOUSTICS OF CONICAL PLUG-NOZZLE JET FLOWS

The model conical plug-nozzle was designed to have the same annulus-radius ratio $K = R_p/R_N$, the same annular throat area and a conical plug of the same surface area as that of the contoured plug. Therefore, the the length of the conical plug was even shorter than that of the contoured plug. For other geometrical specifications of the model conical plug-nozzles see Table 2, p.22 . When operated at the same pressure ratio, the mass flow rate for the conical and the contoured plug-nozzles is the same. For a discussion of the various options considered for the selection of the short conical plug, see Section III. 3. The extent of the accumulated one-third octave sound pressure level data for the conical plug-nozzle is tabulated on p.23 .

Figure 34, shows some typical records of the one-third octave SPL spectra recorded at $\theta = 90°$ for the conical P-N operated in the underexpanded mode at the two highest supercritical pressure ratios $\xi = 4.0$ and 4.5 used in the present studies. Since there are no sudden and sharp peaks in the SPL spectra at either of these pressure ratios, it is concluded that the screech noise component is absent.

The variation of the peak frequency with the azimuthal angle θ for

the conical P-N at pressure ratio $\xi \doteq 3.6$ is shown in Figs. 35. For clarity, the corrected one-third octave SPL spectra at various observer angles have been plotted on a sliding scale. For the contoured and the conical plug-nozzles operated at the same pressure ratio $\xi \doteq 3.6$, the peak frequency f_p = 10 kHz is nearly the same. The Strouhal number St. = $f_p w_t / v_j$ vs θ, for $\xi \doteq 3.05$, 3.6 and 4.5, are plotted in Fig. 36. At each ξ, the Strouhal number varies in steps from low values $\approx$ .06 at $\theta = 15°$, peaks at $\theta = 45°$ to Strouhal number $\approx$ 0.4 and for $\xi = 3.60$ stays nearly constant between $45 < \theta < 90°$; varies in steps for $\xi = 3.05$ and 4.5 approaching $\approx$ 0.2 at $\theta = 120°$.

The comparison of the variation of the Strouhal number vs. θ at the same pressure ratio $\xi \doteq 3.6$ (shockless flow) of a contoured plug (Fig. 16) with that of a conical plug (Fig. 36), shows similar peaks and plateaus. In both cases, at $\theta < 30°$ for each of the three pressure ratios, the Strouhal number $\doteq$ 0.05. At $\xi = 3.6$, its peak value $\doteq$ 0.5 at $\theta = 60°$ for the contoured plug and $\doteq$ 0.4 at $\theta = 45°$ for the conical plug. The St. number for the conical plug operated at different super-critical pressure ratios also shows peaks and plateaus similar to those for the contoured plug at $\xi \doteq 3.6$, the St. number = 0.4 between $\theta = 45°$ to $90°$. At $\xi = 4.5$, St. number exhibits two plateaus; the first St. = 0.3) between $\theta = 60°$ to 75° and another (St = 0.16) at $\theta = 90°$ to 120° (Fig. 36). It is noteworthy that St. number vs. θ variations of the conical plug nozzle at different above-critical pressure ratios are nearly similar to those of a contoured plug nozzle when operated at the same pressure ratios (Fig. 16). This similarity in the acoustic behavior stems from the fact that some of the geometrical features of the short contoured and uncontoured plugs are rather similar and, therefore, the nature of the jet flows from each of the plug-nozzles, when operated at the same pressure ratio, is also not radically different.

V.3.1 Noise Suppression Effectiveness

The 1/3 octave SPL's records for the conical P-N at $\theta = 90°$ for the three typical pressure ratios (ξ = 3.6, 3.05 and 4.5) are compared with those of the contoured P-N and the convergent nozzle in Figs. 2, 25, and 28, respectively. The OASPL directivity comparisons at various angles for supersonic jet flows issuing from these three 'equivalent' nozzles are presented for ξ = 3.6 (the pressure ratio at which the contoured plug-nozzle flow is shockless) in Figure 27, and for underexpanded flows at ξ = 4.5 in Figure 30. The power level spectra of the jet flows from these nozzles are compared for ξ = 3.6, in Figure 23, for ξ = 3.05 in Figure 26, and for ξ = 4.5 in Figure 29.

The directivity (OASPL vs θ) and the power spectra (PWL vs f) plots at the three typical pressure ratios ξ = 3.05, 3.6 and 4.5 clearly demonstrate that at all angles to the jet axis and for the entire frequency range over which the acoustic data are collected, the noise levels from the uncontoured conical P-N jet flows are about 2 to 4 dB higher than those of the contoured plug-nozzle jet flows. However, the comparison of OASPL's vs θ of the equivalent convergent nozzle and the plug-nozzle (in Figs. 23, 26 and 29) shows that by the use of even an uncontoured conical plug as a centerbody in the plug nozzle, the noise reductions of about 6-8 dB are achieved at all θ's. The plug-nozzle with a short conical pointed plug as the centerbody, therefore, effectively suppresses not only the shock-associated noise component (dominant at the higher angles to the jet axis) but also the turbulent mixing noise, the component of the noise dominant at lower angles to the jet axis.

The acoustic data gathered for improperly expanded plug-nozzle flows are also analysed for comparison with the noise intensifies predicted by relations proposed by Stone [40]. The shock-associated noise generated from the premerged flow region in the vicinity of the plug and the shock-associated noise generated from flows downstream of the plug are considered separately. For single stream plug-nozzle flows, the OASPL components for each flow region are represented as follows.

From pre-merged flow region:

$$1.\quad OASPL_p = 159 + 10 \log \left(\frac{p_a}{p_{i\,sA}}\right)^2 \left(\frac{a_a}{a_{i\,sA}}\right)^4 + 10 \log \frac{A_j}{R^2}$$

$$+ 10 \log (1-K) + 10 \log \frac{(M_j^2 - 1)^2}{1 + (M_j^2 - 1)^2}$$

$$+ F \cdot (\theta_m - \theta)$$

From Downstream Flow Region:

$$2.\quad OASPL_D = 159 + 10 \log \left(\frac{p_a}{p_{i\,sA}}\right)^2 \left(\frac{a_a}{a_{i\,sA}}\right)^4 + 10 \log \frac{(M_j^2 - M_{d,p}^2)^2}{1 + (M_j^2 - M_{d,p}^2)^2}$$

$$+ F \cdot (\theta_m - \theta) + 10 \log \frac{A_j}{R^2}$$

where $F\ (\theta_m - \theta) = 0$, for $\theta > \theta_m$

$F\ (\theta_m - \theta) = -0.75$, for $\theta < \theta_m$.

M_{dp} is the design Mach number if a pointed plug is used and is 1.0 if truncated plug is used.

The experimental OASPL's vs θ at three typical pressure ratios ξ = 3.05, 3.6 and 4.5 of the conical plug nozzle are compared with the OASPL's predicted by Stone's scheme, in Figs. 37 to 39, respectively. The experimental and predicted OASPL's at $\theta = 90°$ are compared at a range of fully-expanded flow Mach Number M_j in Fig. 40. At $M_j > 1.5$ the agreement between the experimental and predicted OASPL's is within 3 dB's. At higher angles to the jet flow axis, at all pressure ratios, Stone's relation overpredicts OASPL's by 2 to 5 dB. Some of the likely reasons for the observed differences in the predicted and the experimental OASPL's are outlined below.

The empirical relations by Stone were devised particularly to predict shock associated-noise from plug-nozzle flows. Therefore, poor prediction of OASPL at lower angles to the jet axis (Figs. 37-39), where mixing noise dominates, is understandable. Moreover, it seems that Stone's empirical scheme was based only on the noise-data for the plug- nozzle flows

accumulated by Yamamoto et al. [41]. The annulus-radius- ratio K of this plug nozzle was 0.85. The plugs were long with the ratio of the plug length L_{max} to the radius at the nozzle lip R_N of 2.4, and the conical plug had bluff termination. In the present model conical plug- nozzle configurations, K is only 0.43; the ratio L_{max}/R_N is 0.97 and the plug tip is pointed. The recompression shock from the wake flow of any bluff (truncated) plug-nozzle operated at super critical presence ratios would result in a repetitive shock structure [27]. Because of the different configurational factors K, plug length L and plug termination, even at the same super-critical pressure ratio, the shock structure in the respective jet flows from these two different plug-nozzle configurations is bound to be quite different.

Influence of the Annulus-Radius Ratio K and the Plug Length L.

An examination of the Stone's relation for predicting the OASPL's for plug-nozzle flows shows that at the same M_j , an increase in the annulus-radius-ratio K results in a decrease in OASPL. In the design of plug contours for shockless flow, the parameter K and the design Mach number M_j are uniquely related (See Section III.2). Higher the design flow Mach number, larger the value of K is. Moreover, Stone's relations predict the same noise levels for plugs of the same K, but of different lengths. This assumption of non-dependence on maximum length L_{max} cannot be defended from the gasdynamical considerations. For example, consider a short plug and a much longer plug both having the same K. Both are operated at a pressure ratio for which the long plug just intercepts all the expansion waves emanating from the nozzle lip and for the short plug, part of the wave fronts of the expansion fan are not intercepted. In such conditions, the jet flow of the long P-N will have reflected wave fronts from the surface and form only one family of repetitive shock cells whereas the short P-N jet will have two different families of repetitive shock cells, one due to reflections at the plug surface of the expansion waves (see shock labelled s_1 in Figs. 12 and 51(a)) and the other due to part of the expansion waves from the nozzle lip escaping interception by the plug (see shock labelled (s_2 in Figs. 12 and 50(a)). Hence, the gasdynamical features of the plug-nozzle jet flows with a short plug and a long plug even with the same K factor and operated at the same pressure ratio, are

different. Therefore, the resulting shock-associated noise-component for such two plug-nozzle configurations would also be different.

Influence of the Plug Termination

If the plug termination is bluff or truncated, the base wake-flow results. Consequently, as noted earlier, additional shock fronts originate from the compressive turn of the boundary streamline of the wake flow [27]. Moreover, because of additional flow expansions around the shoulder of the truncated plug, the local flow Mach numbers may also increase, thus resulting in stronger recompression shocks. This additional family of repetitive shock structure in such plug-nozzle flows interact with the highly vortical, mixing layer of the wake flow and generate additional shock-associated noise components from truncated-plug flows. Such would not be the case for a pointed plug of the type used in the present investigation. The acoustic data gathered by Yamamoto et al. [41] using a plug-nozzle with a centerbody (plug) of bluff termination would result in additional complexities in the shock structure of the jet flows associated with wake formation. Stone's choice of the parameter $M_{d,p} = 1$ to account for truncation effect, does not seem to have either an obvious experimental or a physical gasdynamical basis.

The acoustic performance of supersonic plug-nozzle flows reported here is based on the acoustic data gathered using a plug-nozzle with a short conical plug as centerbody of a low annulus-radius-ratio $K = R_p/R_N$, a small L/R_N and a pointed plug-termination. The geometry of the conical plug was selected to be rather similar to a contoured plug. As such, the wake flow at the plug tip is practically absent (Figs. 8-13) and the shock structure at the off-design pressure ratios is comparatively weak. Stone's scheme was developed to fit the acoustic data from plug-nozzle flows which are likely to have stronger shock structure either because the plug was truncated or had a bluff termination. This may be the underlying reason that for the present study of the model solid conical plug, the overall sound pressure levels are lower than those predicted by Stone (Fig. 40).

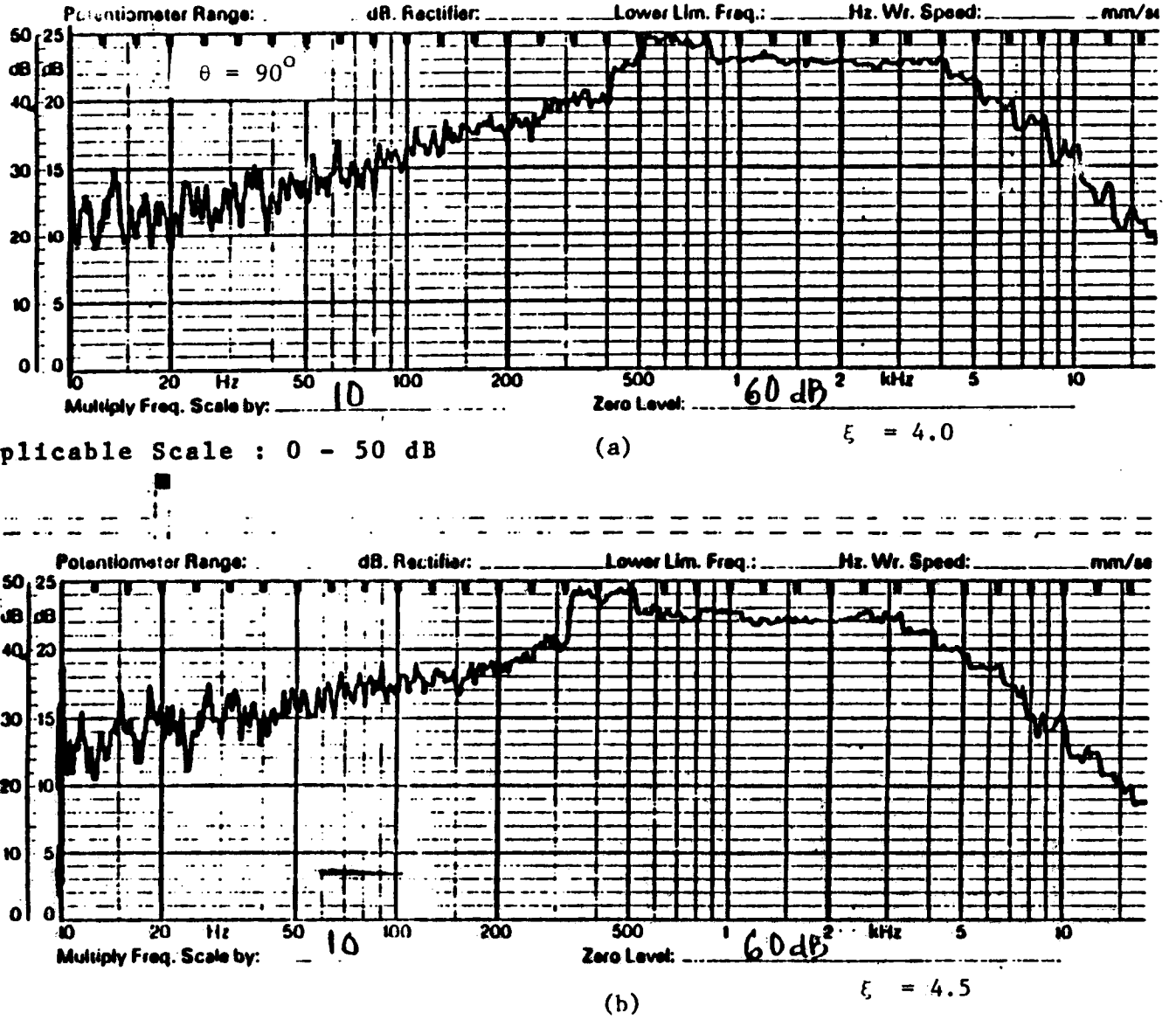

Fig. 34 Typical One-Third Octave Sound Pressure Level Spectra for the Conical Plug-Nozzle Jet Flow.

K = 0.43

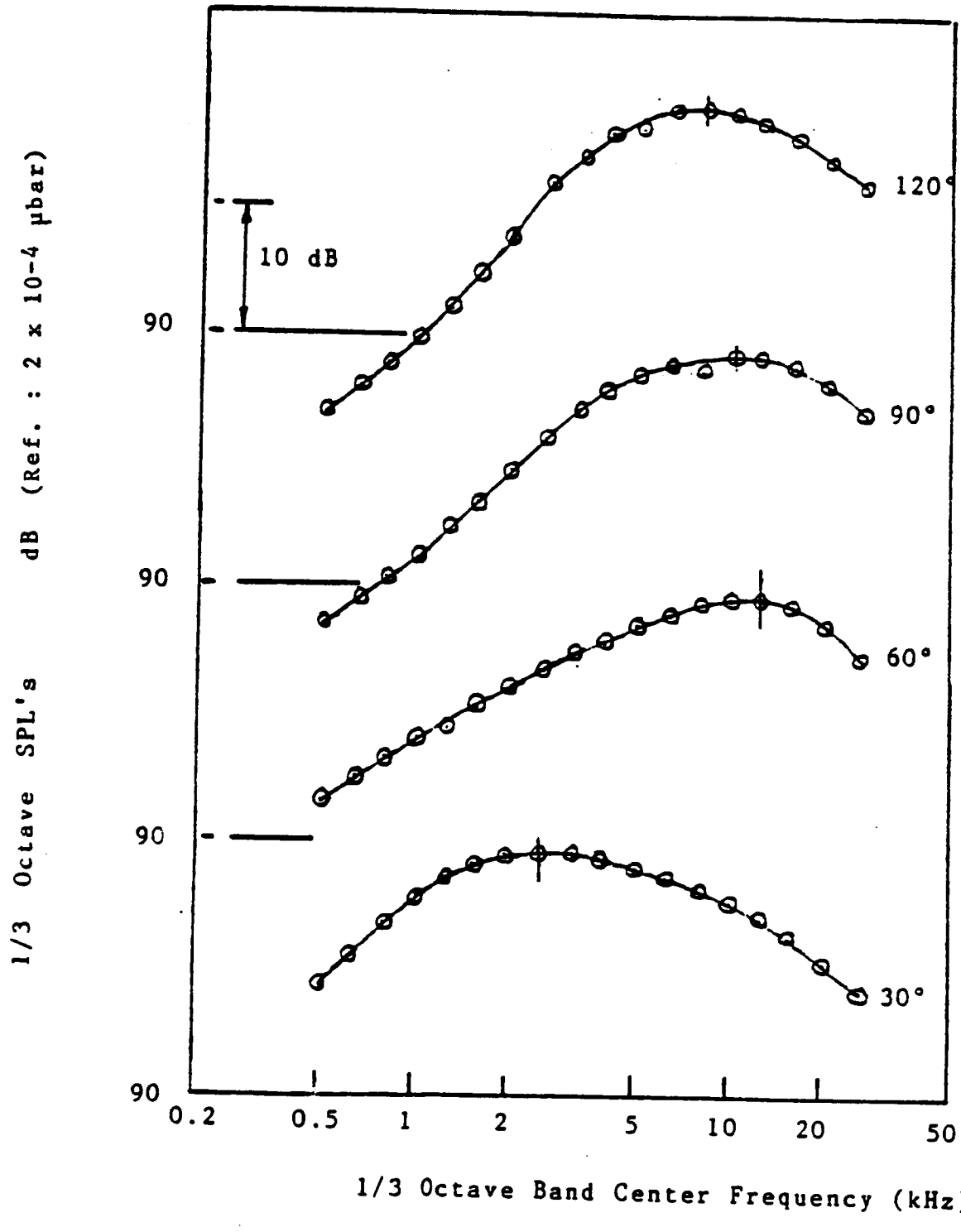

Fig. 35 Variation of Peak Frequency with Azimuthal Angle for Conical Plug-Nozzle Jet Flow at Pressure Ratio $\xi = 3.6$

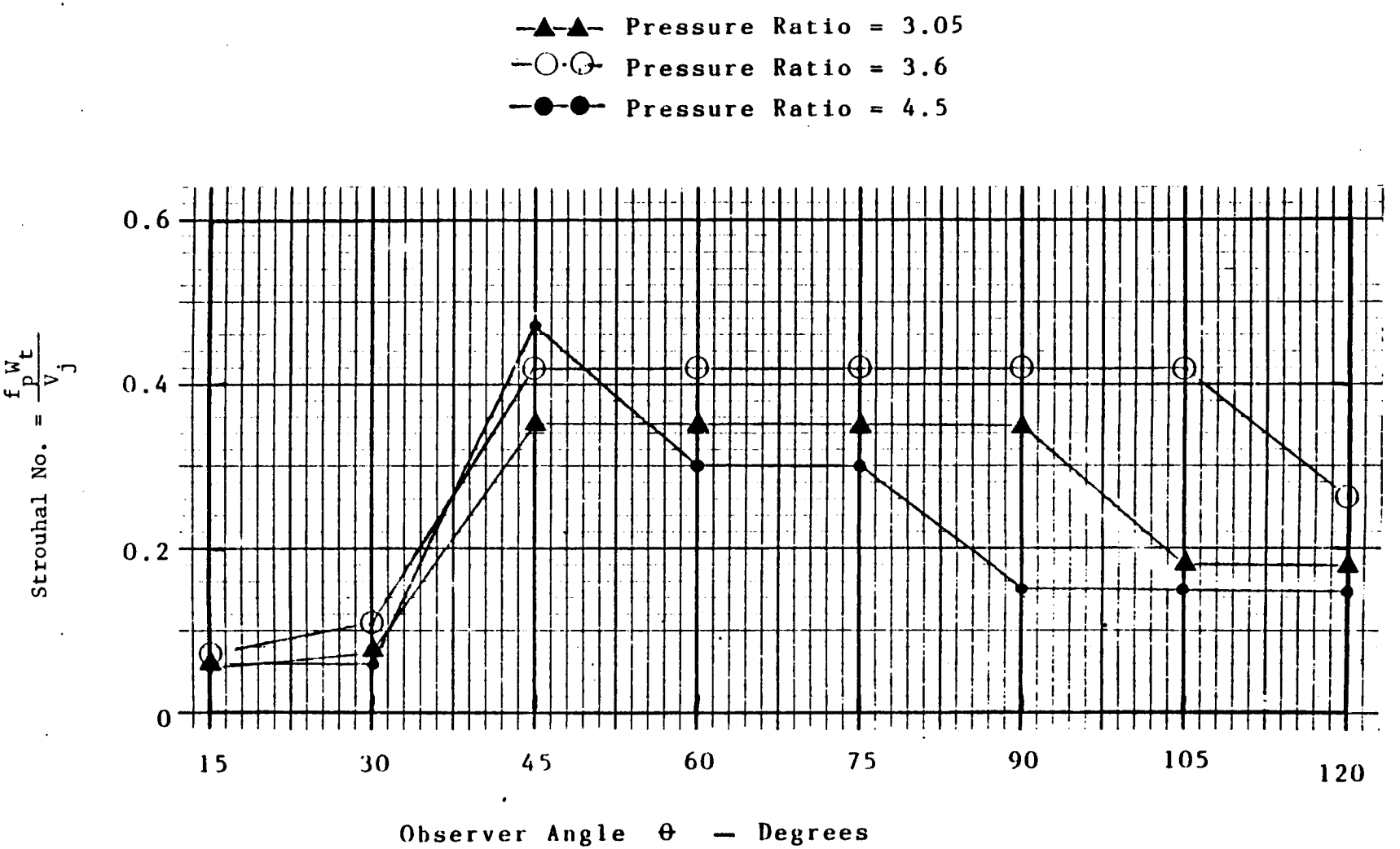

Fig. 36 Variation of Strouhal Number with Azimuthal Angle for the Conical Plug-Nozzle Jet Flow at Different Pressure Ratios.

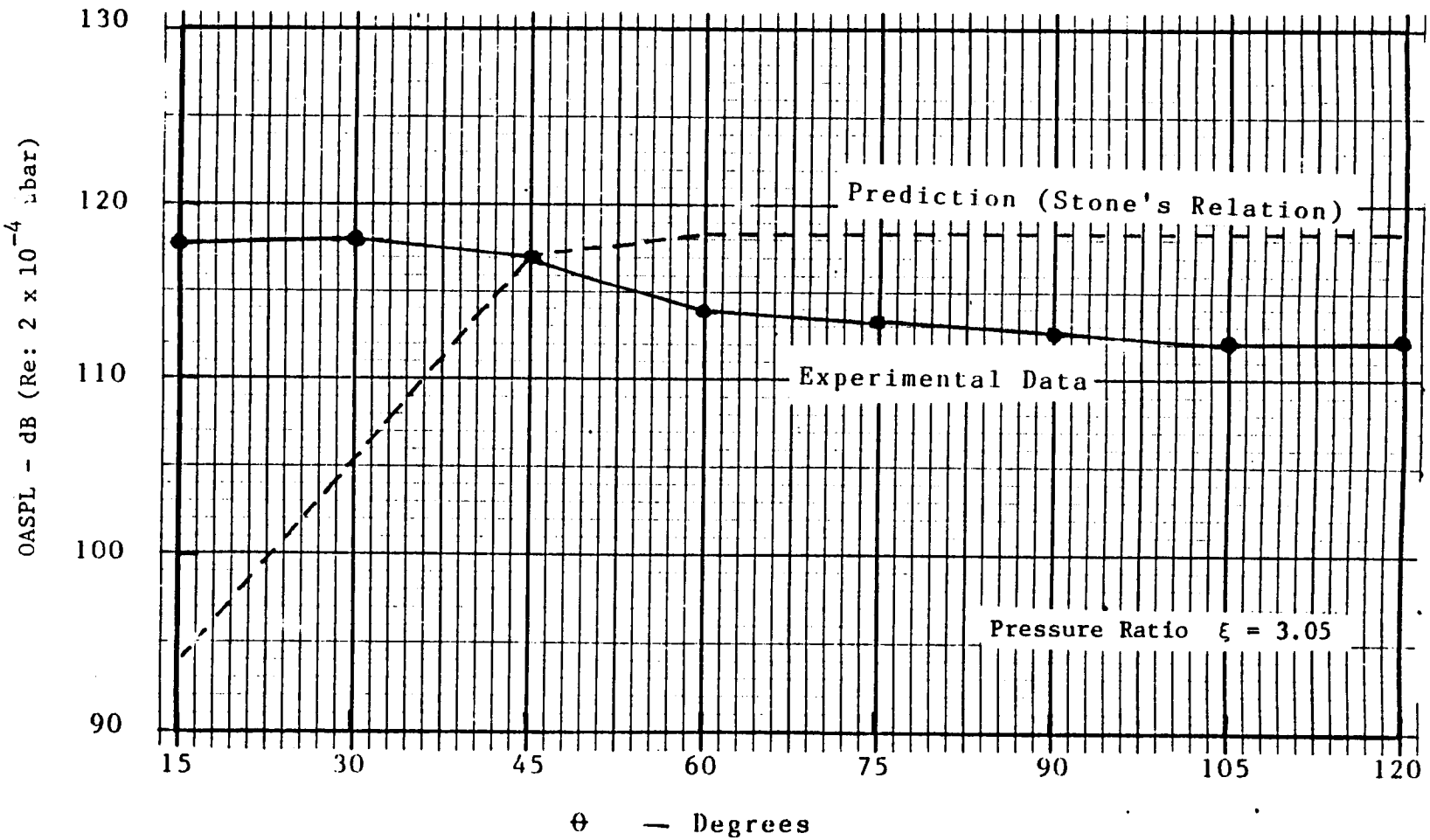

Fig. 37 Comparison of Overall Sound Pressure Level Variations vs. Azimuthal Angle of Conical Plug-Nozzle Jet Flow with those Predicted by Stone [40].

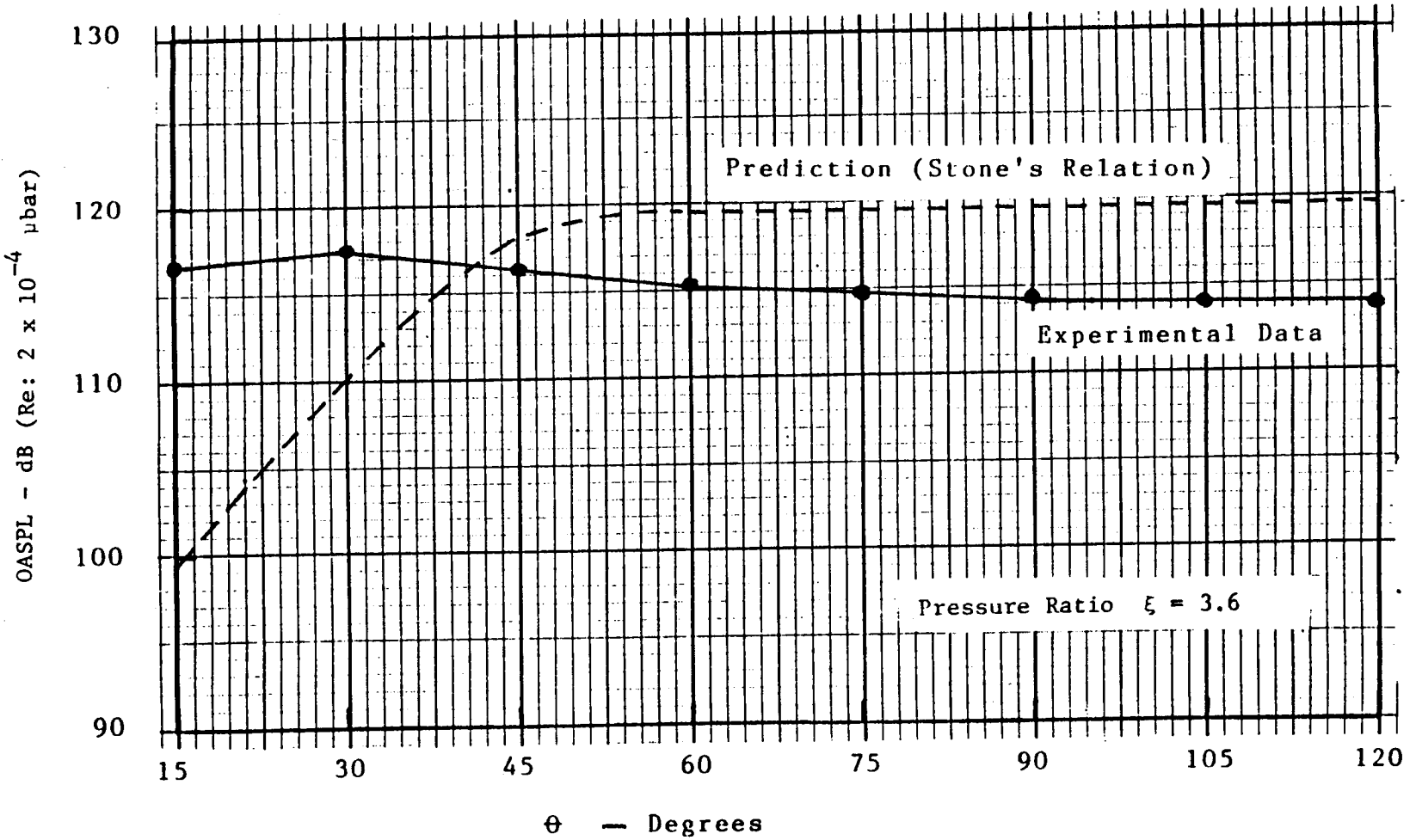

Fig. 38 Comparison of Overall Sound Pressure Levels Variations vs. Azimuthal Angle of Conical Plug-Nozzle Jet Flow with those Predicted by Stone [40].

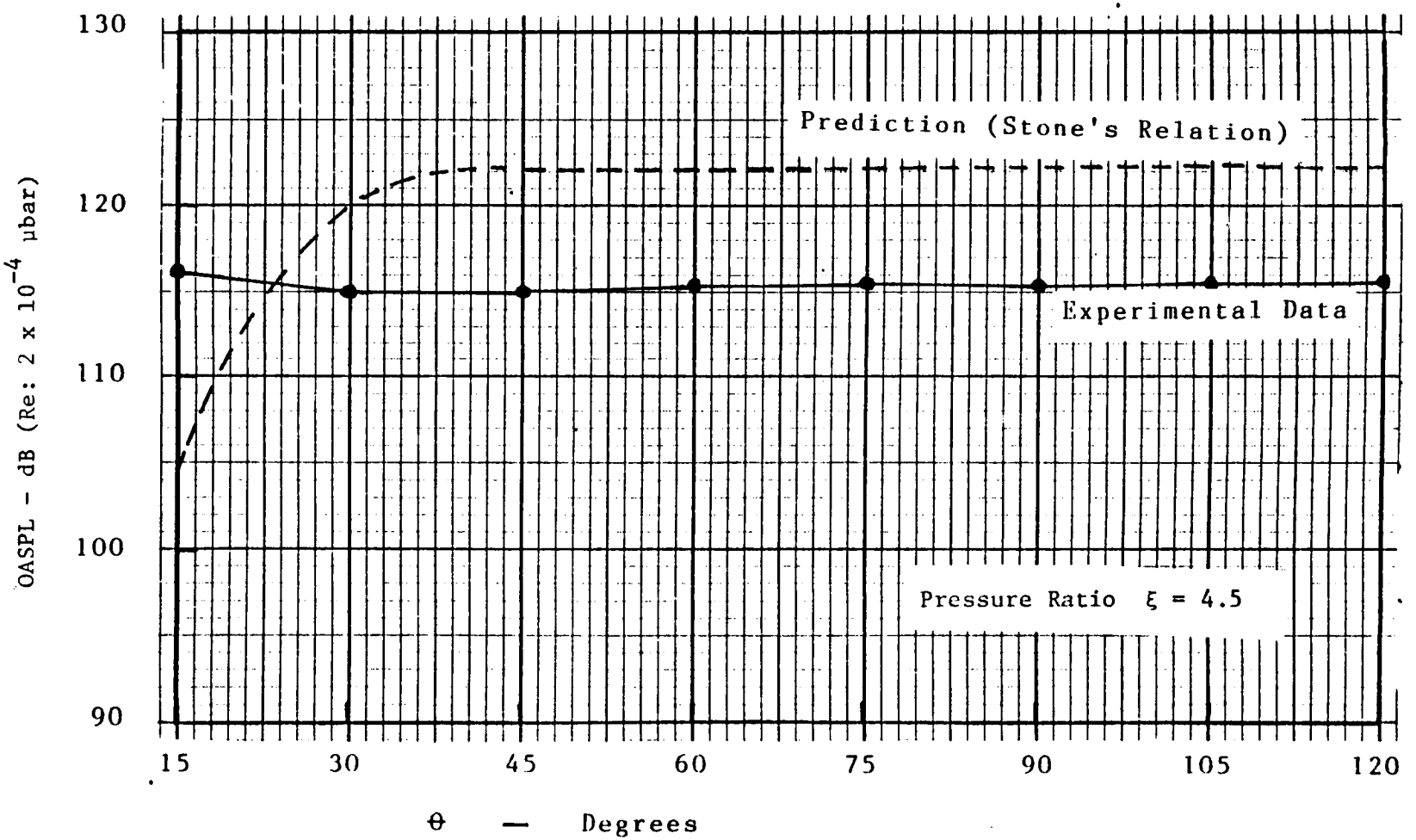

Fig. 39 Comparison of Overall Sound Pressure Level Variations vs Azimuthal Angle of Conical Plug-Nozzle Jet Flow with those Predicted by Stone [40].

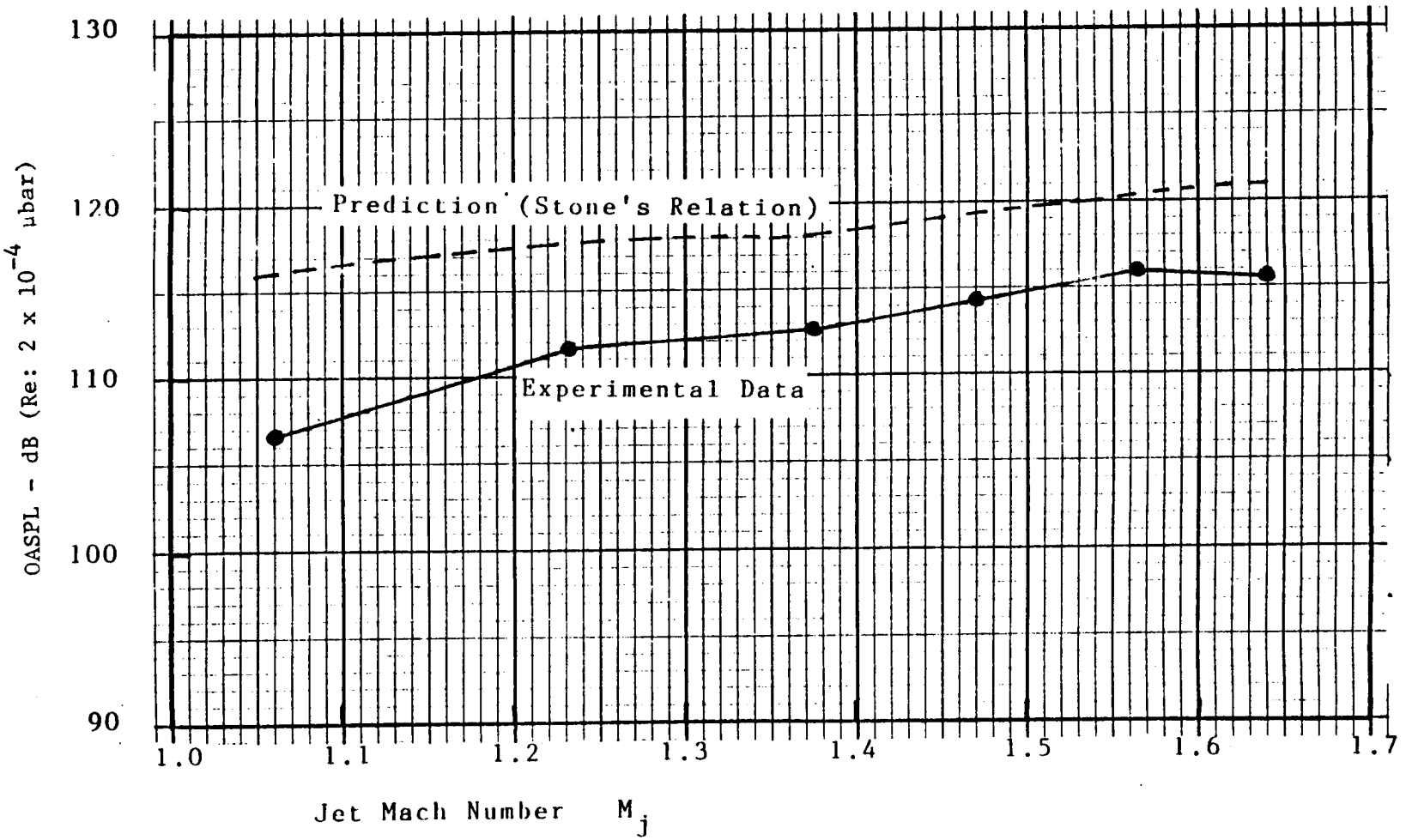

Fig. 40 Comparison of Experimental Overall Sound Pressure Level as a Function of the Jet Mach Number for Conical Plug-Nozzle with those Predicted by Stone [40].

V.3.2 Noise Generation Mechanism of the Conical Plug-Nozzle Flows.

The shock-structure in the jet flows from plug nozzles with a short uncontoured conical plug as its centerbody is noted to be qualitatively different from those in the contoured plug-nozzle flows at off-design pressure ratios (see Figs. 8-13). The conical plug is shorter than the contoured plug. At higher than the design pressure ratios, the conical plug-nozzle flow field has two families of repetitive cellular shock-structures; one family originating due to the reflections of incident expansion waves as expansions from the solid plug-surface (see shock front labelled (s_1) in Figs. 12 and 56(a), and the second family of shock structure originating because the expansion waves from the nozzle lip are not intercepted completely by the conical plug and the escaped expansion fronts reflect as compressions from the opposite jet flow boundary (see shock front labelled (s_2 in Figs. 12 and 56(a)). In an ideal contoured plug-nozzle flow all the expansion waves pertaining to the pressure ratios upto the design pressure ratio, incident on the plug-surface are cancelled and as such in the underexpanded mode of operation ($\xi > \xi_d$), one would expect only one set of weak repetitive shock-structure formed by the expansion waves which escape beyond the plug-tip (See Fig. 32). Thus, it is reasonable to conclude that at $\xi > \xi_d$, the shock-associated noise generated by the solid conical plug-nozzle flow with its two independent families of repetitive shock structure be of higher level than that radiated by the contoured plug-nozzle flow. For comparison of the shock structure in spark shadowgraphs of the solid conical plug-nozzle and contoured plug-nozzle at $\xi = 4.0$ and 4.5, see Figs. 12 and 13. At some operating pressure ratios $\xi < \xi_d$, the shock structure may appear on the plug surface (see Figs. 9 and 10). Comparatively, the shock structure in the contoured plug-nozzle flow is less pronounced because of the cancellation of the incident expansion wave fronts by the initial part of the contoured plug. At pressure ratios $\xi < \xi_d$, the contour of the plug introduces compression waves only from the part of its surface lying beyond the terminating surface of the P-M expansion fan for the operating super-critical pressure ratio (see Fig. 32). Therefore, one may conclude that for the entire range of pressure ratio used in this study, the repetitive shock structure is comparatively more pronounced and stronger in conical plug-nozzle flows and the noise levels

from an equivalent solid conical plug-nozzle flow are comparatively higher than those from the contoured plug-nozzle flows. For experimental support of this argument, compare the OASPL vs θ variations of a contoured and an equivalent conical plug operated at $\xi = 4.5$ (Fig. 30).

The comparisons of the OASPL's vs θ for the conical and the contoured plug nozzles with those of a convergent nozzle operated at the same pressure ratios have shown that substantial noise reductions are achieved at all observer angles $15° < \theta < 120°$. Since at lower θ's generally the turbulent mixing noise is considered to be dominant, the observed reductions at such low angles, therefore, may be attributed to helpful flow modifications in the turbulent jet flows from the plug nozzles. Perhaps the mounting of a short centerbody such as a conical or a contoured plug with a pointed termination in a convergent nozzle has a stablizing effect on the underexpanded turbulent free jet flow from a convergent nozzle.

V.4. AEROACOUSTICS OF POROUS-PLUG-NOZZLE SUPERSONIC JET FLOWS.

The motivation for incorporating porosity in the plug-surface to affect shock-structure modifications and the suppression of shock-associated noise of improperly expanded jet flows issuing from plug-nozzles has been noted earlier (see p. 7). Here, the acoustic performance of the improperly expanded jet flows of a plug nozzle with perforated plugs is compared with that of an 'equivalent' plug-nozzle with a conical plug without perforations. The basic conical plug in each plug-nozzle configuration has the same shape and contour and are mounted as a centerbody in the same convergent nozzle. The acoustic performance of such improperly-expanded jet flows issuing from an externally-expanded plug nozzle with a non-perforated conical plug of pointed termination has been presented in the preceeding section V.3

The one-third octave SPL spectra were recorded when the conical plug had either 10 percent porosity ($\sigma = 10\%$) distributed evenly over the entire plug surface or four percent porosity ($\sigma = 4\%$) distributed evenly over the middle-third of the plug surface. The plug-nozzles with the perforated plugs were operated at pressure ratios $\xi = 2.0$ to 4.5. The specifications of the conical plug-nozzles used in these studies are summarized in Table 2, p.22. For the extent of the recorded experimental

data, see p.23 .

It should be noted that all the plug nozzles have the same annulus-radius-ratio K , the same basic convergent nozzle of radius R_N, and the same annulus width at the nozzle throat. Therefore, for the model plug-nozzles with either a conical plug of entire solid surface or a combination of solid/porous plug surface, the throat areas are the same and when operated at the same pressure ratios and same stagnation temperatures, the mass flow rates are matched.

V.4.1 Acoustic Results with Porous Plugs

Variations of the peak frequency with the observer angle θ , for the porous plug-nozzles at a pressure ratio of 3.6 (at which shockless flow of the contoured plug-nozzle was achieved) are shown in Fig.41 for 10% porosity and in Figure 43 for 4% porosity. For clarity, the one-third octave spectra at various angles are plotted on a sliding scale. The corresponding Strouhal numbers St. = $f_p W_t / V_j$ are plotted in Figs. 42 and 44, respectively. The following observations can be made about the variation of the peak frequency f_p (or St. number) with θ at various super-critical pressure ratios.

1. At $\theta > 60°$, the peak 1/3 octave SPL's occur around 10 kHz. The peak frequencies for the solid conical or contoured plug nozzles operated at the same pressure ratios are comparable and similar to those for the porous plug-nozzles. Compare figures 15, 35, 41 and 43.

2. Strouhal number vs. θ plots (Figs. 42 and 44) exhibit peaks and plateaus. For the same characteristic length W_t and pressure ratio, these also represent similar peaks and plateaus in the peak frequencies. The overall range of the variations in the St. number is between 0.05 to 0.43 with St. number approaching approximately 0.2 at $\theta \approx 120^{\circ}$

With 10% porosity, at ξ = 3.0 and ξ = 3.6, St. number peak = 0.44. For ξ = 3.6, a second peak in St. number = 0.42 occurs at $\theta = 105°$. St. number for both ξ = 3.05 and 3.6 reduce to 0.20 at $\theta = 120°$. For 4% porosity, at ξ = 3.6 a peak plateau is observed in the St. number = 0.35 for $\theta = 45°$ to $75°$. The St. number reduces to 0.2 at $105°$ to $120°$. Similar plateaus of St. number occur at ξ = 3.05 and 4.5 (see Figure 14.)

For $\theta \leq 30°$, the St. number approaches 0.05 for each of the pressure ratios and porosities.

Typical one-third octave SPL spectra at $\theta = 90°$ for the two porous plug-nozzles operated at $\xi = 3.05$, $\xi = 3.6$ and $\xi = 4.5$ are presented in Figs. 45, 46 and 47, respectively. For comparison, the corresponding SPL spectra for the equivalent P-N with a plug of solid surface have been included. The SPL's at a wide-range of band-center frequencies of plug nozzles with the porous plugs are noted to be lower than those for the equivalent plug-nozzle with the plug having solid surface.

The power level spectra of the porous plug-nozzles along with those of the solid conical P-N, are shown for $\xi = 3.05$, $\xi = 3.6$ and $\xi = 4.5$ in Figs. 48, 49 and 50, respectively. At $\xi = 3.05$, the 10% porosity results in lower PWL's as compared to those of the solid P-N and the effect of 4% porosity is noted to be minimal. At $\xi = 3.6$, by the presence of porosity, the PWL's are noted to be significantly reduced at higher band- center frequencies. In the underexpanded mode of operation ($\xi = 4.5$), the reduction in PWL's due to porosity are noted at all band-center frequencies for which the data were recorded. The level of reductions in PWL's for the 10% porosity, as compared to those for the solid conical plug, is about 2 to 3 dB, and for the 4% porosity about 1.5 to 2.5 dB. Therefore, the acoustic performance of the plug having 4% porosity distributed in the middle-third of the conical plug, is often noted to be sometime even better comparable to, sometimes even better then, that of the plug having 10% porosity distributed over the entire plug surface.

Beyond $f_c > 50$ kHz, the PWL's are observed to increase particularly at the higher operating pressure ratios. Moreover, the sharpest increase in PWL's occurs for the plug-nozzle with the solid conical plug. Therefore, the plug-porosity is not the root-cause of this increase. For the possible cause of this sharp increase at $f_c > 50$ kHz and the role of this increase in the analysis of the acoustic data, see Appendix I.

The variations of the OASPL at $\theta = 90°$, for a range of the operating pressure ratios both for the porous and the solid conical plug-nozzles are shown in Fig. 54. At different pressure ratios, due to porosity, noise-reductions of 1 to 4 dB are noted. In Fig. 55, ΔOASPL (= OASPL of the equivalent convergent nozzle minus OASPL of different plug nozzles used in this study) are plotted for $\theta = 120°$. For the entire range of

operating pressure ratios, reductions in the OASPL's of 2.5 dB to 11 dB of the underexpanded convergent nozzle flows are achieved by the use of the plug-nozzle with either a contoured plug or a short conical plug or a conical plug with porous surface. At pressure ratio ξ = 3.6, at which contoured plug-nozzle flow is shockless, the reduction in OASPL for the porous plug nozzle and the contoured plug nozzles are of the same order of magnitude.

When compared with the acoustic performance of improperly expanded jet flows from an equivalent convergent nozzle, the levels of the noise reductions noted in the present investigation of plug-nozzles with short solid/porous conical externally-expanded plugs with pointed terminations are comparable to the levels of noise reductions reported by Maestrello [22] and in a subsequent study by Kibens et al. [23]. As noted earlier, in these studies a combination of a convergent nozzle and long cylindrical porous center-bodies were used extending over almost the entire length of the supersonic parts of the jet flow. Aerodynamically, this type of nozzle configuration has weight and drag disadvantages. The geometrical configurations of the plug-nozzle in the present study are typical of a conventional plug-nozzle [24-26]. Thus, the noise suppression effects of the short solid and solid/porous plugs of pointed termination on the improperly expanded jet flows from plug-nozzles as noted in this investigation are of much greater significance from the point of view of engineering application in propulsion systems.

V.4.2. Observed Shock Modifications in Porous Plug-Nozzle Flows.

Typical spark shadowgraph of the improperly expanded jet flows issuing from the convergent nozzle, the plug-nozzle with a solid conical plug, the contoured plug nozzle, and the plug-nozzles with porous conical plugs operated at a range of pressure ratios are reproduced in Figs. 8-13. Each of these nozzles are operated at above critical pressure ratios ξ = 2.0, 2.5, 3.05, 3.6, 4.0, and 4.5, respectively.

The quantitative measurement of the shock angles from shadowgraphs of jet flows from different nozzles at the same pressure ratio and at the same location downstream of the respective nozzle throats shows that the shock angles of the repetitive shocks for a convergent nozzle are larger than those in the plug nozzle flows. Also, for ξ > 4.0, Mach reflection

with its normal shock-disk appears in convergent nozzle flows while in plug nozzle flows, the crossing shock fronts from opposite jet flow boundaries are oblique. This means that at the same pressure ratio, the shock structure in underexpanded jet flow of the convergent nozzle is stronger. At pressure ratio $\xi = 3.6$, the contoured plug nozzle flows are shock-free. Because of the cancellation of the incident expansion fronts from part of the plug surface, even at the off-design pressure ratios the shock structure in contoured plug-nozzle flows is much weaker than in convergent nozzle jet flows operated at the same pressure ratio.

The shock-modifications by the porosity of the plug surface are affected essentially by the following two factors:

(a) Interaction of Waves of Opposite Polarity:

The reflection of wave fronts (may these be compressions or expansions) incident on a solid surface meet the condition that the flow follows the surface. Therefore, a compression wave front incident on the solid surface reflects as a compression and an expansion front reflects as an expansion. On the other hand for a freely expanded jet flow the pressure along the jet boundary is constant and, therefore, an incident compression front reflects as an expansion and an incident expansion, as a compression.

Over the porous plug surface both the flow direction and constant pressure conditions need to be satisfied from the successive adjacent parts of the plug. Thus, the expansion rays of the fan originating at the nozzle lip will impinge in sequence on the porous and the solid parts of the surface of the porous plug and these will reflect as compressions and expansions, respectively (See illustrations in Fig. 56(b)). These waves on reaching the free jet boundary are reflected as waves of opposite polarity. Thus, the flow field is closely interspersed with the cross-crossing wave fronts of opposite nature of pressure changes, some diverging and some converging and, thus, mutual weakening of the expansion and compression wave fronts occurs. If and when any coalescence of the compression fronts develops, it results in weak oblique shock structure. For illustrations, see flow sketch of Fig. 56(b), which corresponds to the wave weakening visible in shadowgraphs of Fig. 12, $\xi = 4.0$ for porous ($\sigma = 10\%$) plug-nozzle flow.

(b) The Two-Family Shock Structure

In jet flows from a plug-nozzle having a plug of solid surface, the reflections of the incident expansion waves as expansions from the plug surface and their reflections as compressions from the free jet boundary lead to the formation of a repetitive shock structure in the flow (see shocks labelled s_1 in spark shadowgraphs of Figs. 9-13, and the shock labelled s_1 in the flow sketch of Fig. 56. Since the length of the conical plug is shorter than that of the contoured plug, at the same operating pressure ratio ($\xi > \xi_d$) the conical plug fails to intercept some of the expansion waves emanating from the nozzle lip. The escaped waves reflect as compressions wave fronts from the opposite free jet flow boundary; these compression wave fronts may coalesce and form a shock front and finally a second family of repetitive shock cell system is formed (see shock labelled s_2 in Figs. 9-13 and the shock labelled s_2 in flow sketch shown in Fig. 56).

The two independent families of the repetitive shock structure of different origins may be weakened because of the criss-crossing of waves of opposite polarity. Thus, by appropriate use of porosity on short conical plugs, nearly shock-free improperly-expanded plug-nozzle jet flows can be achieved.

As stated before, the focus of these experiments was to study the noise suppression role of plug-nozzles with short plugs as centerbodies. Therefore, to have a conical plug nozzle not any longer than the contoured plug-nozzle, the conical plug used was selected to have the same surface area and annulus radius ratio as the contoured plug. Due to geometrical closeness of the conical plug to the contoured plug, the shock structure in the conical plug-nozzle flows at off-design conditions was weak to start with. As a result, in these studies, the role of porosity of the plug in introducing shock modifications and achieving reduction of shock-associated noise was found to be less important than just the presence of the short conical solid plug as a centerbody. However, should practical considerations dictate the use of a conical solid plug which is of substantially different geometrical specifications than a contoured plug (say a plug of larger annulus-radius ratio K and/or of larger length ratio L_{max}/R_n as compared to the corresponding specifications of either the solid conical plug or the contoured plug used in this study) then the

repetitive shock structure in the jet flows will be more prominent and stronger. For improperly expanded jet flows from such plug-nozzles, the modifications and weakening of the shock structure due to plug-porosity and the reductions achieved in the shock-associated noise are likely to be more significant than was observed to be the case for the conical plug used in the present study.

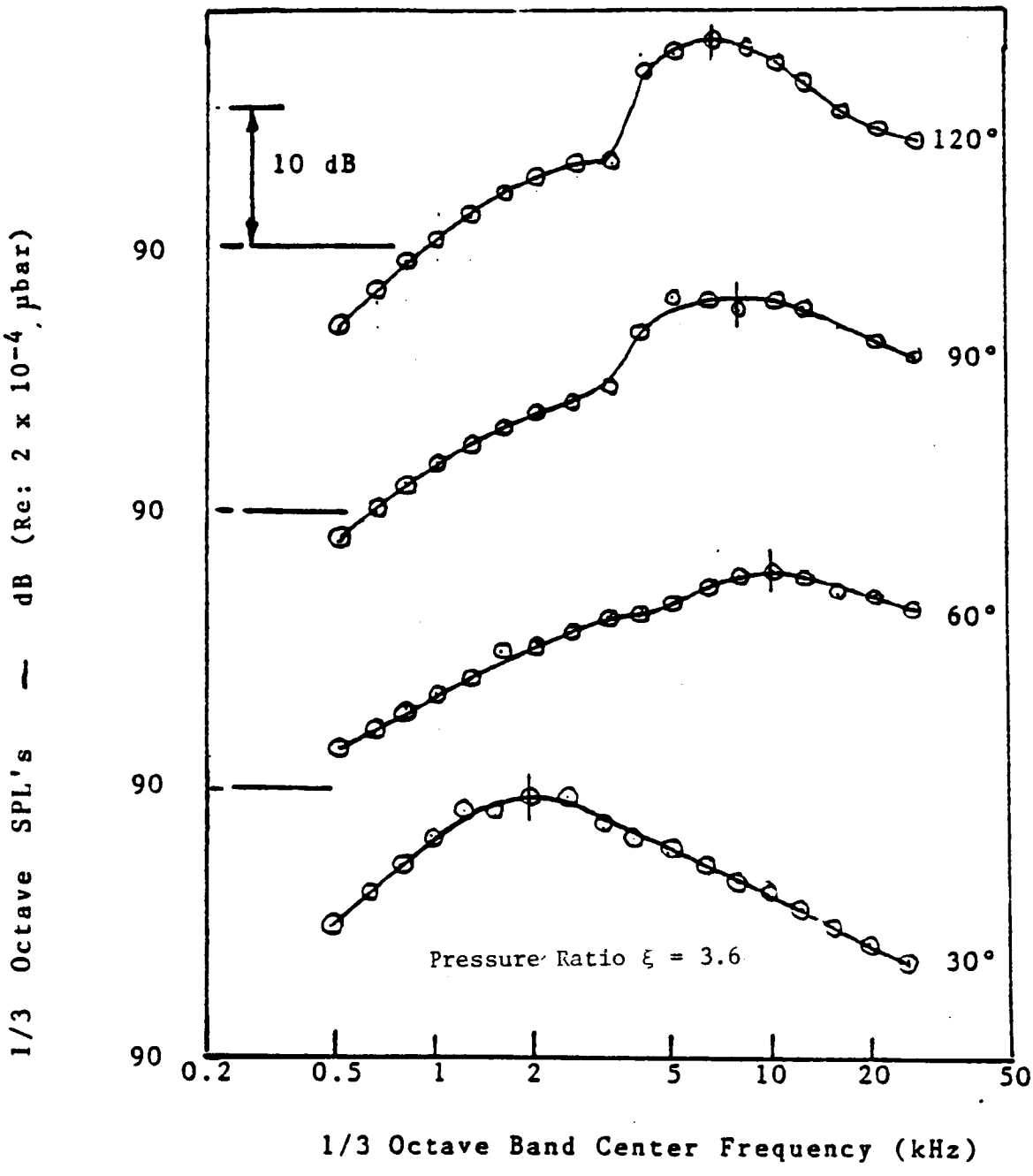

Fig. 41 Variation of Peak-Frequency with Azimuthal Angle for the Ten Percent Porosity Conical Plug-Nozzle Jet Flow

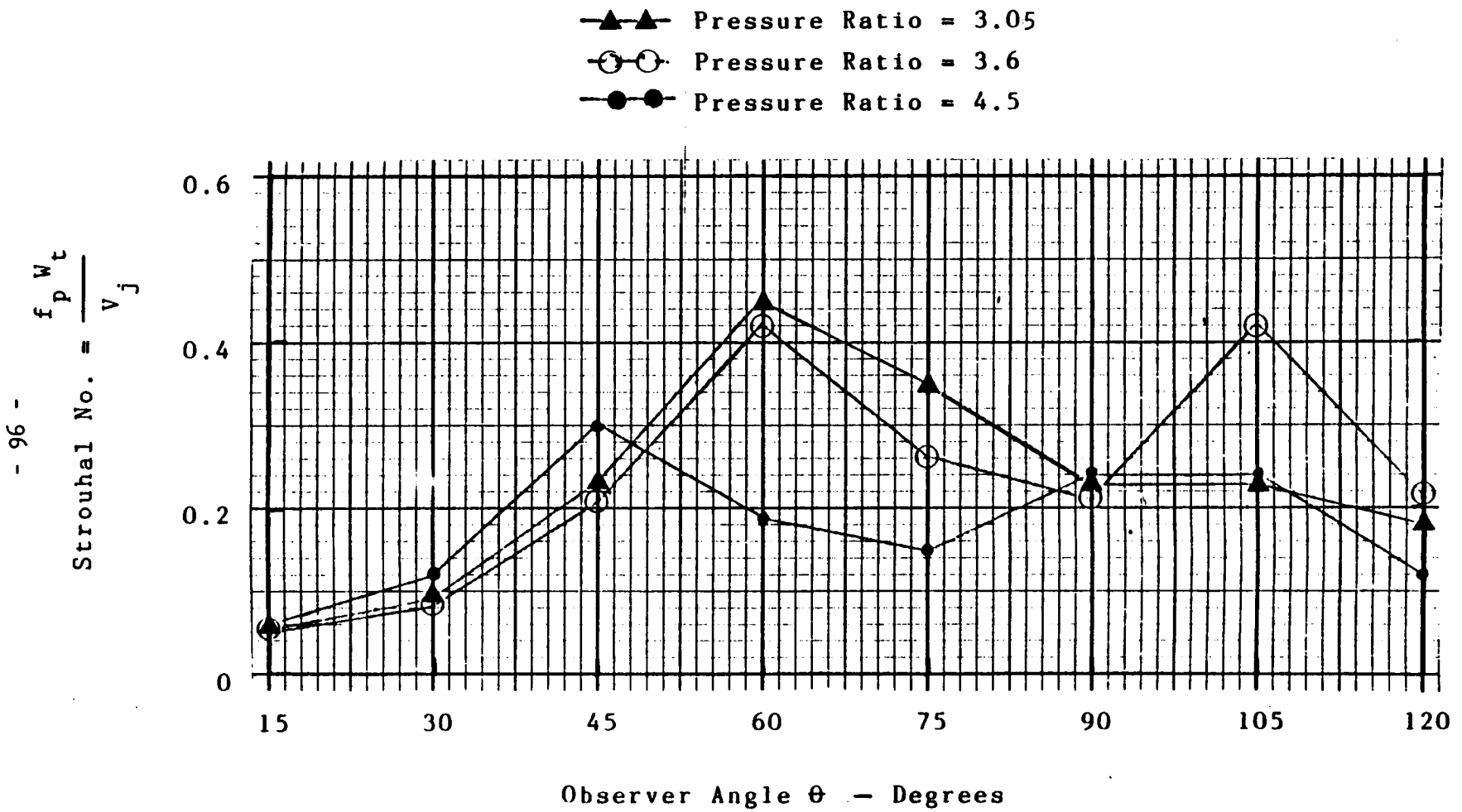

Fig. 42 Variation of Strouhal Number with Azimuthal Angle for the Ten-Percent Porosity-Conical Plug-Nozzle Jet Flows at Different Pressure Ratios.

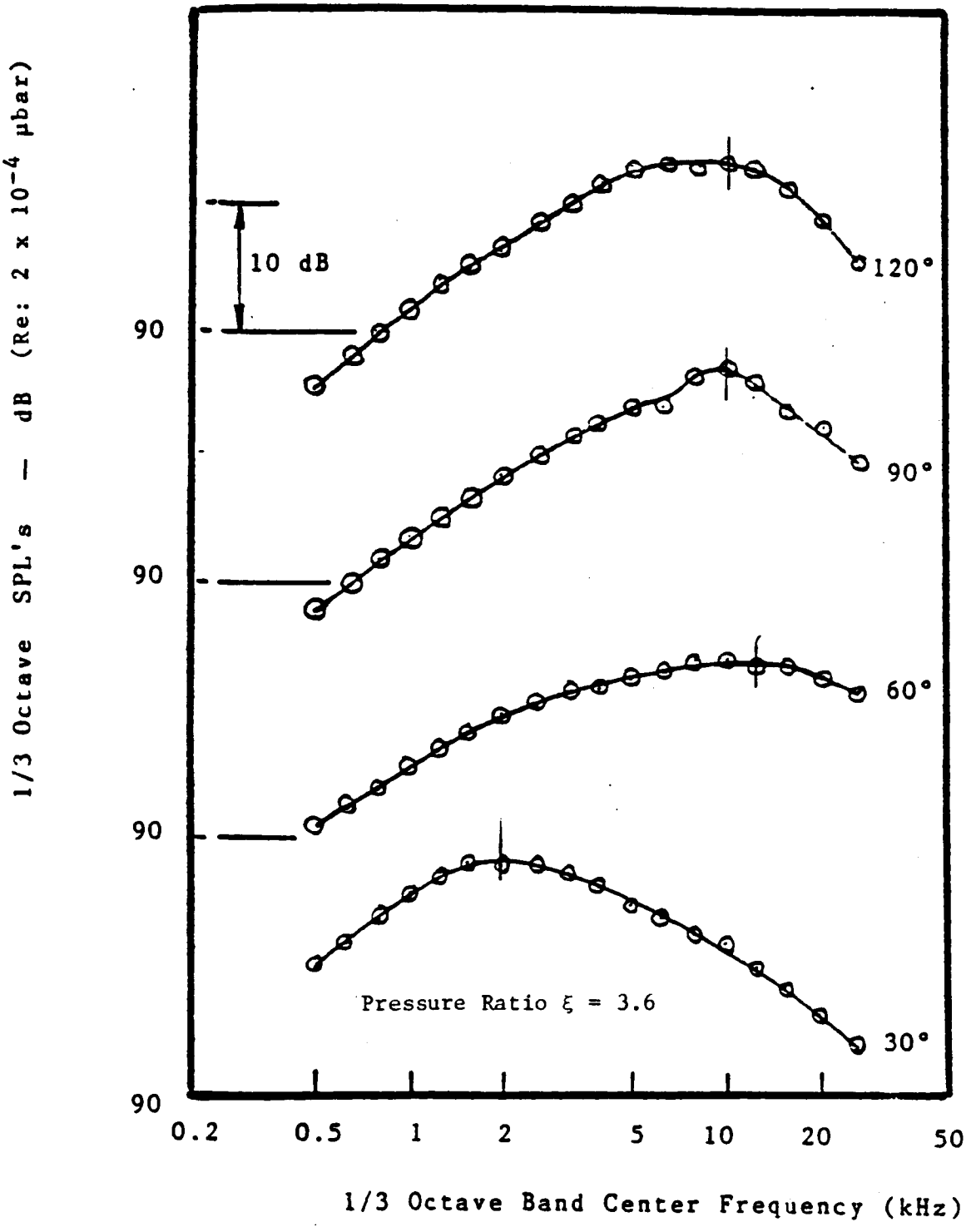

Fig. 43. Variation of Peak-Frequency with Azimuthal Angle for the Four Percent-Porosity-Conical Plug-Nozzle Jet Flow.

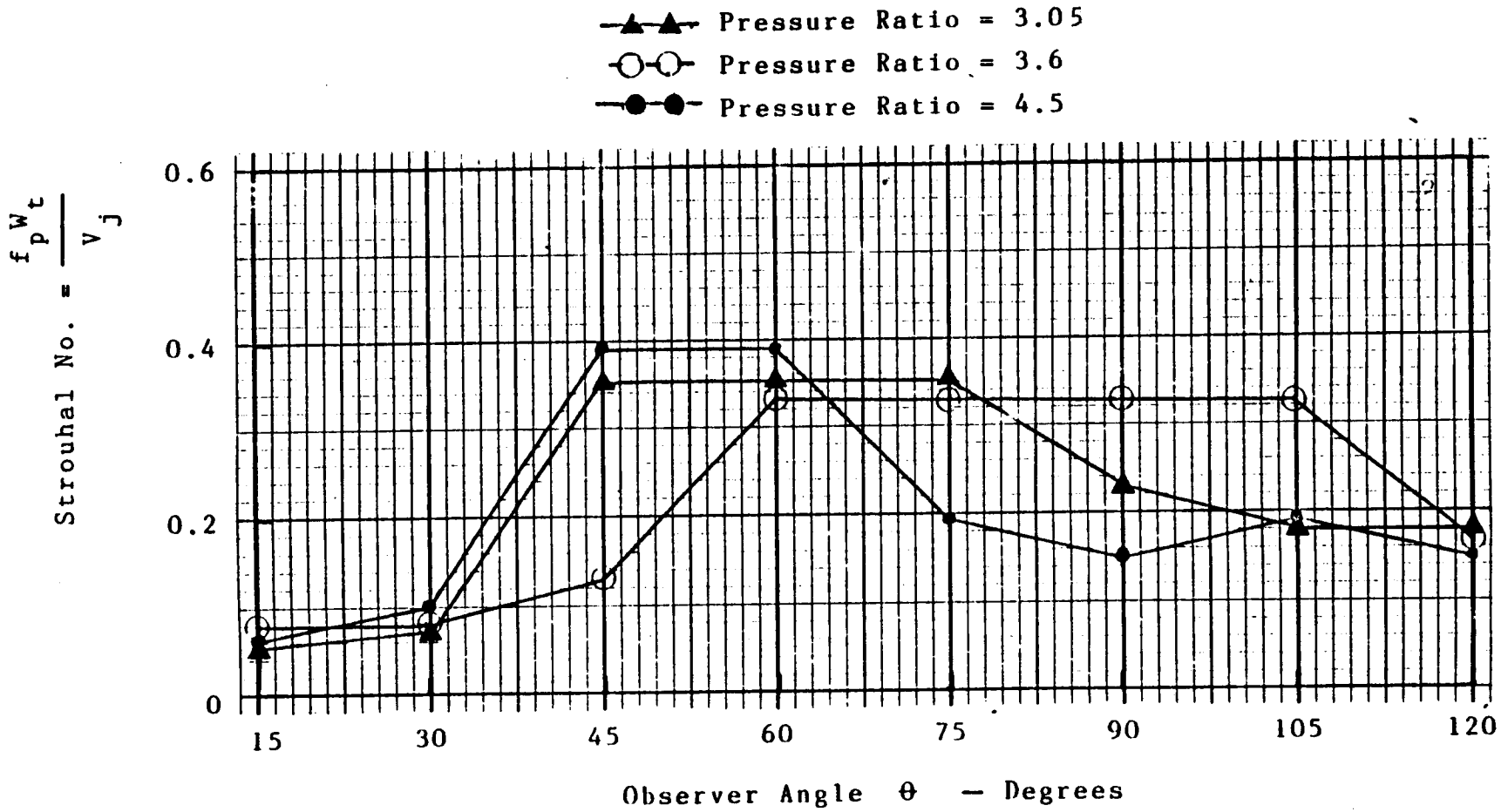

Fig. 44 Variation of Strouhal Number with Azimuthal Angle for the Four-Percent Porosity-Conical Plug-Nozzle Jet Flows at Different Pressure Ratios.

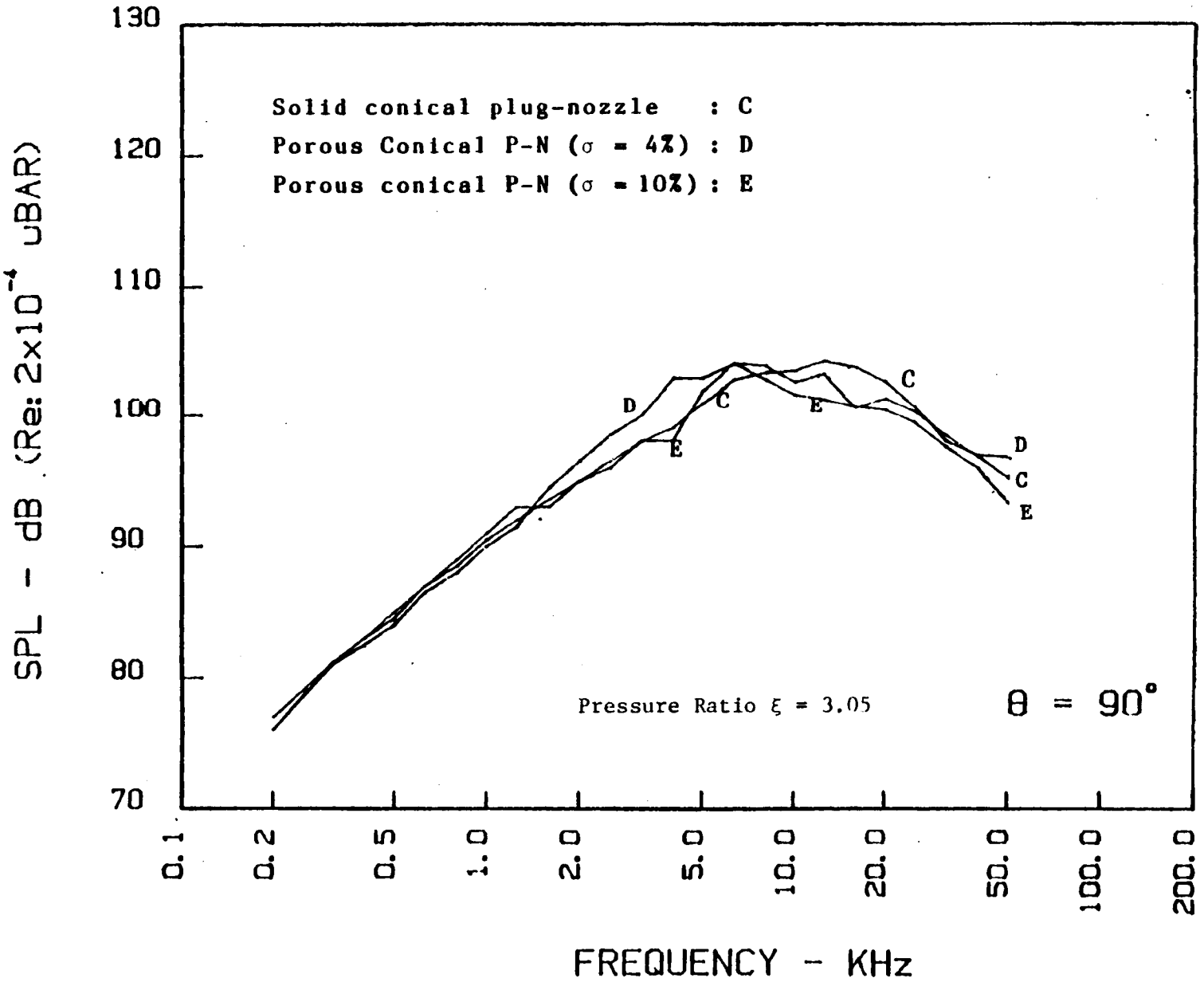

Fig. 45 One-Third Octave Sound Pressure Level Spectra at Azimuthal Angle $\theta = 90^{o}$ of the Solid and Porous Conical Plug-Nozzle Jet Flows.

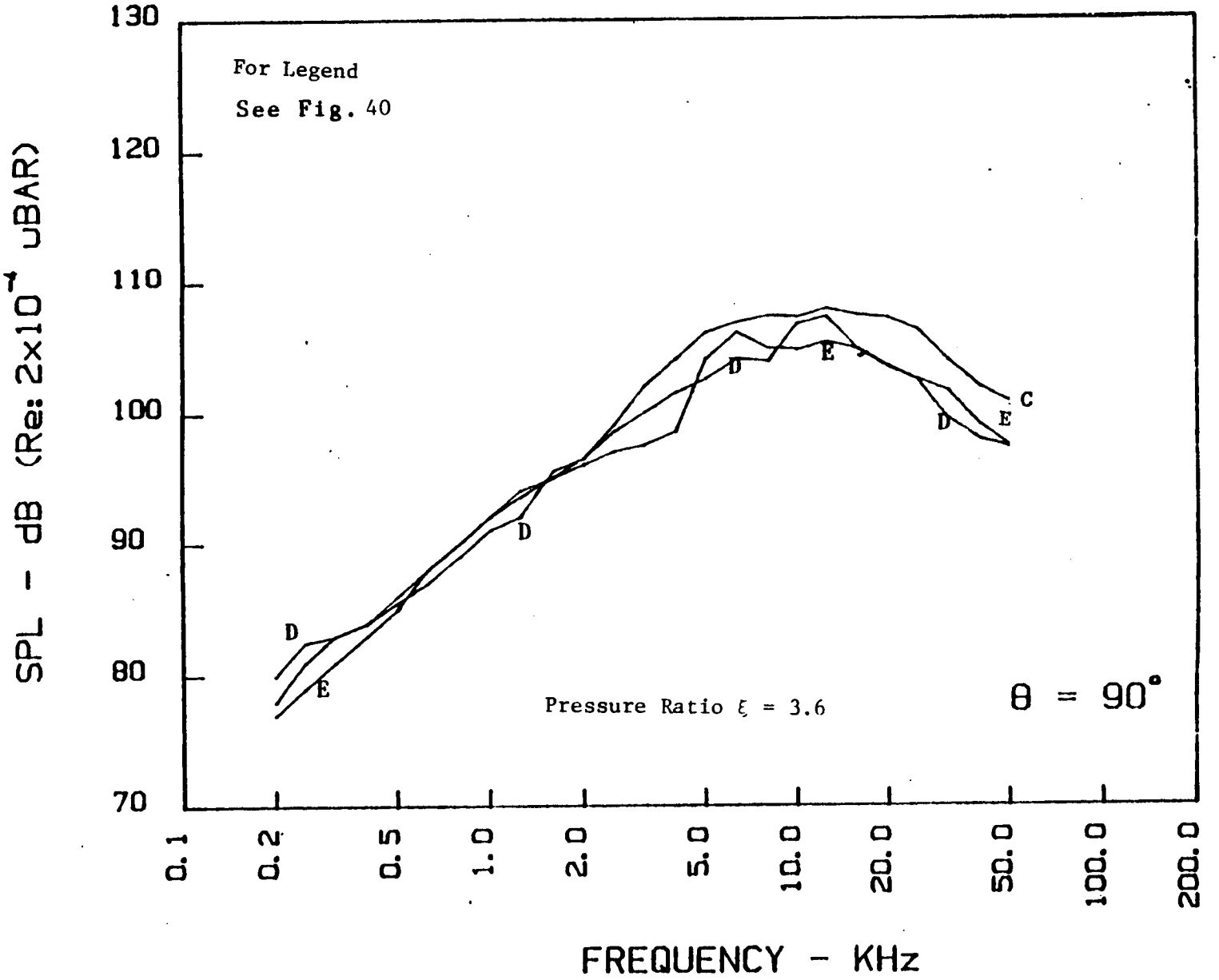

Fig. 46. One-Third Octave Sound Pressure Level Spectra at Azimuthal Angle $\theta = 90^{\circ}$ of the Solid and Porous Conical Plug-Nozzle Jet Flows.

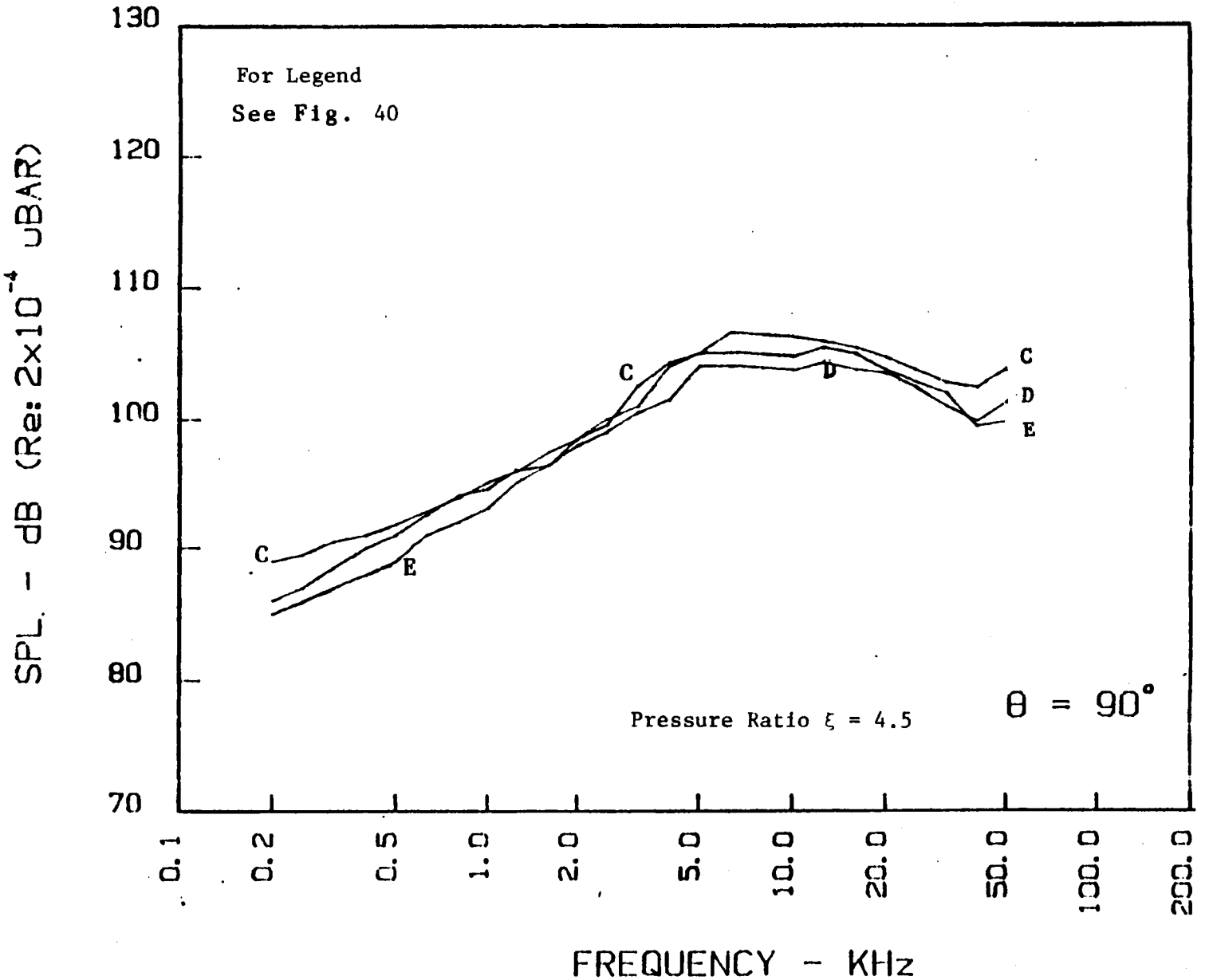

Fig. 47. One-Third Octave Sound Pressure Level Spectra at Azimuthal Angle $\theta = 90^{\circ}$ of the Solid and Porous Conical Plug-Nozzle Jet Flows.

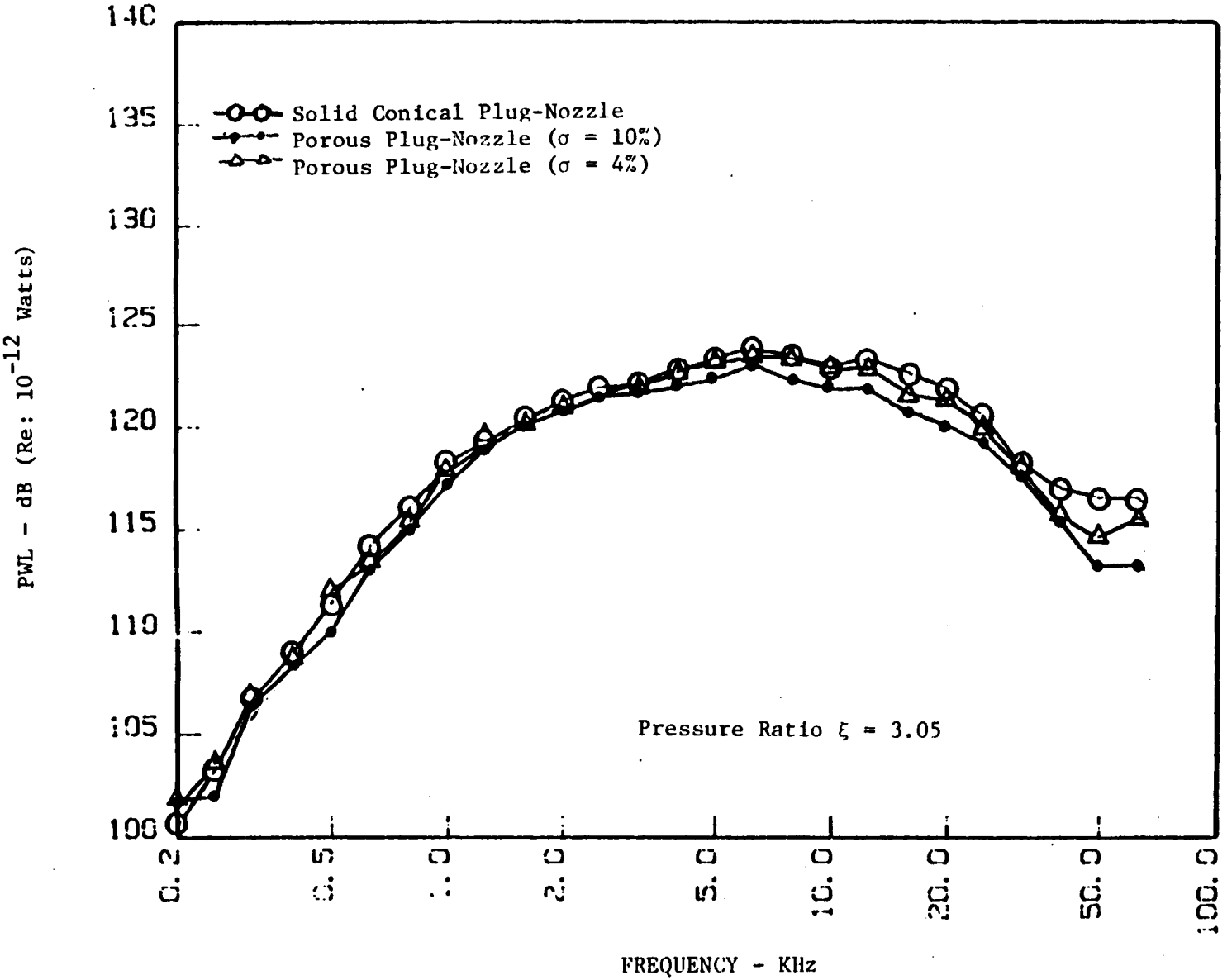

Fig. 48. Comparison of Power Watt Level Variations with Frequency for the Solid and Porous Conical Plug-Nozzles.

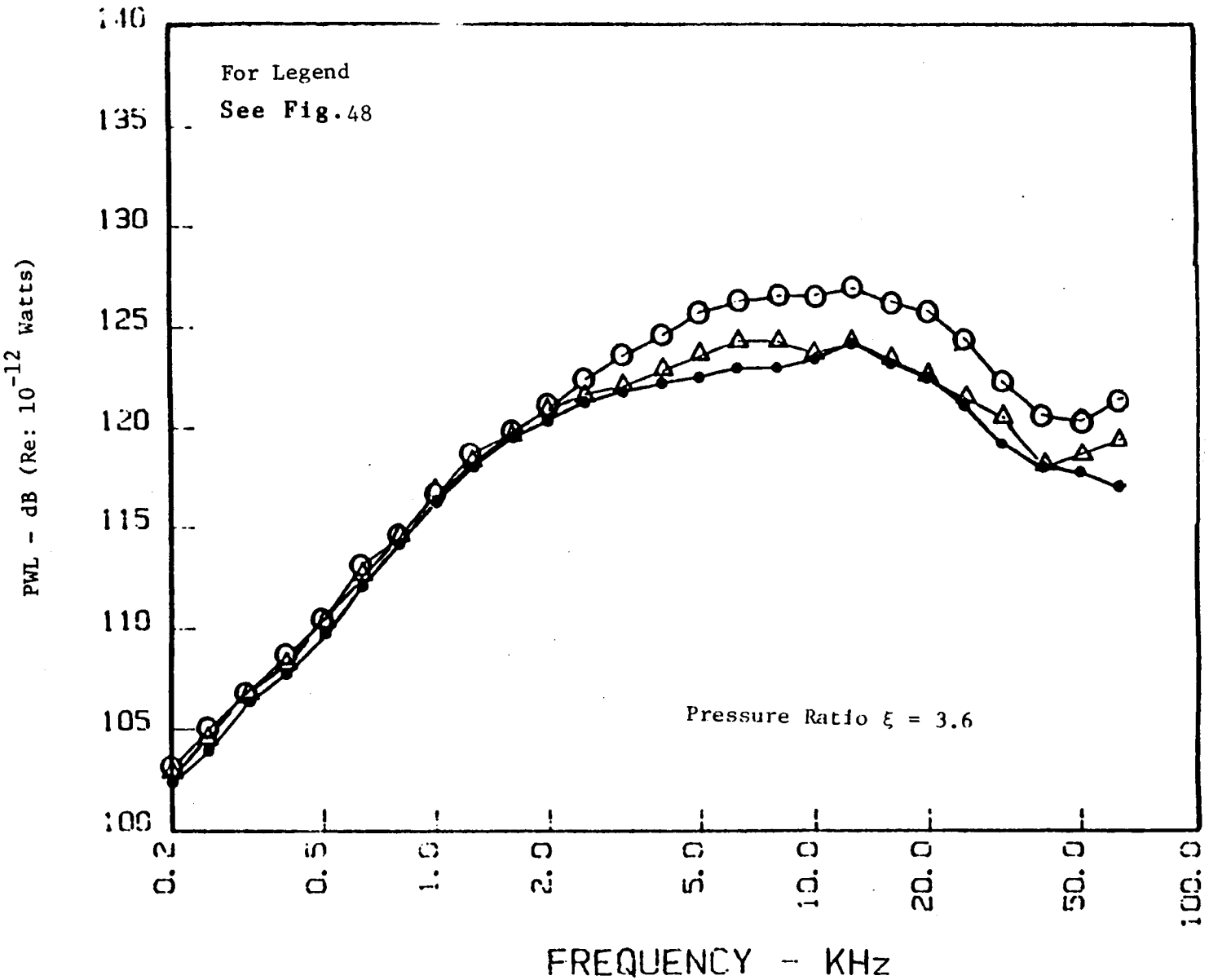

Fig. 49 . Comparison of Power Watt Level Variations with Frequency for the Solid and Porous Conical Plug-Nozzles.

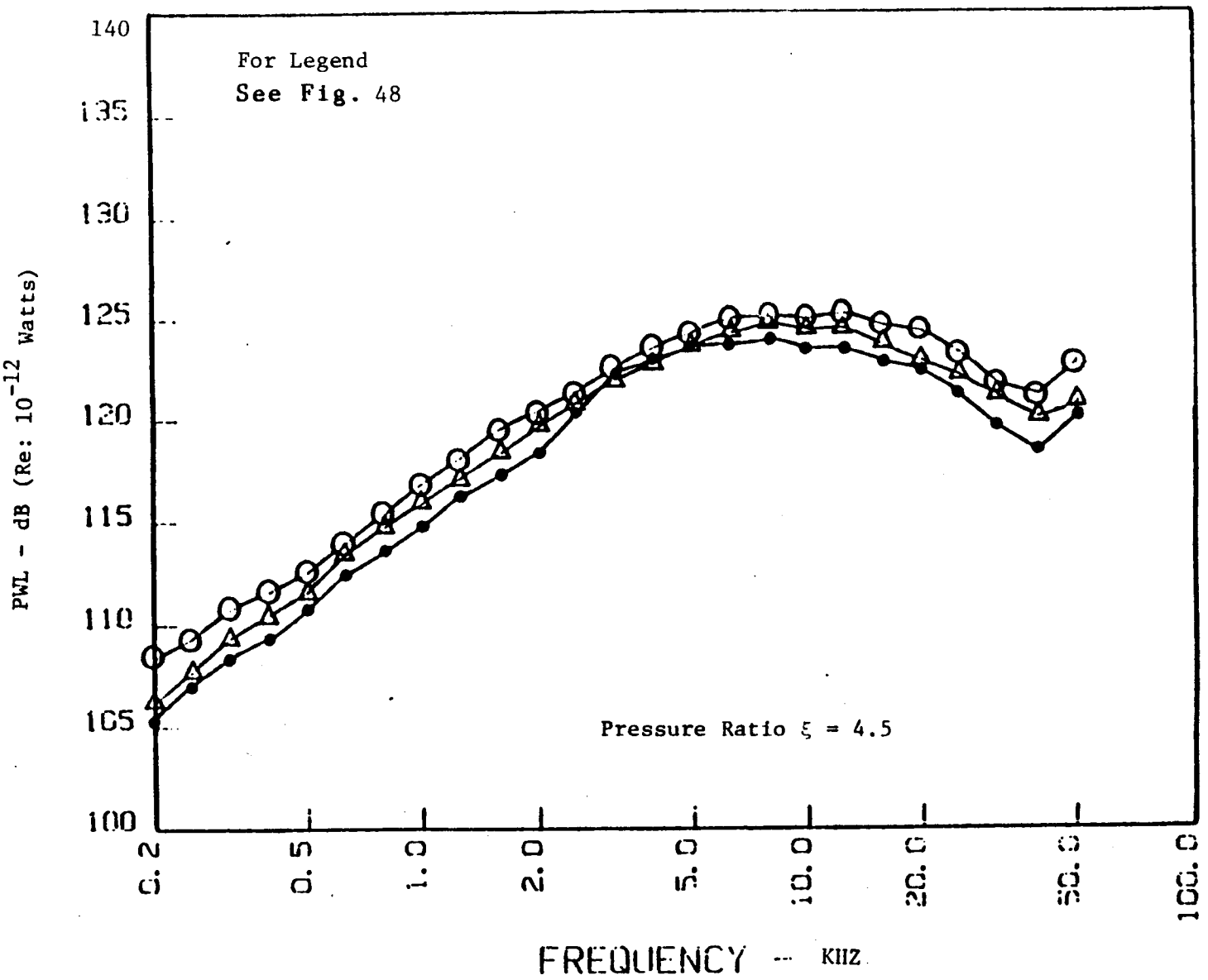

Fig. 50. Comparison of Power Watt Level Variations with Frequency for the Solid and Porous Conical Plug-Nozzles.

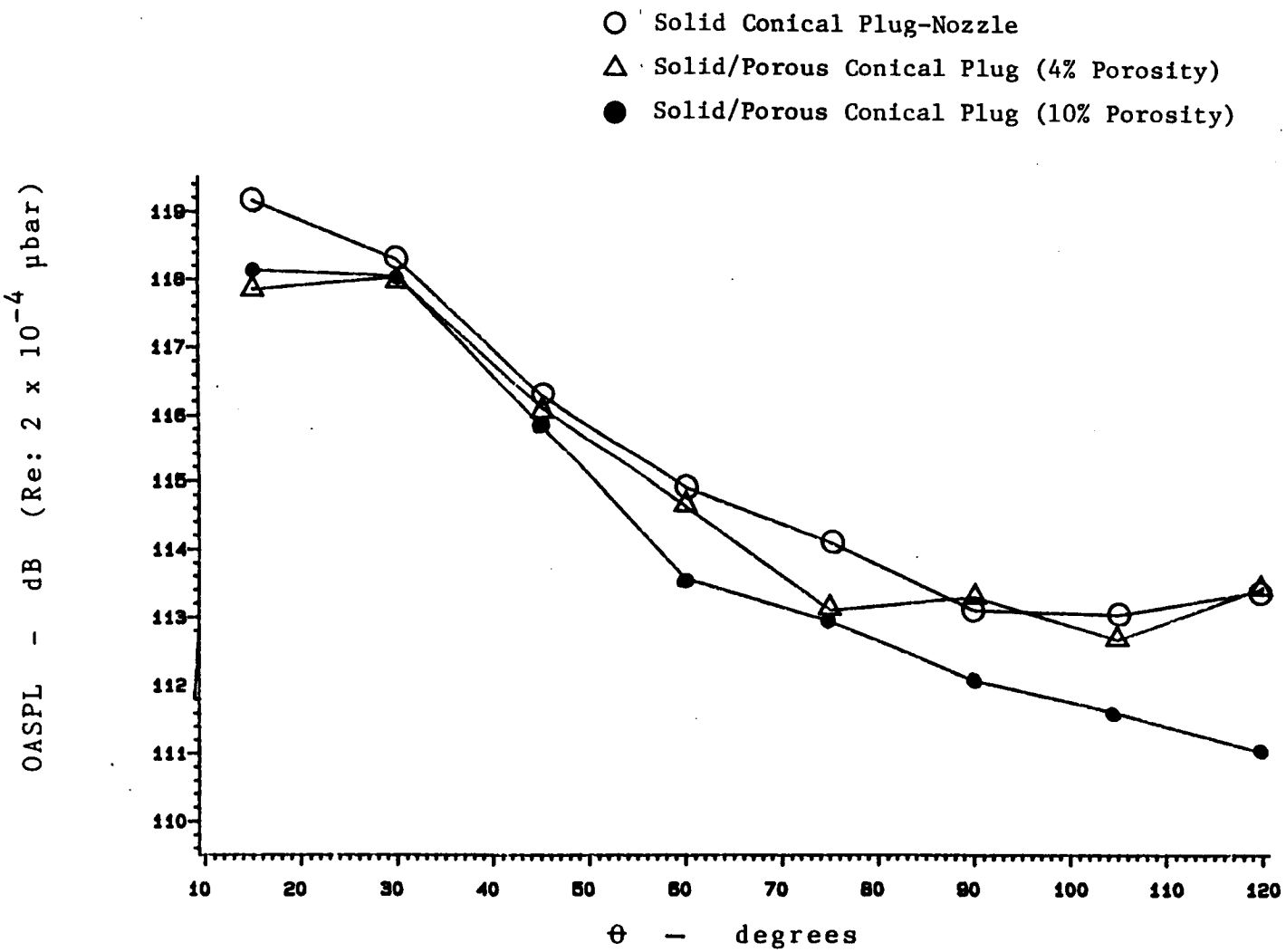

Fig. 51 Comparison of Overall Sound Pressure Level vs Azimuthal Angle of Solid and Porous Conical Plug-Nozzle Flows at Pressure Ratio $\xi = 3.05$

For Legend

see **Fig. 51**

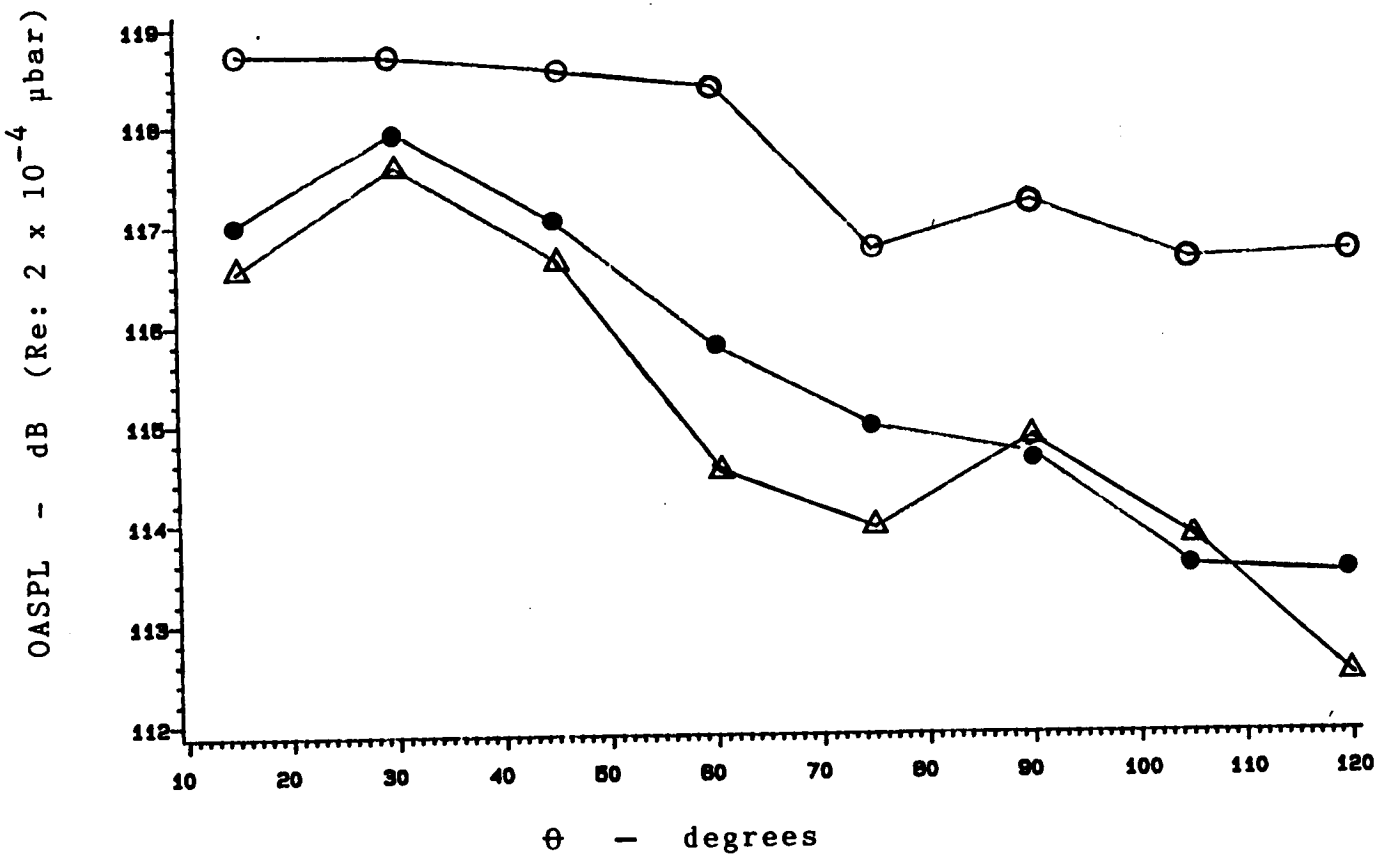

Fig. 52 Comparison of Overall Sound Pressure Level vs Azimuthal Angle of Solid and Porous Conical Plug-Nozzle Flows at Pressure Ratio $\xi = 3.60$

For Legend
see **Fig.** 51

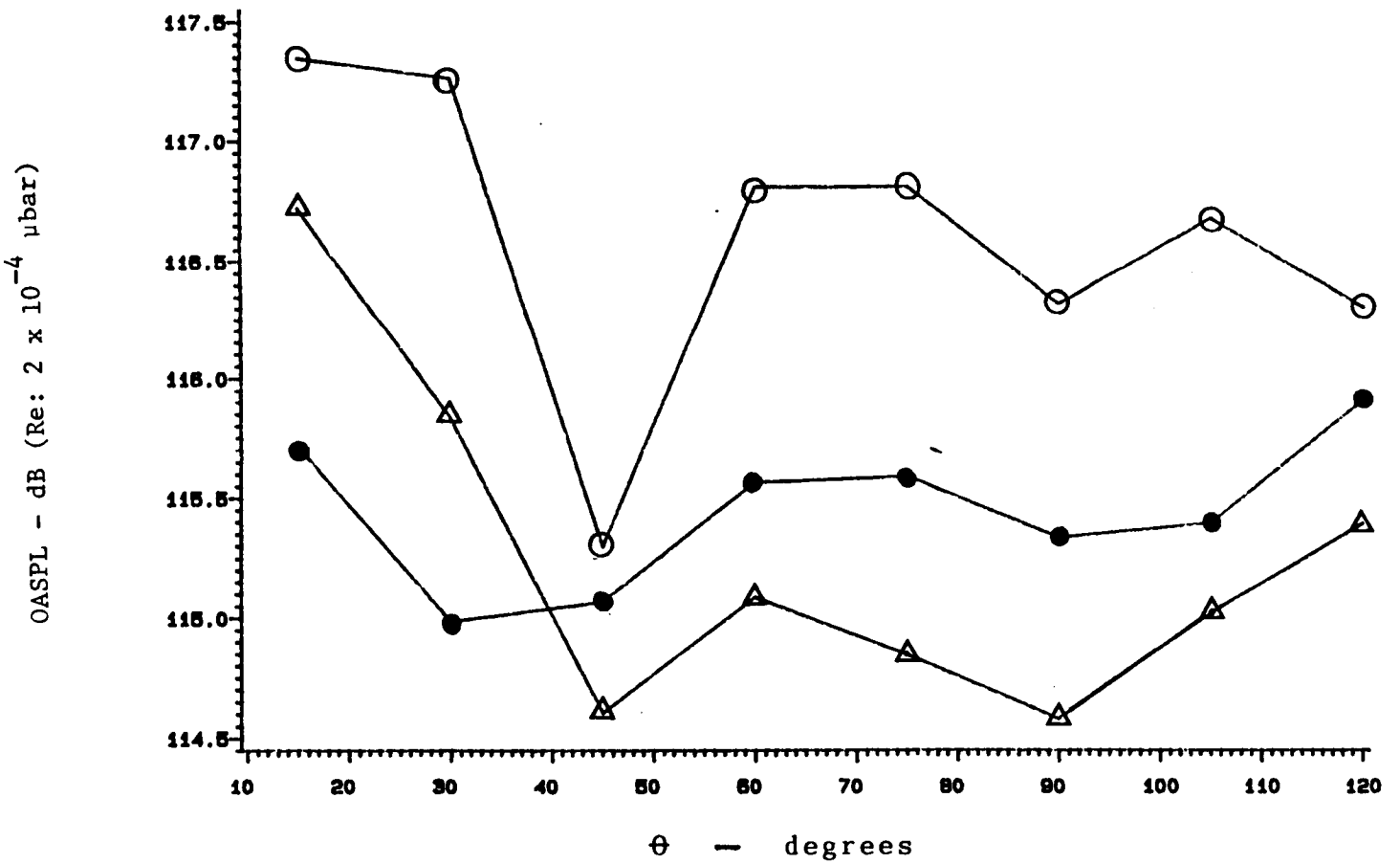

Fig. 53 Comparison of Overall Sound Pressure Level vs Azimuthal Angle of Solid and Porous Conical Plug-Nozzle Flows at Pressure Ratio $\xi = 4.5$

For Legend
see Fig. 51

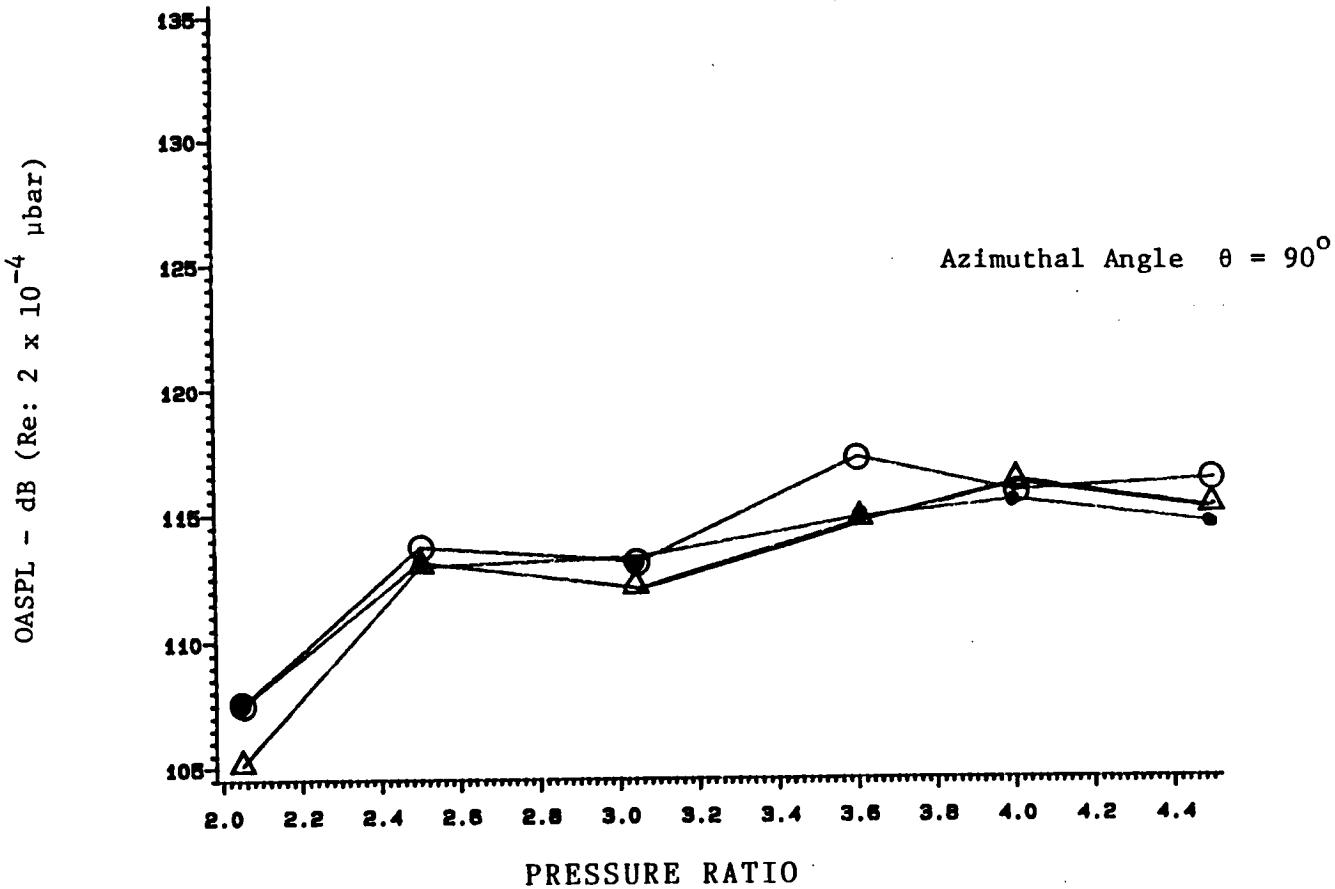

Fig. 54 Overall Sound Pressure Level Variation at a Range of Pressure Ratios of Solid and Porous Conical Plug-Nozzle Jet Flows.

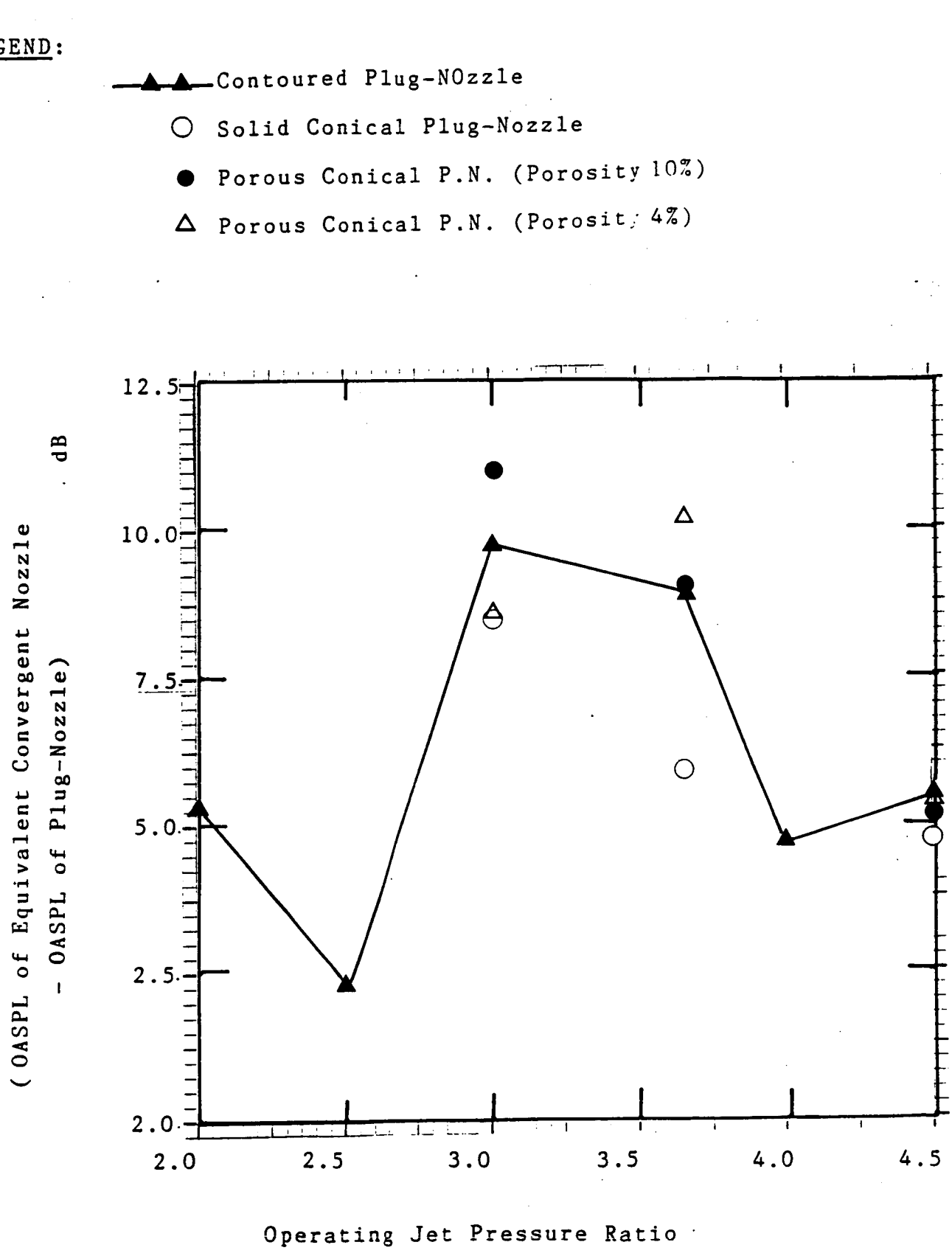

Fig. 55. Shock-Associated Noise Suppression of Various Plug-Nozzle Jet Flows as Compared to the Equivalent Convergent Nozzle at Azimuthal Angle $\theta = 120^{\circ}$.

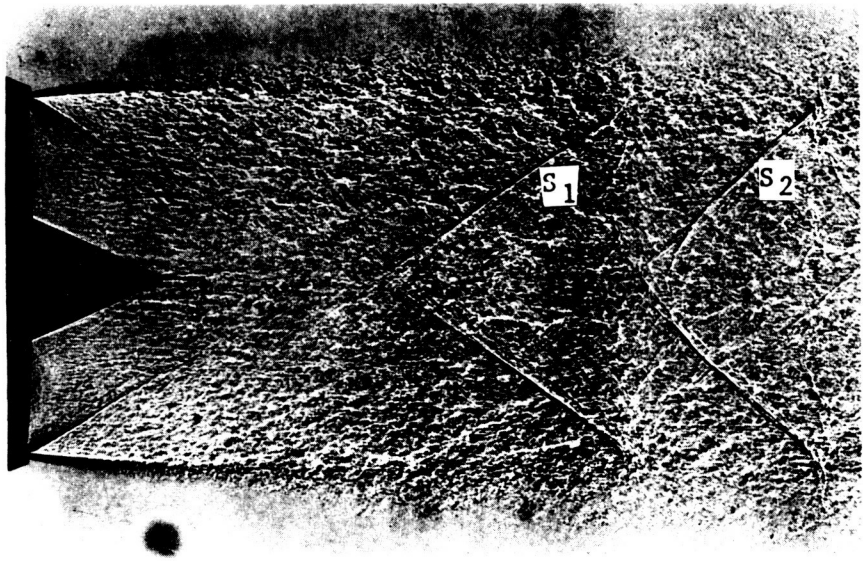

Solid Conical Plug-Nozzle (ξ=4.0)

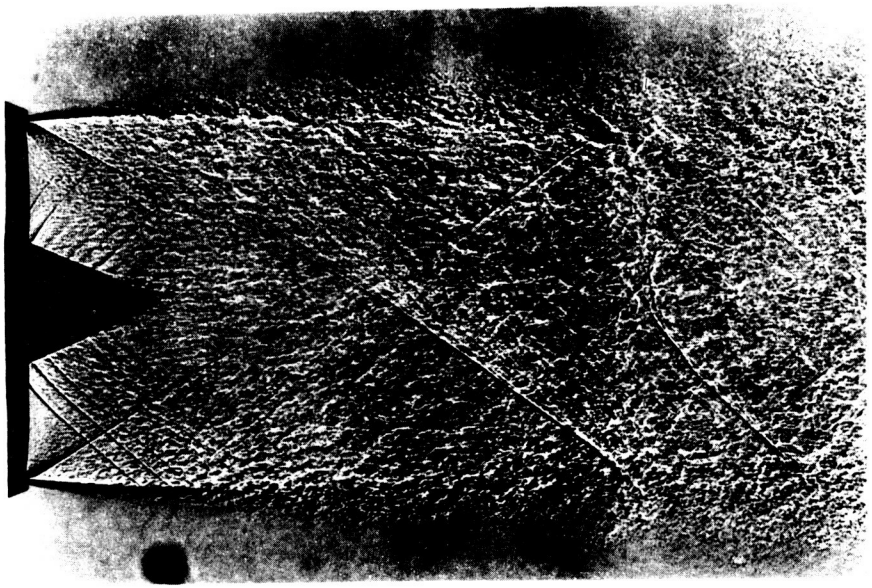

Porous Conical Plug-Nozzle (ξ=4.0 ,σ=10%)

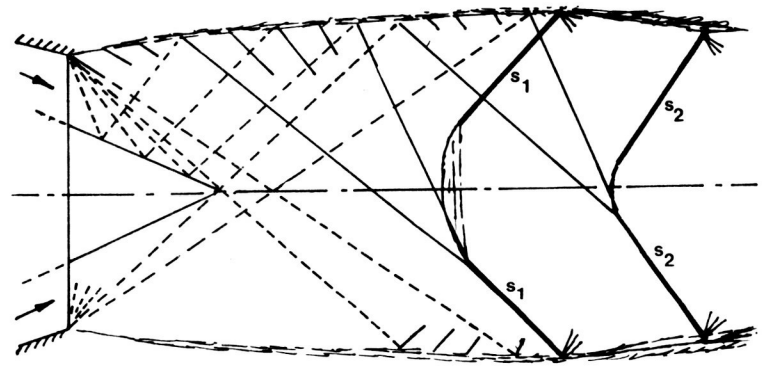

Typical wave structure in solid conical plug-nozzle flow

(a) s_1-shock formation due to solid surface reflections
s_2-shock due to reflections not intercepted by the plug

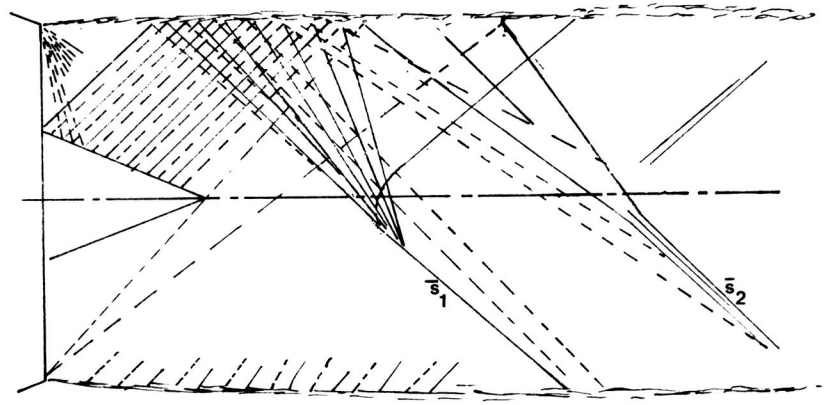

Shock modifications in porous plug-nozzle flow

(b) $\bar{s}_1$-weakened shock s_1 due to porosity
$\bar{s}_2$-degeneration of shock s_2 intc aset of compression waves

Fig. 56 Shock structure Modifications of Underexpanded Jet Flows from Solid and Porous Plug-Nozzles.

VI. CONCLUSIONS

1. The noise levels (SPL's, OASPL's, and PWL's) radiated by the fully-expanded (shockless) jet flows issuing from an externally-expanded contoured plug-nozzle with a pointed plug termination are substantially lower than those from underexpanded jet flows of an equivalent convergent nozzle operated at the same pressure ratio. The OASPL reduction of around 10 dB have been consistently observed at all angular locations $15° < \theta < 120°$ measured with respect to the downstream jet axis. At higher observer angles, these reductions are attributable to the suppression of the shock- associated noise. By similar comparison, significant levels of noise reductions are also observed even when the contoured plug nozzle is operated at a range of off-design pressure ratios in the over- and the underexpanded modes. It is shown that the repetitive oblique shock structure in both the over- and the underexpanded plug-nozzle jet flows is weaker than that in the underexpanded jet flows from an 'equivalent' convergent nozzle operated at the same pressure ratio.

2. The acoustic data gathered for the fully-expanded (shockless) jet flow issuing from a contoured externally expanded plug-nozzle with a pointed plug-termination and annulus-ratius-ratio $K = R_p/R_N = 0.43$ operated at pressure ratio $\xi \doteq 3.6$ are tabulated in (Appendices III lossless) and IV (uncorrected). The lossless acoustic data for the contoured plug-nozzle are used as the baseline data for comparative assessment of the acoustic performance of supersonic jet flows issuing from equivalent plug-nozzles of various configurations operated at a range of super-critical pressure ratios $2.0 \leq \xi \leq 4.5$.

3. The processes of the development of the flows of (a) an underexpanded jet from a convergent nozzle, (b) the over- and underexpanded jet flows from a C-D nozzle operated with its exit flow to be at the design Mach number and (c) a contoured plug nozzle operated in the over- and the underexpanded modes result in shock structures of different configurations and strengths. Therefore, the acoustic performance of the improperly expanded jet flows from the contoured plug-nozzle operated at off-design pressure ratios does not follow either the Harper-Bourne and Fisher scaling for the underexpanded jet flows from a convergent circular nozzle or the Tam-Tanna scaling for the over- and the

underexpanded jet flows from a convergent-divergent symmetric nozzle of a given design Mach number. For the contoured plug-nozzle jet flows, the overall Sound Pressure Levels at either $\theta = 90^{o}$ or 120^{o} over a range of pressure ratios (ie., OASPL's mostly for shock-associated noise) varied approximately as β^2 where shock- strength parameter $\beta = (M_j^2 - 1)^{1/2}$ and not as β^4 as observed by Harper- Bourne and Fisher for the underexpanded jet flows from convergent round nozzles. Similarly for the contoured plug nozzle OASPL's vary approximately as β_*^2 where $\beta_* = (M_j^2 - M_d^2)^{1/2}$ and not β_*^4 as observed by Tam- Tanna [2] for the contoured C-D nozzle jet flows.

4. The aeroacoustic performance of an externally-expanded plug-nozzle with a short solid conical plug of a pointed termination having the same annulus-radius-ratio K, the same throat area, and the same surface area as a contoured plug-nozzle (and thus even shorter than the contoured plug) when operated at the same pressure ratio as a contoured plug is noted to be fairly close to that of the contoured plug-nozzle. The noise levels for the solid conical plug nozzle, though higher, are within 3 dB of the contoured plug-nozzle when operated at the same pressure ratio. Therefore the presence of such short conical plugs with pointed termination in the convergent nozzle itself, acts as an effective suppressor of noise radiated by the improperly expanded jet flows issuing from a convergent nozzle.

5. The evenly distributed porosity over either the entire or the middle third of the plug-surface results in the weakening of the repetitive cellular shock structures in the improperly expanded jet flows of the plug-nozzles having short conical plug of pointed termination. The attendant reductions in the shock-associated noise component are achieved. The reductions in OASPL for the porous short conical plugs as compared to the solid conical plug of the same geometry but without perforations, are noted to be of the order of 2 to 3 dB. If the solid conical plug were to be of a markedly different contour and shape from those of a contoured plug, stronger repetitive shock structure will be present in the conical plug-nozzle jet flows. Because of porosity, the modifications in the shock-structure and the resulting shock-associated noise reductions may be more significant.

6. The conical plug having a porosity of 4% distributed only over the middle-third of the plug surface is found to have an aeroacoustic performance often comparable to that of the same plug having a porosity of 10% distributed over the entire surface of the plug.

7. The noise reductions achieved through the use of porosity over a short solid conical plug with pointed termination are often comparable to those observed for a contoured plug operated at design or at slightly off-design conditions where only weak repetitive shock structures are present. This suggests that by judicious selection of the plug contour, shape, annulus- radius-ratio K, length and the extent and the distribution of porosity, the shock structure in improperly expanded jet flows issuing from plug- nozzles can be modified and weakened to approach those of a contoured plug at its design pressure ratios. Therefore, to achieve noise reductions in improperly expanded jet flows, the use of an externally-expanded plug-nozzle with a short conical porous plug of pointed termination, is an attractive alternative to either a contoured plug-nozzle or a contoured convergent-divergent nozzle operated at their respective off-design conditions.

VII. REFERENCES

1. Powell, A., "On the Mechanism of Choked Jet Noise", Proc. Phys. Soc., Vol. 66, Pt. 12B, pp. 1039-1056, 1953.

2. Dosanjh, D.S. and Yu, J.C., "Noise from Underexpanded Axisymmetric Jet Flows Using Radial Jet Flow Impingement", Proceedings of AFOSR-UTIAS Symposium Toronto, May 1968. Ed. H. Ribner; University of Toronto Press.

3. Nagamatsu, H.T., and Horvay, G., Supersonic Jet Noise, AIAA Paper No. 70-237, 1970.

4. Plumblee, Harry E., The Generation and Radiation of Supersonic Jet Noise Vol. 1 (Summary), Tech. Rept. AFAPL-TR-76-65, June 1976.

5. Seiner, J.M., "Advances in High Speed Jet Aeroacoustics", AIAA/NASA 9th Aeroacoustics Conference, Oct. 1984, Paper No. AIAA-84-2275.

6. Lighthill, M.J., "On Sound Generated Aerodynamically I. General Theory," Proc. R. Soc., London, A., Vol. 221, pp. 564-587, 1952.

7. Vertel, H., "Coherent Structures Producing Mach Waves Inside and Outside of the Supersonic Jet." Proc. of Structure of Complex Shear Flows, Berlin, Springer-Verlag, 1983/

8. Harper-Bourne, M. and Fisher, M.J., "The Noise from Shock Waves in Supersonic Jets", AGARD-CP-131, 1973.

9. Norum, T.D., "Screech Suppression in Supersonic Jets", AIAA J., Vol. 21, No. 2, 1983.

10. Lighthill, M.J., "On the Energy Scattered from the Interaction of Turbulence with Sound or Shock Waves", Proceedings of the Cambridge Philosophical Society, Vol. 49, 1953.

11. Ribner, H.S., "Cylindrical Sound Waves Generated by Shock-Vortex Interaction", AIAA J. Vol. 23, No. 11, 1985.

12. Dosanjh, D.S. and Weeks, T., "Interaction of a Starting Vortex as well as a Vortex Street with a Travelling Shock Wave," AIAA J., Vol. 3, Feb. 1965.

13. Dosanjh, D.S., Yu, J.C., and Abdelhamid, A.N., "Reduction of Noise from Supersonic Jet Flows", AIAA J., Vol. 9, No. 12, pp. 2346-2353, 1971.

14. Dosanjh, D.S., Ahuja, K.K., Bassiouni, M.R., and Bhutiani, P.K., "Some Recent Developments in Supersonic Jet Noise Reduction", AIAA paper No. 75-502, 1975. Also AIAA Series on Progress in Astronautics and Aeronautics on Aeroacoustics, Vol. 43, 1976.

15. Dosanjh, D.S., Bhutiani, P.K. and Ahuja, K.K., "Supersonic Jet-Noise Suppression by Coaxial Cold/Heated Jet Flows", AIAA J., Vol. 16, No. 3, March 1978.

16. Tanna, H.K., Tam, C.K.W., and Brown, W.H., "Shock Associated Noise Reduction from Inverted-Velocity Profile Coannular Jets", NASA Contractor Rep. 3454, 1981.

17. Janardan, B.A., Yamamoto, K., Majjigi, R.K. and Brausch, J.F., "Experimental Investigations of Shock-Cell Noise-Reduction for Dual-Stream Nozzles in Simulated Flight", NASA CR 3846, 1984.

18. Yu, J.C., and Dosanjh, D.S., "Noise Field of a Supersonic Mach 1.5 Cold Model Jet", NASA Vol. 51, Nov. 5, 1972.

19. Tam, C,K.W., and Tanna, H.K., "Shock Associated Noise of Supersonic Jets from Convergent-Divergent Nozzles", J. Sound and Vib., Vol. 81, No. 3, pp. 337-358, 1982.

20. Das, I., and Dosanjh, D.S., "Noise Suppression of Supersonic Jets by Contoured and Porous Conical Plug-Nozzles, AIAA Paper #84-2363 AIAA/NASA 9th Aeroacoustics Conference, Oct. 1984.

21. Knott, P.R., Janardan, B.A., Plajjigi, R.K., Bhutiani, P.K. and Vogt, P.G., "Free-Jet Acoustic Investigation of High-Radius-Ratio Coannular Plug Nozzles. NASA Contractor Report 3818, Oct. 1984.

22. Maestrello, L., "An Experimental Study on Porous Plug Jet Noise Suppressor", AIAA Paper No. 79-0673, March 1979.

23. Kibens, V., and Wiezien, R.W., "Noise Reduction Mechanisms in Supersonic Jet with Porous Center-bodies", AIAA, J., Vol. 23, No. 5, May 1985.

24. Krase, W.H., "Performance of Plug Nozzles for Turbojet and Rocket Exhausts", presented at ASME Gas Turbine Power Divn. Meeting, Cincinnati, 1960.

25. Berman, K., "The Plug Nozzle - A New Approach to Engine Design", Astronautics, Vol. 5, No. 4, 1960.

26. Migdal, D., "Supersonic Annular Nozzles", Space Craft Vol. 9, No. 1, Jan. 1972.

27. Saule, W.P., and Mueller, T.J., "Annular Truncated Plug Nozzle Flow Field and Base Pressure Characteristics", AIAA Paper No. 73-137, AIAA 11th Aerospace Sciences Meeting, Washington, DC, Jan. 1973.

28. Evans, L.B., and Bass, K.E., "Tables of Absorption and Velocity of Sound in Still Air at 20^{O} C', Wyle Lab. Report WR72-2, Jan. 1972.

29. Das, I.S., Matambo, T.J., and Dosanjh, D.S., "Aeroacoustics of Supersonic Porous Plug-Nozzle Flows", AIAA Paper No. 83-0075, 1983.

30. Connors, J.F., and Meyer, R.C., "Design Criteria for Axisymmetric and Two-Dimensional Supersonic Inlets and Exits," NASA TN 3589, October 1956.

31. Zucrow, M.J., and Hoffman, J.D., Gas Dynamics, John Wiley and Sons, 1976.

32. Owczarek, J.A., "Fundamentals of Gas Dynamics", International Textbook Co., Scranton, PA, 1964.

33. Spigel, J.M., Tunnell, P.J., and Wilson, W.S., "Measurements of the Effects of Wall Outflow and Porosity on Wave Attenuation in a Transonic Wind Tunnel with Perforated Wall," NACA TN 4360, 1958.

34. Tsui, C.Y., and Flandro, G.A., "Self-Induced Sound Generation by Flow Over Perforated Duct Liners", J. Sound and Vibration, 50, pp. 315-331, 1950.

35. Bauer, A.B., and Chapkis, R.L., "Noise Generated by Boundary Layer Interaction with Perforated Acoustic Liners," AIAA J. of Aircraft, 14, pp. 157-160, 1977.

36. Krull, J.F., Beale, W.T., and Schmiedlin, R.F., "Effect of Several Design Variables on Internal Performance of Convergent-Plug Exhaust Nozzles", NACA RM E56G20, 1956.

37. Tam, C.K.W., Seiner, J.M., and Yu, J.C., "On the Relationship between Broadband Shock Associated Noise and Screech Tones", AIAA Paper No. 84-2276, 1984.

38. Tanna, H.K., "An Experimental Study of Jet Noise Part II: Shock Associated Noise; J. of Sound and Vibration Vol. 50, No. 3, 1977.

39. Seiner, J.M. and Norum, T.D., "Experiments on Shock-Associated Noise of Supersonic Jets", AIAA Paper No. 79-1526, July 1979.

40. Stone, J.R., "Supersonic Jet Shock Noise Reduction" NASA TM 83799 Presented at 9th Aeroacoustic Conference Sponsored by AIAA, Oct. 1984.

41. Yamamoto, K., Brausch, J.F., Balsa, T.F., Janardan, B.A., and Knott, P.R., "Experimental Investigation of Shock-Cell Noise reduction for Single Stream Nozzles in Simulated Flight," NASA Contractor Report 3845, 1984.

42. Greer, H., "Rapid Method for Plug-Nozzle Design", ARS J., Vol. 32, No. 4. April 1961.

43. Das, I., "Far-Field Noise of Contoured and Solid/Porous Conical Plug-Nozzle Jet Flows," Ph.D. Dissertation, Syracuse University, May 1985.

44. Dosanjh, D.S. and Das, I.S., "Aeroacoustics of Contoured Plug-Nozzle Supersonic Jet Flows," AIAA-86-1946, 10th Aeroacoustics Conference July 1986.

APPENDIX I

Corrected Acoustic Spectral Data and the Upper Cut-Off Band-Center-Frequency

In the present investigation, the one-third octave SPL spectral data recorded over the frequency range between the band-center frequencies f_c = 200 Hz and f_c = 100 kHz were corrected for the microphone corrections as well as for the acoustic absorption due to humidity in the anechoic chamber. The microphone corrections for the 1/4" B & K condenser microphone with grid, used in the normal-incidence mode, were applied as listed in Table I-1. The humidity corrections were calculated based on the relation by Evan and Bass [28]. A typical sound absorption in the atmosphere at 30% humidity vs frequencies is shown in Fig. I-1. For details, see Ref. 43.

It may be noted that the annular-throat-width of the model plug-nozzles is 13.56 mm and the exit radius R_N of the model convergent nozzle is 22.5 mm (Table 2, p.23. For model plug-nozzles with such small annular throat, the SPL's at upper band-center frequencies will be higher than those for an equivalent convergent nozzle. The peak frequencies in the one-third octave SPL spectra for the model convergent nozzle were noted to be of the order of 4 to 6 kHz and for the model plug-nozzles were generally of the order of 10 kHz. For the convergent nozzle flows ($\xi \doteq 4.0$, $\theta = 90°$), approximately 10 dB drop in the uncorrected SPL's occurs around an upper band-center frequency f_c = 20 kHz (Fig. 4(a) and a similar drop in the uncorrected SPL's for the conical plug-nozzle flows at the same pressure ratio and angular location occurs around $f_c \doteq 50$ kHz (Fig. 34(a). Therefore, for the plug nozzle flows, comparatively higher levels of acoustic signals are present at higher band-center frequencies. Moreover, the noise attenuations at higher frequencies due to relative humidity in the anechoic chamber will also be higher for the plug-nozzle spectra. Therefore, the corresponding levels of corrections at higher band-center frequencies are larger in magnitude. The significance of these corrections vis-a-vis the choice of upper cut-off frequency in the analysis of the present 1/3 octave spectral data is discussed in what follows.

The corrected (lossless) data were analyzed over the frequency range between the one-third octave band-center frequencies f_c = 200 Hz to 100 kHz. A typical set of the uncorrected and the corrected 1/3 octave spectral data at θ = 90° are tabulated in Table I-3, for the model solid conical plug-nozzle operated at ξ = 4.5. The microphone and the humidity corrections are listed separately. It is noted that the level of the combined microphone and humidity corrections applied to the acoustic data at higher band-center frequencies (f_c = 63 kHz; 80 kHz and 100 kHz) are rather high and that the absorption corrections are dominant. With such large corrections, the corrected one-third SPL spectra show a sharp increase at band-center frequency f_c > 63 kHz. This increase is most pronounced for the SPL's of jet flows from conical plug-nozzles with the solid as well as the solid/porous surfaces. For the model convergent nozzle this peculiarity of the rising trend in the corrected acoustic data at higher band-center frequencies is generally absent (see Ref. 43 for details).

The observed increase at higher center-frequency bands (f_c > 50 kHz) in the corrected SPL's, could perhaps be attributed to the higher acoustic levels at higher band-center frequencies generated by the jet flows from the model plug-nozzles with narrow annular-throats. The nature and the levels of this increase in the corrected SPL's at f_c > 63 kHz are substantially similar for the model plug-nozzles with either the solid or the porous plugs (Fig. 42). Since the increase is observed to occur both from solid as well as porous plug nozzle flows, it is surmised that this increase in SPL's at f_c > 63 kHz is not caused by the presence of the perforations of the porous plug. Moreover this type of increase is not present for convergent-nozzle flows. The narrow annular throat of the plug-nozzle, therefore, seems to play a primary role in the generation of acoustic spectra with higher frequency content which at higher band-center frequencies requires higher levels of corrections. If the humidity corrections at f_c > 50 kHz, are overestimated by the Evan and Bass relation [28], then the corrected spectral data may result in an increase in SPL's of the type seen in these studies [Ref. 43].

Assuming that the over-shoot in the corrected SPL's at f_c = 63, 80 and 100 kHz is primarily the result of such an over-estimation of the

corrections due to absorption and is not due to the higher acoustic levels generated at higher band-center frequencies by jet flows from model plug- nozzles with small annulus-height, it was considered advisable to set the upper cut-off band-center frequency at 50 kHz for the analysis of the corrected acoustic spectral data. Though the magnitude of the reductions in OASPL's changed somewhat with the upper band-center cut-off frequency [Table I-3], yet the nature of the results and conclusions about OASPL vs θ at different ξ's; the ΔOASPL's as compared to those of an equivalent convergent nozzle and comparisons with the predicted OASPL by Stone for the contoured and the plug nozzles, remain essentially similar [43].

If absorption corrections due to Evans and Bass [28] at band-center frequencies 63 kHz, 80 kHz, and 100 kHz turn out to be of questionable validity, then for the analysis of the acoustic data in the present study, the upper cut-off frequency f_c = 50 kHz would be a more reasonable choice. If a more accurate relation predicting the atmospheric absorptions-corrections were to become available in the future, then to facilitate the inclusion of such corrections (if needed), the uncorrected SPL spectral also have been tabulated in Appendix IV, where the needed values of the ambient conditions, and the radial distance at which these acoustic data were recorded, are also listed. The corresponding microphone corrections are tabulated in Table I-1.

TABLE I-1

Microphone Corrections

B and K Condenser Microphone Diameter 1/4"
Cartridge Type B & K 4135
Serial Number 101169
Used at Normal Incidence (i.e. at zero angle of incidence): with microphone grid in place).
Pre-amplifier: Type B & K 2615
Microphone Adaptor: Type UA 0035

Microphone corrections are taken from calibration provided by B and K and are to be added algebraically to the 1/3 octave SPL's obtained from acoustic spectra recorded on the Level Recorder.

kHz	Correction dB	kHz	Correction dB	kHz	Correction dB
0.100	0	1.000	0	10.000	-.50
0.125	0	0.250	0	12.5000	0
0.160	0	0.600	0	16.000	-0.8
0.200	0	2.000	0	20.000	-1.4
0.250	0	2.500	0	25.000,	-2.9
0.315	0	3.150	0	31.500	-4.5
0.400	0	4.000	0	40.000	-5.2
0.500	0	5.000	0	50.000	-3.2
0.630	0	6.200	0	63.000	+0.7
0.800	0	8.000	-.25	80.000	+3.1
				100.00	+9.5

AMBIENT CONDITIONS (AVERAGE VALUES)

Atmospheric Pressure P_o = 14.6 PSIa

Chamber Temperature T_o = 68°F

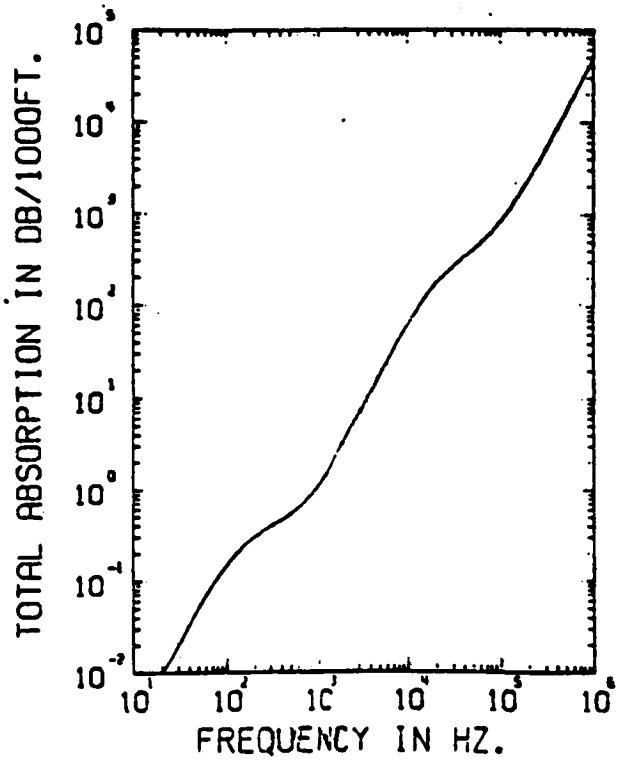

Fig. I-1 Sound Absorption in Atmosphere at Relative-Humidity of 30%. (Reference 28).

TABLE I-2

Typical Comparison of Corrected and Recorded 1/3 Octave SPL's

Model: Solid Conical Plug-Nozzle K = 0.43 R = 3.05 m

Pressure Ratio: ξ = 4.5. Azimuthal angle at the Measuring Station: θ = 90°

f_c (kHz)	1/3 Octave SPL's		Correction	
	Recorded	Corrected	Microphone	Atm.Absorp.
0.200	89.0	89.0	0	0
0.250	89.5	89.5	0	0
0.315	90.5	90.5	0	0
0.400	91.0	91.6	0	0
0.500	91.8	91.8	0	0
0.630	92.8	92.8	0	0
0.800	93.8	93.8	0	0
1.000	95.0	95.0	0	0
1.250	96.0	96.0	0	0
1.600	97.5	97.5	0	0
2.000	98.5	98.5	0	0
2.500	99.5	99.5	0	0
3.150	102.5	102.5	0	0
4.000	104.3	104.4	0	+0.1
5.000	105.0	105.1	0	+0.1
6.300	106.5	106.6	0	+0.1
8.000	106.5	106.4	-0.25	+0.15
10.00	106.5	106.3	-0.50	+0.3
12.50	105.5	106.0	0	+0.5
16.00	105.5	105.4	-0.8	+0.7
20.00	105.0	104.7	-1.4	+1.1
25.00	105.0	103.7	-2.9	+1.6
31.50	104.8	102.7	-4.5	+2.4
40.00	104.0	102.4	-5.2	+3.6
50.00	102.0	103.8	-3.2	+5.0
63.00	100.0	107.5	+0.7	+6.8
80.00	97.0	109.2	+3.1	+9.1
100.00	93.0	114.2	+9.5	+11.7

APPENDIX II

Aeroacoustics of Solid/Porous Conical Plug-Nozzles with an Approximately Contoured Plug

An approximate method for a relatively quick design of plug contours for high pressure ratio plug-nozzles for rocket engines was developed by Greer [42]. This method, when tried in the present plug-nozzle study at relatively low super-critical pressure ratios (the design Mach number $M_d \doteq 1.5$), resulted in a convexity downstream of the sonic region in the predicted plug surface contour. The expansion waves generated in supersonic flow past such a convexity of the plug surface, develop, on subsequent reflections from free jet boundary as compression, into an unacceptable shock structure. Therefore, in the course of the present investigation, a simple alternate approximate method for plug-contour design was developed.

II.1. Approximate Method of Plug Contour Design

In the corner expansion over the shoulder of an axially symmetric body, the flow locally (at the shoulder) may be considered to be two-dimensional (Prandtl-Meyer expansion). If the expanded flow over the contoured plug were to be directed along the axis of the plug-nozzle, the wall of the convergent round nozzle should be inclined at an angle α which is equal and opposite to the Prandtl-Meyer angle ν (M) corresponding to the design Mach number M_d at the plug-exit.

Thus, for an ideal gas with constant specific heats and in absence of the boundary layer effects,

$$\nu(M) = \sqrt{\frac{\gamma+1}{\gamma-1}} \cdot \tan^{-1}\sqrt{\frac{\gamma-1}{\gamma+1}\cdot(M^2-1)} - \tan^{-1}\sqrt{M^2-1} \qquad (1)$$

where

$$|\alpha| = |\nu(M_d)|$$

For nomenclature of the externally-expanded plug-nozzle geometry and flow, see Fig. 1.

In axisymmetric corner flows, the Mach surfaces in general are curved. However, in the present case the curvature of the waves is assumed to be negligible. In the absence of the viscous effects, the plug surface is assumed to be a streamline of the flow. Then, using the conservation of mass between the throat OP and any section OQ (both sections being surfaces of conefrustums having the same axis as that of the jet),

$$\rho_t A_t V_t = \rho A V \sin \mu$$

or,

$$\frac{A \sin \mu}{A_t} = \frac{\rho_t V_t}{\rho V} = f(M) \tag{3}$$

where f(M) represents the area-Mach number relation for isentropic flow in a streamtube, given by

$$f(M) = \frac{1}{M}\left[\frac{2}{\gamma + 1}\left(1 + \frac{\gamma - 1}{2} M^2\right)\right]^{\frac{(\gamma + 1)}{2(\gamma - 1)}} \tag{4}$$

The area A formed by revolution of the Mach line OQ about the jet-axis is

$$A = 2\pi r \cdot \frac{R_N + (R_N - Y)}{2}$$

where

$$r = y/\sin \phi$$

Solving this quadratic equation in y and noting that y cannot be greater than the nozzle radius R_N,

$$y = R_N - \sqrt{R_N^2 - \frac{A \sin \phi}{\pi}} \tag{5}$$

Using the relations (3) and (4)

$$y = R_N - \frac{1}{\pi}\left[A_e - \frac{f(M).A_t \sin\phi}{\sin\mu}\right]^{1/2}$$

Since the geometrical relations,

$$\phi = \mu + \alpha - \nu \tag{6}$$

$$y = r \sin\phi \tag{7}$$

and

$$x = r \cos\phi \tag{8}$$

are available, therefore, for a given nozzle radius R_N and design exit Mach number M_e $(=M_d)$, the plug coordinates can be determined by use of equations (1) through (8).

It may be noted that for a given nozzle radius R_N and exit Mach number M_d, the length of the isentropic plug is fixed. Also, the annulus-radius-radio $K = (R_p/R_N)$ of the plug-nozzle given by

$$K = \sqrt{1 - \frac{\cos[\upsilon(M_d)]}{f(M_d)}}$$

is fixed if the exit (design) Mach number M_d is fixed. Thus for given M_d and R_N, the parameters K, the annulus width W_t and the maximum length L_{max} of the plug are uniquely fixed.

II.2 Model Configurations

The coordinates of plug-contour obtained by the approximate method are tabulated in Table II-1. The approximately contoured plug-nozzle for design Mach number $\doteq$ 1.5 had an annulus-radius-ratio K = 0.41 and the inner wall slope of 21.1° at the sonic point.

The corresponding uncontoured solid conical plug had K = 0.41, inner wall slope of 21° and L_{max} = 28.8 mm and L_{max}/R_N = 1.28. The noise suppression effect of porosity was also studied on this solid conical

plug. Porosity of 10% distributed over the entire surface and porosity of 4% distributed over the middle-third of the plug were investigated. The diameter and the depth of the perforation were, respectively 1 mm. and 2 mm. All the plug-nozzles (contoured and solid/porous conical) had the same throat area.

II.3 Experimental Observations

The acoustic measurements and shadowgraphic records of the approximate plug-nozzle jet flows are presented in Figs. II.1 and II.2 respectively.

At an operating pressure ratio $\xi = 3.04$ (when the design pressure ratio $\xi_{design} = 3.67$), in the spark shadowgraphs (Fig. II.2) the contoured plug-nozzle jet flow was observed to be reasonably free of shock structure. Moreover, the free jet boundary is nearly horizontal and straight at the nozzle exit. Therefore, at this pressure ratio the flow is nearly isentropic. The shock (b) as visible in Fig. II.2 (A): $\xi = 3.04$) is too weak to form, on subsequent reflections, a repetitive shock structure farther downstream. Thus, the contoured plug designed by the approximate method when used at a pressure ratio noticeably different and lower than the design pressure ratio resulted in a jet flow which is reasonably free of shock-structure.

The acoustic results and the optical data of the jet flows of the set of plug-nozzle based on the approximate plug-nozzle design ($K = 0.41$ but for $\xi \doteq 3.00$ or $M = 1.37$ instead of $\xi \doteq 3.67$ (or $M_d = 1.5$)) are found to be in qualitative agreement with the results for the contoured plug-nozzle designed by MOC for $M = 1.5$ having $K = 0.43$ presented in the main body of this report. The order of magnitudes of the comparative noise suppression effects of the contoured and solid/porous conical plug-nozzle for each case are noted to be similar. The noise suppression effects of porosity are also comparable for both configurations of plug-nozzles. This is so because the near-shockless flow is achieved for both cases when $K = 0.43$ (exact method of plug design) and $K = 0.41$ (approximate method of plug design) respectively. It should be noted that for the exact method the shockless jet flow is achieved at pressure ratio ($\xi \doteq 3.60$) which is very nearly the same as the design pressure ratio ($\xi \doteq 3.67$).

For further details of the experimental data gathered with the approximate contoured plug and the corresponding solid/porous conical plug-nozzles, see Ref. 29 and 43.

TABLE II-1: PLUG COORDINATES IN CMS.

X	Y		X	Y	
	contoured	conical		contoured	conical
-0.277	1.313	1.313	1.083	1.827	1.835
-0.-10	1.415	1.415	1.177	1.858	1.871
0.112	1.463	1.462	1.274	1.890	1.908
0.214	1.503	1.501	1.374	1.922	1.947
0.306	1.540	1.537	1.478	1.954	1.987
0.394	1.574	1.571	1.586	1.986	2.028
0.479	1.607	1.603	1.698	2.019	2.072
0.563	1.639	1.635	1.816	2.052	2.117
0.647	1.671	1.668	1.938	2.086	2.163
0.731	1.702	1.700	2.066	2.120	2.213
0.816	1.733	1.733	2.200	2.155	-
0.903	1.764	1.766	2.340	2.190	-
0.992	1.796	1.800	2.488	2.225	-

(Note: Origin is at the nozzle lip)

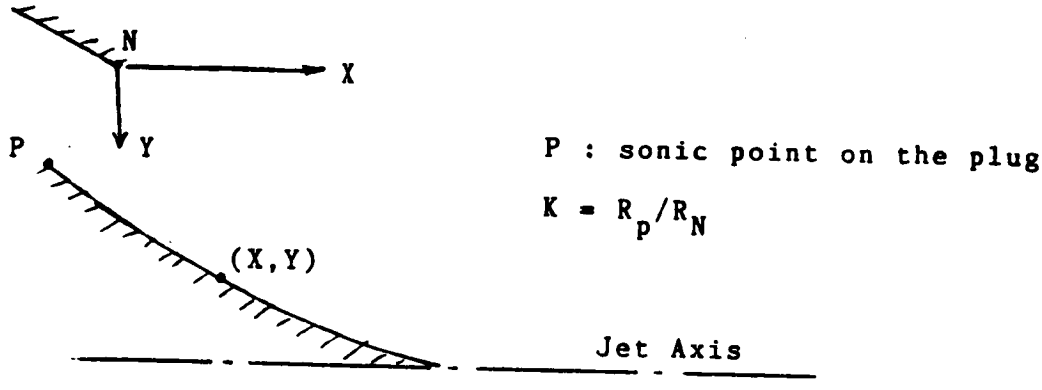

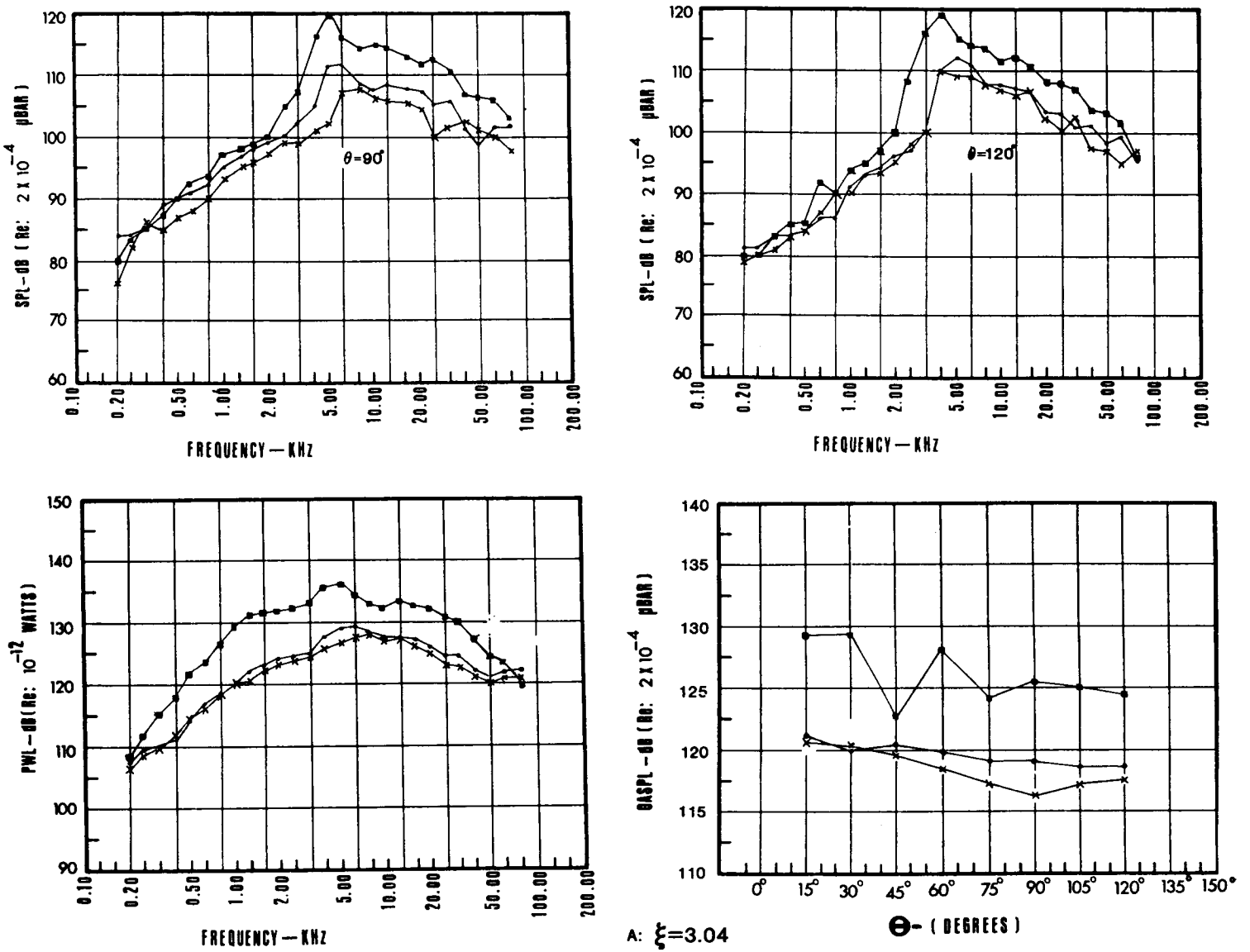

Fig. II-1. Comparison of 1/3 Octave SPL Spectra, Power watt level Spectra, and OASPL of Converging Nozzle and different Plug-Nozzles at the same pressure ratio. k=.41

■ converging nozzle
● solid conical plug-nozzle
x contoured plug-nozzle

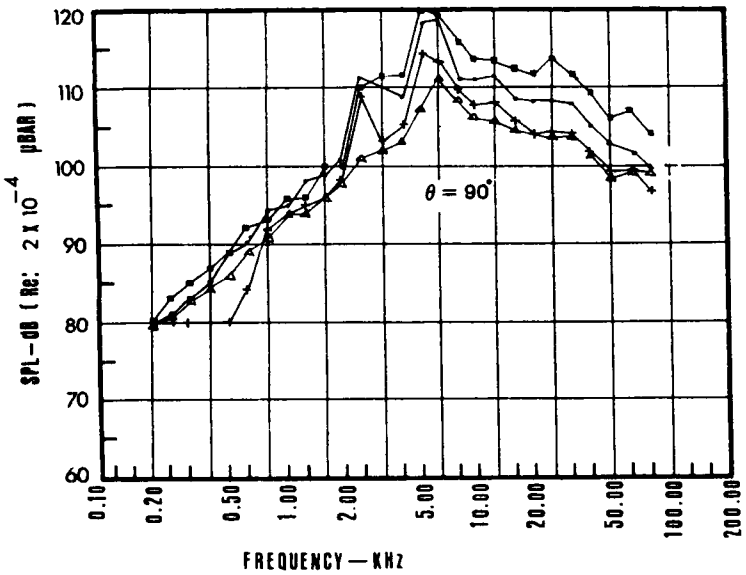

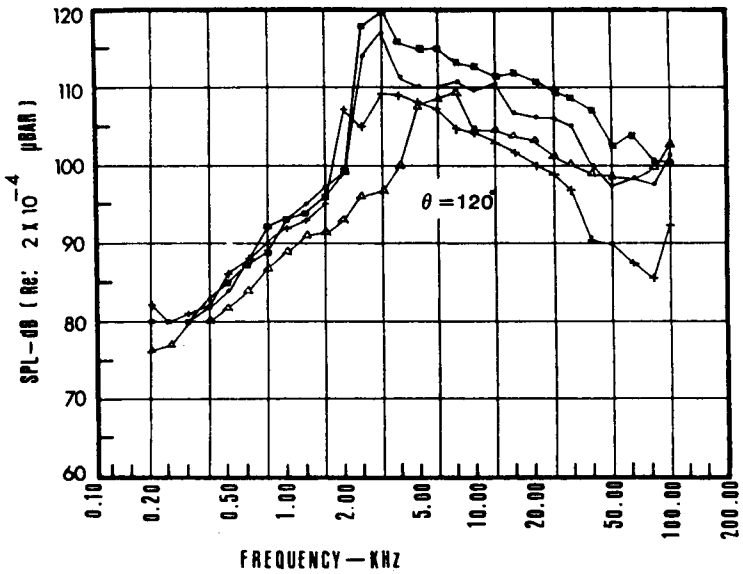

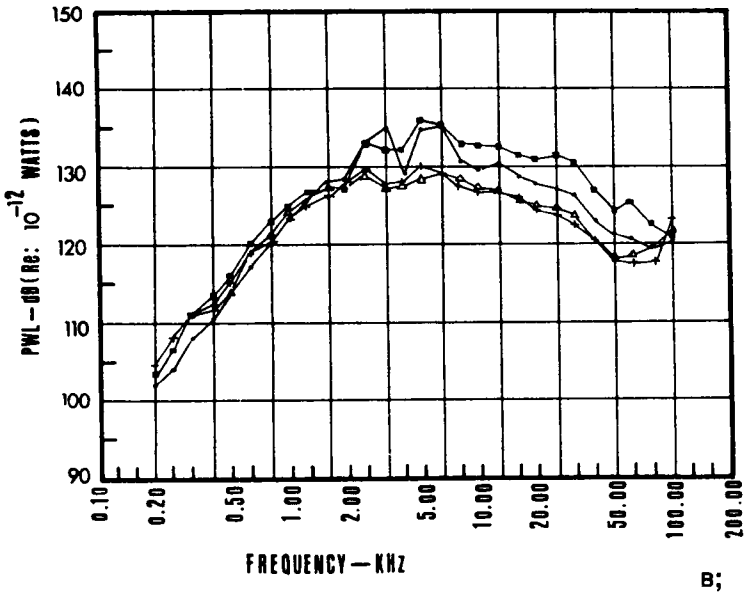

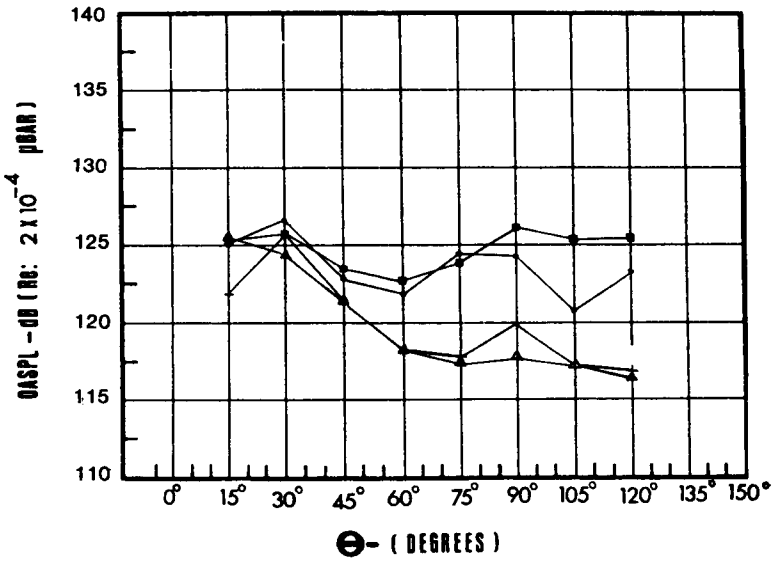

B; $\xi = 2.85$

Fig. II-1. Cont'd

■ conveging nozzle
● solid conical plug-nozzle
+ porous conical plug-nozzle (σ=4% holes locally distributed)
△ porous conical plug-nozzle (σ=10% holes uniformly distributed)

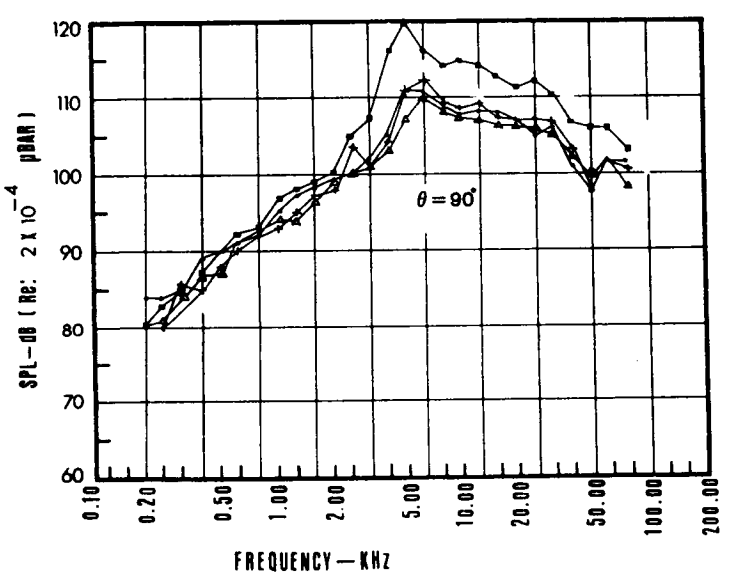

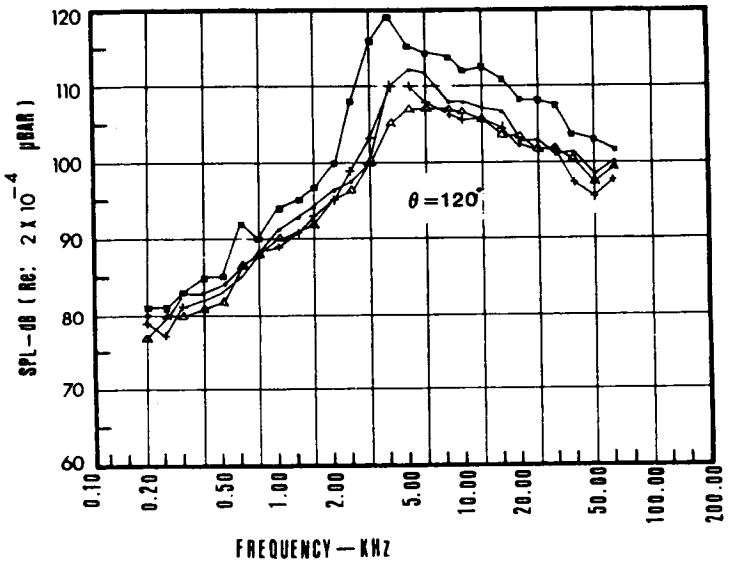

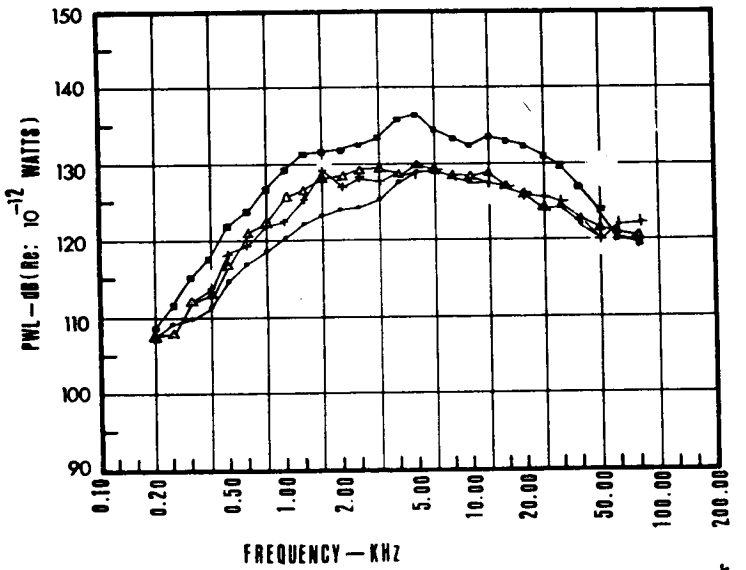

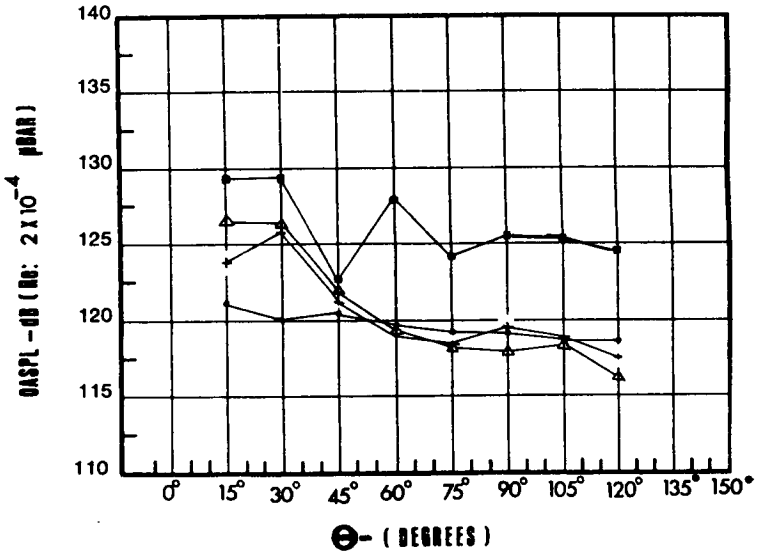

c : ξ = 3.04

Fig. II-1. Cont'd.

■ converging nozzle
● solid conical plug-nozzle
+ porous conical plug-nozzle (σ=4% holes locally distributed)
△ porous conical plug-nozzle (σ=10% holes uniformly distributed)

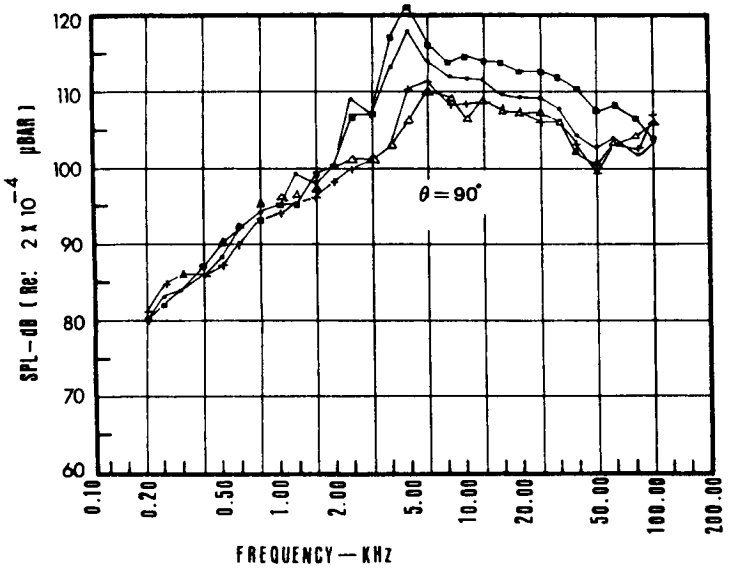

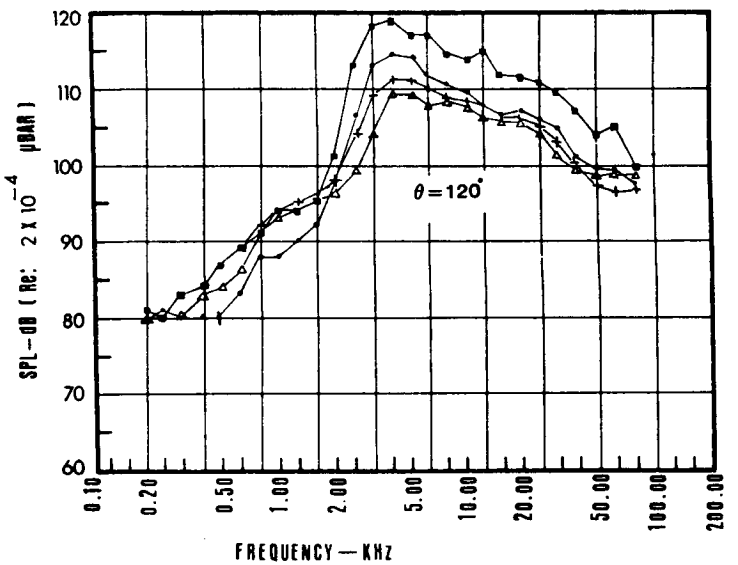

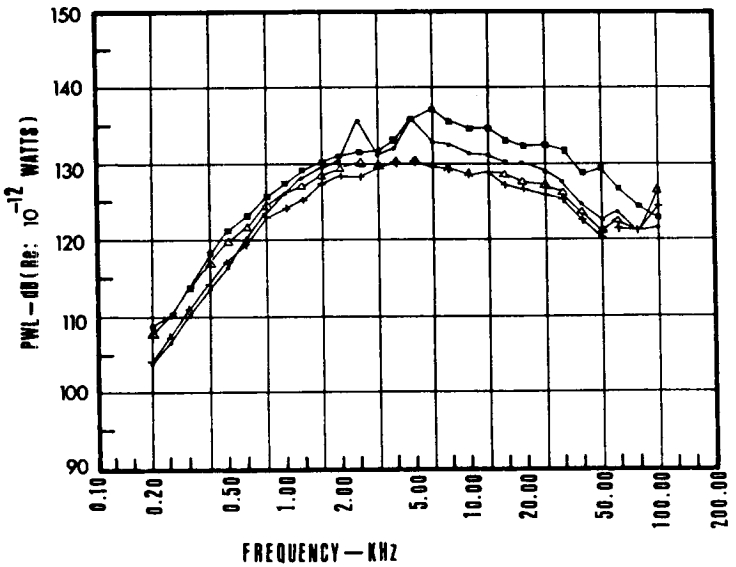

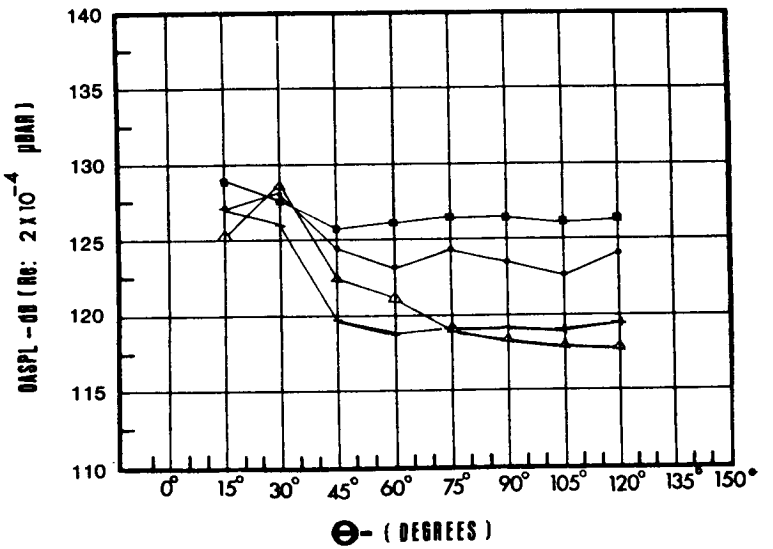

D : ξ=3.26

Fig. II-1 Cont'd.

■ converging nozzle
● solid conical plug-nozzle
+ porous conical plug-nozzle (σ=4% holes locally distributed)
△ porous conical plug-nozzle (σ=10% holes uniformly distributed)

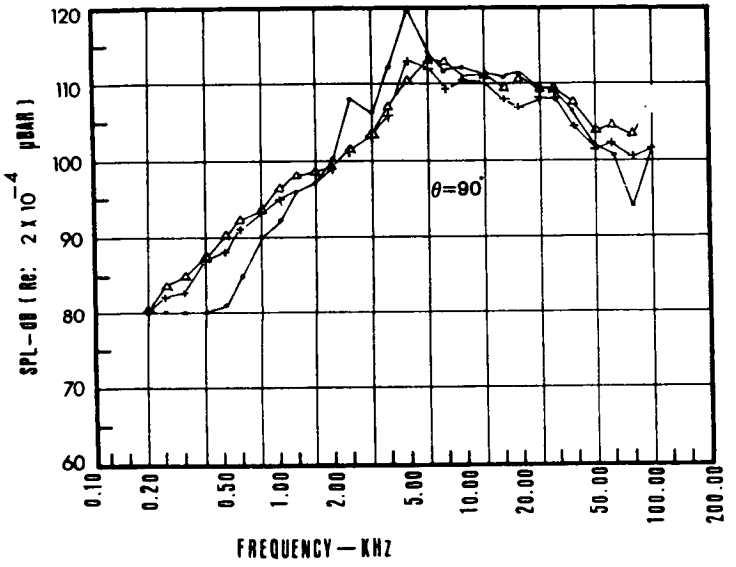

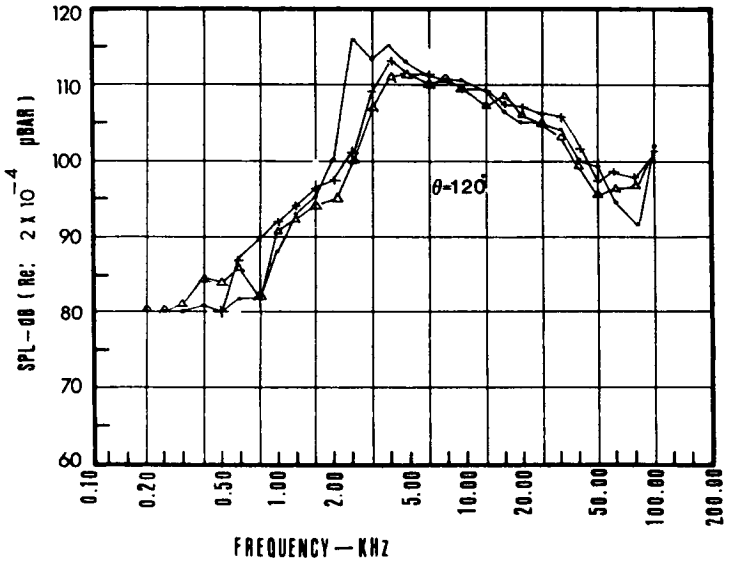

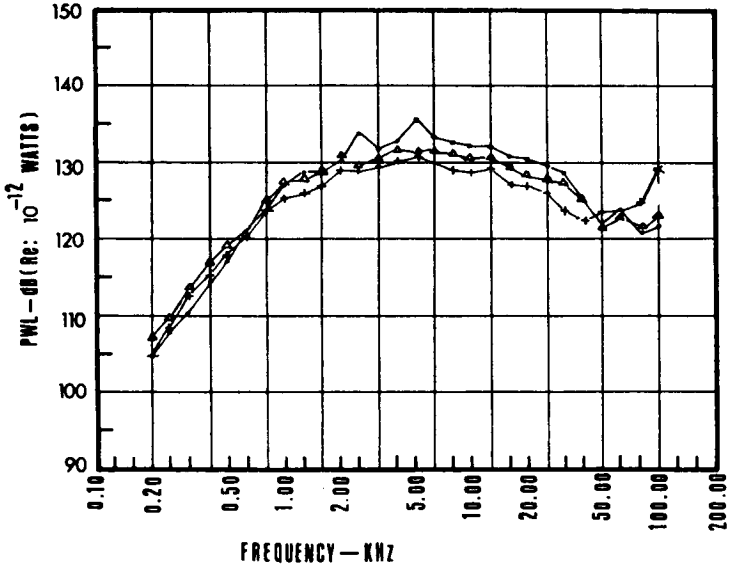

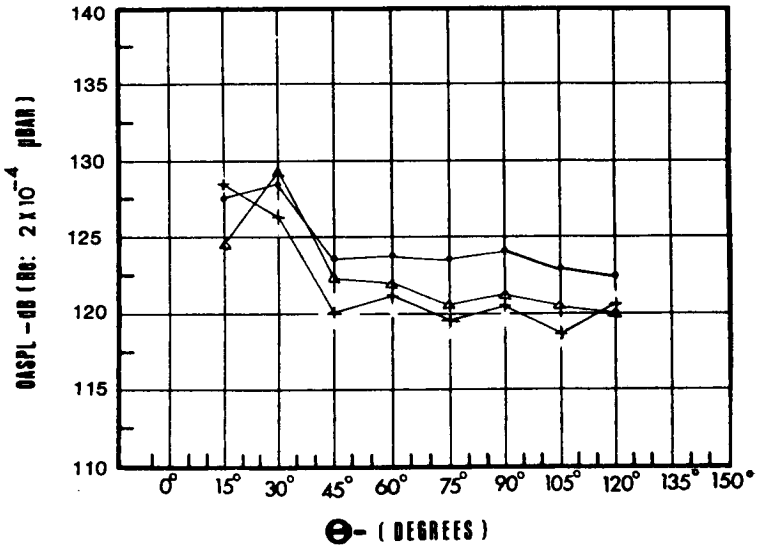

Fig. II-1. Cont'd

E: $\xi = 3.47$

- solid conical plug-nozzle
+ porous conical plug-nozzle (σ=4% holes locally distributed)
△ porous conical plug nozzle (σ=10% holes uniformly distributed)

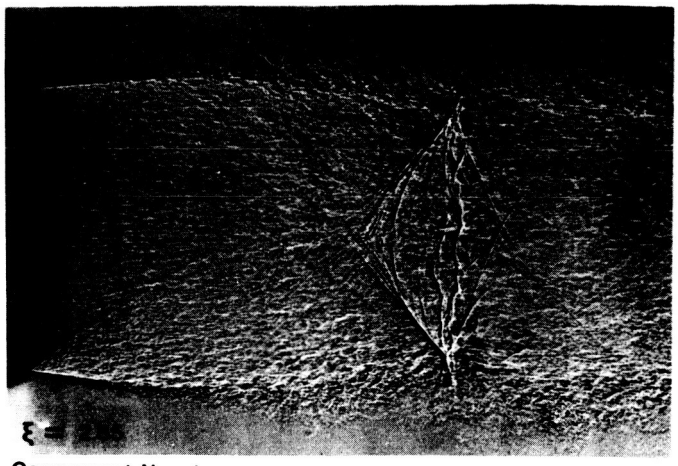

Convergent Nozzle

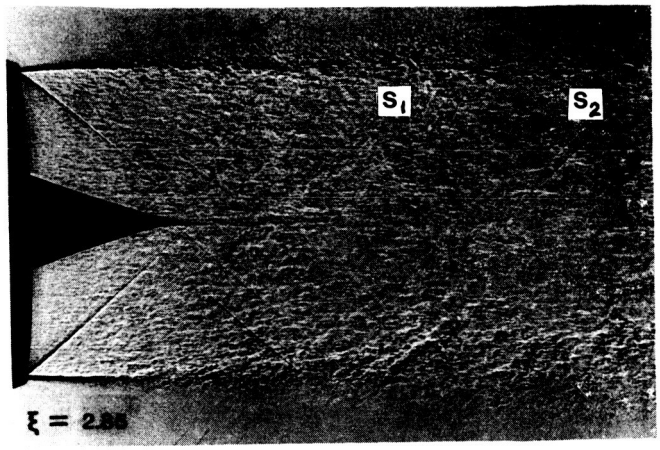

Contoured Plug-Nozzle

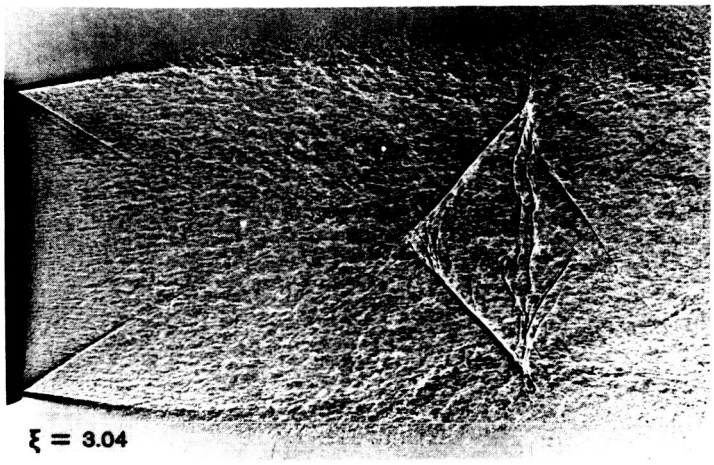

Convergent Nozzle

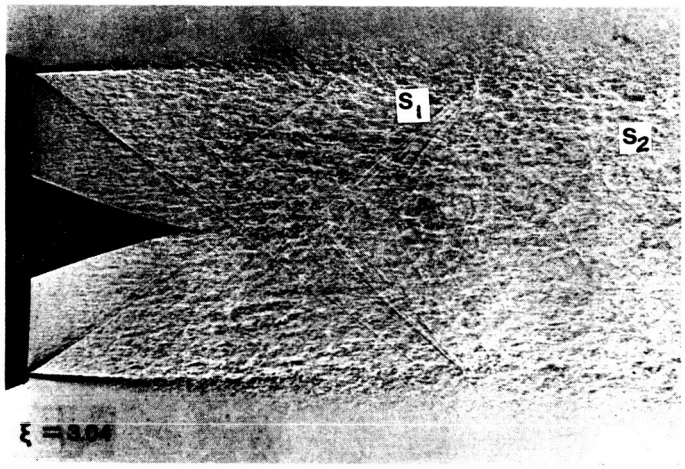

Contoured Plug-Nozzle

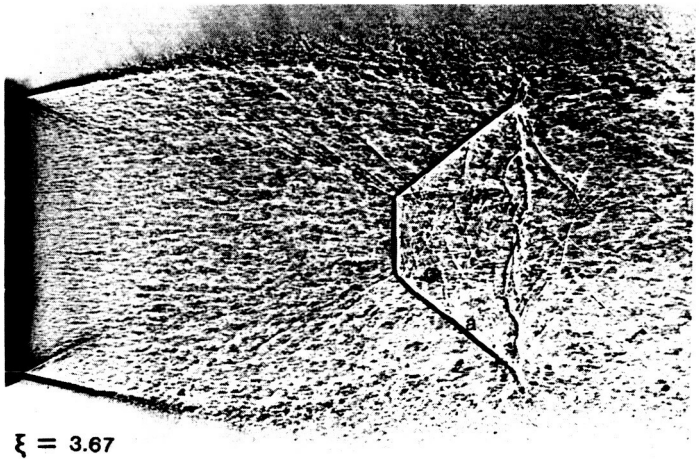

Convergent Nozzle

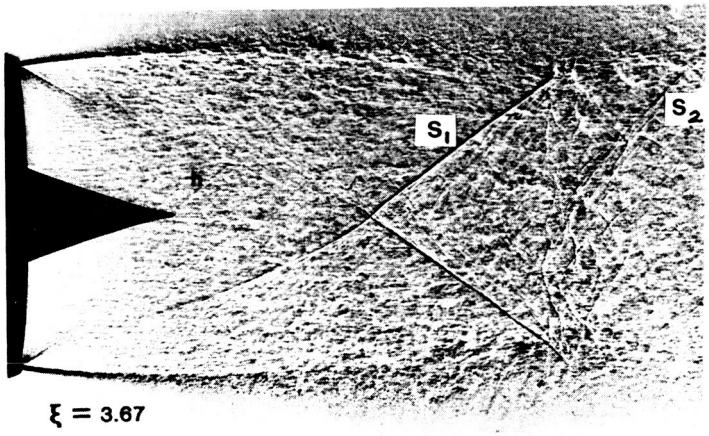

Contoured Plug-Nozzle

A

Fig. II-2 Typical Spark Shadowgrphs of Supersonic Jet Flows

Legend of Flow Features in shadowgraphs

(a) Repetitive shock structure
(b, or s_1) Shocks related to reflections from plug surface
(c) Lambda shock at jet flow boundary
(d, or s_2) Shock formed from the reflection of expansions unintercepted by the plug
(e) Compression wave front
(f) Mach disk
(g) Slip surface
(h) Weak shock from plug lip
(i) Compression waves generated at the porous plug surface.

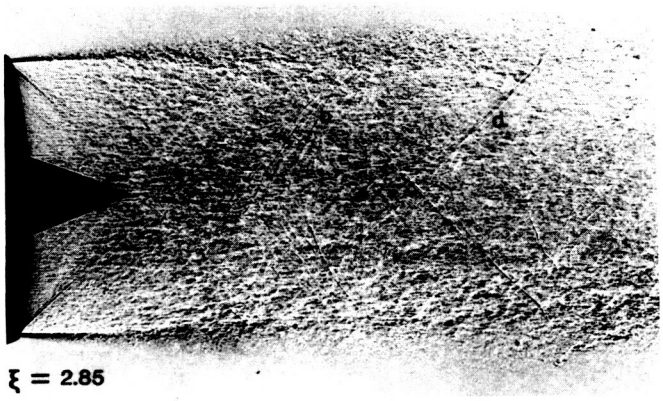

$\xi = 2.85$

Solid Conical Plug-Nozzle

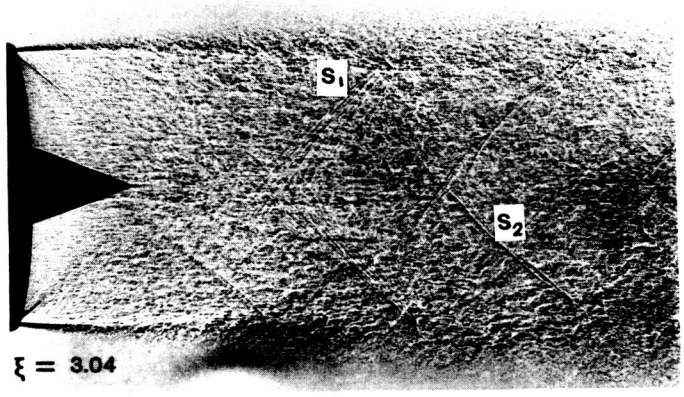

$\xi = 3.04$

Solid Conical Plug-Nozzle

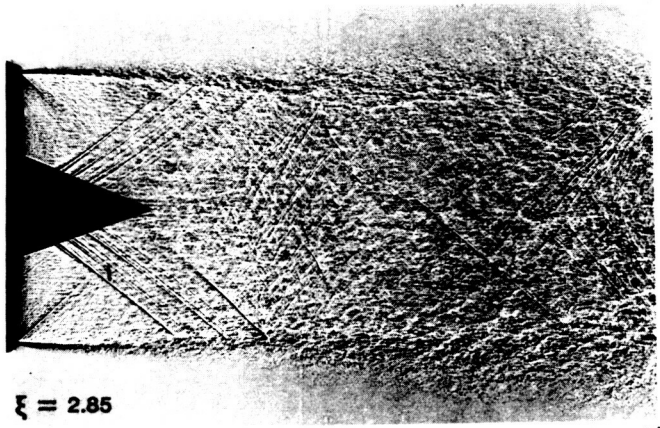

$\xi = 2.85$

Porous Conical Plug-Nozzle (σ= 4% , holes locally distributed)

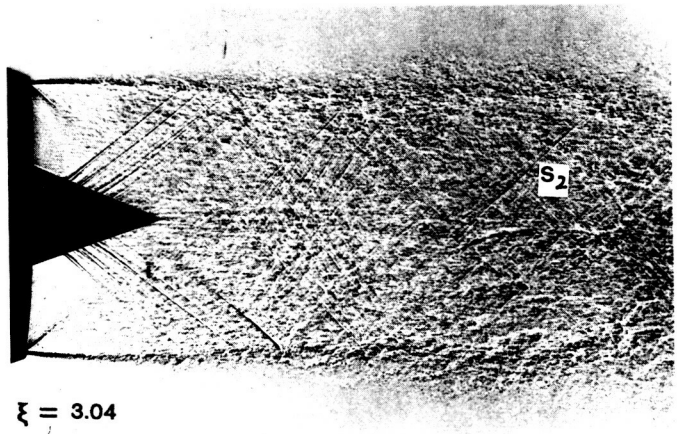

$\xi = 3.04$

Porous Conical Plug-Nozzle (σ= 4% , holes locally distributed)

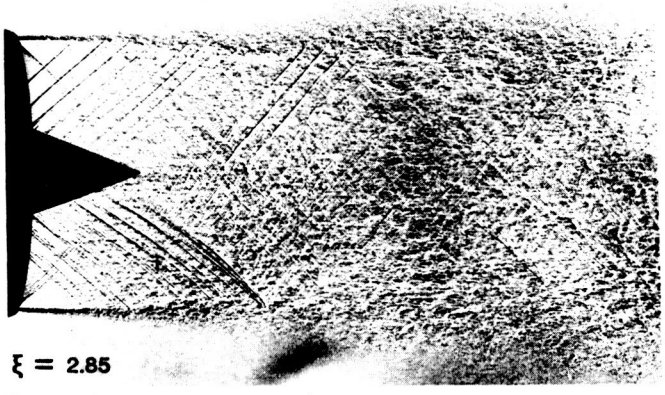

$\xi = 2.85$

Porous Conical Plug-Nozzle (σ= 10% , holes uniformly distributed)

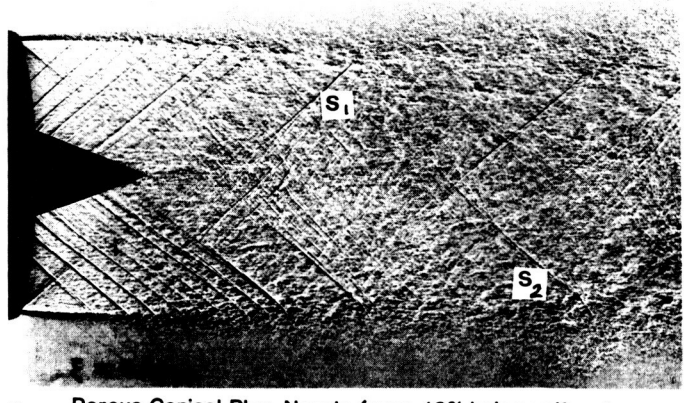

Porous Conical Plug-Nozzle (σ= 10%,holes uniformly distributed)

Fig. 11-2 Cont'd

B

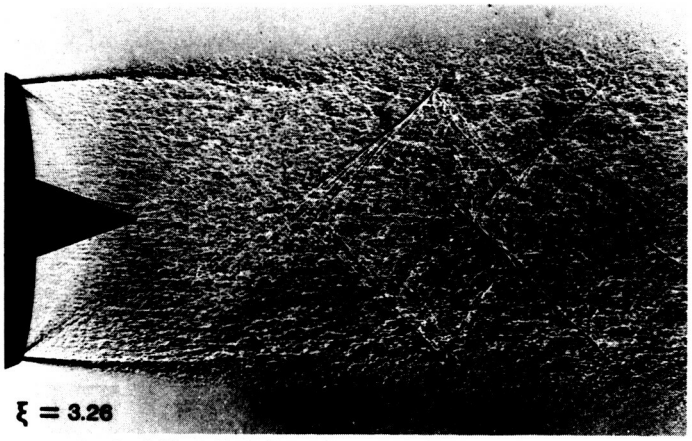

Solid Conical Plug-Nozzle

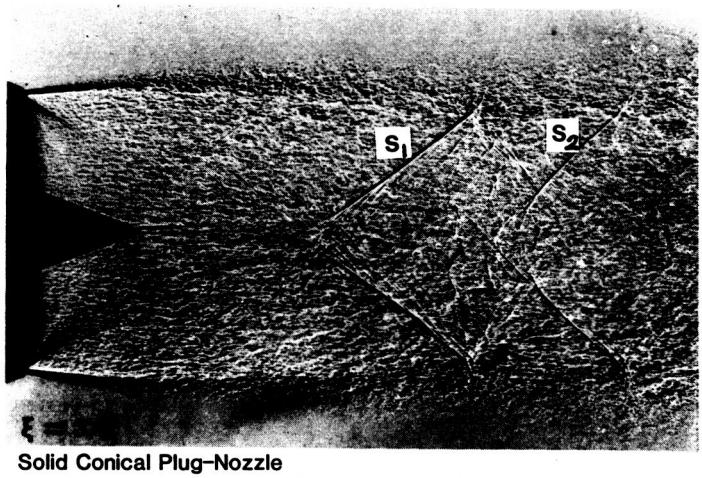

Solid Conical Plug-Nozzle

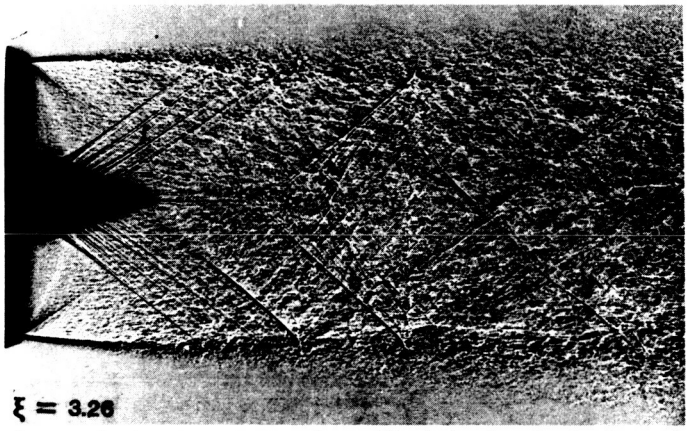

Porous Conical Plug-Nozzle (σ= 4% , holes locally distributed)

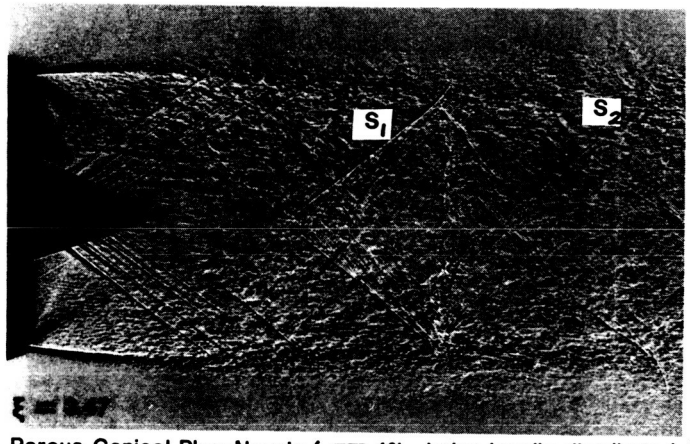

Porous Conical Plug-Nozzle (σ= 4% , holes locally distributed)

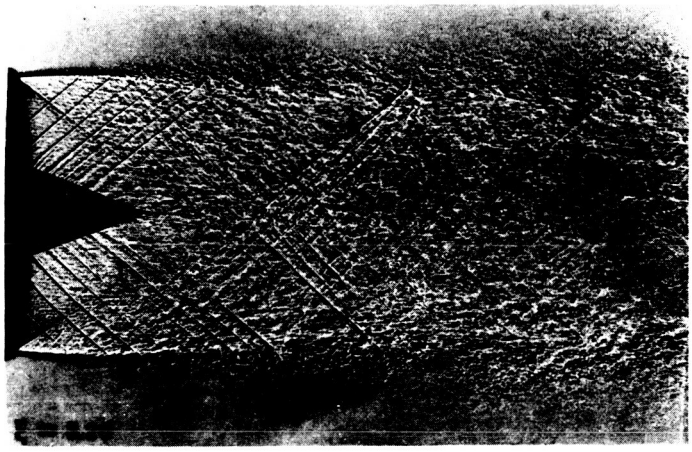

Porous Conical Plug-Nozzle (σ= 10% , holes uniformly distributed)

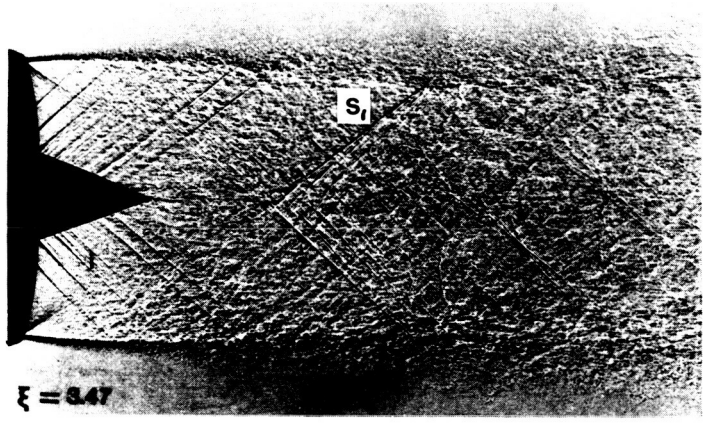

Porous Conical Plug-Nozzle (σ= 10%, holes uniformly distributed

C

Fig. II-2 Cont'd

APPENDIX III

The 1/3 octave sound pressure level data corrected for the microphone and atmospheric absorption corrections over the band-center frequencies f_c = 200 HZ to 50 KHZ at all observer angles θ for each of the nozzle configurations and pressure ratios are tabulated on pp. 137-159 For the microphone and absorption corrections see Appendix I. The acoustic results presented in the main body of this report are based on these corrected (lossless) SPL data. The corresponding OASPL's at all observer angles θ calculated for the pressure ratios ξ = 2.0 to 4.5 for each of the nozzle configurations are tabulated on p. 160.

Corrected 1/3 Octave SPL's

Test Model: Convergent Nozzle
Reservoir Pressure = 15 psig
Atmospheric Pressure = 29.42 in Hg

Measurement - Radius R = 3.05 m
Dry Bulb Temp. = 83° F
Wet Bulb Temp. = 71° F

f_c (kHz)	Theta in degrees								
	15	30	45	60	75	90	105	120	PWL
0.200	87.0	81.0	76.0	76.0	71.0	74.0	74.0	74.0	96.8
0.250	90.0	87.0	79.0	78.0	75.0	76.0	75.0	75.0	100.2
0.315	93.0	90.0	82.0	81.0	79.0	78.0	76.0	76.0	103.1
0.400	96.0	92.0	84.0	82.0	80.0	80.0	78.0	78.0	105.4
0.500	99.0	94.0	87.0	84.0	82.0	82.0	80.0	82.0	108.0
0.630	100.0	96.0	89.0	85.0	85.0	83.0	82.0	81.0	109.4
0.800	104.0	101.0	91.0	88.0	87.0	85.0	84.0	83.0	113.4
1.000	104.0	103.0	94.0	91.0	89.0	87.0	85.0	85.0	114.8
1.250	104.0	104.0	96.0	91.0	90.5	88.0	87.0	86.0	115.6
1.600	104.0	104.0	97.0	93.0	91.0	90.0	88.0	87.0	115.9
2.000	104.0	104.0	98.0	95.0	93.0	91.0	90.0	88.0	116.4
2.500	103.0	103.5	100.0	95.0	94.0	92.0	91.0	90.0	116.6
3.150	101.0	102.0	100.0	96.0	95.0	92.5	91.0	90.0	116.1
4.000	99.1	100.1	100.1	97.1	96.1	98.1	91.6	92.1	116.5
5.000	99.1	98.1	100.1	98.1	98.1	99.1	93.1	101.1	118.1
6.300	96.1	96.1	100.1	97.1	98.1	99.1	95.1	101.1	117.9
8.000	94.0	96.0	100.0	97.0	98.0	99.0	100.0	102.0	118.6
10.00	92.8	94.8	97.8	96.8	98.8	99.8	99.8	101.8	118.5
12.50	92.5	94.5	97.5	97.5	99.5	101.5	101.5	101.5	119.2
16.00	89.0	93.0	97.0	97.0	99.0	100.0	100.0	99.0	117.9
20.00	88.8	92.8	96.8	97.8	97.8	98.8	97.8	97.8	116.9
25.00	87.9	91.9	95.9	96.9	97.9	97.9	95.9	96.9	116.0
31.50	85.1	87.6	95.1	97.1	97.1	97.1	96.1	95.1	115.3
40.00	82.5	82.5	92.5	92.5	94.5	94.5	92.5	92.5	112.2
50.00	78.8	79.8	88.8	90.8	91.8	93.8	90.8	90.8	110.4

Corrected 1/3 Octave SPL's

Test Model: Convergent Nozzle

Reservoir Pressure = 22 psig

Atmospheric Pressure = 29.42 in Hg

Measurement - Radius R = 3.05 m

Dry Bulb Temp. = 83° F

Wet Bulb Temp. = 71° F

f_c (kHz)	Theta in degrees								
	15	30	45	60	75	90	105	120	PWL
0.200	90.0	85.0	78.0	77.0	75.0	74.0	76.0	74.0	99.4
0.250	93.0	88.5	84.0	81.0	79.0	78.0	78.0	76.0	102.9
0.315	97.0	92.5	87.0	85.0	83.0	82.0	80.0	78.0	106.7
0.400	101.0	96.0	89.0	86.0	85.0	84.0	80.0	80.0	109.9
0.500	104.0	98.0	92.0	88.0	87.0	86.0	83.0	84.0	112.5
0.630	105.0	102.5	95.0	91.0	90.0	88.0	85.0	85.0	115.0
0.800	107.0	106.0	97.0	93.0	92.0	90.0	87.0	86.0	117.7
1.000	108.0	108.0	100.0	95.0	94.0	92.0	90.0	90.0	119.5
1.250	109.0	110.0	101.0	96.0	95.0	94.0	91.0	91.0	121.1
1.600	109.0	111.0	102.5	99.0	97.0	95.0	93.0	92.0	122.1
2.000	109.0	112.0	104.0	100.0	98.0	96.0	95.0	93.5	123.0
2.500	109.0	110.0	105.0	101.0	100.0	99.0	95.0	95.0	122.6
3.150	108.0	109.0	105.0	102.0	102.0	100.0	100.0	103.0	123.1
4.000	106.1	107.1	105.1	101.6	102.1	103.1	103.1	105.1	123.4
5.000	104.1	106.1	105.1	102.1	104.1	105.1	106.1	107.1	124.6
6.300	100.1	105.1	105.1	104.1	105.1	106.1	107.1	107.1	125.2
8.000	98.0	104.0	105.0	106.0	105.0	105.0	105.0	107.0	124.6
10.00	97.8	101.8	104.8	106.8	104.8	103.8	104.8	104.8	124.1
12.50	97.5	101.5	105.5	107.5	103.5	104.5	105.5	105.5	124.5
16.00	96.0	101.0	105.0	104.0	103.0	102.0	103.5	102.0	122.4
20.00	94.8	100.8	104.8	103.8	102.8	102.8	103.3	101.8	122.3
25.00	93.9	98.9	101.9	102.9	101.9	100.9	101.9	100.9	120.8
31.50	93.1	98.1	99.1	98.1	100.1	99.1	101.1	100.1	118.9
40.00	87.5	94.5	96.5	94.5	96.5	98.5	98.5	96.5	116.2
50.00	84.9	88.8	92.8	93.8	94.8	94.8	97.8	93.8	114.0

Corrected 1/3 Octave SPL's

Test Model: Convergent Nozzle

Reservoir Pressure = 30 psig

Atmospheric Pressure = 29.42 in Hg

Measurement - Radius R = 3.05 m

Dry Bulb Temp. = 83° F

Wet Bulb Temp. = 71° F

f_c (kHz)	Theta in degrees								
	15	30	45	60	75	90	105	120	PWL
0.200	94.5	88.0	85.0	81.0	84.0	82.0	81.0	80.0	104.5
0.250	98.0	91.5	86.5	84.0	85.5	84.0	82.5	81.5	107.3
0.315	101.0	95.0	89.0	87.0	88.0	86.0	84.0	83.0	110.1
0.400	104.5	100.0	91.0	90.0	89.0	87.8	86.0	84.2	113.6
0.500	106.5	103.0	93.5	92.2	91.0	89.5	87.0	85.2	115.9
0.630	109.5	106.0	96.0	95.0	93.0	91.5	89.5	87.2	118.8
0.800	111.5	109.5	99.0	97.0	95.0	94.0	91.2	89.0	121.4
1.000	113.0	113.0	101.0	99.0	96.5	95.0	93.0	91.0	124.0
1.250	114.0	115.0	104.0	101.0	98.0	97.3	95.0	93.5	125.8
1.600	114.5	117.0	107.0	103.0	101.0	98.0	96.0	95.0	127.6
2.000	115.0	118.0	109.0	104.5	103.0	101.0	98.5	101.0	128.7
2.500	115.0	117.5	110.5	106.0	105.5	104.0	101.0	109.0	129.4
3.150	115.0	116.0	110.5	107.5	108.7	107.8	107.0	114.0	130.6
4.000	114.1	114.1	111.1	109.1	110.1	112.1	109.6	116.1	131.7
5.000	113.1	112.7	111.1	111.1	112.1	115.1	111.6	115.1	132.5
6.300	111.6	111.1	111.1	112.1	113.1	115.1	112.1	113.6	132.4
8.000	110.5	110.0	111.5	114.0	113.0	113.0	111.8	112.0	131.8
10.00	108.8	108.8	111.8	114.4	112.8	111.3	110.8	110.8	131.3
12.50	108.5	108.2	113.0	115.1	112.7	110.7	111.1	109.5	131.4
16.00	106.5	107.0	113.0	114.6	111.2	109.2	109.5	108.0	130.4
20.00	104.3	106.8	112.3	111.8	109.8	108.8	108.8	107.3	129.1
25.00	102.9	105.9	110.9	109.9	107.4	107.5	106.9	105.4	127.3
31.50	100.6	104.3	108.6	105.1	104.1	105.1	105.1	102.3	124.5
40.00	98.5	102.5	106.5	101.5	100.5	103.0	102.5	100.0	122.0
50.00	97.3	100.0	105.8	98.8	99.8	100.8	99.8	96.8	120.3

Corrected 1/3 Octave SPL's

Test Model: Convergent Nozzle

Reservoir Pressure = 37 psig

Atmospheric Pressure = 29.42 in Hg

Measurement - Radius R = 3.05 m

Dry Bulb Temp. = 83° F

Wet Bulb Temp. = 71° F

f_c (kHz)	Theta in degrees								
	15	30	45	60	75	90	105	120	PWL,
0.200	99.0	95.0	89.0	85.5	84.5	83.0	82.6	82.0	108.7
0.250	102.0	97.5	90.5	87.0	86.5	84.0	83.0	83.0	111.1
0.315	105.5	100.0	92.0	89.5	87.8	86.0	84.0	84.0	113.9
0.400	109.0	103.0	94.0	92.0	89.0	87.0	86.0	85.2	117.0
0.500	111.0	106.0	96.5	94.2	91.0	88.5	87.5	87.0	119.3
0.630	114.0	109.0	99.0	96.0	93.0	90.5	89.5	88.5	122.2
0.800	115.5	111.0	101.5	98.5	95.0	92.5	91.0	90.2	124.0
1.000	117.0	115.0	104.5	100.0	96.5	94.5	93.0	92.0	126.7
1.250	117.0	117.5	106.5	101.2	98.0	96.2	94.6	95.0	128.2
1.600	117.0	119.5	108.2	103.8	99.5	98.0	96.5	99.0	129.8
2.000	117.5	119.5	109.5	104.5	101.7	100.5	99.0	105.0	130.2
2.500	117.5	119.0	110.5	106.0	104.0	103.5	103.0	112.0	130.9
3.150	117.0	117.0	110.5	107.5	107.0	107.0	107.0	116.2	131.6
4.000	116.6	115.4	111.3	109.1	109.6	111.1	113.1	116.1	132.3
5.000	115.6	114.1	111.4	110.8	111.6	115.1	117.1	114.1	133.5
6.300	114.6	112.6	112.3	112.1	114.6	117.1	115.7	112.6	133.9
8.000	113.5	111.0	113.0	113.0	115.0	115.6	113.5	111.2	133.0
10.00	111.1	110.8	113.8	113.8	114.8	113.5	111.8	110.8	132.5
12.50	110.0	110.5	116.5	114.5	113.7	113.5	111.5	110.5	132.7
16.00	108.0	109.5	115.7	114.0	112.0	112.5	110.6	110.0	131.8
20.00	106.8	109.3	114.3	113.5	110.8	112.3	110.0	108.4	131.0
25.00	104.4	108.4	111.9	111.9	108.9	110.4	108.6	106.9	129.2
31.50	101.6	107.1	108.6	108.6	107.3	109.1	107.1	104.1	126.9
40.00	99.0	103.5	104.5	105.5	106.8	107.5	106.5	100.5	124.9
50.00	98.5	101.3	102.8	103.3	106.8	106.3	104.8	96.8	123.7

Corrected 1/3 Octave SPL's

Test Model: Convergent Nozzle

Reservoir Pressure = 44 psig

Atmospheric Pressure = 29.42 in Hg

Measurement - Radius R = 3.05 m

Dry Bulb Temp. = 83° F

Wet Bulb Temp. = 71° F

f_c (kHz)	Theta in degrees								
	15	30	45	60	75	90	105	120	PWL
0.200	101.0	93.0	88.0	86.0	83.0	82.0	81.0	81.0	109.0
0.250	104.0	96.0	90.0	89.0	85.0	84.0	83.0	82.5	111.8
0.315	107.0	101.0	92.0	90.0	87.0	86.0	85.0	83.0	115.0
0.400	110.0	104.0	94.0	92.0	89.0	88.0	87.0	84.0	117.9
0.500	112.0	107.0	98.0	94.0	92.0	90.0	88.0	86.0	120.3
0.630	114.6	110.0	100.0	96.0	93.0	91.0	90.0	88.0	123.0
0.800	116.0	113.0	103.0	99.0	95.0	94.0	93.0	91.0	125.2
1.000	117.0	116.0	105.0	100.0	97.0	96.0	95.0	92.5	127.2
1.250	118.0	117.5	107.0	101.0	99.0	97.0	96.0	95.0	128.6
1.600	119.5	119.0	108.0	102.0	100.0	98.0	96.0	95.0	130.0
2.000	119.2	119.0	109.0	104.0	102.0	100.0	99.0	100.0	130.2
2.500	119.0	118.5	110.0	105.0	104.0	103.0	104.0	106.0	130.3
3.150	118.0	117.5	110.0	105.5	106.0	108.0	111.0	114.0	131.5
4.000	117.6	117.1	111.1	107.1	108.1	114.1	113.1	114.1	132.5
5.000	116.1	116.1	111.1	109.1	112.1	115.1	113.1	114.1	132.9
6.300	115.1	115.1	112.6	113.1	114.1	114.1	112.1	111.1	132.8
8.000	114.0	113.0	113.0	116.0	113.0	112.0	112.0	111.0	132.5
10.00	112.4	112.3	114.8	115.8	110.8	111.8	110.8	110.8	132.2
12.50	111.5	112.5	116.5	115.5	111.5	111.5	111.5	109.5	132.5
16.00	110.0	111.0	116.0	113.5	111.0	111.0	111.0	109.0	131.5
20.00	108.8	110.8	113.8	112.8	110.8	110.8	109.8	108.8	130.6
25.00	106.4	109.9	112.9	111.9	109.9	109.9	108.9	106.9	129.6
31.50	104.1	108.6	112.1	111.1	109.1	109.1	107.1	105.6	128.6
40.00	100.5	106.5	107.5	107.5	107.5	106.5	103.5	104.5	125.7
50.00	98.8	102.8	105.8	105.8	104.8	102.8	101.8	101.8	123.2

Corrected 1/3 Octave SPL's

Test Model: Convergent Nozzle

Reservoir Pressure = 51 psig

Atmospheric Pressure = 29.42 in Hg

Measurement - Radius R = 3.05 m

Dry Bulb Temp. = 83° F

Wet Bulb Temp. = 71° F

f_c (kHz)	Theta in degrees								
	15	30	45	60	75	90	105	120	PWL
0.200	102.0	97.5	91.0	88.0	86.0	84.0	111.16	82.0	111.9
0.250	105.0	100.0	94.0	90.0	88.0	86.0	113.85	83.0	114.5
0.315	109.0	104.0	96.0	91.5	89.5	87.0	117.42	84.0	117.8
0.400	112.0	107.0	98.0	94.5	92.0	89.0	120.29	86.0	120.6
0.500	114.0	110.0	105.5	96.0	93.5	91.0	123.25	87.5	123.5
0.630	116.0	113.0	103.0	98.5	95.0	93.0	125.17	89.5	125.4
0.800	118.0	115.5	106.0	100.5	97.0	95.0	127.44	91.7	127.6
1.000	119.5	117.0	107.5	102.0	98.5	97.0	129.3	94.0	129.2
1.250	120.5	119.0	109.0	103.0	99.7	99.0	130.5	96.5	130.8
1.600	121.0	120.0	110.5	105.0	101.5	101.3	131.4	99.0	131.8
2.000	121.0	121.0	111.0	106.0	103.5	103.5	132.17	103.5	132.8
2.500	120.0	121.0	112.0	107.0	105.5	106.0	132.38	109.0	133.9
3.150	119.7	120.0	112.5	108.0	109.0	111.0	132.86	113.0	135.5
4.000	119.1	119.1	113.1	110.1	110.1	114.1	133.18	113.6	136.2
5.000	117.6	117.6	114.1	112.1	111.6	114.1	133.00	113.1	136.1
6.300	116.1	116.6	114.6	114.6	112.6	113.1	132.87	111.6	135.8
8.000	115.0	115.5	115.5	116.5	113.0	112.5	132.47	110.5	135.8
10.00	112.8	114.8	115.8	115.8	112.8	111.8	132.67	109.8	135.4
12.50	112.5	114.5	117.0	115.5	113.5	112.2	133.97	110.0	135.8
16.00	111.0	113.0	116.0	113.5	113.0	111.7	131.78	109.0	134.7
20.00	110.3	112.8	115.3	113.8	111.8	111.5	131.48	108.3	134.2
25.00	107.9	110.9	113.4	113.9	110.4	110.6	130.30	106.9	132.7
31.50	105.1	108.6	111.1	110.6	108.1	109.1	127.86	105.6	130.3
40.00	102.5	105.5	106.5	106.5	105.5	108.5	124.6	103.5	127.1
50.00	101.8	102.8	102.8	104.8	104.3	103.8	122.35	100.3	125.1

Corrected 1/3 Octave SPL's

Test Model: Contoured Plug Nozzle

Reservoir Pressure = 15 psig

Atmospheric Pressure = 29.64 in Hg

Measurement - Radius R = 3.05 m

Dry Bulb Temp. = 55° F

Wet Bulb Temp. = 51° F

RH = 60%

f_c (kHz)	Theta in degrees								
	15	30	45	60	75	90	105	120	PWL
0.200	81.0	74.0	73.0	70.0	72.0	72.0	72.0	72.0	92.4
0.250	86.0	80.0	76.0	73.0	75.0	74.0	73.0	73.0	96.0
0.315	90.0	85.0	79.0	76.5	78.0	76.0	76.0	74.0	99.6
0.400	92.0	87.0	81.0	78.0	79.0	78.0	77.0	74.0	101.4
0.500	95.0	90.0	84.0	81.0	80.0	80.0	80.0	77.0	104.2
0.630	98.5	93.0	86.0	84.0	83.0	82.0	80.0	79.0	107.2
0.800	103.0	95.0	87.5	86.0	83.0	84.0	83.0	79.0	110.5
1.000	103.0	98.0	90.0	88.0	86.5	85.5	85.0	82.0	111.7
1.250	104.5	100.0	93.0	90.0	87.0	87.0	87.0	83.0	113.5
1.600	105.0	103.0	94.0	91.0	88.0	88.0	88.0	84.0	115.0
2.000	105.0	103.0	95.0	92.0	89.0	89.5	88.0	85.0	115.2
2.500	105.0	103.0	97.0	94.5	92.0	90.0	89.0	87.0	115.8
3.150	102.0	103.0	98.0	95.0	92.0	91.0	90.0	87.5	115.5
4.000	100.1	102.1	98.1	96.1	92.1	95.1	90.1	88.1	115.3
5.000	98.1	101.1	98.1	97.1	94.1	96.1	92.1	90.1	115.5
6.300	96.1	99.1	97.1	96.6	94.6	95.1	93.1	93.1	114.9
8.000	94.0	98.0	98.0	96.0	94.0	97.0	96.0	95.0	115.4
10.00	91.8	97.3	96.8	96.3	94.8	97.8	97.8	96.8	116.0
12.50	91.5	97.5	97.5	97.0	97.5	97.5	95.5	96.5	116.1
16.00	88.0	95.0	97.0	98.0	97.0	95.0	93.0	94.0	114.9
20.00	87.8	94.3	96.8	97.8	96.8	94.8	91.8	92.8	114.5
25.00	86.8	92.8	93.8	96.8	95.8	93.8	91.8	92.8	113.4
31.50	85.0	92.0	94.0	95.5	94.5	91.0	91.0	91.0	112.2
40.00	82.5	90.5	92.5	94.5	95.5	88.5	89.5	88.5	111.3
50.00	81.8	86.8	91.8	93.8	95.8	86.8	84.8	85.8	110.5

Corrected 1/3 Octave SPL's

Test Model: Contoured Plug Nozzle — Measurement - Radius R = 3.05 m

Reservoir Pressure = 22 psig — Dry Bulb Temp. = 55° F

Atmospheric Pressure = 29.64 in Hg. — Wet Bulb Temp. = 48° F

f_c (kHz)	Theta in degrees								
	15	30	45	60	75	90	105	120	PWL
0.200	86.0	83.0	76.0	76.0	74.0	73.0	74.0	72.0	96.8
0.250	90.0	86.0	81.0	80.0	78.0	77.0	76.0	74.0	100.4
0.315	93.0	90.0	84.0	82.0	80.0	80.0	78.0	77.0	103.5
0.400	95.0	93.0	87.0	85.0	81.0	82.0	80.0	78.0	105.9
0.500	98.0	97.0	90.0	86.0	83.0	83.0	82.0	82.0	109.0
0.630	102.0	100.0	91.0	88.0	85.0	85.0	83.0	83.0	112.0
0.800	104.0	103.0	93.0	91.0	87.0	87.0	86.0	84.0	114.5
1.000	106.0	105.0	95.0	93.0	89.0	89.0	88.0	86.0	116.5
1.250	107.0	106.0	97.0	95.0	90.0	90.0	89.0	87.0	117.6
1.600	108.0	107.0	99.0	97.0	92.0	92.0	90.0	89.0	118.9
2.000	109.0	108.0	100.0	98.0	93.0	93.0	90.0	90.0	119.8
2.500	108.0	106.0	102.0	99.0	95.0	94.0	93.0	94.0	119.4
3.150	108.0	105.0	102.0	100.0	97.0	95.0	95.0	100.0	119.9
4.000	107.1	105.1	103.1	100.1	97.1	96.9	98.1	100.1	120.2
5.000	106.1	103.1	102.1	99.6	100.1	97.1	100.1	104.1	120.7
6.300	104.1	102.1	102.1	100.1	105.1	98.1	106.1	106.1	123.1
8.000	102.0	100.0	102.0	100.0	107.0	99.0	106.0	104.0	122.9
10.00	99.8	99.8	101.8	101.8	104.8	101.8	103.8	102.8	122.0
12.50	98.5	99.5	103.5	103.5	102.5	104.5	102.5	101.5	122.0
16.00	97.0	99.0	104.0	104.0	101.0	101.0	100.0	100.0	120.8
20.00	95.8	98.8	103.8	102.8	100.8	99.8	99.8	98.8	120.1
25.00	93.8	97.8	101.8	100.8	100.8	99.8	100.8	96.8	119.3
31.50	92.0	92.0	99.0	100.0	98.0	100.0	98.0	94.0	117.4
40.00	91.5	88.5	97.5	98.0	95.5	100.5	96.5	93.5	116.2
50.00	91.8	88.8	95.8	95.8	95.8	100.8	91.8	91.8	115.4

Corrected 1/3 Octave SPL's

Test Model: Contoured Plug-Nozzle

Reservoir Pressure = 30 psig

Atmospheric Pressure = 29.43 in Hg.

Measurement - Radius R = 3.05 m

Dry Bulb Temp. = 68° F

Wet Bulb Temp. = 62° F

f_c (kHz)	Theta in degrees								
	15	30	45	60	75	90	105	120	PWL
0.200	90.0	89.0	80.0	78.0	80.0	76.0	77.0	74.0	101.4
0.250	93.0	91.0	82.0	79.5	81.5	78.0	79.0	76.0	103.6
0.315	95.0	92.5	85.0	82.0	84.0	81.0	81.5	79.0	105.7
0.400	97.0	94.5	87.0	84.0	86.0	82.0	82.5	80.0	107.6
0.500	100.0	96.5	89.0	86.0	88.0	84.5	85.0	81.0	109.9
0.630	102.0	99.0	92.0	89.0	89.7	86.5	87.0	84.0	112.2
0.800	104.5	102.5	94.0	91.0	92.0	88.0	88.0	86.0	114.9
1.000	106.0	104.0	96.0	94.0	93.8	90.0	90.0	88.0	116.6
1.250	107.0	106.5	99.0	96.0	95.0	92.0	91.0	89.5	118.5
1.600	107.0	108.0	101.0	97.0	96.0	94.0	93.0	91.5	119.7
2.000	108.0	108.0	103.0	98.0	97.0	95.0	94.0	92.0	120.4
2.500	108.0	108.0	104.0	99.5	98.0	97.0	95.0	95.5	121.0
3.150	107.5	108.0	105.0	101.0	100.5	99.0	98.0	99.0	121.9
4.000	107.0	108.0	105.0	101.0	100.0	99.0	100.0	102.0	122.2
5.000	106.6	107.1	105.1	101.1	100.1	101.1	102.1	104.1	122.6
6.300	105.6	106.1	105.1	102.1	103.1	104.1	102.1	104.1	123.2
8.000	103.9	104.9	104.9	101.9	103.9	102.9	102.9	101.9	122.7
10.00	102.3	103.8	104.8	103.3	103.8	102.8	102.8	101.8	122.5
12.50	101.4	101.4	105.4	104.4	103.4	103.4	102.9	101.4	122.7
16.00	99.8	100.8	104.8	103.8	102.3	102.3	101.8	100.8	121.9
20.00	98.6	100.1	104.6	103.6	102.1	101.6	100.6	99.6	121.2
25.00	96.1	98.6	103.6	102.6	101.1	100.1	99.6	98.6	120.1
31.50	93.7	95.7	101.7	101.7	99.2	99.2	97.7	97.7	118.7
40.00	92.1	94.1	100.1	100.1	97.6	97.1	96.1	95.1	117.0
50.00	92.6	93.6	99.6	99.6	96.6	94.1	93.6	91.6	115.6

Corrected 1/3 Octave SPL's

Test Model: Contoured Plug Nozzle — Measurement - Radius R = 3.05 m

Reservoir Pressure = 37 psig — Dry Bulb Temp. = 68° F

Atmospheric Pressure = 29.43 in Hg — Wet Bulb Temp. = 62° F

f_c (kHz)	Theta in degrees								
	15	30	45	60	75	90	105	120	PWL
0.200	91.0	88.0	79.0	80.0	79.0	78.5	77.0	72.0	101.4
0.250	92.5	90.0	82.0	83.0	81.0	81.0	78.0	75.0	103.4
0.315	94.0	92.5	85.0	85.0	84.5	83.5	80.5	78.0	105.8
0.400	96.0	94.0	87.5	87.5	86.5	84.5	82.0	80.0	107.6
0.500	98.0	96.0	90.0	90.0	88.5	86.5	84.0	81.0	109.7
0.630	100.0	99.0	93.0	91.5	91.0	88.5	86.0	84.0	112.1
0.800	101.5	101.0	95.5	94.0	93.0	90.0	88.0	87.0	114.1
1.000	103.0	103.0	98.0	95.5	94.0	91.5	91.0	89.0	116.0
1.250	104.5	105.5	100.0	97.0	96.0	93.0	92.0	91.5	118.0
1.600	105.5	106.0	102.0	98.5	98.0	94.5	94.0	93.0	119.2
2.000	106.0	107.5	103.0	100.0	99.0	96.0	95.0	95.0	120.4
2.500	106.0	107.5	104.0	101.0	100.0	97.0	96.0	97.0	121.0
3.150	106.0	107.0	105.0	102.0	101.0	98.7	98.0	100.0	121.7
4.000	105.5	106.5	105.0	102.0	101.0	100.0	99.0	102.0	121.9
5.000	105.6	106.6	105.1	102.1	102.1	101.1	101.1	103.1	122.5
6.300	106.1	105.6	105.1	103.1	104.1	102.6	103.1	103.1	123.2
8.000	104.9	104.9	104.9	103.9	104.9	102.9	104.4	104.9	123.7
10.00	103.8	104.3	104.8	103.8	104.8	104.3	105.8	104.8	124.0
12.50	102.4	102.9	105.4	105.4	105.4	105.4	105.9	104.9	124.5
16.00	100.8	101.3	104.8	105.3	104.8	104.8	104.8	103.8	123.8
20.00	98.6	99.6	104.6	105.6	104.6	104.6	103.6	102.6	123.3
25.00	97.6	97.6	103.6	104.6	103.6	103.6	102.1	100.6	122.1
31.50	95.7	95.2	101.7	101.7	100.7	102.7	99.2	97.7	119.9
40.00	95.1	94.6	99.1	100.1	99.1	100.1	98.1	96.1	118.0
50.00	95.6	96.6	100.6	99.6	98.6	98.6	98.6	95.6	117.8

Corrected 1/3 Octave SPL's

Test Model: Contoured Plug Nozzle

Reservoir Pressure = 44 psig

Atmospheric Pressure = 29.57 in Hg

Measurement - Radius R = 3.05 m

Dry Bulb Temp. = 63° F

Wet Bulb Temp. = 51° F

f_c (kHz)	Theta in degrees								
	15	30	45	60	75	90	105	120	PWL
0.200	91.0	90.0	86.0	84.0	84.0	86.0	87.0	87.0	105.9
0.250	95.0	92.0	87.0	95.0	85.0	87.0	88.0	88.0	109.6
0.315	97.0	94.0	88.0	87.0	87.0	88.0	89.5	89.0	109.2
0.400	98.0	96.0	88.0	88.0	88.0	90.0	89.0	90.0	110.3
0.500	100.0	98.0	89.0	90.0	89.0	90.0	91.0	91.0	111.9
0.630	101.0	100.0	91.0	91.0	91.0	91.0	91.0	92.0	113.2
0.800	102.0	102.0	93.0	92.0	92.0	92.5	92.0	94.0	114.7
1.000	104.0	104.0	96.0	94.0	94.0	94.0	92.0	94.0	116.5
1.250	105.0	105.0	97.0	95.0	95.0	95.0	94.0	94.0	117.5
1.600	106.0	107.0	98.0	97.0	96.5	95.0	95.0	95.0	119.0
2.000	106.5	107.0	99.0	97.0	97.0	97.0	96.0	96.5	119.4
2.500	107.0	107.0	100.0	101.0	100.0	99.0	98.0	102.0	121.1
3.150	106.5	105.5	101.0	100.0	101.0	100.0	102.0	107.0	122.4
4.000	106.1	105.1	101.6	100.1	103.1	105.1	105.1	107.1	123.7
5.000	105.1	104.1	102.1	102.1	105.1	106.1	107.1	107.1	124.6
6.300	104.6	104.1	103.1	104.1	107.1	106.1	107.1	106.6	125.1
8.000	103.4	102.9	103.4	107.4	106.9	104.9	106.9	106.4	125.2
10.00	100.8	101.8	104.8	107.3	106.8	105.3	105.8	105.8	124.9
12.50	101.0	101.5	106.0	106.5	106.5	105.5	105.5	106.0	124.8
16.00	99.9	100.9	105.9	105.9	105.9	104.9	103.9	103.9	124.0
20.00	99.7	100.7	105.2	105.7	105.7	103.7	103.7	103.7	123.6
25.00	98.7	99.7	104.2	104.7	104.7	103.7	102.7	101.7	122.6
31.50	96.9	97.9	103.4	103.9	103.9	102.9	101.9	101.9	121.9
40.00	95.4	98.4	102.4	104.4	103.4	102.4	102.4	99.4	121.5
50.00	96.8	98.8	102.8	104.8	103.8	101.8	101.8	100.8	121.6

Corrected 1/3 Octave SPL's

Test Model: Contoured Plug Nozzle — Measurement - Radius R = 3.05 m

Reservoir Pressure = 51 psig — Dry Bulb Temp. = 68° F

Atmospheric Pressure = 29.43 in Hg — Wet Bulb Temp. = 62° F

Theta in degrees

f_c (kHz)	15	30	45	60	75	90	105	120	PWL
0.200	91.0	89.0	84.0	85.0	85.0	87.0	86.0	86.0	105.8
0.250	91.5	90.5	86.0	86.0	86.0	87.0	87.5	86.5	106.7
0.315	92.5	92.0	87.0	88.0	87.0	88.0	88.5	88.0	108.0
0.400	94.0	93.0	89.0	89.0	88.0	89.0	89.0	89.0	109.0
0.500	99.0	94.0	90.5	90.0	89.5	91.0	89.0	90.0	110.9
0.630	101.0	96.5	92.5	92.0	91.0	91.5	91.8	91.5	112.7
0.800	103.0	98.0	94.0	93.5	92.0	92.5	93.0	92.5	114.2
1.000	105.0	100.0	95.5	95.0	93.5	94.0	94.0	94.0	115.9
1.250	105.5	101.5	97.0	96.0	95.0	94.5	94.0	94.5	116.8
1.600	106.0	102.5	98.5	97.0	96.5	95.5	95.0	96.0	117.8
2.000	106.0	104.0	100.0	98.0	98.0	97.0	96.5	99.0	119.1
2.500	106.0	104.5	101.0	99.0	100.0	99.5	100.0	103.0	120.8
3.150	105.5	104.5	102.0	100.5	101.0	103.0	104.0	104.5	122.4
4.000	105.5	104.0	102.0	101.5	103.0	104.0	106.0	106.0	123.6
5.000	104.6	104.1	103.1	103.1	105.1	105.1	106.1	106.1	124.2
6.300	103.6	104.1	104.1	104.1	106.1	106.1	106.1	106.1	124.8
8.000	102.4	102.9	103.9	104.9	104.9	104.9	105.9	105.4	124.2
10.00	101.3	102.3	103.8	104.8	104.8	104.8	104.8	105.3	123.8
12.50	100.4	102.4	104.9	105.4	105.4	104.4	104.9	104.4	123.9
16.00	98.8	101.3	104.3	104.8	104.8	103.8	103.3	103.8	123.2
20.00	97.6	100.6	104.1	105.1	104.6	103.6	103.1	102.6	122.9
25.00	96.1	98.6	103.1	104.1	103.6	102.6	102.1	100.6	121.7
31.50	93.7	96.7	101.7	102.7	101.2	101.2	100.2	99.7	120.1
40.00	93.1	95.6	101.1	101.6	100.1	100.1	98.1	98.1	119.0
50.00	94.6	97.6	102.6	102.6	100.6	101.1	99.6	97.6	119.9

Corrected 1/3 Octave SPL's

Contoured Plug+Nozzle

90 degrees

P_R Psig

f_c (kHz)	2,	4,	6,	8,	10,	15,	22,	44.
0.200	68.0	70.0	72.0	72.0	73.0	75.0	78.0	86.0
0.250	69.5	71.5	72.5	72.5	74.0	76.0	79.0	87.0
0.315	71.0	72.0	73.0	73.0	74.5	76.0	80.0	88.0
0.400	72.0	73.0	74.0	74.0	75.0	78.0	82.0	89.0
0.500	73.5	74.0	75.0	75.0	77.0	81.0	83.0	89.0
0.630	74.0	74.0	75.0	76.0	78.0	81.5	84.0	90.0
0.800	74.0	74.0	76.0	77.0	80.0	83.0	87.0	90.5
1.000	74.0	74.0	76.0	78.0	80.5	85.0	88.0	92.0
1.250	73.0	75.0	77.0	79.0	82.0	86.0	90.0	93.0
1.600	71.0	74.0	78.0	80.0	83.0	87.0	92.0	94.0
2.000	67.0	74.0	78.0	80.0	84.0	89.0	93.0	95.0
2.500	66.0	74.0	79.0	81.0	86.0	90.0	94.0	98.0
3.150	66.0	74.0	79.0	81.5	86.0	91.0	98.0	99.0
4.000	66.1	74.1	79.1	82.1	87.1	92.1	100.1	99.1
5.000	66.1	74.1	79.1	82.1	87.1	93.1	100.1	106.1
6.300	66.1	74.1	79.1	82.1	88.1	94.1	104.1	106.1
8.000	66.0	74.0	79.0	82.0	88.0	96.0	105.0	106.0
10.00	63.8	73.8	78.8	81.8	87.8	95.8	104.8	103.8
12.50	65.0	72.5	78.5	82.5	88.5	96.5	104.5	104.5
16.00	64.0	72.0	77.5	81.0	87.5	95.0	103.0	104.0
20.00	63.8	71.8	76.8	80.8	87.8	94.8	101.8	103.8
25.00	63.3	70.8	76.8	80.3	86.8	93.8	100.8	102.8
31.50	62.5	68.0	76.0	79.0	87.0	93.0	100.0	102.0
40.00	62.5	68.5	72.5	77.5	86.5	90.5	98.5	101.5
50.00	59.8	66.8	72.8	80.8	85.8	89.8	97.8	102.8

Corrected 1/3 Octave SPL's

Test Model: Conical Plug

Reservoir Pressure = 30 psig

Atmospheric Pressure = 29.64 in. Hg

Measurement - Radius R = 3.05 m

Dry Bulb Temp. = 55° F

Wet Bulb Temp. = 48° F

f_c (kHz)	Theta in degrees								
	15	30	45	60	75	90	105	120	PWL
0.200	90.0	88.0	78.0	78.0	77.0	77.0	77.0	72.0	100.6
0.250	93.0	90.5	82.0	80.2	80.0	79.0	78.0	74.0	103.2
0.315	97.0	94.0	86.0	84.0	83.0	81.2	80.0	76.5	106.8
0.400	99.5	96.0	88.5	85.8	85.0	83.0	82.0	78.0	109.0
0.500	102.0	98.5	91.0	87.8	87.0	84.5	84.0	80.0	111.4
0.630	105.0	101.0	94.0	90.8	90.0	87.0	86.0	82.0	114.2
0.800	106.0	104.0	96.0	92.0	91.6	88.5	87.5	84.0	116.1
1.000	107.0	106.0	98.5	94.0	93.5	90.5	88.5	86.0	117.8
1.250	108.0	107.0	101.0	95.5	95.0	92.0	90.0	88.5	119.1
1.600	108.5	108.5	103.0	96.5	96.5	93.6	91.5	90.5	120.4
2.000	109.0	108.5	103.5	98.0	98.0	95.0	93.0	92.0	120.9
2.500	109.0	108.5	104.5	100.0	99.5	96.5	94.0	95.0	121.5
3.150	109.0	108.2	104.5	101.0	101.0	98.0	96.0	100.0	122.0
4.000	108.6	108.1	104.9	101.9	102.1	99.1	100.1	103.1	122.7
5.000	108.1	107.1	104.9	102.6	103.1	101.1	103.1	105.1	123.4
6.300	107.1	105.1	104.9	103.1	103.6	102.9	105.1	106.1	123.9
8.000	106.0	104.0	104.8	104.0	104.0	103.5	104.5	105.0	123.5
10.00	103.8	103.3	104.6	103.8	103.8	103.6	103.8	102.8	122.9
12.50	102.5	103.5	105.3	105.5	104.5	104.3	103.1	102.5	123.4
16.00	101.0	101.5	104.8	105.5	104.0	103.8	102.0	100.5	122.6
20.00	99.8	100.8	104.6	104.8	103.3	102.8	100.8	99.8	121.9
25.00	98.0	98.3	103.6	103.8	101.3	100.8	99.8	98.3	120.5
31.50	95.2	95.5	101.5	102.0	98.5	98.0	97.5	96.0	118.2
40.00	94.5	94.5	99.5	100.5	98.5	97.0	96.5	95.0	117.0
50.00	93.8	94.8	97.8	99.8	98.8	96.8	95.8	94.3	116.5

Corrected 1/3 Octave SPL's

Test Model: Conical Plug

Reservoir Pressure = 37 psig

Atmospheric Pressure = 29.57 in. Hg

Measurement - Radius R = 3.05 m

Dry Bulb Temp. = 51° F

Wet Bulb Temp. = 45° F

f_c (kHz)	Theta in degrees								
	15	30	45	60	75	90	105	120	PWL
0.200	92.0	89.0	83.0	82.0	82.0	80.0	79.0	78.0	103.0
0.250	94.5	90.0	85.5	84.0	84.5	82.5	81.0	79.0	105.0
0.315	96.0	92.0	88.0	87.0	86.0	83.0	82.0	80.0	106.8
0.400	98.0	94.0	89.0	88.0	87.0	84.0	83.0	81.0	108.4
0.500	100.0	96.0	91.8	91.0	88.0	85.5	84.0	82.5	110.4
0.630	102.0	98.5	94.0	93.0	90.0	87.0	86.5	84.0	112.6
0.800	103.8	101.0	96.0	94.8	91.5	89.0	88.0	86.0	114.6
1.000	105.0	103.5	98.0	96.5	93.5	91.0	90.5	88.0	116.5
1.250	107.0	106.0	100.0	98.0	96.0	92.0	93.0	90.0	118.7
1.600	107.5	107.0	102.0	99.0	97.5	95.5	94.5	92.0	119.9
2.000	108.0	108.0	103.5	100.5	98.0	96.5	97.5	95.0	121.0
2.500	109.0	108.8	105.0	102.0	100.0	99.0	100.5	98.0	122.5
3.150	107.5	108.8	106.5	103.5	102.0	102.0	103.0	102.0	123.6
4.000	108.1	108.7	107.1	104.1	103.6	104.1	105.6	104.1	124.7
5.000	108.1	108.3	107.1	105.6	104.7	106.1	107.1	106.6	125.7
6.300	107.6	107.6	108.1	107.1	106.1	106.9	107.1	106.6	126.3
8.000	105.9	106.9	107.9	107.9	106.4	107.4	106.7	107.9	126.5
10.00	105.3	106.3	107.8	108.8	106.8	107.3	106.3	107.8	126.6
12.50	104.5	105.0	108.5	109.5	107.5	108.0	107.0	107.5	126.9
16.00	103.4	103.4	107.9	108.9	106.9	107.4	105.9	106.4	126.2
20.00	102.7	102.2	107.2	108.7	106.7	107.2	105.2	105.7	125.8
25.00	99.7	100.2	105.7	106.9	105.2	106.2	104.7	104.2	124.4
31.50	96.9	98.4	103.9	104.9	103.4	103.9	101.9	101.9	122.3
40.00	95.9	97.9	102.9	103.4	102.4	101.9	99.2	99.9	120.7
50.00	97.3	99.3	103.4	103.3	101.8	100.8	98.8	98.8	120.4

Corrected 1/3 Octave SPL's

Test Model: Conical Plug

Reservoir Pressure = 51 psig

Atmospheric Pressure = 29.57 Hg.

Measurement - Radius R = 3.05 m

Dry Bulb Temp. = 51° F

Wet Bulb Temp. = 45° F

f_c (kHz)	Theta in degrees								
	15	30	45	60	75	90	105	120	PWL
0.200	93.5	91.0	87.0	87.0	88.0	89.0	91.0	87.0	108.4
0.250	95.0	92.0	88.0	88.0	89.0	89.5	91.5	89.0	109.4
0.315	97.0	94.0	89.3	89.0	90.0	90.5	92.4	91.0	110.7
0.400	97.5	95.0	90.3	90.2	91.0	91.0	93.0	92.5	111.6
0.500	99.0	96.0	91.8	91.2	91.8	91.8	93.5	93.0	112.5
0.630	101.0	98.0	93.0	92.2	93.0	92.8	94.5	94.5	114.0
0.800	103.0	100.6	94.5	93.2	94.0	93.8	95.0	95.0	115.4
1.000	104.5	103.0	95.6	94.5	95.0	95.0	95.5	96.0	116.8
1.250	105.0	105.0	97.0	96.0	96.0	96.0	96.0	97.0	118.1
1.600	106.4	106.8	98.0	97.0	97.0	97.5	97.0	99.0	119.6
2.000	107.0	107.0	99.0	97.5	98.3	98.5	98.8	101.0	120.4
2.500	107.0	107.0	100.0	98.6	99.6	99.5	101.0	103.0	121.3
3.150	107.0	106.0	100.5	100.0	101.8	102.5	104.0	104.6	122.6
4.000	107.1	105.7	101.1	101.1	103.1	104.4	105.9	105.6	123.6
5.000	106.9	105.1	102.1	103.1	104.7	105.1	106.6	106.1	124.3
6.300	105.1	104.6	103.1	105.1	105.7	106.6	106.6	106.8	125.0
8.000	103.4	103.9	102.9	106.9	105.5	106.4	106.7	106.3	125.1
10.00	102.8	103.6	103.8	106.8	106.5	106.3	105.8	105.8	125.0
12.50	102.3	103.8	105.0	107.5	107.2	106.0	106.0	105.5	125.2
16.00	101.6	102.9	104.9	106.9	106.6	105.4	104.9	104.4	124.6
20.00	99.7	102.7	105.7	106.7	106.4	104.7	104.5	103.7	124.3
25.00	97.5	101.7	104.7	105.7	105.4	103.7	103.5	101.7	123.2
31.50	96.9	100.5	102.9	103.9	103.9	102.7	101.7	99.9	121.7
40.00	95.9	99.4	102.9	103.4	102.9	102.4	101.4	99.4	121.1
50.00	96.6	100.8	104.8	104.8	104.8	103.8	102.8	101.3	122.7

Corrected 1/3 Octave SPL's

Conical Plug Nozzle

90 Degrees

P_R Psig

f_c (kHz)	2,	4,	6,	8,	10,	15,	22,	44	PSIG
0.200	54.0	68.0	64.0	66.0	66.0	68.5	76.0	83.0	
0.250	60.0	69.0	66.0	66.5	68.0	71.0	78.0	83.5	
0.315	63.0	71.0	68.0	70.0	70.0	74.5	80.0	85.0	
0.400	65.0	71.5	68.0	71.0	72.0	76.0	82.5	86.0	
0.500	66.0	72.0	70.0	73.0	74.0	78.5	84.0	87.0	
0.630	68.0	73.0	72.0	75.0	76.0	82.0	86.0	88.5	
0.800	69.0	74.0	73.0	77.0	78.0	83.0	88.5	90.0	
1.000	71.0	75.0	75.0	79.0	79.5	84.5	91.0	92.0	
1.250	72.0	75.0	76.0	81.0	81.5	87.0	92.0	94.0	
1.600	73.0	75.0	77.0	81.5	83.0	88.5	95.0	96.0	
2.000	74.0	75.0	78.0	83.0	84.0	90.0	97.0	97.0	
2.500	74.0	73.0	79.0	84.0	85.5	91.0	100.0	99.0	
3.150	74.0	73.0	79.0	84.0	86.0	93.0	103.0	100.0	
4.000	74.0	73.0	79.0	84.0	87.0	94.5	104.0	102.0	
5.000	74.1	73.1	79.1	84.1	87.1	95.6	104.1	104.1	
6.300	74.1	73.1	79.1	84.1	87.1	97.1	104.1	105.1	
8.000	73.9	72.9	78.9	83.9	86.9	97.9	103.9	105.9	
10.00	73.8	72.8	78.8	82.8	86.8	97.8	103.8	105.8	
12.50	73.4	72.9	78.4	83.4	87.4	98.9	103.4	105.9	
16.00	72.3	71.8	77.3	81.8	86.8	97.3	101.8	105.3	
20.00	71.6	71.1	76.6	81.6	86.1	97.6	100.6	105.1	
25.00	70.6	70.1	74.6	80.6	85.1	94.6	99.6	104.1	
31.50	69.7	69.2	72.7	76.7	84.2	93.7	97.7	103.2	
40.00	70.1	68.1	72.1	76.1	82.1	91.1	94.1	103.6	
50.00	69.6	67.6	71.6	75.6	82.1	90.6	93.6	103.6	

Corrected 1/3 Octave SPL's

Test Model: Porous (10%)

Reservoir Pressure = 30 psig

Atmospheric Pressure = 29.23

Measurement - Radius R = 3.05 m

Dry Bulb Temp. = 62° F

Wet Bulb Temp. = 58° F

Theta in degrees

f_c (kHz)	15	30	45	60	75	90	105	120	PWL
0.200	92.0	89.0	81.0	77.0	78.0	76.0	73.0	72.0	101.8
0.250	84.5	91.0	83.0	80.0	79.0	78.5	77.0	74.0	102.0
0.315	97.0	93.0	86.0	83.0	82.0	81.0	79.0	77.0	106.4
0.400	98.0	96.0	88.0	86.0	85.0	83.0	82.0	79.0	108.6
0.500	100.0	98.0	90.0	88.0	96.0	85.0	82.0	81.0	112.0
0.630	103.0	101.0	93.0	90.0	89.0	87.0	85.0	83.0	113.4
0.800	105.0	102.5	97.0	92.0	90.0	89.0	88.0	86.0	115.4
1.000	106.0	107.0	99.0	94.0	93.0	91.0	90.0	88.5	118.3
1.250	107.0	108.0	100.0	96.0	94.5	93.0	91.0	90.0	119.4
1.600	108.0	108.0	102.0	97.0	96.0	93.0	92.0	92.0	120.0
2.000	108.0	108.0	104.0	99.0	97.0	95.0	93.0	94.0	120.7
2.500	108.0	109.0	104.0	100.0	98.5	96.0	94.0	96.0	121.4
3.150	108.0	108.0	105.0	101.0	99.0	98.0	96.0	97.0	121.6
4.000	108.0	107.5	105.0	101.0	100.0	98.0	99.0	101.5	122.0
5.000	106.1	106.1	105.1	101.1	101.1	102.1	102.1	102.6	122.4
6.300	106.1	105.6	105.1	102.1	103.1	104.1	103.1	102.1	123.1
8.000	103.9	102.9	104.9	102.9	102.9	102.9	101.9	101.9	122.3
10.00	102.7	101.7	103.7	103.7	103.7	101.7	101.7	99.7	121.9
12.50	102.4	101.4	104.4	104.4	102.4	101.4	102.4	100.9	121.9
16.00	98.8	99.8	103.8	102.8	101.8	100.8	100.8	98.8	120.7
20.00	98.5	99.5	103.5	101.5	101.5	100.5	99.5	98.0	120.1
25.00	96.5	98.5	102.5	101.5	100.5	99.5	98.5	97.0	119.2
31.50	95.6	96.6	99.6	100.6	98.6	97.6	97.6	95.6	117.6
40.00	93.0	96.0	96.0	98.0	97.5	96.0	95.0	93.0	115.4
50.00	91.4	92.4	94.4	97.4	94.4	93.4	91.4	90.4	113.2

Corrected 1/3 Octave SPL's

Test Model: Porous (10%)

Reservoir Pressure = 37 psig

Atmospheric Pressure = 29.23

Measurement - Radius R = 3.05 m

Dry Bulb Temp. = 62° F

Wet Bulb Temp. = 58° F

f_c (kHz)	Theta in degrees								
	15	30	45	60	75	90	105	120	PWL
0.200	90.5	90.8	81.0	80.0	80.0	77.0	76.0	73.0	102.5
0.250	93.0	92.5	83.5	82.5	83.0	79.0	78.0	77.0	104.6
0.315	94.5	95.0	86.0	85.0	85.0	81.0	81.0	79.0	106.9
0.400	97.0	96.0	90.0	87.0	87.0	83.0	82.0	80.0	108.7
0.500	98.0	98.0	92.0	89.0	89.0	85.0	84.0	82.0	110.5
0.630	102.0	100.0	93.5	93.0	91.0	88.0	87.0	84.0	113.2
0.800	102.0	102.0	95.8	94.0	93.0	90.0	88.0	86.0	114.6
1.000	104.0	104.0	98.5	96.0	94.5	92.0	91.0	89.0	116.7
1.250	104.0	106.0	100.0	97.0	95.0	93.5	92.0	92.0	118.1
1.600	105.0	108.0	102.5	98.0	96.0	95.0	93.0	92.0	119.8
2.000	107.0	108.0	104.0	100.0	99.0	96.0	95.0	94.0	120.9
2.500	107.0	109.0	105.0	101.0	99.0	97.0	96.0	95.0	121.7
3.150	107.0	109.0	105.5	102.0	100.0	97.5	97.5	96.0	122.1
4.000	107.0	107.0	106.0	103.0	100.0	98.5	102.0	104.0	122.9
5.000	106.1	106.1	106.1	103.1	102.1	104.1	104.1	104.1	123.6
6.300	105.1	105.1	106.1	104.1	104.1	106.1	104.1	105.1	124.3
8.000	103.9	103.9	105.9	104.9	105.9	104.9	103.9	104.9	124.3
10.00	103.7	102.7	105.7	104.7	104.7	104.7	103.7	103.7	123.7
12.50	102.4	102.4	106.4	106.4	104.9	105.4	104.4	103.4	124.2
16.00	99.8	100.8	105.8	105.8	104.8	104.8	102.8	101.8	123.4
20.00	99.5	99.5	105.5	104.5	104.5	103.5	102.0	99.5	122.5
25.00	97.5	98.5	103.5	104.5	103.5	102.5	100.5	98.5	121.5
31.50	94.6	97.6	102.6	103.6	102.6	101.6	99.6	97.6	120.6
40.00	94.0	96.0	100.0	101.0	100.0	99.0	96.0	97.5	118.1
50.00	95.4	95.4	98.4	101.4	100.4	97.4	96.4	95.4	117.8
									117.0

Corrected 1/3 Octave SPL's

Test Model: Porous (10%)

Reservoir Pressure = 51 psig

Atmospheric Pressure = 29.37

Measurement - Radius R = 3.05 m

Dry Bulb Temp. = 73° F

Wet Bulb Temp. = 64° F

Theta in degrees

f_c (kHz)	15	30	45	60	75	90	105	120	PWL
0.200	91.0	89.0	83.0	85.0	85.0	85.0	86.0	86.0	105.4
0.250	92.5	91.0	85.0	86.0	86.0	86.0	89.0	87.0	107.1
0.315	94.5	92.0	86.5	87.5	87.0	87.0	90.5	88.0	108.4
0.400	96.0	93.5	88.0	88.0	88.0	88.0	91.0	88.5	109.4
0.500	98.0	95.0	90.0	89.5	89.0	89.0	92.0	89.0	110.8
0.630	100.0	97.0	92.0	91.0	91.0	91.0	93.0	90.5	112.5
0.800	101.0	98.5	94.0	92.0	92.0	92.0	93.5	91.5	113.6
1.000	102.0	100.0	95.0	93.0	93.0	93.0	94.0	94.0	114.8
1.250	104.0	101.0	97.0	95.0	95.0	95.0	94.5	94.0	116.3
1.600	105.0	102.0	98.0	96.0	96.0	96.5	96.0	94.0	117.3
2.000	105.0	103.0	99.0	98.0	97.0	98.5	96.0	97.0	118.4
2.500	105.0	104.0	101.0	99.0	99.0	100.0	100.0	102.0	120.4
3.150	105.0	104.0	101.0	99.0	100.5	101.0	102.5	107.0	122.3
4.000	105.1	104.6	101.1	99.1	100.1	104.1	104.1	107.1	123.0
5.000	105.1	104.1	102.1	100.1	104.1	105.1	105.1	106.1	123.6
6.300	103.6	103.1	102.6	104.1	106.1	105.1	105.1	106.1	124.3
8.000	103.0	103.0	104.0	106.8	106.0	105.0	106.0	106.0	124.8
10.00	101.8	102.3	103.8	106.3	105.8	104.8	104.8	105.8	124.4
12.50	101.5	102.5	105.0	106.5	105.5	105.5	105.5	104.5	124.5
16.00	99.7	101.9	104.9	104.9	104.9	104.9	103.9	102.9	123.6
20.00	98.7	100.7	104.7	104.7	103.7	103.7	103.7	101.7	122.8
25.00	96.8	98.8	103.8	103.8	103.8	102.8	102.8	101.8	122.1
31.50	95.6	98.0	103.0	103.0	103.0	102.0	101.0	100.0	121.1
40.00	94.4	98.4	102.4	102.4	102.4	99.4	99.4	98.4	120.0
50.00	95.8	98.8	103.8	102.8	103.8	99.8	98.8	97.8	120.7

Corrected 1/3 Octave SPL's

Test Model: Porous (4%)

Reservoir Pressure = 30 psig

Atmospheric Pressure = 29.32 in Hg

Measurement - Radius R = 3.05 m

Dry Bulb Temp. = 60° F

Wet Bulb Temp. = 57° F

f_c (kHz)	Theta in degrees								
	15	30	45	60	75	90	105	120	PWL
0.200	91.0	89.0	81.0	79.0	78.0	76.0	76.0	75.0	101.6
0.250	94.0	90.0	83.0	81.0	79.0	78.5	78.0	76.0	103.6
0.315	96.0	92.5	85.5	83.0	82.0	81.0	80.0	78.0	105.9
0.400	99.0	95.0	87.0	85.5	84.0	82.5	82.0	80.0	108.4
0.500	101.0	96.0	89.0	88.0	86.0	84.0	83.0	82.0	110.1
0.630	103.0	100.5	92.0	91.0	88.5	86.5	85.0	83.5	113.1
0.800	104.0	103.0	95.0	92.5	91.0	88.0	88.0	85.5	115.1
1.000	106.0	105.0	98.0	95.0	93.5	90.0	90.5	87.5	117.2
1.250	107.0	107.0	100.0	97.0	95.0	91.5	93.0	90.0	119.0
1.600	108.0	108.0	102.0	98.0	96.5	94.5	93.0	92.0	120.2
2.000	108.0	109.0	104.0	99.5	98.0	96.5	94.0	92.0	121.3
2.500	108.0	109.0	105.0	101.0	100.0	98.5	96.0	95.0	122.0
3.150	108.0	108.0	105.0	101.0	101.0	100.0	98.0	100.0	122.2
4.000	107.0	107.5	105.0	101.0	101.0	102.0	102.0	103.0	122.9
5.000	106.1	106.6	105.1	101.1	101.1	103.1	104.1	104.1	123.1
6.300	105.1	105.1	105.1	102.6	103.1	104.1	104.1	105.1	123.5
8.000	103.9	103.9	104.9	103.9	102.9	103.9	103.9	104.9	123.3
10.00	101.7	102.7	104.7	104.7	102.7	102.7	102.2	104.7	122.8
12.50	101.3	101.8	105.3	105.3	103.3	103.3	102.3	103.3	123.0
16.00	99.8	100.8	104.8	104.8	101.8	100.8	99.8	101.8	121.6
20.00	97.4	99.4	104.4	104.4	101.4	101.4	100.4	99.4	121.2
25.00	96.4	98.4	102.4	103.4	100.4	100.4	99.4	98.4	120.0
31.50	91.5	96.5	100.5	100.5	98.5	98.5	97.5	97.5	117.9
40.00	89.8	92.8	97.8	97.8	96.8	96.8	95.3	94.8	115.6
50.00	89.3	91.3	96.3	97.3	96.3	95.3	94.3	94.3	114.6

Corrected 1/3 Octave SPL's

Test Model: Porous (4%)

Reservoir Pressure = 37 psig

Atmospheric Pressure = 29.32 in Hg

Measurement - Radius R = 3.05 m

Dry Bulb Temp. = 60° F

Wet Bulb Temp. = 57° F

f_c (kHz)	Theta in degrees								
	15	30		60	75	90	105	120	PWL
0.200	89.0	91.0	83.0	81.0	76.0	78.0	74.0	75.0	102.4
0.250	91.0	92.0	85.5	82.5	78.0	81.0	76.0	77.0	104.0
0.315	93.0	94.5	87.5	85.0	80.5	83.0	78.0	79.5	106.3
0.400	94.5	96.0	89.0	87.0	82.5	84.0	80.0	81.5	107.8
0.500	96.5	97.5	92.0	89.0	84.6	86.0	82.0	83.5	109.8
0.630	99.6	100.0	94.0	91.0	87.0	88.0	84.0	85.6	112.2
0.800	101.5	102.0	97.0	92.5	89.5	90.0	86.0	88.0	114.3
1.000	104.0	104.0	99.0	94.0	91.5	92.0	88.0	90.0	116.4
1.250	105.0	106.0	101.0	96.0	94.0	94.0	91.0	91.0	118.2
1.600	105.5	107.5	102.5	97.5	95.5	95.0	92.5	93.0	119.6
2.000	106.0	108.0	104.0	98.6	97.0	96.5	94.0	95.0	120.5
2.500	107.0	108.0	105.0	100.0	98.5	98.5	96.0	97.0	121.3
3.150	107.0	107.5	106.0	100.6	100.0	100.0	97.0	98.5	121.9
4.000	106.5	107.5	106.0	101.5	100.5	101.5	99.0	100.0	122.3
5.000	106.1	106.6	106.1	102.1	101.1	102.6	100.6	102.1	122.6
6.300	105.6	105.1	106.1	102.6	102.1	104.1	102.1	103.1	123.0
8.000	104.9	103.9	105.9	103.4	102.4	103.9	102.9	102.9	123.0
10.00	103.7	102.7	104.7	103.7	102.7	106.7	103.7	102.7	123.5
12.50	102.3	101.8	105.3	104.3	104.3	107.3	105.3	103.3	124.3
16.00	101.3	100.3	104.3	103.8	103.8	104.8	105.8	102.8	123.3
20.00	99.4	98.4	103.4	103.9	104.4	103.4	104.4	101.4	122.6
25.00	97.4	96.4	102.4	102.9	103.4	102.4	102.4	98.4	121.1
31.50	95.0	93.5	99.5	102.0	101.5	99.5	101.5	95.5	119.3
40.00	93.8	92.8	97.8	101.8	99.8	97.8	99.8	91.8	118.0
50.00	95.8	92.3	98.3	103.3	101.3	97.3	99.3	91.3	118.6

Corrected 1/3 Octave SPL's

Test Model: Porous (4%)

Reservoir Pressure = 51 psig

Atmospheric Pressure = 29.32 in Hg

Measurement - Radius R = 3.05 m

Dry Bulb Temp. = 60° F

Wet Bulb Temp. = 57° F

Theta in degrees

f_c (kHz)	15	30	45	60	75	90	105	120	PWL
0.200	92.0	90.0	86.0	85.0	84.0	86.0	87.0	87.0	106.2
0.250	94.0	92.0	88.0	86.0	85.0	87.0	88.0	88.5	107.7
0.315	96.5	94.0	89.5	87.5	86.5	88.5	89.5	89.0	109.4
0.400	98.0	95.0	90.5	89.0	87.5	90.0	90.0	90.0	110.5
0.500	99.0	96.5	92.0	90.0	88.5	91.0	90.5	90.8	111.6
0.630	102.0	98.0	93.5	91.5	90.5	92.5	91.8	92.0	113.4
0.800	103.5	99.5	95.0	93.0	91.5	94.0	92.5	93.0	114.8
1.000	104.5	101.0	96.0	94.0	93.0	94.5	94.0	94.0	115.9
1.250	105.5	102.0	97.0	96.0	94.0	96.0	95.0	95.7	117.1
1.600	106.0	103.5	99.0	97.0	95.0	96.5	97.0	98.0	118.4
2.000	106.0	105.0	100.0	98.0	97.0	98.0	99.0	100.0	119.6
2.500	106.0	105.0	100.0	100.0	99.0	99.0	100.5	103.0	120.8
3.150	106.0	105.0	101.5	100.6	100.5	100.5	103.0	104.5	121.9
4.000	106.0	105.0	101.5	102.0	101.0	101.5	104.0	106.0	122.8
5.000	105.6	105.1	102.1	102.6	103.6	104.1	105.1	106.1	123.6
6.300	104.1	104.1	102.1	102.6	105.1	104.1	105.1	106.1	123.7
8.000	102.9	103.9	103.9	104.9	104.9	103.9	104.9	105.9	124.0
10.00	101.7	102.7	103.7	104.7	104.7	103.7	104.7	104.2	123.4
12.50	101.3	103.3	104.3	105.3	104.3	104.3	104.3	103.3	123.5
16.00	99.8	100.8	103.8	104.8	103.8	103.8	103.8	102.8	122.8
20.00	98.4	100.4	103.4	104.4	103.4	103.4	103.4	101.4	122.4
25.00	96.4	99.4	102.4	103.4	102.4	102.4	101.9	100.4	121.2
31.50	95.0	97.5	101.5	101.5	101.5	101.0	99.5	98.5	119.7
40.00	93.3	96.8	98.8	100.8	100.8	99.8	97.8	96.8	118.4
50.00	94.8	98.3	101.3	102.3	103.3	101.3	98.3	98.3	120.1

Model	Observer Angle θ								Pressure Ratio ξ
	15°	30°	45°	60°	75°	90°	105°	120°	
Convergent Nozzle	112.7	112.3	109.9	108.0	108.5	109.2	108.0	109.5	2.0
	117.7	119.1	115.6	114.6	113.8	113.8	114.4	114.7	2.5
	124.2	125.2	122.3	122.3	121.2	121.6	120.0	122.0	3.05
	127.0	126.9	123.7	122.5	122.4	123.3	122.6	122.6	3.65
	128.1	127.5	124.1	123.2	121.3	122.2	121.3	121.3	4.0
	129.8	129.4	125.3	124.0	121.9	122.4	122.0	121.1	4.5
Contoured Plug-Nozzle	113.5	112.3	108.7	108.0	106.8	106.4	104.8	104.3	2.0
	117.7	116.2	113.9	112.8	113.2	111.6	112.9	112.5	2.5
	117.8	117.9	116.2	113.9	113.3	112.8	112.2	112.2	3.05
	116.7	117.3	116.3	115.2	114.9	114.2	114.1	113.8	3.65
	116.8	116.8	115.6	116.4	116.7	115.9	116.1	116.6	4.0
	116.2	115.1	115.0	115.3	115.4	115.3	115.5	115.6	4.5
Solid Conical Plug-Nozzle	119.2	118.3	116.3	114.9	114.1	113.1	113.0	113.4	3.05
	118.7	118.7	118.6	118.4	116.7	117.2	116.6	116.7	3.65
	117.3	117.3	115.3	116.8	116.8	116.3	116.7	116.3	4.5
Porous Conical PN (4% Porosity)	117.9	118.0	116.1	114.6	113.1	113.3	112.7	113.4	3.05
	116.5	117.6	116.6	114.5	113.9	114.8	113.8	112.4	3.65
	116.7	115.8	114.6	115.1	114.8	114.6	115.0	115.4	4.5
Porous Conical PN (10% Porosity)	118.1	118.1	115.9	113.6	113.0	112.1	111.6	111.0	3.05
	117.0	117.9	117.0	115.8	115.0	114.7	113.5	113.5	3.65
	115.7	115.0	115.1	115.6	115.6	115.3	115.4	115.9	4.5

OASPL's of the Convergent Nozzle, Contoured Plug-Nozzle, Solid Conical and Porous Conical Plug-Nozzles.

APPENDIX IV

The absorption corrections based on the Evans and Bass relation [28], are quite large at higher band-center frequencies f_c > 63 kHz (see Table I-3). The SPL's so corrected and the calculated PWL's show a sharp increase for $f_c \geq 63$ kHz. Such an increase in the radiated noise levels suggests that the predicted magnitude of the absorption corrections at higher band-center frequencies may be questionable. For further details see Appendix I. Therefore the acoustic results presented in the main body of the report are based on corrected SPL data for band-center frequencies up to f_c = 50 kHz. To facilitate any future analysis of the original acoustic data by an alternate approach for calculating the absorption corrections, the uncorrected SPL data for f_c = 200 HZ to 100 kHz are also tabulated on pp. 161-183.

Uncorrected 1/3 Octave SPL's

Test Model : Conv Nozzle

Reservoir Pressure = 15 psig Dry Bulb Temp. = 83°F

Atmospheric Pressure = 29.42 in Hg Wet Bulb Temp. = 71°F

f (kHz)	Theta in degrees							
	15	30	45	60	75	90	105	120
0.200	87	81	76	76	71	74	74	74
0.250	90	87	79	78	75	76	75	75
0.315	93	90	82	81	79	78	76	76
0.400	96	92	84	82	80	80	78	78
0.500	99	94	87	84	82	82	80	82
0.630	100	96	89	85	85	83	82	81
0.800	104	101	91	88	87	85	84	83
1.000	104	103	94	91	89	87	85	85
1.250	104	104	96	91	90.5	88	87	86
1.600	104	104	97	93	91	90	88	87
2.000	104	104	98	95	93	91	90	88
2.500	103	103.5	100	95	94	92	91	90
3.150	101	102	100	96	95	92.5	91	90
4.000	99	100	100	97	96	98	91.5	92
5.000	99	98	100	98	98	99	93	101
6.300	96	96	100	97	98	99	95	101
8.000	94	96	100	97	98	99	100	102
10.00	93	95	98	97	99	100	100	102
12.50	92	94	97	97	99	101	101	101
16.00	89	93	97	97	99	100	100	99
20.00	89	93	97	98	98	99	98	98
25.00	89	93	97	98	99	99	97	98
31.50	87	89.5	97	99	99	99	98	97
40.00	84	84	94	94	96	96	94	94
50.00	77	78	87	89	90	92	89	89
63.00	69	70	81	81	82	83	80	81
80.00	60	64	74	76	76	78	74	75
100.0	56	62	64	64	66	72	74	71

Uncorrected 1/3 Octave SPL's

Test Model : Conv Nozzle

Reservoir Pressure = 22 psig Dry Bulb Temp. = 83°F

Atmospheric Pressure = 29.42 in Hg Wet Bulb Temp. = 71°F

f (kHz)	Theta in degrees							
	15	30	45	60	75	90	105	120
0.200	90	85	78	77	75	74	76	74
0.250	93	88.5	84	81	79	78	78	76
0.315	97	92.5	87	85	83	82	80	78
0.400	101	96	89	86	85	84	80	80
0.500	104	98	92	88	87	86	83	84
0.630	105	102.5	95	91	90	88	85	85
0.800	107	106	97	93	92	90	87	86
1.000	108	108	100	95	94	92	90	90
1.250	109	110	101	96	95	94	91	91
1.600	109	111	102.5	99	97	95	93	92
2.000	109	112	104	100	98	96	95	93.5
2.500	109	110	105	101	100	99	95	95.0
3.150	108	109	105	102	102	100	100	103
4.000	106	107	105	101.5	102	103	103	105
5.000	104	106	105	102	104	105	106	107
6.300	100	105	105	104	105	106	107	107
8.000	98	104	105	106	105	105	105	107
10.00	98	102	105	107	105	104	105	105
12.50	97	101	105	107	103	104	105	105
16.00	96	101	105	104	103	102	103.5	102
20.00	95	101	105	104	103	103	103.5	102
25.00	95	100	103	104	103	102	103	102
31.50	95	100	101	100	102	101	103	102
40.00	89	96	98	96	98	100	100	98
50.00	83	87	91	92	93	93	96	92
63.00	76	80	83	81	85	86	88	85
80.00	72	75	77	75	80	82	80	77
100.0	71	71	72	70	72	70	70	70

Uncorrected 1/3 Octave SPL's

Test Model : Conv Nozzle

Reservoir Pressure = 30 psig Dry Bulb Temp. = 83°F

Atmospheric Pressure = 29.42 in Hg Wet Bulb Temp. = 71°F

f (kHz)	Theta in degrees							
	15	30	45	60	75	90	105	120
0.200	94.5	88	85	81	84	82	81	80
0.250	98	91.5	86.5	84	85.5	84	82.5	81.5
0.315	101	95	89	87	88	86	84	83
0.400	104.5	100	91	90	89	87.8	86	84.2
0.500	106.5	103	93.5	92.2	91	89.5	87	85.2
0.630	109.5	106	96	95	93	91.5	89.5	87.2
0.800	111.5	109.5	99	97	95	94	91.2	89
1.000	113	113	101	99	96.5	95	93	91
1.250	114	115	104	101	98	97.3	95	93.5
1.600	114.5	117	107	103	101	98	96	95
2.000	115	118	109	104.5	103	101	98.5	101
2.500	115	117.5	110.5	106	105.5	104	101	109
3.150	115	116	110.5	107.5	108.7	107.8	107	114
4.000	114	114	111.0	109	110	112	109.5	116
5.000	113	112.6	111.0	111	112	115	111.5	115
6.300	111.5	111	111.0	112	113	115	112	113.5
8.000	110.5	110	111.5	114	113	113	111.8	112
10.00	109	109	112	114.6	113	111.5	111	111
12.50	108	107.7	112.5	114.6	112.2	110.2	110.6	109
16.00	106.5	107	113	114.6	111.2	109.2	109.5	108
20.00	104.5	107	112.5	112	110	109	109	107.5
25.00	104	107	112	111	108.5	108.6	108	106.5
31.50	102.5	106.2	110.5	107	106	107	107	104.2
40.00	100	104	108	103	102	104.5	104	101.5
50.00	95.5	98.2	104	97	98	99	98	95
63.00	87	92	96	89	91.5	91	91	89
80.00	80	84	88.5	83	845	86	86	84
100.0	74	76	81	75	76	80	80	78

Uncorrected 1/3 Octave SPL's

Test Model : Conv Nozzle

Reservoir Pressure = 37 psig Dry Bulb Temp. = 83°F

Atmospheric Pressure = 29.42 in Hg Wet Bulb Temp. = 71°F

f (kHz)	Theta in degrees							
	15	30	45	60	75	90	105	120
0.200	99	95	89	85.5	84	83	82.6	82
0.250	102	95.5	90.5	87	86.5	84	83.0	83
0.315	105.5	100	92.0	89.5	87.8	86	84	84
0.400	109	103	94	92	89	87	86	85.2
0.500	111	106	96.5	94.2	91	88.5	87.5	87
0.630	114	109	99	96	93	90.5	89.5	88.5
0.800	115.5	111	101.5	98.5	95	92.5	91	90.2
1.000	117	115	104.5	100	16.5	94.5	93	92
1.250	117	117.7	106.5	101.2	98	96.2	94.6	95
1.600	117	119.5	108.2	103.8	99.5	98	96.5	99
2.000	117.5	119.5	109.5	104.5	101.7	100.5	99	105
2.500	117.5	119	110.5	106	104	103.5	103	112
3.150	117	117	110.5	107.5	107	107	107	116.2
4.000	116.5	115.2	111.2	109	109.5	111	113	116
5.000	115.5	114	111.3	110.7	111.5	115	117	114
6.300	114.5	112.5	112.2	112	114.5	117	115.6	112.5
8.000	113.5	115	113.0	113	115	115.6	113.5	111.2
10.00	111.3	111	114	114	115	113.7	112	111
12.50	109.5	110	116	114	113.2	113	111	110
16.00	108	109.5	115.7	114	112	112.5	110.6	110
20.00	107	109.5	114.5	113.7	111	112.5	110.2	108.6
25.00	105	109.5	113	113	110	111.5	109.7	108
31.50	103.5	109	110.5	110.5	109.2	119	109	106
40.00	100.5	105	106	107	108.3	109	108	102
50.00	96.7	99.5	101	101.5	105	104.5	103	95
63.00	91.5	93.0	95	96	98	98	97	89
80.00	85	86	88	88.5	92	91	91	83
100.0	80	80	78	78	83	82	83	80

Uncorrected 1/3 Octave SPL's

Test Model : Conv Nozzle

Reservoir Pressure = 44 psig
Atmospheric Pressure = 29.42 in Hg

Dry Bulb Temp. = 83°F
Wet Bulb Temp. = 71°F

f (kHz)	Theta in degrees							
	15	30	45	60	75	90	105	120
0.200	101	93	88	86	83	82	81	81
0.250	104	96	90	89	85	84	83	82.5
0.315	107	101	92	90	87	86	85	83
0.400	110	104	94	92	89	88	87	84
0.500	112	107	98	94	92	90	88	86
0.630	114.6	110	100	96	93	91	90	88
0.800	116	113	103	99	95	94	93	91
1.000	117	116	105	100	97	96	95	92.5
1.250	118	117.5	107	101	99	97	96	95
1.600	119.2	119	108	102	100	98	96	95
2.000	119.2	119	109	104	102	100	99	100
2.500	119	118.5	110	105	104	103	104	106
3.150	118	117.5	110	105.5	106	108	111	114
4.000	117.7	117	111	107	108	114	113	114
5.000	116	116	111	109	112	115	113	114
6.300	115	115	112.5	113	114	114	112	111
8.000	114	113	113	116	113	112	112	111
10.00	112.6	112.5	115	116	111	112	111	111
12.50	111	112	116	115	111	111	111	109
16.00	110	111	116	113.5	111	111	111	109
20.00	109	111	114	113	111	111	110	109
25.00	107.5	111	114	113	111	111	110	108
31.50	106	110.5	114	113	111	111	109	107.5
40.00	102	108	109	109	109	108	105	106
50.00	97	101	104	104	103	101	100	100
63.00	88	94	96	98	96	95	92	90
80.00	87	90	90	90	90	88	86	86
100.0	76	81	80	80	80	80	80	80

Uncorrected 1/3 Octave SPL's

Test Model : Conv Nozzle

Reservoir Pressure = 51 psig
Atmospheric Pressure = 29.42

Dry Bulb Temp. = 83°F
Wet Bulb Temp. = 71°F

f (kHz)	Theta in degrees							
	15	30	45	60	75	90	105	120
0.200	102	97.5	91	88	86	84	83	82
0.250	105	100	94	90	88	86	85	83
0.315	109	104	96	91.5	89.5	85	86	84
0.400	112	107	98	94.5	92	89	88	86
0.500	114	110	105.5	96	93.5	91	90	87.5
0.630	116	113	103	98.5	95	93	91.5	89.5
0.800	118	115.5	106	100.5	97	95	92	91.7
1.000	119.5	117	107.5	102	98.5	97	96	94.0
1.250	120.5	119	109	103	99.7	99	98	96.5
1.600	121	120	110.5	105	101.5	101.3	100	99
2.000	121	121	111	106	103.5	103.5	103	103.5
2.500	120	121	112	107	105.5	106	107.5	109
3.150	119.7	120	112.5	108	109	111	111	113
4.000	119	119	113	110	110	114	111	13.5
5.000	117.5	117.5	114	112	111.5	114	112	113
6.3000	116	116.5	114.5	114.5	112.5	113.0	111.5	111.5
8.000	115	115.5	115.5	116.5	113	112.5	111.5	110.5
10.00	113	115	116	116	113	112	111.2	110
12.50	112	114	116.5	115	113	111.7	111	109.5
16.00	111	113	116	113.5	113	111.7	110.5	109
20.00	110.5	113	115.5	114	112	111.7	110	108.5
25.00	109	112	114.5	115	111.5	111.7	109	108
31.50	107	110.5	113	12.5	110	111	107.5	107.5
40.00	104	107	108	108	107	108	104	107
50.00	100	101	101	103	102.5	102	99	98.5
63.00	94	96	96	97	98	95	94	94
80.00	88	89	87	86	89	88.5	84	85.5
100.0	80	80	80	80	80	80	72	80

Uncorrected 1/3 Octave SPL's

Test Model : Contoured PN

Reservoir Pressure = 15 psig

Atmospheric Pressure = 29.64 in Hg

Dry Bulb Temp. = 55°F

Wet Bulb Temp. = 51°F

RH = 60

f (kHz)	Theta in degrees							
	15	30	45	60	75	90	105	120
0.200	81	74	73	70	72	72	72	72
0.250	86	80	76	73	75	74	73	73
0.315	90	85	79	76.5	78	76	76	74
0.400	92	87	81	78	79	78	77	74
0.500	95	90	84	81	80	80	80	77
0.630	98.5	93	86	84	83	82	80	79
0.800	103	95	87.5	86	83	84	83	79
1.000	103	98	90	88	86.5	85.5	85	82
1.250	104.5	100	93	90	87	87	87	83
1.600	105	103	94	91	88	88	88	84
2.000	105	103	95	92	89	89.5	88	85
2.500	105	103	97	94.5	92	90	89	87
3.150	102	103	98	95	92	91	90	87.5
4.000	100	102	98	96	92	95	90	88
5.000	98	101	98	97	94	96	92	90
6.300	96	99	97	96.5	94.5	95	93	93
8.000	94	98	98	96	94	97	96	95
10.00	92	97.5	97	96.5	97	98	98	97
12.50	91	97	97	96.5	97	97	95	96
16.00	88	95	97	98	97	95	93	94
20.00	88	94.5	97	98	97	95	92	93
25.00	88	94	95	98	97	95	93	94
31.50	87	94	96	97.5	96.5	93	93	93
40.00	84	92	94	96	97	90	91	90
50.00	80	85	90	92	94	85	83	84
63.00	73	74	84	84	87	80	78	75
80.00	68	70	78	75	82	73	71	69
100.0	58	58	67	66	74	60	58	58

Uncorrected 1/3 Octave SPL's

Test Model : Contoured PN

Reservoir Pressure = 22 psig. Dry Bulb Temp.= 55°F

Atmospheric Pressure = 29.64 in Hg. Wet Bulb Temp.= 48°F

f (kHz)	Theta in degrees							
	15	30	45	60	75	90	105	120
0.200	86	83	76	76	74	73	74	72
0.250	90	86	81	80	78	77	76	74
0.315	93	90	84	82	80	80	78	77
0.400	95	93	87	85	81	82	80	78
0.500	98	97	90	86	83	83	82	82
0.630	102	100	91	88	85	85	83	83
0.800	104	103	93	91	87	87	86	84
1.000	106	105	95	93	89	89	88	86
1.250	107	106	97	95	90	90	89	87
1.600	108	107	99	97	92	92	90	89
2.000	109	108	100	98	93	93	90	90
2.500	108	106	102	99	95	94	93	94
3.150	108	105	102	100	97	95	95	100
4.000	107	105	103	100	97	96.8	98	100
5.000	106	103	102	99.5	100	97	100	104
6.300	104	102	102	100	105	98	106	106
8.000	102	100	102	100	107	99	106	104
10.00	100	100	102	102	105	102	104	103
12.50	98	99	103	103	102	104	102	101
16.00	97	99	104	104	101	101	100	100
20.00	96	99	104	103	101	100	100	99
25.00	95	99	103	102	102	101	102	98
31.50	94	94	101	102	100	102	100	96
40.00	93	90	99	99.5	97	102	98	95
50.00	90	87	94	94	94	99	90	90
63.00	94	79	88	88.5	88	93	87	84
80.00	80	72	82	83	81	86	78	76
100.0	72	66	74	84	73	81	73	70

Uncorrected 1/3 Octave SPL's

Test Model : Contoured PN

Reservoir Pressure = 30 psig
Atmospheric Pressure = 29.43 in Hg

Dry Bulb Temp. = 68°F
Wet Bulb Temp. = 62°F

f (kHz)	Theta in degrees							
	15	30	45	60	75	90	105	120
0.200	90	89	80	78	80	76	77	74
0.250	93	91	82	79.5	81.5	78	79	76
0.400	97	94.5	87	84	86	82	82.5	80
0.500	100	96.5	89	86	88	84.5	85	81
0.630	102	99	92	89	89.7	86.5	87	84
0.800	104.5	102.5	94	91	92	88	88	86
1.000	106	104	96	94	93.8	90	90	88
1.250	107	106.5	99	96	95	92	01	89.5
1.600	107	108	101	97	96	94	93	91.5
2.000	108	108	103	98	97	95	94	92
2.500	108	108	104	99.5	98	97	95	95.5
3.150	107.5	108	105	101	100.5	99	98	99
4.000	107	108	105	101	100	99	100	102
5.000	106.5	107	105	101	100	101	102	104
6.300	105.5	106	105	102	103	104	102	104
8.000	104	105	105	102	104	103	103	102
10.00	102.5	104	105	103.5	104	103	103	102
12.50	101	101	105	104	103	103	102.5	101
16.00	100	101	105	104	102.5	102.5	102	101
20.00	99	100.5	105	104	102.5	102	101	100
25.00	97.5	100	105	104	102.5	101.5	101	100
31.50	96	98	104	104	101.5	101.5	100	100
40.00	94	102	102	99.5	99	98	97	
50.00	91	92	98	98	95	92.5	92	90
63.00	87	87	92	93	89	87	86	84
80.00	83	83	86	87	83	82	80	76
100.0	77	77	80	82	74	75	73	67

Uncorrected 1/3 Octave SPL's

Test Model : Contoured PN

Reservoir Pressure = 37 psig Dry Bulb Temp. = 68°F

Atmospheric Pressure =29.43 in Hg Wet Bulb Temp. = 62°F

f (kHz)	Theta in degrees							
	15	30	45	60	75	90	105	120
0.200	91	88	79	80	79	78.5	77	72
0.250	92.5	90	82	83	81	81	78	75
0.315	94	92.5	85	85	84.5	83.5	80.5	78
0.400	96	94	87.5	87.5	86.5	84.5	82	80
0.500	98	96	90	90	88.5	86.5	84	81
0.630	100	99	93	91.5	91	88.5	86	84
0.800	101.5	101	95.5	94	93	90	88	87
1.000	103	103	98	95.5	94	91.5	91	89
1.250	104.5	105.5	100	97	96	93	92	91.5
1.600	105.5	106	102	98.5	98	94.5	94	93
2.000	106	107.5	103	100	99	96	95	95
2.500	106	107.5	104	101	100	97	96	97
3.150	106	107	105	102	101	98.7	98	100
4.000	105.5	106.5	105	102	101	100	99	102
5.000	105.5	106.5	105	102	102	101	101	103
6.300	106	105.5	105	103	104	102.5	103	103
8.000	105	105	105	104	105	103	104.5	105
10.00	104	104.5	105	104	105	104.5	106	105
12.50	102	102.5	105	105	105	105	105.5	104.5
16.00	101	101.5	105	105.5	105	105	105	104
20.00	99	100	105	106	105	105	104	103
25.00	99	99	105	106	105	105	103.5	102
31.50	98	97.5	104	104	103	105	101.5	100
40.00	97	96.5	101	102	101	102	100	98
50.00	94	95	99	98	97	97	97	94
63.00	89	90	95	92.5	92	91	91	81
80.00	88	85	90	87	86	85	85	84
100.0	83	80	84	80	79	79	80	78

Uncorrected 1/3 Octave SPL's

Test Model : Contoured PN

Reservoir Pressure = 44 psig
Atmospheric Pressure = 29.57 in Hg

Dry Bulb Temp. = 63°F
Wet Bulb Temp. = 51°F

f (kHz)	Theta in degrees							
	15	30	45	60	75	90	105	120
0.200	91	90	86	84	84	86	87	87
0.2500	95	92	87	85	85	87	88	88
0.315	97	94	88	87	87	88	89.5	89
0.400	98	96	88	88	88	90	81	90
0.500	100	98	89	90	89	90	91	91
0.630	101	100	91	91	91	91	91	92
0.800	102	102	93	92	92	92.5	92	94
1.000	104	104	96	94	94	94	92	94
1.250	105	105	97	95	95	95	94	94
1.600	106	107	98	97	96.5	95	95	95
2.000	106.5	107	99	97	97	97	96	96.5
2.500	107	107	100	101	100	99	98	102
3.150	106.5	105.5	101	100	101	100	102	107
4.000	106	105	101.5	100	103	105	105	107
5.000	105	104	102	102	105	106	107	107
6.300	104.5	104	103	104	107	106	107	106.5
8.000	103.5	103	103.5	107.5	107	105	107	106.5
10.00	101	102	105	107.5	107	105.5	106	106
12.50	100.5	101	105.5	106	106	105	105	105.5
16.00	100	101	106	106	106	105	104	104
20.00	100	101	105.5	106	106	104	104	104
25.00	100	101	105.5	106	106	105	104	103
31.50	99	100	105.5	106	106	105	104	104
40.00	97	100	104	106	105	104	104	101
50.00	95	97	101	103	102	100	100	00
63.00	91	95	100	100	100	99	96	94
80.00	88	89	97	96.5	97	95	93	92
100.0	84	87	94	92	91	90	92	89

Uncorrected 1/3 Octave SPL's

Test Model : Contoured PN

Reservoir Pressure = 51 psig Dry Bulb Temp. = 68°F

Atmospheric Pressure = 29.43 in Hg Wet Bulb Temp. = 62°F

f (kHz)	Theta in degrees							
	15	30	45	60	75	90	105	120
0.200	91	89	84	85	85	87	86	86
0.250	91.5	90.5	86	86	86	87	87.5	86.5
0.315	92.5	92	87	88	87	88	88.5	88
0.400	94	93	89	89	88	89	89	89
0.500	99	94	90.5	90	89.5	91	89	90
0.630	101	96.5	92.5	92	91	91.5	91.8	91.5
0.800	103	94	94	93.5	92	92.5	93	92.5
1.000	105	100	95.5	95	93.5	94	94	94
1.250	105.5	101.5	97	96	95	94.5	94	94.5
1.600	106	102.5	98.5	97	96.5	95.5	95	96
2.000	106	104	100	98	98	97	96.5	99
2.500	106	104.5	101	99	100	99.5	100	103
3.150	105.5	104.5	102	100.5	101	103	104	104.5
4.000	105.5	104	102	101.5	103	104	106	106
5.000	104.5	104	103	103	105	105	106	106
6.300	103.5	104	104	104	106	106	106	106
8.000	102.5	103	104	105	105	105	106	105.5
10.00	101.5	102.5	104	105	105	105	105	105.5
12.50	100	102	104.5	105	105	104	104.5	104
16.00	99	101.5	104.5	105	105	104	103.5	104
20.00	98	101	104.5	105.5	105	104	103.5	103
25.00	97.5	100	104.5	105.5	105	104	103.5	102
31.50	96	99	104	105	103.5	103.5	102.5	102
40.00	95	97.5	103	103.5	102	102	100	100
50.00	93	96	101	101	99	99.5	98	96
63.00	91	94	97	98	96	95.5	93	91
80.00	89	92	94	94	92	92	88	87
100.0	84	88.5	90	90	88	88	83	83

Uncorrected 1/3 Octave SPL's

Test Model : Conical Plug

Reservoir Pressure = 30 psig. Dry Bulb Temp. = 55°F

Atmospheric Pressure = 29.64 in. Hg Wet Bulb Temp. = 48°F

f (kHz)	Theta in degrees							
	15	30	45	60	75	90	105	120
0.200	90	88	78	78	77	77	77	72
0.250	93	90.5	82	80.2	80	79	78	74
0.315	97	94	86	84	83	81.2	80	76.5
0.400	99.5	96	88.5	85.8	85	83	82	78
0.500	102	98.5	91	87.8	87	84.5	84	80
0.630	105	101	94	90.8	90	87	86	82
0.800	106	104	96	92	91.6	88.5	87.5	84
1.000	107	106	98.5	94	93.5	90.5	88.5	86
1.250	108	107	101	95.5	95	92	90	88.5
1.600	108.5	108.5	103	96.5	96.5	93.6	91.5	90.5
2.000	109	108.5	103.5	98	98	95	93	92
2.500	109	108.5	104.5	100	99.5	96.5	94	95
3.150	109	108.2	104.5	101	101	98	96	100
4.000	108.5	108	104.8	101.8	102	99	100	103
5.000	108	107	104.8	102.5	103	101	103	105
6.300	107	105	104.8	103	103.5	102.8	105	106
8.000	106	104	104.8	104	104	103.5	104.5	105
10.00	104	103.5	104.8	104	104	103.8	104	103
12.50	12	103	104.8	105	104	103.8	102.6	102
16.00	101	101.5	104.8	105.5	104	103.8	102	100.5
20.00	100	101	104.8	105	103.5	103	101	100
25.00	99.2	99.5	104.8	105	102.5	102	101	99.5
31.50	97.2	97.5	103.5	104	100.5	100	99.5	98
40.00	96	96	101	102	100	98.5	98	96.5
50.00	92	93	96	98	97	95	94	92.5
63.00	87	88	91	92	92	88	88	87
80.00	80	83	86	87	84	82	81	80
100.0	72	78	81	82	76	74	72	66

Uncorrected 1/3 Octave SPL's

Test Model : Conical Plug

Reservoir Pressure = 37 psig Dry Bulb Temp. = 51°F

Atmospheric Pressure = 29.57 in. Hg Wet Bulb Temp. = 45°F

f (kHz)	Theta in degrees							
	15	30	45	60	75	90	105	120
0.200	92	89	83	82	82	80	79	78
0.250	94.5	90	85.5	84	84.5	82.5	81	79
0.315	96	92	88	87	86	83	82	80
0.400	98	94	89	88	87	84	83	81
0.500	100	96	91.8	91	88	85.5	84	82.5
0.630	102	98.5	94	93	90	87	86.5	84
0.800	103.8	101	96	94.8	91.5	89	88	86
1.000	105	103.5	98	96.5	93.5	91	90.5	88
1.250	107	106	100	98	96	92	93	90
1.600	107.5	107	102	99	97.5	95.5	94.5	92
2.000	108	108	103.5	100.5	98	96.5	97.5	95
2.500	109	108.8	105	102	100	99	100.5	98
3.150	107.5	108.8	106.5	103.5	102	102	103	102
4.000	108	108.6	107	104	103.5	104	105.5	104
5.000	108	108.2	107	105.5	104.6	106	107	106.5
6.300	107.5	107.5	108	107	106	106.8	107	106.5
8.000	106	107	108	108	106.5	107.5	106.8	108
10.00	105.5	106.5	108	109	107	107.5	106.5	108
12.50	104	104.5	108	109	107	107.5	106.5	107
16.00	103.5	103.5	108	109	107	107.5	106	106.5
20.00	103	102.5	107.5	109	107	107.5	105.5	106
25.00	101	101.5	107	108.2	106.5	107.5	106	105.5
31.50	99	100.5	106	107	105.5	106	104	104
40.00	97.5	99.5	104.5	105	104	103.5	100.8	101.5
50.00	95.5	97.5	101.6	101.5	100	99	97	97
63.00	93	95	97.8	97	94.8	94	91	90
80.00	91	92	93	92	91	90	86	84
100.0	86	88	88	87	86	87.5	81	80

Uncorrected 1/3 Octave SPL's

Test Model : Conical Plug

Reservoir Pressure = 51 psig
Atmospheric Pressure = 29.57 Hg.

Dry Bulb Temp. = 51°F
Wet Bulb Temp. = 45°F

f (kHz)	Theta in degrees							
	15	30	45	60	75	90	105	120
0.200	93.5	91	87	87	88	89	99	87
0.250	95	92	88	88	89	89.5	91.5	89
0.315	97	94	89.3	89	90	90.5	92.4	91
0.400	97.5	95	90.3	90.2	91	91	93	92.5
0.500	99	96	91.8	91.2	91.8	91.8	93.5	93
0.630	101	98	93	92.3	93	92.8	94.5	94.5
0.800	103	100.6	94.5	93.2	94	93.8	95	95
1.000	104.3	103	95.6	94.5	95	95.0	95.5	96.0
1.250	105.2	105	97	96.0	96	96	96	97
1.600	106.4	106.8	98	97.0	97	97.5	97	99
2.00	107	107	99	97.5	98.3	98.5	98.8	101
2.500	107	107	100	98.6	99.6	99.5	101	103
3.150	107	106	100.5	100	101.8	102.5	104	104.6
4.000	107	105.6	101	101	103	104.3	105.8	105.5
5.000	106.8	105	102	103	104.6	105	106.5	106
6.300	105	104.5	103	105	105.6	106.5	106.5	106.7
8.000	103.5	104	103	107	105.6	106.5	106.8	106.4
10.00	103	103.8	104	107	106.7	106.5	106	106
12.50	101.8	103.3	104.5	107	106.7	105.5	105.5	105
16.00	101.7	103	105	107	106.7	105.5	105	104.5
20.00	100	103	106	107	106.7	105	104.8	104
25.00	98.8	103	106	107	106.7	105	104.8	103
31.50	99	102.6	105	106	106	104.8	103.8	102
40.00	97.5	101	104.5	105	104.5	104	103	101
50.00	94.8	99	103	103	103	102	101	99.5
63.00	91.6	98.6	100.5	100	101	100	98	97
80.00	89	93.5	97.5	98.5	98.8	97	95	94
100.0	86	90.5	95.0	95.5	96	93	92.6	89

Uncorrected 1/3 Octave SPL's

Measuring Station : $\theta = 90°$

Models	Ambient Conditions		
	P_{atm} (in. of Hg)	DBT °F	WBT °F
(i) Solid Conical Plug	29.43	68	62
(ii) Porous Plug (10%)	29.37	73	64
(iii) Porous Plug (4%)	29.32	60	57

f	(i)			(ii)			(iii)		
—	2.0	2.5	4.0	2.0	2.5	4.0	2.0	2.5	4.0
0.200	68.5	76	83	66	76	80	69	77	82
0.250	71	78	83.5	70	79	83	72	79	83
0.315	74.5	80	85	73	81	84	75	81	84
0.400	76	82.5	86	76	82	86	76	82.5	85
0.500	78.5	84	87	78	85	87	78.5	84	86
0.630	82	86	88.5	80	87	89	81	86.5	88
0.800	83	88.5	90	82	90	91	83	88	90
1.000	84.5	91	92	85	91	92	85	90	92
1.250	87	92	94	87	92	95	86	93	93
1.600	88.5	95	96	87.5	95	95	87	94.5	95
2.000	90	97	97	90	96	97	89	96	96
2.500	91	100	99	90	97	98	90.5	97	98
3.150	93	103	100	91	102	100	91	101	99
4.000	94.5	104	102	92	104	104	93	101	101
5.000	95.5	104	104	95	104	106	95	102	103
6.300	97	104	105	98	105	107	96	104	105
8.000	98	104	106	98	104	106.5	96	104	106
10.00	98	104	106	98	102	106	96	104	106
12.50	98.5	103	105.5	99	101	106	95	103	106
16.00	97.5	102	105.5	97	100	105.5	94	102	106
20.00	98	101	105.5	97	100	105	94	101	105
25.00	96	101	105.5	97	101	105	93	100	105
31.50	96	100	105.5	96	97	105	91	99.5	105
40.00	93	96	105.5	94	94	102	88	97	104
50.00	89	92	102	90	90	100	82	92	102
63.00	83	87	98	85	84	95	75	86	90
80.00	75	81	95	76	78	91	66	79	95
100.0	66	76	91	60	71	86	58	73	91

Uncorrected 1/3 Octave SPL's

Test Model : Porous (10%)

Reservoir Pressure = 30 psig
Atmospheric Pressure = 29.23

Dry Bulb Temp. = 62°F
Wet Bulb Temp. = 58°F

f (kHz)	Theta in degrees							
	15	30	45	60	75	90	105	120
0.200	92	89	81	77	78	76	73	72
0.250	94.5	91	83	80	79	78.5	77	74
0.315	97	93	86	83	82	81	79	77
0.400	98	96	88	86	85	83	82	79
0.500	100	98	90	88	86	85	82	81
0.630	103	101	93	90	89	87	85	83
0.800	105	102.5	97	92	90	89	88	86
1.000	106	107	99	94	93	91	90	88.5
1.250	107	108	100	96	94.5	93	91	90
1.600	108	108	102	97	96	93	92	92
2.000	108	108	104	99	97	95	93	94
2.500	108	109	104	100	98.5	96	94	96
3.150	108	108	105	101	99	98	96	97
4.000	108	107.5	105	101	100	98	99	101.5
5.000	106	106	105	101	101	102	102	102.5
6.300	106	105.5	105	102	103	104	103	102
8.000	104	103	105	103	103	103	102	102
10.00	103	102	104	104	104	102	102	100
12.50	102	101	104	104	102	101	102	100.5
16.00	99	100	104	103	102	101	101	99
20.00	99	100	104	102	102	101	100	98.5
25.00	98	100	104	103	102	101	100	98.5
31.50	98	99	102	103	101	100	100	98
40.00	95	98	98	100	99.5	98	97	95
50.00	90	91	93	96	93	92	90	89
63.00	87	85	88	90	87	86	84	82
80.00	81	79	82	84	80	80	78	75
100.0	75	74	76	77	72	68	68	68

Uncorrected 1/3 Octave SPL's

Test Model : Porous (10%)

Reservoir Pressure = 37 psig
Atmospheric Pressure = 29.23

Dry Bulb Temp. = 62°F
Wet Bulb Temp. = 58°F

f (kHz)	Theta in degrees							
	15	30	45	60	75	90	105	120
0.200	90.5	90.8	81	80	80	77	76	73
0.250	93	92.5	83.5	82.5	83	79	78	77
0.315	94.5	95	86	85	85	81	81	79
0.400	97	96	90	87	87	83	82	80
0.500	98	98	92	89	89	85	84	82
0.630	102	100	93.5	93	91	88	87	84
0.800	102	102	95.8	94	93	90	88	86
1.000	104	104	98.5	96	94.5	92	91	89
1.250	104	106	100	97	95	93.5	92	92
1.600	105	108	102.5	98	96	95	93	92
2.000	107	108	104	100	99	96	95	94
2.500	107	109	105	101	99	97	96	95
3.150	107	109	105.5	102	100	97.5	97.5	96
4.000	107	107	106	103	100	98.5	102	104
5.000	106	106	106	103	102	104	104	104
6.300	105	105	106	104	104	106	104	105
8.000	104	104	106	105	106	105	104	105
10.00	104	103	106	105	105	105	104	104
12.50	102	102	106	106	104.5	105	104	103
16.00	100	101	106	106	105	105	103	102
20.00	100	100	106	105	105	104	102.5	100
25.00	99	100	105	106	105	104	102	100
31.50	97	100	105	106	105	104	102	100
40.00	96	98	102	103	102	101	98	99.5
50.00	94	94	97	100	99	96	95	94
63.00	88	91	92	92	92	90	88	86
80.00	86	85	88	88	87	84	84	80
100.0	82	79	84	84	82	76	76	74

Uncorrected 1/3 Octave SPL's

Test Model : Porous (10%)

Reservoir Pressure = 51 psig
Atmospheric Pressure = 29.37

Dry Bulb Temp. = 73°F
Wet Bulb Temp. = 64°F

f (kHz)	Theta in degrees							
	15	30	45	60	75	90	105	120
0.200	91	89	83	85	85	85	86	86
0.250	92.5	91	85	86	86	86	89	87
0.315	94.5	92	86.5	87.5	87	87	90.5	88
0.400	96	93.5	88	88	88	88	91	88.5
0.500	98	95	90	89.5	89	89	92	89
0.630	100	97	92	91	91	91	03	90.5
0.800	101	98.5	94	92	92	92	93.5	91.5
1.000	102	100	95	93	93	93	94	94
1.250	104	101	97	95	95	95	94.5	94
1.600	105	102	98	96	96	96.5	96	94
2.000	105	103	99	98	97	98.5	96	97
2.500	105	104	1C1	99	99	100	100	102
3.150	105	104	101	99	100.5	101	102.5	107
4.000	105	104.5	101	99	100	104	104	107
5.000	105	104	102	100	104	105	105	106
6.300	103.5	103	102.5	104	106	105	105	106
8.000	103	103	104	106.8	106	105	106	106
10.00	102	102.5	104	106.5	106	105	105	106
12.50	101	102	104.5	106	105	105	105	104
16.00	99.8	102	105	105	105	105	104	103
20.00	99	101	105	105	104	104	104	102
25.00	98	100	105	105	105	104	104	103
31.50	97.6	100	105	105	105	104	103	102
40.00	96	100	104	104	104	101	101	100
50.00	94	97	102	101	102	98	97	96
63.00	88	94	99.5	99	99	95	92	90
80.00	87	92	97	95	96	92	88	88
100.0	84	88	94	92	92	86	84	82

Uncorrected 1/3 Octave SPL's

Test Model : Porous (4%)

Reservoir Pressure = 30 psig
Atmospheric Pressure = 29.32 in Hg

Dry Bulb Temp. = 60°F
Wet Bulb Temp. = 57°F

f (kHz)	Theta in degrees							
	15	30	45	60	75	90	105	120
0.200	91	89	81	79	78	76	76	75
0.250	94	90	83	81	79	78.5	78	76
0.315	96	92.5	85.5	83	82	81	80	78
0.400	99	95	87	85.5	84	82.5	82	80
0.500	101	96	89	88	86	84	83	82
0.630	103	100.5	92	91	88.5	86.5	85	83.5
0.800	104	103	95	92.5	91	88	88	85.5
1.000	106	105	98	95	93.5	90	90.5	87.5
1.250	107	107	100	97	95	91.5	93	90
1.600	108	108	102	98	96.5	94.5	93	92
2.000	108	109	104	99.5	98	96.5	94	92
2.500	108	109	105	101	100	98.5	96	95
3.150	108	108	105	101	101	100	98	100
4.000	107	107.5	105	101	101	103	102	103
5.000	106	106.5	105	101	101	103	104	104
6.300	105	105	105	102.5	103	104	104	105
8.000	104	104	105	104	103	104	104	105
10.00	102	103	105	105	103	103	102.5	105
12.50	101	101.5	105	105	103	103	102	101
16.00	100	101	105	105	102	101	100	102
20.00	98	100	105	105	102	102	101	100
25.00	98	100	104	105	102	102	101	100
31.50	94	99	103	103	101	101	100	100
40.00	92	95	100	100	99	99	97.5	97
50.00	88	90	95	96	95	94	93	93
63.00	84	86	89	92	88	90	88	88
80.00	79	81	83	86	84	83	81	82
100.0	74	75	77	78	76	76	74.5	71

Uncorrected 1/3 Octave SPL's

Test Model : Porous (4%)

Reservoir Pressure = 37 psig
Atmospheric Pressure =29.32 in Hg

Dry Bulb Temp. = 60°F
Wet Bulb Temp. = 57°F

f (kHz)	Theta in degrees							
	15	30	45	60	75	90	105	120
0.200	89	91	83	81	76	78	74	75
0.250	91	92	85.5	82.5	78	81	76	77
0.315	93	94.5	87.5	85	80.5	83	78	79.5
0.400	94.5	96	89	87	82.5	84	80	81.5
0.500	96.5	97.5	92	89	84.6	86	82	83.5
0.630	99.6	100	94	91	87	88	74	85.6
0.800	101.5	102	97	92.5	89.5	90	86	88
1.000	104	104	99	94	91.5	92	88	90
1.250	105	106	101	96	94	94	91	91
1.600	105.5	107.5	102.5	97.5	95.5	95	92.5	93
2.000	106	108	104	98.6	97	96.5	94	95
2.500	107	108	105	100	98.5	98.5	96	97
3.150	107	107.5	106	100.6	100	100	97	98.5
4.000	106.5	107.5	106	101.5	100.5	101.5	99	100
5.000	106	106.5	106	102	101	102.5	100.5	102
6.300	105.5	105	106	102.5	102	104	102	103
8.000	105	104	106	103.5	102.5	104	103	103
10.00	104	103	105	104	103	107	104	103
12.50	102	101.5	105	104	104	107	105	103
16.00	101.5	100.5	104.5	104	104	105	106	103
20.00	100	99	104	104.5	105	104	105	102
25.00	99	98	104	104.5	105	104	104	100
31.50	97.5	96	102	104.5	104	102	104	98
40.00	96	95	100	104	102	100	102	94
50.00	94.5	91	97	102	100	96	98	90
63.00	92	87	92	97	95	89	93	85.5
80.00	88	83	88	92	90	84	88	81
100.0	83	78	81	87	85	78	82	73

Uncorrected 1/3 Octave SPL's

Test Model : Porous (4%)

Reservoir Pressure = 51 psig Dry Bulb Temp. = 60°F

Atmospheric Pressure = 29.32 in Hg Wet Bulb Temp. = 57°F

f (kHz)	Theta in degrees							
	15	30	45	60	75	90	105	120
0.200	92.0	90	86	85	84	86	87	87
0.250	94	92	88	86	85	87	88	88.5
0.315	96.5	94	89.5	87.5	86.5	88.5	89.5	89
0.400	98	95	90.5	89	87.5	90	90	90
0.500	99	96.5	92	90	88.5	91	90.5	90.8
0.630	102	98	93.5	91.5	90.5	92.5	91.8	92
0.800	103.5	99.5	95	93	91.5	94	92.5	93
1.000	104.5	101	96	94	93	94.5	94	94
1.250	105.5	102	97	96	94	96	95	95.7
1.600	106	103.5	99	97	95	96.5	97	98
2.000	106	105	100	98	97	98	99	100
2.500	106	105	100	100	99	99	100.5	103
3.150	106	105	101.5	100.6	100.5	100.5	103	104.5
4.000	106	105	101.5	102	101	101.5	104	106
5.000	105.5	105	102	102.5	103.5	104	105	106
6.300	104	104	102	102.5	105	104	105	106
8.000	103	104	104	105	105	104	105	106
10.00	102	103	104	105	105	104	105	104.5
12.50	101	103	104	105	104	104	104	103
16.00	100	101	104	105	104	104	104	103
20.00	99	101	104	105	104	104	104	102
25.00	98	101	104	105	104	104	103.5	102
31.50	97.5	100	104	104	104	103.5	102	101
40.00	95.5	99	101	103	103	102	100	99
50.00	93.5	97	100	101	102	100	97	97
63.00	90	94	97	98	99	96	94	93
80.00	87.5	93	94.5	95	97	93	90	88
100.0	84	90	91	92	95	89	85	84

Standard Bibliographic Page

1. Report No.	2. Government Accession No.	3. Recipient's Catalog No.
NASA CR-178095		

4. Title and Subtitle	5. Report Date
Aeroacoustics of Supersonic Jet Flows from Contoured and Solid/Porous Conical Plug-Nozzles	January 1987
	6. Performing Organization Code
7. Author(s)	8. Performing Organization Report No.
Darshan S. Dosanjh and Indu S. Das	
9. Performing Organization Name and Address	10. Work Unit No.
Department of Mechanical and Aerospace Engineering Syracuse University, Syracuse, N.Y. 13244	11. Contract or Grant No. NAG1-129
12. Sponsoring Agency Name and Address	13. Type of Report and Period Covered Contractor Report
National Aeronautics and Space Administrations Langley Research Center, Hampton, VA 23665	14. Sponsoring Agency Code 505-61-11

15. Supplementary Notes

Technical Officer for the Grant
John M. Seiner, Senior Research Scientist
NASA (Langley Research Center), Hampton, VA 23665
Final Report

16. Abstract

The results of an experimental study of the acoustic far-field, the shock associated noise, and the nature of the repetitive shock structure of supersonic jet flows issuing from plug-nozzles having externally-expanded plugs with pointed termination operated at a range of supercritical pressure ratios $\xi \doteq 2.0$ to 4.5 are reported. The plug of one of these plug-nozzles was contoured. The other plug-nozzles had short conical plugs with either a solid surface or a combination of solid/porous surface of different porosities. The contoured and the uncontoured plug-nozzles had the same throat area and the same annulus-radius ratio $K = R_p/R_N = 0.43$.

By comparison with the noise characteristics of underexpanded jet flows from an 'equivalent' convergent nozzle, the reductions of the order of 10 dB in the combined (mixing and the shock associated) overall sound pressure levels are achieved at all observer locations ($15^o < \theta < 120^o$) when the contoured plug-nozzle with a pointed plug termination is operated at pressure ratio $\xi = 3.6$ ($M_j \doteq 1.49$) in its fully-expanded (shock-free) and virtually wakeless mode. The noise intensity levels radiated by supersonic jet flows at higher θ's from such a contoured plug nozzle operated at a range of supercritical pressure ratios follow β^2 and not the Harper-Bourne Fisher β^4 scaling for the underexpanded jet flows from a convergent round nozzle, where $\beta^2 = M_j^2 - 1$. Similarly $\beta^2_* = M_j^2 - M_d^2$ and not the Tam-Tanna scaling β^4_* is followed.

When a plug-nozzle incorporating an uncontoured conical plug with a pointed termination of the same annulus-radius ratio and the same surface area as that of the contoured plug is operated at the pressure ratio at which shock-free flow is achieved by the contoured plug-nozzle, reductions in noise intensity levels of the order of 7 dB, were recorded. Additional reductions in the noise intensity level of up to 3 dB were attained when the surface of the uncontoured conical short plug was perforated either with 10% porosity distributed evenly over the entire plug surface or 4% porosity distributed evenly over the middle-third of the plug-surface. As a result of modifications of the shock structure, the acoustic performance of improperly expanded jet flows of an externally-expanded short uncontoured plug of an appropriate geometry with suitably perforated plug and a pointed termination, is shown to approach the acoustic performance of a shock-free supersonic jet issuing from an 'equivalent' externally-expanded contoured plug-nozzle.

17. Key Words (Suggested by Authors(s))	18. Distribution Statement
Supersonic jet flows. Supersonic jet noise. Plug-nozzles with contoured and uncontoured plugs with pointed termination. Plugs with porous surface. Shock-structure modification.	unclassified-unlimited Subject Category 71

19. Security Classif.(of this report)	20. Security Classif.(of this page)	21. No. of Pages	22. Price
unclassified	unclassified	187	A09

For sale by the National Technical Information Service, Springfield, Virginia 22161

NASA Langley Form 63 (June 1985)